CLINICAL PHENOTYPES AND CELLULAR MEDIATORS IN DIABETIC RETINOPATHY

Dawn Alexandra Su Ying Sim

UCL

Thesis submitted in fulfilment of the requirements for the degree of

Doctor of Philosophy

Supervised by Dr. Marcus Fruttiger

2015

I, Dawn Sim confirm that the work presented in this thesis is my own. Where information has been derived from other sources, I confirm that this has been indicated in the thesis.

22nd October 2015

Acknowledgements:

I wish to thank:

All the members of the lab for their support, invaluable assistance, and friendship throughout this project, including Michael Powner, Kristis Vevis, Senth Selvam, and Elmira Jailian;

Grazyna Galatowicz and Colin Chu for help and guidance with Flow cytometry;

Marcus Fruttiger, Adnan Tufail, Catherine Egan, and Pearse Keane for the excellent guidance and challenges they set forth throughout the project;

And last but not least, my family.

Abstract:

The aim of this work was to establish meaningful clinical end-points and surrogate markers for diabetic macular ischaemia, a condition for which there is no treatment. The relationship between diabetic eye disease and circulating cellular mediators of angiogenesis and inflammation was further explored with a view to developing therapy in the longer term.

Visual loss in diabetic macular ischaemia was observed to occur only in moderate to severe disease, progresses at a rate of 5-10% increase in area per year and associated with thinning of the retinal nerve fibre layer. Direct visualisation of cells in the vitreous was achieved using optical coherence tomography. Novel methods for this were further developed in inflammatory eye disease, with a view for application in diabetic eye disease. A method for in vivo labelling of cells using ICG to enhance visualisation was described. In the field of regenerative medicine, this technique may allow direct visualisation of cell-mediated inflammation regardless of the type of cell or tissue transplanted. EPC and monocyte profiles were analysed in the context of diabetic eye disease. Elevated levels of EPCs as defined by CD34+ CD309+ were observed in diabetes, but no associations were observed with progression. There were no initial associations between monocyte subsets and diabetic eye disease severity at the outset but differences were observed in the context of progression. Observations from this work support the notion that inflammation plays an important role in diabetic eye disease and will inform development of new treatments in this field.

Contents

List of tables

List of figures

Abbreviations:

CME	Cystoid macular oedema
CR	Coefficient of repeatability
CSME	Clinically significant macular oedema
DRCR.net	Diabetic Retinopathy Clinical Research Network
EAU	Experimental autoimmune uveoretinitis
EDI-OCT	Enhanced depth optical coherence tomography
EIU	Endotoxin-induced uveitis
EPC	Endothelial progenitor cell
FBS	Fetal bovine serum
FCS	foveal central subfield
FDA	US Food and Drug Administration
FMO	Fluorescence-minus-one
ICC	Intraclass correlation coefficient
ICG	Indocyanine Green
IL	Interleukin
iM	intermediate monocytes
ip	Intraperitoneal
IRMA	Intraretinal microvascular abnormalities
iv	Intravenous
LogMAR	logarithm of the minimum angle of resolution
LPS	Lipopolysaccharide
M-CSF	Macrophage colony-stimulating factor
M1	Non classical monocytes

M2	Classical monocytes
mm	millimeters
NIR	Near infrared
NVD	Neovascularisation at the disk
NVE	Neovascularisation elsewhere
PBMCs	Peripheral blood mononuclear cells
PE	R-Phycoerythrin
PI	Propidium Iodide
PIC	Punctate inner choroidopathy
SD	Standard deviation
SD-OCT	Spectral-domain optical coherence tomography
TB	Tuberculosis
TMC	total macular circle
TNFα	Tumour necrosis factor
UK NSC	United Kingdom National Screening Committee
uwFA	Ultra widefield fluorescein angiography
VA	Visual acuity
VEGF	vascular endothelial growth factor
VEGFR	Vascular endothelial growth factor receptor
VKH	Vogt-Koyanagi-Harada
χ^2	Chi-squared

1. General introduction

1.1 Diabetic retinopathy

1.1.1 Historical perspective

Diabetes was one of the first diseases to be described in medicine. In 1500 BC, it was mentioned in an Egyptian manuscript as the excessive passing of urine. The knowledge of diabetes did not increase for over a thousand years, and over the turn of the 1st century it continued to be described as an incurable condition with "honey urine" for which its name was derived; Diabetes, a Greek work meaning to "pass through" or "siphon", and Mellitus, Latin for "sweet" or "honeyed". It was not until the discovery of insulin by Frederick Banting and Charles Best in 1922, that patients with diabetes had a substantial increase in survival and life expectancy.(1) With the development of modern insulin and glucose monitoring devices, patients with diabetes are now living longer, and in doing so, are at a greater risk of developing diabetes-related complications. It is estimated that over half of these individuals will at some point in the course of their disease develop diabetic retinopathy, representing an insurmountable burden on healthcare systems worldwide.(2-5) By the year 2030, there will be an estimated 552 million people diagnosed with diabetes globally.

Vision loss as a consequence of diabetes is now well known. However, it was only the invention of the direct ophthalmoscope that allowed the first description of diabetic retinopathy in 1856, when Eduard Jaeger reported his then controversial observations of "yellowish spots and extravasations" in the central macular of a diabetic patient.(6) However, a causal relationship between diabetes and diabetic vascular changes in the retina was treated with skepticism by European ophthalmologists, largely because of open opposition by Albrecht von Graefe, an influential German ophthalmologist in his time. Diabetic retinopathy, as a disease entity only gained acceptance after 1872 when Edward Nettleship published the first histopathological proof in his seminal paper "On oedema or cystic disease of the retina".(7)

1.1.2 Epidemiology

In the 21st century, diabetic retinopathy is now recognised as the most common microvascular complication of diabetes and the leading cause of blindness in working-age persons. As such, it is a condition that is of an important public health concern with significant economic consequences. Our knowledge of the onset, progression, and impact of diabetic retinopathy derives from large epidemiological studies such as the Wisconsin Epidemiologic Study of Diabetes (WESDR)(4, 5, 8), Beaver Dam Eye Study (BDES) (9), and Blue Mountains Eye Study (BMES) (10, 11).

The WESDR, a population-based cohort study, shows that the prevalence of diabetic retinopathy in type 1 diabetes range from 17% (less than 5 years duration of disease) to 100% (more than 15 years duration of disease). In the corresponding type 2 population, the prevalence ranged from 29% to 78%. The factors that influenced the development of diabetic retinopathy were confirmed in two landmark clinic trials; the Diabetes Control and Complications Trial (DCCT) for type 1 diabetes (12), and the UK Prospective Diabetes Study (UKPDS) for type 2 diabetes (13), and include glycaemic control, duration of diabetes, dyslipidaemia, and blood pressure.(14, 15) Of note, both inflammation and vascular endothelial dysfunction have also been associated with the presence of diabetic retinopathy in large population-based studies. Serum levels of C-reactive protein (CRP), soluble intercellular adhesion molecule-1 (sICAM-1), and urinary albumin:creatinine ratio (16) , as well as chemokines such as stromal cell-derived factor (SDF)-1 alpha, RANTES, and monocyte chemoattractant protein (MCP)-1 (12), have been associated with diabetic retinopathy prevalence and severity.

1.2 Phenotypic manifestations of diabetic retinopathy

The abnormalities observed in the retina in diabetic retinopathy can be conceptually classified according to the behaviour of the retinal vasculature- (1) hyperperfusion (leakage and oedema), which results in the development of lesions such as macular oedema, peripheral hard exudates and microaneurysms, and (2) hypoperfusion (ischaemia), which results in enlargement of the foveal avascular zone (FAZ) in the

macula, and capillary non perfusion and retinal neovascularisation in the retinal periphery.

Historically, classification for diabetic retinopathy was developed for the purposes of communication between researchers and clinicians. In 1968, the “Airlie House” classification was developed by the US public health service, based on five standard colour photographic fields.(17) Vascular lesions were classified into three categories; absent, mild to moderate, and severe. This system was deemed over-simplistic, with only three categories of severity, in particular, the broad category of “mild to moderate”. Subsequently, the Diabetic Retinopathy Study (DRS), whose principal aim was to determine the efficacy of retinal laser photocoagulation in preventing severe vision loss in “high-risk” proliferative diabetic retinopathy, created the modified Airlie House classification system.(18) This included a further 2 colour photographic fields and separation of severity grades in order to allow the researchers to grade more consistently. Although the DRS, a landmark study in the field of diabetic retinopathy treatment, showed that visual function was preserved with laser treatment of those with “high-risk” retinal features, it failed to examine whether those with early features of proliferative diabetic retinopathy would benefit from similar therapy.

The Early Treatment Diabetic Retinopathy Study (ETDRS) was designed in the 1970s to answer this question, and the efficacy of laser photocoagulation for macular oedema. In the ETDRS, classification of diabetic retinopathy features were further split to include 17 factors, examples of which include microaneurysms, intraretinal microvascular abnormalities (IRMA), new vessels, hard exudates, cotton wool spots, venous beading/narrowing/sheathing, perivascular exudates, fibrosis. Combined with several severity steps, this presented a complicated grading scheme of over 100 grades. In spite of this, the ETDRS diabetic retinopathy scale remains the gold-standard for grading for researchers and clinicians alike.(19) An attempt to simplify the ETDRS grading system was developed by the Global Diabetic Retinopathy Project Group- the International Classification Scheme.(20) This international collaborative effort towards consensus regarding disease severity classification was designed to

detect both proliferative diabetic retinopathy and diabetic macular oedema at a threshold, which required laser therapy, for the purposes of facilitating communication and discussion amongst clinicians who attend to these patients.

It is important to note that the historical classification of diabetic retinopathy is based solely on colour photography. Fluorescein angiography, although performed in ETDRS, had poor agreement in grading of the FAZ size (74% agreement), FAZ outline and perifoveal capillary loss (47% agreement)(21). Because of the questionable reproducibility of grading, the resources required, and invasive nature of fluorescein angiography, it has not been used in more recent clinical trials of diabetic retinopathy such as the Diabetic Retinopathy Clinical Research Network (DRCR.net).(22) A fundamentally new way of assessing retinal disease was introduced by the advent of optical coherence tomography (OCT) was a completely different story. Its non-invasive nature, rapid acquisition, and cross-sectional view of the retina, has led to widespread use in both research and clinical practice. As such, the future of diabetic retinopathy classification is likely to incorporate multi-modal, non-invasive imaging technology, such as OCT, but also OCT angiography, and ultra widefield fundus photography.

1.2.1 Retinal Neovascularisation

Retinal neovascularisation in the diabetes occurs as a result of areas of retinal non-perfusion. It can occur at the optic nerve head; neovascularisation at the disk (NVD) or along retinal veins and postcapillary venules; neovascularisation elsewhere (NVE). In diabetic retinopathy, neovascularisation may also occur in the anterior segment in the form of new vessels in the iris, or iris rubeosis, with resultant bleeding into the anterior chamber of the eye, and/or blockage of the trabecular meshwork (drainage angle) and elevated intraocular pressure. The new blood vessels grow along the retina and vitreous gel. They have thin fragile walls, leak plasma (as observed using fluorescein angiography), and may bleed into the vitreous cavity. Visual loss from retinal neovascularisation can occur with vitreous haemorrhage, or later fibrosis of

new vessels with and consequent tractional forces on the retina causing retinal breaks and detachment.

The spectrum of disease in retinal neovascularisation is wide. Clinically, it can be classified as non-proliferative or proliferative diabetic retinopathy (PDR).(19, 20) PDR, which occurs in up to 50% in type 1, and 15% in type 2 diabetes, remains a major cause of visual disability in this age group.(4) Therefore, the timely detection of neovascularisation and the monitoring of new vessel activity is important in managing these patients. In the landmark clinical trials of the DRS and ETDRS, colour photography was used to detect retinal neovascularisation with fluorescein angiography (examples of which can be seen in **Figure 1.1a-d**) as an adjunct for the classification of disease severity, guiding laser therapy and evaluating the response to treatment.(21, 23, 24) In current large multicenter clinical trials, fluorescein angiography is usually not required, and performed at the investigator's discretion.(25) In clinical practice however, it is often used to ascertain new vessel activity in the context of evaluating the response to treatment. As fluorescein angiography is an invasive procedure, it is not performed with the same frequency as OCT.

OCT, first described by Huang et al., in 1991, obtains a cross-sectional image of the retina, using a non-invasive technique with micrometre resolution.(26, 27) In the last decade, this technology has advanced rapidly, and currently, spectral-domain OCT (SD-OCT), which uses spectral interferometry and a Fourier transform algorithm, has an increased sensitivity, higher scan acquisition rate, and potentially greater depth penetration.(27) The evolution of SD-OCT has changed how diabetic retinopathy is investigated, and has been widely adopted for the assessment of diabetic macular oedema, both in clinical practice and clinical trials. This non-invasive technique has not only allowed for more frequent assessment and close monitoring of patients with diabetic retinopathy, but has also increased our understanding of how the disease affects the different layers of the retina and choroid, in particular, for the identification of retinal thickening, intra-retinal oedema and changes of the vitreoretinal interface.(28-31)

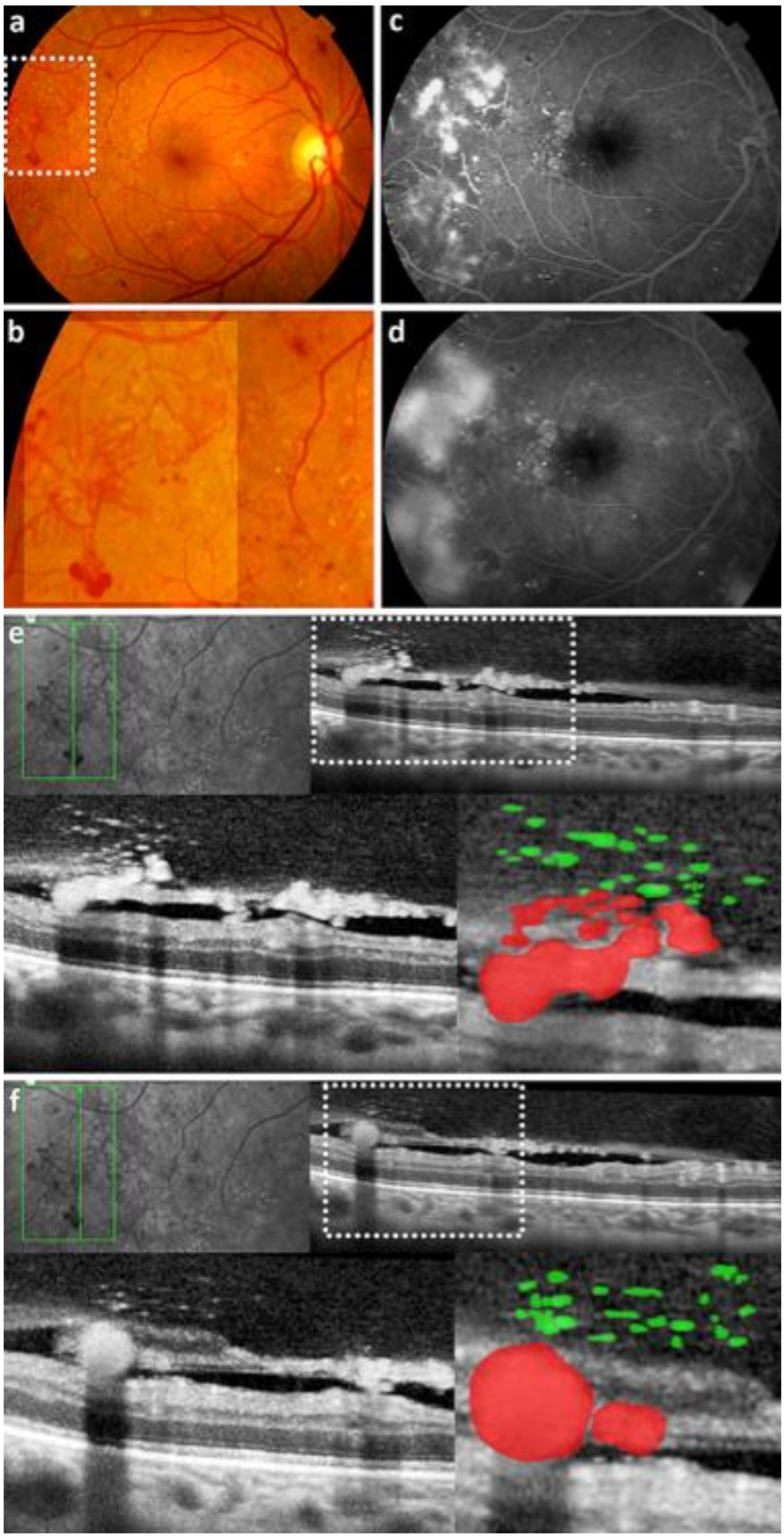
a
c
b
d
e
f

Figure 1.1. Retinal neovascularisation.

(a) Colour fundus photograph of a patient with active neovascularisation elsewhere (NVE). (b) Magnification of the annotated area in 2a showing the NVE in detail. (c) Early phase fluorescein angiogram demonstrating temporal capillary non-perfusion and leakage from the NVE complex, which (d) increased in size and intensity through the study, corresponding to active disease. (e-f) Green horizontal lines represent spectral-domain optical coherence tomography B-scans through the NVE. (e) Depicted area is enlarged and shows a flat NVE complex with vitreous invasion (red) and associated vitreous hyperreflective dots (green). (f) Magnification of the delineated area shows in more detail the dilated tips of the NVE (red) and the hyperreflective dots (green). Figure prepared from my own data.

There is limited evidence regarding the usefulness of SD-OCT for the investigation of the morphologic features of PDR, namely NVD and NVE. Although vitreoretinal changes may be observed when extramacular SD-OCT scans are obtained through new vessels, there have been no studies that address its potential to assess new vessel activity.(32) Identifying SD-OCT derived features of new vessel activity will enable the clinician to more closely monitor patients, and consequently tailor management decisions according to the individual's response to treatment – i.e., during a course of pan-retinal laser photocoagulation, or intravitreal pharmacotherapy. An example of an OCT image of an active neovascular complex is demonstrated in **Figure 1.1**, showing invasion into the vitreous cavity hyperreflective dots above the lesion, which may indicate sub-clinical bleeds into the vitreous cavity or inflammatory cells homing to these sites of neovascularisation.

1.2.2 Macular ischaemia

Diabetic macular ischaemia (DMI) is characterized by disruption to the FAZ, loss of capillaries in the perifoveal and non-contiguous areas of the macula. The presence of DMI is recognised as an important cause of visual loss in diabetic retinopathy, and implicated in poor treatment outcomes in diabetic macular oedema (DMO) and PDR.(24, 33, 34) Furthermore, macular ischaemia has been observed to be a risk factor for the development of PDR, DMO, and a poor visual outcome after vitrectomy.(24, 35, 36) At the present time, there is no effective treatment for DMI,

and consequently, major population studies, and clinical trials for targeting DMO, have not been geared towards identifying macular ischaemia.(5, 37)

The paucity of information evaluating DMI may be explained, in part, by the requirement of an invasive procedure, fluorescein angiography, for its diagnosis. Despite the risk, albeit small, of serious adverse effects, fluorescein angiography is the current gold standard as it allows excellent visualization of the foveal capillary network. The EDTRS first described standardized grading of DMI using angiography; in their system, severity of DMI is assessed on the basis of criteria such as degree of capillary loss, capillary dilatation, the size and outline of the FAZ, perifoveal capillary spacing, and abnormalities of retinal arterioles.(21) Examples of the different DMI severity levels are shown in **Figure 1.2**. The EDTRS study only included a few cases of severe macular ischaemia (2.3% of eyes at baseline), and though limited by a 36% attrition rate, remains as the only large prospective study to grade specifically for DMI. Although some studies have adopted the EDTRS method of DMI grading,(38, 39) many others use only the FAZ area and outline, which has been shown to be a reliable measure of DMI, as a substitute for detailed ETDRS grading.(33, 40) As a result the effects of ischaemia outside the FAZ are often not accounted for.

The clinical significance of DMI is that it confers a poor prognosis in diabetic retinopathy, complicates management decisions of DMO, may impart a poor response to treatment, and most importantly, has effects on visual function. Although previous studies have demonstrated the correlation of macular ischaemia with impaired visual acuity,(41) this relationship is not always straightforward. Morphological changes do not always correspond with functional endpoints and – in many cases – good visual acuity may be maintained even in the presence of seemingly advanced ischaemia.(42, 43)

1.2.3 Retinal choroidopathy

The choroidal circulation forms an integral part of metabolic exchange in the outer retina.(44) This is of particular significance in the macula, due to the lack of retinal

vasculature – the FAZ, and a high metabolic demand from an increased photoreceptor density. Dysfunction of the choroidal circulation has been long implicated in diabetic retinopathy and maculopathy.(45) Since the advent of enhanced depth OCT (EDI-OCT) imaging, allowing non-invasive examination of the choroid in vivo,(46) there has been renewed interest in diabetic choroidopathy as a disease entity.(47-50)

Evidence for diabetic choroidopathy were first noted in histopathological studies, where abnormalities such as arteriosclerosis, choriocapillaris degeneration, focal scarring, and neovascularisation were observed.(51-53) This was followed by indocyanine green angiographic findings in the diabetic choroid, showing hyper- and hypofluorescent spots at the level of the choriocapillaris suggested to represent aneurysms or deficits in the choroidal vasculature.(54, 55)

A number of preliminary studies have used OCT, either EDI-OCT or long-wavelength OCT research prototype systems, to examine the choroid in patients with diabetic retinopathy. These studies have reported a thinner choroid compared to healthy eyes, with an increased disparity in eyes with a greater severity of diabetic retinopathy, the presence of macular oedema, and prior pan-retinal laser photocoagulation.(47-50) However, the thinning observed in eyes of patients with diabetic retinopathy has been described to exceed the magnitude of possible choriocapillaris atrophy in isolation.(47) It is therefore conceivable that choroidal vascular changes observed in patients with diabetes occur not only in the choriocapillaris, but also within its medium (Sattler's) and large (Haller's) vessel layers. To date, analysis of these choroidal vascular sublayers using OCT has been restricted to small studies using long wavelength OCT in normal subjects.(56, 57)

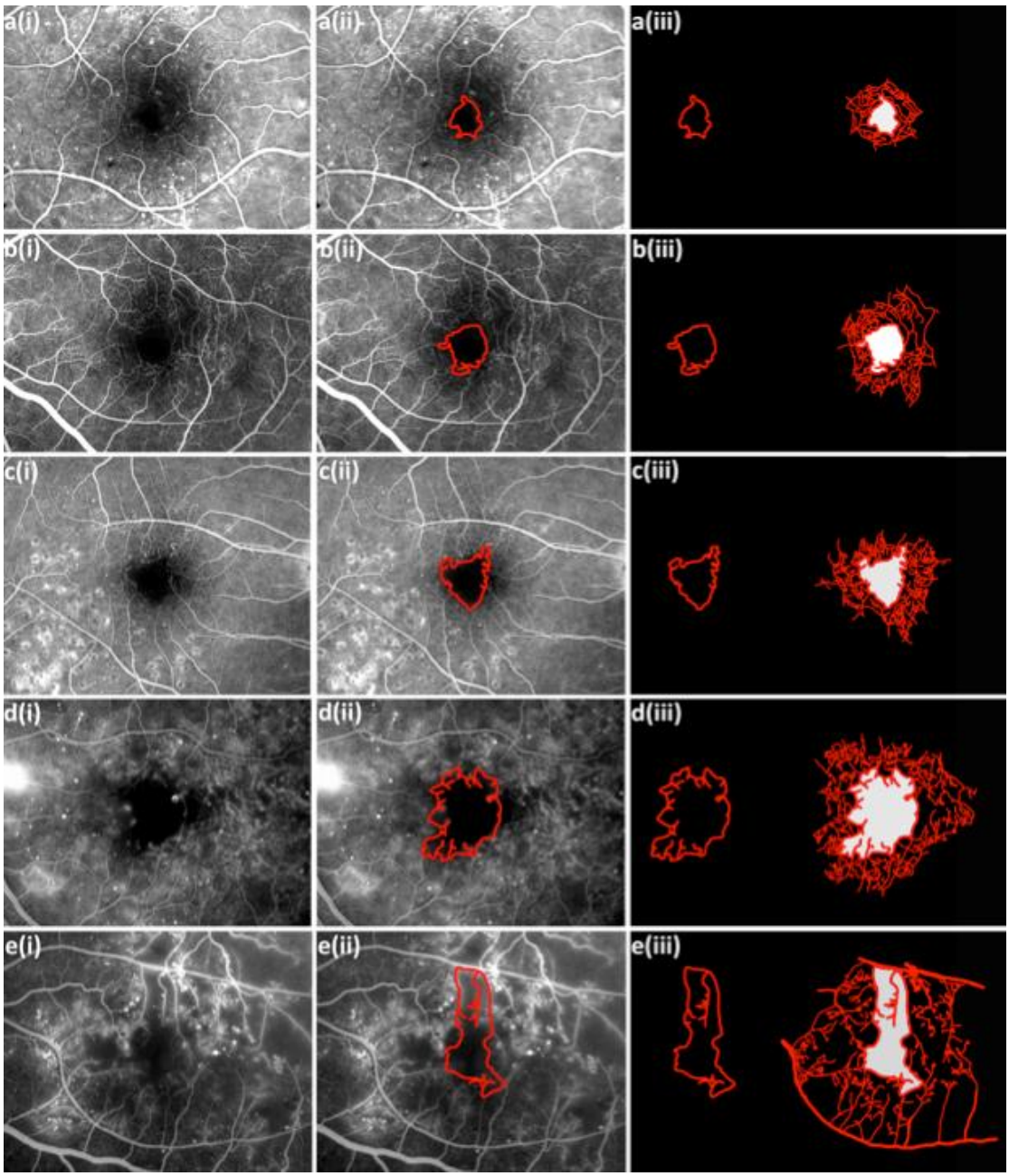

Figure 1.2. Diabetic macular ischaemia severity grades.

(i) Examples of an early phase fundus fluorescein angiogram demonstrating (a) none, (b) questionable, (c) mild, (d) moderate, and (e) severe diabetic macular ischaemia. (ii) Annotated fluorescein angiogram, with the foveal avascular zone outlined in red. (iii) The foveal avascular zone outline alone on the left (red), and on the right, the foveal avascular zone area (white), and perifoveal vasculature (red). Figure prepared from my own data.

1.3 Cellular mediators in diabetic retinopathy

In adults, neovascularisation – the growth of new blood vessels – is typically thought to occur via "angiogenesis" (i.e. by the proliferation, migration, and remodelling of fully differentiated endothelial cells in existing vascular networks).(58) However, since 1997, circulating endothelial progenitor cells (EPCs) have been found to contribute to this process – a form of "vasculogenesis" (the formation of blood vessels from individually migrating precursor cells), previously only described in the embryo.(59) Since this seminal finding, EPCs have been used to promote tissue vascularisation in a number of non-ocular models,(60) and the therapeutic opportunity they present, for patients with diabetic retinopathy, has been recognised.(61) A number of studies have demonstrated evidence of EPC dysfunction in patients with diabetes mellitus;(62-64) There are fewer EPCs in peripheral blood in patients with diabetes compared with healthy subjects and diabetic EPCs exhibit impaired mobilisation from the bone marrow, impaired migratory response to chemokines, proliferation, adhesion and deformability.(62-65)

Diabetic retinopathy is a phenotypically heterogeneous disorder and the association between EPC number/function and each disease subtype is not yet known.(61) Therefore, as a first step in the application of EPCs for the treatment of diabetic retinopathy, characterisation of EPCs in each diabetic retinopathy subgroup is required. The knowledge acquired from such characterisation may provide useful prognostic information for these patients, as well as guiding the development of translational cellular therapies.

1.3.1 Endothelial progenitor cells (EPCs)

The EPC was first isolated in in human peripheral blood by Asahara et al using cell surface markers CD34 and vascular endothelial growth factor receptor (VEGFR2).(59) They observed that these cells were able to differentiate in to mature endothelial cells in culture, form vascular structures, and incorporate into sites of active angiogenesis restoring vascular integrity.(66, 67) EPCs are found mainly in the adult

bone marrow. In the peripheral circulation, these cells are relatively rare at 0.01% of peripheral blood mononuclear cells (PBMCs).(61, 66) However, their numbers increase in response to injury; such as inflammation or ischaemia where they are recruited to sites requiring vascular repair.(68)

EPCs have been previously defined by their surface markers and behaviour in culture. In its initial discovery, CD34+ and VEGFR2+ hematopoietic progenitor cells were shown to differentiate to an endothelial phenotype. However, CD34 is not exclusively expressed on haematopoietic stem cells but also on mature endothelial cells. CD133, an immature haematopoietic stem cell marker, was used to distinguish between the two.(69) There is also evidence showing that CD14+ myeloid cells are capable of transdifferentiating along the endothelial cell lineage, and can participate in the formation of new vessels in vivo.(69-74) Controversy remains, with respect to the identification and origin of EPCs from peripheral blood mononuclear cells. Putative sources that have been suggested include (1) hematopoietic stem cells, (2) myeloid cells and (3) circulating mature endothelial cells. (75, 76)

Controversy regarding the potential identity and origin of the EPC are further muddied by its progeny; the heterogeneous nature of the vascular endothelium is exemplified not only by its behaviour in health and disease, but also its variability in gene expression, morphology and function according to its location within the circulatory system.(77) However, such diversity is key to the specialised role of its function. In particular, the microvascular endothelium, among its many roles, regulates fluid and nutrient transport and acts as a gatekeeper for inflammation, adapting to local fluctuations in metabolism.(78) In diabetes, endothelial dysfunction and early senescence have been demonstrated in response to hyperglycaemic conditions (79), with impaired nitric oxide production(80) and increased circulating apoptotic microparticles found in the circulation of these patients.(81) The reparative function of the endothelium has also been shown to be impaired in diabetes. EPCs in diabetes have been observed to have impaired mobilization, migration, and homing to sites of injury.(82) In culture, a decreased proliferative capacity and shorten survival have been further observed.(82) Defects in intracellular signalling, a response

to inflammation, reactive oxygen species, and insulin have all been implicated.(83, 84)

EPCs have been reported to be reduced in numbers in newly diagnosed type 2 diabetes, with a partial recovery during the intervening years, before a dramatic reduction at 20 years after diagnosis.(85) Functional impairment of EPCs have also been associated with its affiliated complications. In animal models of critical limb ischaemia, collateralisation of vessels was enhanced by EPCs from control but not diabetic animals.(86) In diabetic kidney disease, renal transplantation has been shown to improve EPC function (in vitro migration and adhesion) but paradoxically decreased its numbers.(87) In diabetic neuropathy, intramuscular administration of EPCs has been shown to reverse impairment of sciatic nerve conduction velocity and blood flow in diabetic rats.(88) This was similarly observed in streptozotocin-induced diabetic mice after hind-limb injection of EPCs.(89) Interestingly, portions of injected EPCs were localised to the vasa nervorum suggesting that EPCs may reverse the effects of diabetic neuropathy. In fact, bone marrow neuropathy itself (in a rat model of type 2 diabetes), has been found to be a cause for the reduction of bone marrow release of EPCs.(90) Interestingly, these changes were observed prior to the development of diabetic retinopathy in this model.

In diabetic eye disease, EPCs have been observed in both type 1 and type 2 diabetes to be reduced in number but have a higher clonogenic potential and an enhanced ability to differentiate into mature endothelial cells in culture.(91, 92) It has been suggested that this may, in part, explain the paradoxical “hyperactive” pathological angiogenesis that occurs in proliferative diabetic retinopathy, which occurs when there is profound areas of retinal ischaemia. In proliferative diabetic retinopathy, these aberrant new vessels display characteristics of “poorly-made’ vasculature; leaking, growing into the avascular vitreous, prone to fibrosis with consequent contraction that applies unwanted tractional forces which wrinkle, tear and detach the neural retina. Evidence from patients with type 1 diabetes, indicates that it may be a stage-related regulation of EPCs that occurs with duration of diabetes that plays a role in this phenomena. Reduced numbers of EPCs were

observed in patients with mild and moderate non-proliferative diabetic retinopathy, whereas “mature” EPCs which co-expressed CD34 and CD31 were dramatically increased in proliferative disease.(93) Indeed, these “mature” EPCs may have a causative role in the generation of aberrant new vessels, and reflect a phenotypic shift in patients who develop proliferative diabetic retinopathy. However, they may just as likely be a consequence of “abnormal” EPCs, either produced by the bone marrow or as a result of shedding from the neovascular complexes themselves. There are no studies that examine the relationship between EPCs and diabetic maculopathy.

1.3.2 Circulatory Monocytes

Under prolonged ischaemia, large numbers of circulating monocytes are attracted to sites of injury. The biological goal of this response is to promote healing of damaged tissue by removal of dead cells, aid in the replacement of necrotic areas by connective tissue (fibrosis), and ultimately restore vascularisation at a microcirculatory level. Circulating monocytes and their tissue decedents, macrophages, produce a myriad of cytokines to orchestrate this repair process. This has been observed in various conditions where tissues/organs are exposed to periods of prolonged ischaemia; myocardial infarction, stroke, critical limb ischaemia, and chronic renal disease.(94-97) In the retina, leukocytes have been long implicated in the pathogenesis of diabetic retinopathy. (98) More specifically, targeted suppression of circulating monocytes with clodronate liposomes has been observed to suppress pathological neovascularisation in rat models of proliferative retinopathy. (99) This suggests that alterations in monocyte profiles in diabetes may not only play a role in the pathogenesis of diabetic eye disease, but also differentially steer individual eyes toward divergent phenotypic manifestations of diabetic retinal or macular disease.

Monocytes populations show a great diversity within the circulation; in their proportions, cytokines secreted, and role they play in an inflammatory response. Presently, subsets of the monocyte population are defined by their differential

expression of CD14 (lipopolysaccharide receptor) and CD16 (Fc receptor). The major subset (~85%) is "classical monocyte" (also known as M2), which expresses CD14++ CD16- and produce large amounts of proinflammatory cytokines such as interleukin (IL)-1, IL-6, reactive oxygen species (ROS), prostaglandin E_2, and plasminogen activator.(100, 101) The 2nd most common subset (~15%) is the "non-classical monocytes" (also known as M1), which express CD14low CD16+. These cells exhibit potent antigen-presenting capacity and produces interferon-α, tumour necrosis factor, and IL-12.(102) The smallest subset (<5%) is the "intermediate monocyte" (iM), which express CD14+ CD16+. It is unknown if intermediate monocytes have a discrete biological role or whether they are an "intermediate", as the name suggests, in the journey of transition from classical to non-classical monocytes.(103) It has been observed that intermediate monocytes are increased in different disease states, such as rheumatoid arthritis, severe asthma, and sarcoidosis.(104-106) Interestingly, they are increased by intense physical activity, but found in lower percentages in physically active individuals.(107, 108)

In diabetes, phenotypes of circulating immune cells have been observed to occur in distinct frequencies in type 1 and type 2 disease, and monocytes in particular have been positively correlated with age, body mass index and insulin sensitivity.(109) Flow cytometric analysis have further shown that proportions of monocyte subsets differ in patients with type 1 diabetes compared with healthy controls, with significantly higher classical and non-classical subsets.(110) Both intermediate and non-classical subsets have also been observed to be predictive of the development of diabetic retinopathy in these patients.(110) Conversely, Fadini et al did not observe any difference in monocyte subsets in patients with type 2 diabetes compared to controls.(111) However, a trend towards a decrease in classical monocytes was observed in patients with nephropathy or retinopathy. When the authors compared the ratio of non-classical to classical monocytes (M1/M2 ratio) a significant difference was observed with macroangiopathy but not microangiopathy. To the author's knowledge, there are no studies that examine monocyte profiles in patients with different phenotypic manifestations of diabetic eye disease.

1.3.3 Implications for the clinical management of DR

Diabetic retinopathy, a microvascular complication of diabetes mellitus, is the leading cause of blindness among people of working-age in the United Kingdom.(112) Diabetic retinopathy is a vasodegenerative disorder in which the sequence of pathologic changes has been well established: progressive dysfunction and death of the endothelial cells and pericytes is followed by vascular occlusion and ischaemia, with subsequent ischaemia-related events such as vascular leakage and/or retinal neovascularisation.(113) While both endothelial cells and pericytes undergo premature death in diabetic retinopathy, there is some evidence to suggest that the endothelium has a capacity for replication and repair, at least in the short-term.(114) Despite these findings, the balance of experimental and clinical evidence suggests that reparative neovascular processes in patients with diabetic retinopathy are limited – contrary to its perception as a pro-neovascular disorder, the proliferative phase of diabetic retinopathy only develops after long periods of ischaemia occurring in the context of impaired or absent vascular repair and remodelling.(115) In contrast, microvascular repair and remodelling is a notable feature of other ischaemic retinopathies such as retinal venous occlusion.(61) Thus, if reparative neovascularisation can be harnessed appropriately, the potential exists to contain or reverse the ischaemia that drives macular oedema and pathologic retinal neovascularisation in patients with diabetic retinopathy.

It is widely accepted that neovascularisation occurs in 2 ways: angiogenesis, a process where new blood vessels form by the remodelling of fully differentiated endothelial cells in existing vascular networks (58), and vasculogenesis, which involves de novo formation of blood vessels (primarily during embryogenesis) from migrating precursor cells.(116) The discovery that in some instances these precursor cells may be derived from the adult bone marrow (59) presents a number of diagnostic and therapeutic opportunities; in particular, EPCs may have the ability to act as circulating biomarkers for disease onset and progression, as well as acting as promoters of reparative neovascularisation.(61)

Pioneering preclinical and clinical studies have shown that administration of EPCs can restore tissue vascularisation after ischaemic events in other parts of the body e.g. ischaemic limbs.(60) Thus, EPCs could conceivably fulfil a similar role in patients with diabetic retinopathy. However, a number of studies have shown that patients with diabetes mellitus have fewer numbers of circulating EPCs, with decreased function, relative to age-matched healthy controls.(62-64) These findings are consistent with the known impairment of reparative neovascular processes in patients with diabetic retinopathy.(115) However, diabetic retinopathy is a structurally heterogeneous disorder and the association between each disease subtype, and EPC number/dysfunction, is not yet known. Characterisation of EPCs in this manner thus represents a vital first step for their potential therapeutic application in this disease.

Although there are no studies that have assessed the use of monocytes in diabetic retinopathy as a means for cell replacement therapy, multiple independent groups have demonstrated that CD14+ monocytes are integral to the efficacy of bone marrow or cord blood transplantation in regenerative medicine.(117) Mononuclear fractions of cord blood depleted of CD14+ monocytes have shown a reduced therapeutic value in a rat stroke model. In addition, the value of CD14+ monocytes did not depend on its source as interchangeable results were obtained with cells derived from peripheral blood. Similar results have been observed in hind limb ischaemia models with both human peripheral and mouse bone marrow derived monocytes.(118) The therapeutic value of monocytes has been increasing recognised over the past decade with some in the field postulating that there is more evidence for the therapeutic value of mature cells (monocytes) than stem cells.(119) A paradigm shift in regenerative medicine has moved in the direction of endogenous tissue repair by controlling host inflammatory pathways. However, this development has been largely confined to research in inflammatory and autoimmune diseases and has not been fully explored in predominantly microvascular diseases such as diabetic eye disease. Arguably, there is sufficient preliminary evidence and scope to consider the CD14+ monocyte as a potential candidate for cell therapy.

1.3.4 The effects of lipid-lowering therapy

It is well accepted that dyslipidaemia increases the risk of retinopathy and its progression.(120, 121) However, findings from large randomized controlled trials have not been consistent. For example, the Collaborative Atorvastatin Diabetes Study (CARDS) (n=2830) failed to observe the reduction of progression of retinopathy in patients with type 2 diabetes.(122) In contrast, the FIELD Study, which compared fenofibrate and placebo in stain-naïve patients with type 2 diabetes (n=9795) observed that in 5 years, patients on fenofibrate required less laser or retinopathy or maculopathy (3.6% versus 5.2%).(123) Furthermore, post-hoc analysis of the FIELD Study (n=1012) found a reduced incidence of 2-step progression of retinopathy (by ETDRS criteria), but only in those with retinopathy prior to trial enrolment (3.1% versus 14.6%).(124) The ACCORD trial (n=2856), where all patients were on open-label simvastatin, similarly observed a reduced in progression of diabetic retinopathy.(125) Of note, the reduction obtained with fenofibrate combined with simvastatin was 40%, higher than the 33% reduction obtained in the intensive glycaemic control arm. This highlights the importance of consideration of statin therapy when studying patients with diabetic retinopathy.

Fenofibrate if a peroxisome proliferactor- activated receptor (PPAR)- α that is indicated for the treatment of hypertriglyceridemia and mixed lipidaemia. In addition to its main action fenofibrate has other non-lipid medicated mechanisms by which it could be effective in slowing the progression of diabetic retinopathy. This includes effects on endothelial cell apoptosis(126), angiogenesis (127), and its antioxidant and anti-inflammatory activity.(128-130) Of relevance to this thesis, fenofibrate has further been shown to alter gene transcription of apolipoprotein A1, a potent scavenger of reactive oxygen species in macrophages and fibroblasts in the liver.(131)

1.4 Why should we study cellular mediators in DR?

It is well known that the process of neovascularisation occurs as a result of elevated vascular endothelial growth factor (VEGF) levels in the eye. More recently, the role of inflammation in the pathogenesis of diabetic retinopathy has gained wider acceptance. Elevated levels of inflammatory cytokines such as IL-4, IL-6, IL-8, IL17A, MCP-1, and tumour necrosis factor (TNF)α have been observed in vitreous samples from eyes with proliferative diabetic retinopathy compared to controls, along with raised circulating inflammatory biomarkers in these patients.(132-134) Furthermore, there is evidence to suggest that elevated levels of macrophage colony-stimulating factor (M-CSF) and IL-13, which are elevated in vitreous samples of patients with proliferative diabetic retinopathy, may result in M2 polarisation of macrophages.(135) A recent proof-of-concept clinical trial has observed that the use of a low-dose oral anti-inflammatory agent, doxycycline, has shown promising results in improvement of retinal function in eyes with severe nonproliferative, and proliferative diabetic retinopathy. (136) These suggest that cellular mediators play a large role in both severity and the phenotypic manifestation of diabetic eye disease. A greater understanding of the part inflammation play may aid in tailoring treatment regimes (steroid therapy, laser, anti-VEGF therapy or a combinations of these) to individual patients. The implications of which will have long-term consequences, both to the patients' visual function, as well as quality of life.

1.5 Thesis Hypothesis

Effective biomarker research has increasingly become one of the cornerstones of early drug development in order to identify optimal biological doses for treatment. In fact, imaging-based biomarkers have also been applied to other fields such as cardiology and oncology to understand mechanisms of disease and predict outcomes of novel therapy. This thesis hypothesizes that the synergistic use of state-of-the-art retinal imaging techniques to visualise the eye and its associated blood vessels, combined with putative cellular mediators of diabetic retinopathy; EPCs and

monocytes, will make a powerful biomarker for the identification, definition, and prognosis of diabetic eye disease.

1.6 Thesis Aims

Recent research has shown that diabetes can affect both EPCs and monocytes with significant overlap between both cell types. The relationships between these cells and the phenotypic manifestations of diabetic eye disease are less well known. This project aims to firstly, characterise a clinical phenotype of diabetic eye disease- diabetic macular ischaemia, for which no therapy is currently available, as it is likely to represent a cohort of patients who would be suitable for replacement cell therapy. Secondly, novel methods for monitoring inflammation were investigated in the retinae of both animal models and humans, in an attempt to develop quantitative outcome measures that may be applicable to a clinical trial. And finally, examine the characteristics of EPCs and circulating monocytes in different diabetic eye disease phenotypes in order to identify if relationships exists between these entities. Overall this work may contribute, in the near future, to the development of a suitable cell replacement therapy in diabetic eye disease.

1. To elucidate the natural history of diabetic macular ischaemia, for which there is no existing therapy. Understanding the natural progression of disease will be important as patients with diabetic macular ischaemia may be ideal candidates for regenerative therapy in the future.

2. To validate methods of retinal image analysis; which will be used for the characterisation of diabetic macular ischaemia.

3. To explore different imaging techniques of measuring inflammation in the retina.

4. To profile circulating endothelial progenitor cells and monocytes of patients with diabetic eye disease and explore their relationships with retinal disease phenotype.

2. Clinical Imaging in diabetic macular ischaemia

2.1 Introduction:

DMI was first established using fluorescein angiography (FA) in the ETDRS.(21, 43, 137) Due to the requirement of angiography for its evaluation, DMI has not been studied in the pivotal epidemiological studies of diabetic retinopathy, and is consequently not well understood.(9, 138, 139) Increasing our understanding of how quickly DMI progresses, in whom it occurs, and its association with visual impairment, is important in the clinical management of diabetic maculopathy. This may be of particular relevance due to emerging evidence for intravitreal pharmacotherapies, such as anti-VEGF for the treatment of diabetic macular oedema (DMO).(37, 140, 141)

In type 1 diabetes, the role of peripheral ischaemia and consequent proliferative diabetic retinopathy, has been long established. Proliferative diabetic retinopathy occurs in approximately 50% of patients with Type 1 as compared to 15% in those with Type 2 diabetes.(4) Similarly, in adolescents, the prevalence and severity of all retinopathy has been reported to be higher in Type 1 compared to Type 2 diabetes, with a relatively high cumulative rate of progression to proliferative disease- 42% after 25 years.(142, 143) DMO, which affects 6.8% of all patients with diabetes, has also been reported to affect a greater proportion of those with Type 1 diabetes (14% in Type 1, compared to 6% in Type 2).(144, 145) The prevalence and severity of macular ischaemia in Type 1 diabetes, however, is less clear.

The distinction between Type 1 and Type 2 diabetes has become blurred in recent years with the increasing waistlines of the Western world. Although both syndromes share common metabolic pathways characterised by hyperglycaemia, their classification remains distinct and defined by their pathophysiology, such as the lack of insulin production in Type 1, and insulin resistance in Type 2. There is limited evidence regarding macular ischaemia in Type 1 diabetes. Although it has been reported to occur sooner after diagnosis in Type 2 compared to Type 1 disease, it is well known that the duration of disease in patients with Type 2 diabetes can be difficult to pinpoint, and patients can be diagnosed many years after the onset of

disease. In Type 1 diabetes, it is not known whether there is similar, greater, or a reduced propensity for macular ischaemia, compared to its counterpart- peripheral ischaemia.

Increasing our understanding of how quickly DMI progresses, in whom it occurs, and its association with visual impairment, is important in the clinical management of diabetic maculopathy. The ongoing controversy regarding the potential adverse effects of anti-VEGF therapies on macular ischaemia, is largely based on case reports, and non-comparative cases series - in patients receiving treatment for DME,(33, 146, 147) as an adjunctive treatment with pars plana vitrectomy in diabetic retinopathy,(148) and in eyes treated for exudative age-related macular degeneration (AMD).(149, 150) These studies report that in the presence of macular ischaemia, there is an adverse effect on outcomes, or a limit to the benefits of treatments, however, the deleterious effects of these intravitreal treatments on DMI is far from clear. Firstly, larger prospective studies, such as the RESTORE, RISE/RIDE, and the DRCR net studies, did not address the potential effects of anti-VEGF therapy on ischaemia.[37, 140, 141] Secondly, the BOLT study, the only prospective study which examined macular perfusion, found no clear associations between intravitreal injections of bevacizumab and DMI at 4 months.(39) A recent analysis of eyes with retinal vein occlusions, suggests that VEGF blockade with ranibizumab prevents worsening of “retinal nonperfusion”.(151)

It is not known if, or how quickly DMI progresses. Addressing the shortcomings in our knowledge of “DMI progression” is likely to be of critical importance for a number of reasons. Firstly, the identification of those patients who are likely to progress may have considerable implications in those in a working age group. Secondly, it would aid in discerning between DMI progression, due to the natural history of the disease itself, from the effects of treatments received, and may prevent the unnecessary exclusion of patients, or untimely cessation of therapy.

Diabetic retinopathy encompasses a group of predominantly vascular anomalies which if left untreated, ultimately results in visual loss. The overall global prevalence of any diabetic retinopathy is 34.6%, with up to 28 million persons

worldwide with vision-threatening diabetic retinopathy.(152) Broadly, the spectrum of disease has been classified according the behaviour of the retinal vasculature- (1) hyperperfusion (leakage and oedema), which results in the development of lesions such as macular oedema, peripheral hard exudates and microaneurysms, and (2) hypoperfusion (ischaemia), which results in enlargement of the foveal avascular zone (FAZ) in the macula, and capillary non perfusion and retinal neovascularisation in the retinal periphery.

It is not known what causes the differential regional distribution of these vascular lesions (i.e. peripheral compared central retina), why they occur in some patients but not others, and how they might affect visual function. Epidemiological studies have suggested that age may be a key component to the different patterns of diabetic retinopathy observed; i.e. the predominance of macular oedema in older patients with type 2, and proliferative retinopathy in younger patients with type 1 diabetes.(153, 154) Several possible mechanisms have been suggested, including, the loss of autoregulation in retinal arterioles and microvascular degeneration in older persons causing capillary leakage and consequent macular oedema, and in the younger age group, an intact posterior hyaloid acting as a scaffold for the formation of aberrant neovascularisation.(155, 156) However, the pathobiology of diabetic retinopathy remains unclear, and is unlikely that age alone is solely responsible.

The advent of ultra widefield fluorescein angiography (uwFA) has provided for the first time, the opportunity to visualize both the central and peripheral retina in a single examination. Although widefield imaging of the retina has been in development over the past eighty years, older systems encountered obstacles which precluded its wide application in patients with diabetic retinopathy; such as the requirement of a contact lens, and clear ocular media for the acquisition of good peripheral images.(157, 158) In recent times, the Optos camera (Optos PLC, Dunfermline, UK) has incorporated both a scanning laser ophthalmoscope (which permits imaging through moderate media opacities), and an optical systemic with an ellipsoid mirror which allows reliable imaging of the peripheral retina up to the ora serrata.(159) This provides visualization of up to 200 degrees, compared to the 75

degrees achieved by piecing together the early treatment diabetic retinopathy study (ETDRS) 7-standard fields, taken using the traditional 50 degree-view digital fundus camera. As such, the logical next step was to investigate the applicability fluorescein angiography, superior to colour photography in detecting vascular lesions, to ultra widefield imaging. Several studies have already demonstrated, in diabetic eyes, a greater detection (compared to conventional fluorescein angiography) of peripheral lesions such as areas of capillary non perfusion, leakage, and.(160-164) Therefore, the development of uwFA offers the opportunity to examine, in the diabetic eye, the relationships between both peripheral and central vascular lesions, and may provide new insights into the pathophysiology behind the differential patterns of distribution of diabetic retinopathy lesions observed in patients.

Although the visual importance of macular ischemia was established by a number of seminal fluorescein angiographic studies in the 1970s, many clinical questions remain unclear.(165-167) In particular, the appearance or consequences of macular ischemia on OCT imaging remains ill defined – a significant shortcoming given the widespread adoption of OCT for monitoring of treatment in clinical trials of diabetic retinopathy. A number of preliminary studies have suggested severe macular ischemia is associated with thinning and disorganization of retinal layers on OCT.(28, 168, 169) In the bulk of OCT studies in diabetic retinopathy, however, the effects of macular ischemia are masked by coexisting macular oedema. It is perhaps not surprising then, that only modest correlations have been observed to date, between OCT-derived retinal thickness and visual acuity in these studies.(28, 170) Fortunately however, recent advances in OCT imaging offer the opportunity to more precisely characterize diabetic macular ischemia morphology using OCT. In particular, analysis of OCT image sets has become more sophisticated in recent years, with a move from simple measurements of retinal thickness to more detailed quantitative subanalysis of individual retinal layers and specific disease features.(171) In addition, the formulation of “enhanced depth imaging” scanning protocols now allows high-resolution visualization of choroidal anatomy using the current generation of commercial OCT systems.(46)

In this chapter, the relationships between macular ischaemia, retinopathy severity, presence of concurrent macular oedema, age of patients, and visual function, in an effort to determine its prevalence and clinical significance in this cohort of patients. The impact of macular ischaemia, both in the central macula and paramacular areas, on visual function in patients with both type 1 and type 2 diabetes mellitus are examined. Furthermore, in-depth, longitudinal qualitative and quantitative analyses of the rate of progression for macular ischaemia was performed. The clinical features at the baseline FA which may predict progression are examined in an effort to identify parameters of interest for both clinical practice and future clinical trials using qualitative and quantitative analyses of capillary non-perfusion and leakage, both in the central and peripheral retina. Finally, the relationships between these parameters and OCT-derived measurements of retinal thickness and visual acuity were analysed, in an effort to elucidate its clinical significance.

2.2 Aim:

To investigate the prevalence, natural history, and relationships of diabetic retinopathy, and its impact on retinal structure and function through the analysis of clinical retinal images in order to identify imaging biomarkers for diabetic eye disease.

2.3 Materials and Methods:

Institutional Review Board (IRB)/Ethics Committee approval for data collection and analysis at the UCL Institute of Ophthalmology and Moorfields Eye Hospital, London was in place.

Technical acknowledgements: I would like to thank Srinvas Sadda, Doheny Eye Institute, University of Southern California, Los Angeles, United States, for the provision of custom written software OCTOR and GRADOR for the analysis of clinical images used in this chapter, and also Gerald Liew, Center for Vision Research, Westmead Millenium Institute, University of Sydney, Sydney, Australia, for the provision of a validated, semi-automated software for the grading of retinal vessel calibre.

2.3.1 Inclusion Criteria and Data Collection

Clinical and imaging data were collected retrospectively from patients attending a single consultant-led medical retinal clinic, with a focus on diabetic eye disease, at Moorfields Eye Hospital, London, United Kingdom. All data were collected over a six-month time period (December 1st 2010 to June 30th 2011).

Patient demographic data, visual acuities, and retinopathy/maculopathy grades, were obtained from standardized electronic reports in the United Kingdom National Screening Committee (UK NSC) - Diabetic Eye Screening Programme. Patient age at time of attendance, and presence of ocular co-morbidity, were obtained from electronic patient records. Patients attending the clinic with a diagnosis of Type 2 diabetes mellitus were included (patients with Type 1 diabetes mellitus are being analysed in a separate study). Patients with ocular comorbidities, including retinal arterial or venous occlusion, epiretinal membrane, neovascular age-related macular degeneration (AMD), inherited macular disease, or macular scarring of any etiology, were excluded.

In most cases, FA and OCT images were obtained on the date of attendance in the clinic; however, patients were also included in the study if angiography had been performed within six months of the study attendance date. In patients with bilateral

disease of symmetrical severity, a single eye was selected using permuted-block randomization for inclusion in the study. In patients with bilateral asymmetrical disease, the eye with the greatest degree of ischemic maculopathy was selected. For inclusion in the study, all angiographic image sets had to be of sufficient quality to allow visualization of FAZ capillaries to allow grading of DMI severity.

For the purpose for DMI progression analysis, FAs were graded according to ETDRS protocols (see below) and eyes with ETDRS DMI grades "mild", "moderate" or "severe", and at least two macular centred FA images, separated by a minimum interval of 6 months were identified. Patients with a definite presence of DMI – i.e. those with "mild", "moderate" or "severe" ETDRS DMI grades were included, in order to assess the rate of progression and associations of this clinical entity.

2.3.2 Fluorescein Angiography

Grading methods for macular ischaemia: All angiographic images were acquired with a digital retinal camera system (Topcon TRC 50IX, Topcon Medical Systems Inc., Paramus, NJ). One early to mid-phase image (at 20-40 seconds), centred on the macula, was chosen for analysis (at later phases, fluorescence abnormalities commonly impair visualization of the retinal capillary network) **(Figure 2.1).** The FA images were chosen for optimal focus and intensity levels, which allowed visualisation of macular capillaries. No image manipulation was performed prior to grading. Macular ischaemia was dual-graded by two masked assessors using protocols and standard photographs from ETDRS Report No. 11 in which severity is determined by FAZ size, capillary loss or dilatation, and retinal arteriolar abnormalities.(21) According to these criteria, DMI was classified as none, questionable, mild, moderate, or severe. In the case of disagreement between graders, open adjudication was used to resolve the final grading decision.

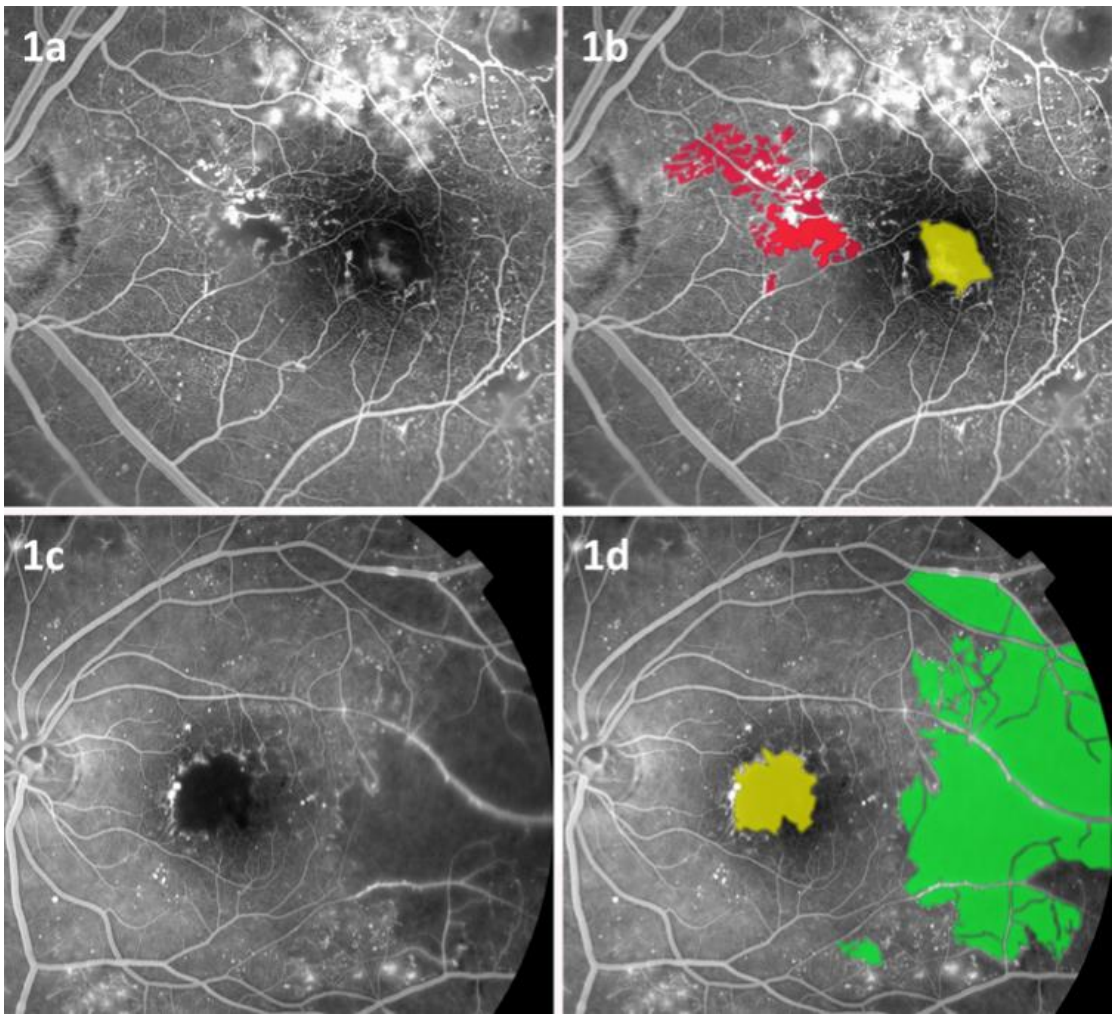

Figure 2.1. Papillomacular and temporal ischaemia

(a) An example of an early phase Fundus Fluorescein Angiography (FA) image centred at the macula demonstrating papillomacular capillary dropout, non-contiguous with the foveal avascular zone (FAZ). (b) Annotated image of 1a with papillomacular ischaemia highlighted in red and the enlarged FAZ highlighted in yellow. (c) An example of an early phase FA image demonstrating temporal capillary dropout non-contiguous with the FAZ. (d) Annotated image of 1c with temporal ischaemia highlighted in green and the enlarged FAZ highlighted in yellow.

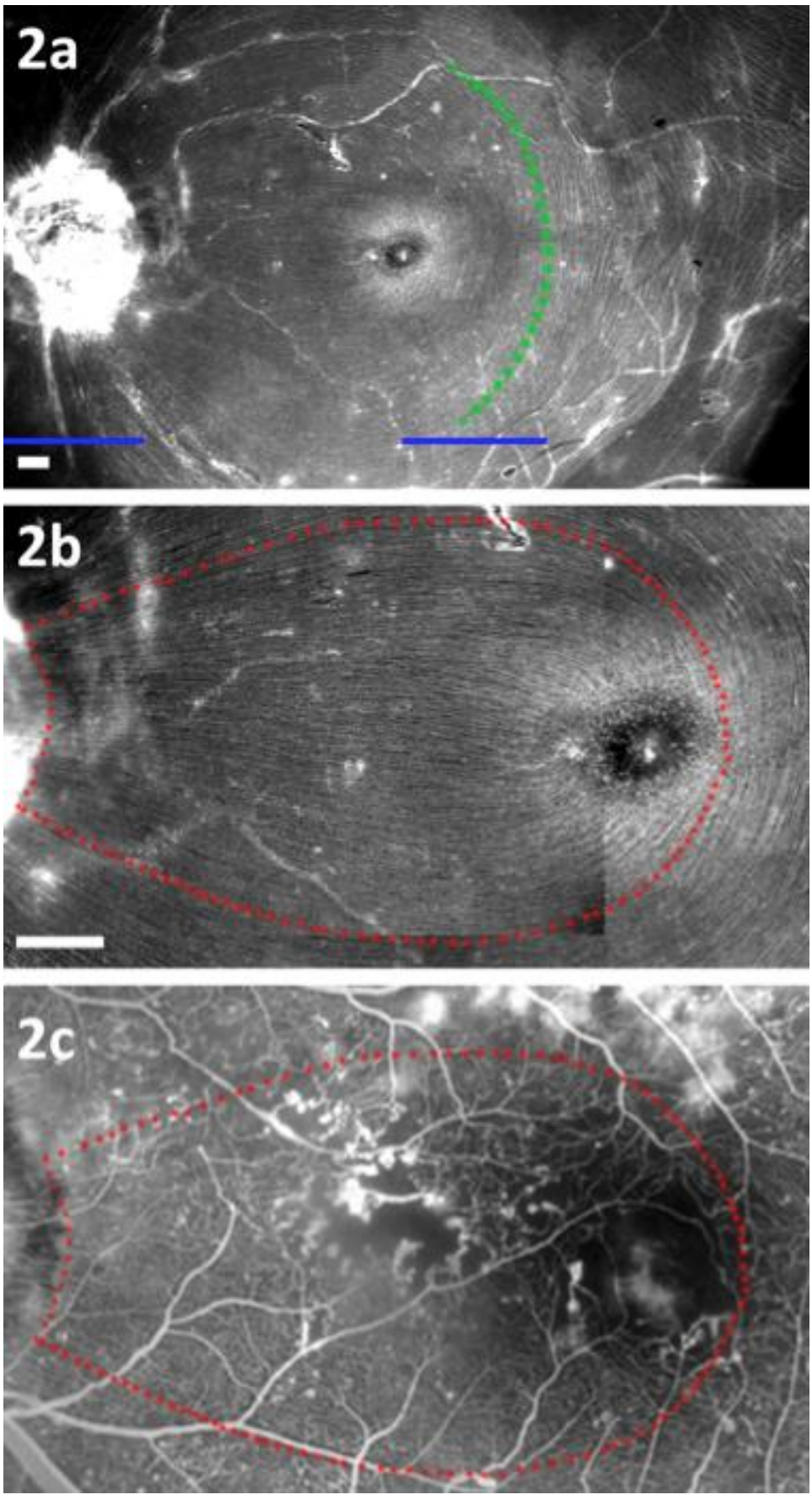
2a
2b
2c

Figure 2.2. Definition of the papillomacular and temporal areas for ischaemia quantification.

a) Tubulin beta III immunostaining of the retinal nerve fibre layer in postmortem human eye tissue. After fixation in 4% paraformaldehyde for 24 hours, the retina was dissected and whole mounted for immunohistochemistry. The dotted green line delineates the boundary for temporal ischaemia, located one disc diameter temporal to the central fovea. Solid blue lines represent one disc diameter. Solid white scale bars equal to 0.5mm. (b) The dotted red line delineates the boundary for the papillomacular area where increased density of nerve fibres/axons originating from the FAZ are located. Solid white scale bars equal to 0.5mm. (c) Overlay of equivalent papillomacular boundary onto FA depicting areas of capillary dropout. (Immunohistochemistry images from figures 2a, and 2b were kindly provided by Dr Michael Powner)

Grading methods for temporal and papillomacular ischaemia: The presence of additional areas of capillary non-perfusion, non-contiguous with the FAZ, was also noted at the time of grading, "Papillomacular ischaemia" was defined by its location within the nasal quadrant of the ETDRS grid and/or the area of retina bordered by the temporal edge of the optic disc and the nasal edge of the FAZ, along the papillomacular nerve fibre raphe **(Figure 2.2).** "Temporal ischaemia" was defined as the area located one disc diameter temporal to the central fovea and within the superior and inferior temporal vascular arcades.

2.3.3 Optical Coherence Tomography

Grading Methods: Spectral domain OCT images were obtained using the Spectralis imaging system (Heidelberg Engineering, Germany). All OCT image sets contained a minimum of 13 B-scans distributed in a horizontal raster pattern overlying the area covered by the nine subfields of the Early Treatment Diabetic Retinopathy Study (ETDRS) grid. Custom image analysis software (OCTOR, Doheny Image Reading Center, Los Angeles) was used for quantitative analysis of OCT image sets. OCTOR has been described and validated in previous reports.(172, 173)

2.3.4 Ultra Widefield Imaging

All uwFA images were acquired with the Optos C200 MA ultra widefield retinal imaging system (Optos PLC, Scotland, United Kingdom), which allows imaging of up to 200 degrees (82%) of the retina in a single image. All patients received a standard infusion of 5 millilitres of 20% sodium fluorescein through the antecubital vein. One early to mid-phase image (at 20-40 seconds), and a second late-phase image (at 5-7 minutes) centred on the optic disc, was chosen for analysis. The early to mid-phase was graded for peripheral and macular ischaemia, and late-phase image for peripheral leakage. All uwFA images were exported as .tiff files and analysed on commercially available software Adobe Photoshop CS4 extended (Photoshop, Adobe Systems, San Jose, CA). No image manipulation was performed prior to grading.

2.3.5 Image analysis

Quantification of the foveal avascular zone and other areas of capillary non-perfusion: Quantitative analysis of all images was performed using a validated image viewer and grading software package ("GRADOR", Doheny Image Reading Center, Los Angeles) that facilitates planimetric measurements. Using this software, the areas of the FAZ, and other areas of capillary non-perfusion, were assessed in square millimetres (mm^2). After manual delineation of each area, measurements were calculated using a scale factor based on the camera's angle of view. Temporal and papillomacular ischaemia were calculated in a similar fashion.

Quantification of uwFA-derived areas of peripheral ischaemia and leakage: An ischemic index was calculated from the early to mid-phase FA using previously described methodology.(174-176) Briefly, areas of capillary nonperfusion, outside the temporal vascular arcades were expressed as a percentage of the total image area in pixels **(Figure 2.3)**.

In addition, for this study, the “total area” was defined as an area in which retinal vasculature was in sharp focus, thereby allowing accurate visualisation of smaller retinal capillaries. Due to the spherical curvature of the eye, ultra widefield images commonly exhibit “blurred” areas in the far periphery when the central portion of the image is in focus. In excluding these “blurred” areas from “total area” measurements, the resultant image is smaller than the 200 degree scanning angle that can be achieved by the ellipsoidal mirror within the Optos imaging system. However, it avoids underestimating the peripheral ischemic index by the inclusion of parts of retina where capillary non perfusion cannot be visualised.

A peripheral “leakage” index was adapted from the ischemic index, similarly calculated; where areas of FA leakage outside the temporal vascular arcades were quantified in pixels and expressed as a percentage of the total area **(Figure 2.3)**.

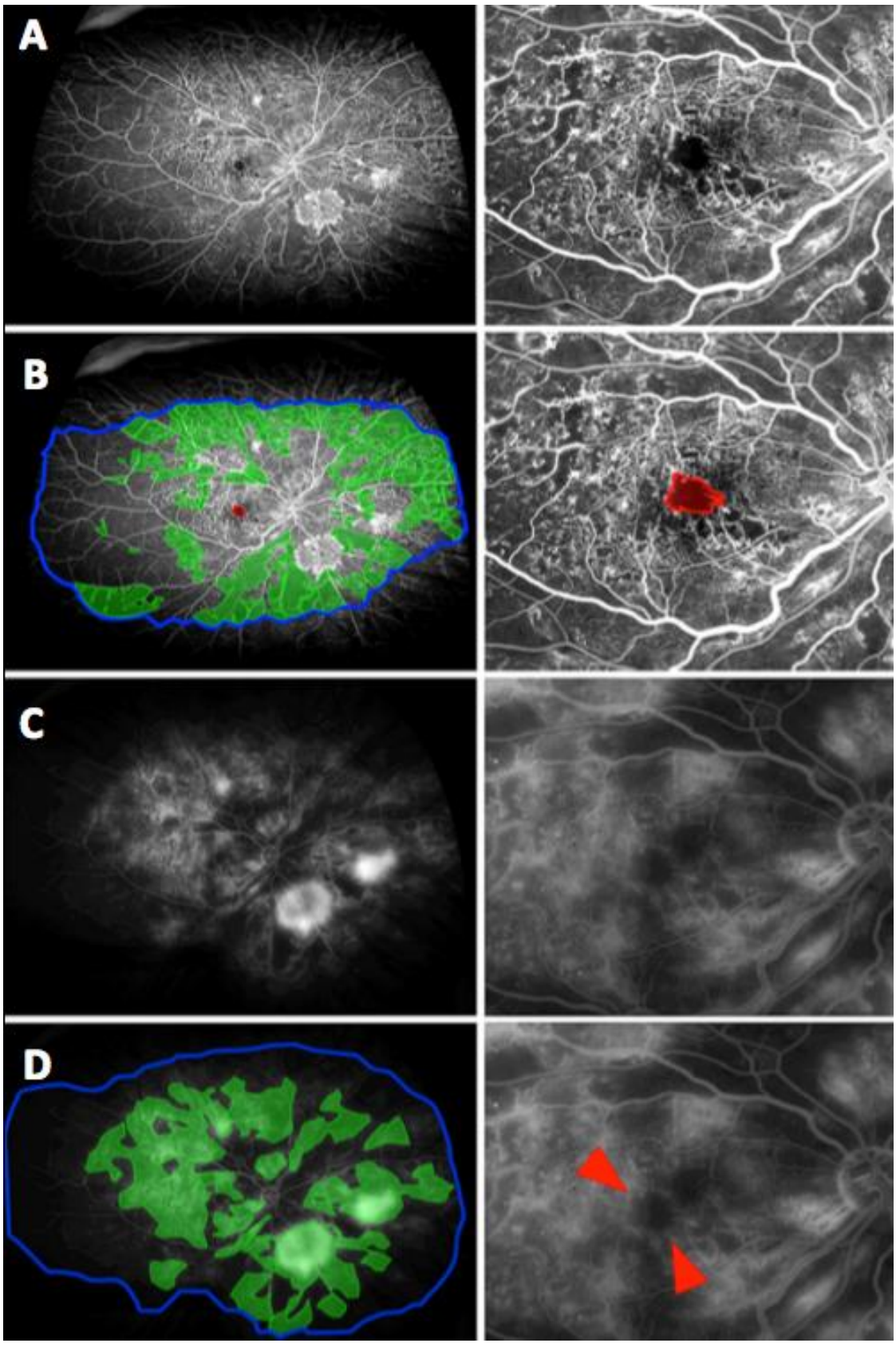
A
B
C
D

Figure 2.3. Early and late-phase ultra widefield fluorescein angiogram image.

A patient with diabetic retinopathy comprising of both peripheral and macular capillary non perfusion. (A, left) An early-phase uwFA image, acquired at 20 seconds. (A, right) 10X magnified early-phase ultra uwFA image, centred on the foveal avascular zone. (B, left) Annotated solid blue line delineates the boundary of the retina where capillaries are in sharp focus. This area was taken to be the "total retinal area", which was the denominator as the peripheral ischemic index. Annotated solid green lines delineates areas of capillary non perfusion in the retinal periphery. The peripheral ischemic index was calculated as the percentage of the "total area of capillary non perfusion" over the "total retinal area". (B, right) Annotated solid red line delineates the boundary of the foveal avascular zone area. (C, left) A late-phase uwFA image, acquired at 6 minutes. (C, right) 10X magnified uwFA image, centred on the foveal avascular zone. (D, left) Annotated solid blue line delineates the boundary of the retina where peripheral vasculature was in sharp focus. This area was also taken to be the "total retinal area" for the purpose for calculating the peripheral leakage index. Annotated solid green lines delineates areas of "vascular leakage" in the retinal periphery. The peripheral leakage index was similarly calculated as the percentage of the "total area of vascular leakage" over the "total retinal area". (D, right) Annotated solid red arrowheads points to diffuse leakage from the perifoveal capillaries. uwFAs were graded for the presence of macular capillary leakage and classified as "none", "focal leakage", and "diffuse leakage".

Quantification of uwFA-derived areas of macular ischaemia and leakage: Boundaries for the FAZ were manually delineated, and area measurements were calculated, and analysed in pixels, but subsequently converted into square millimeters (mm^2) for the purpose of clinical interpretation, using a scale factor based on the assumption that the disc area was $2.7mm^2$.(177)

uwFAs were graded for the presence of macular capillary leakage- i.e. oedema in late-phase angiograms. The uwFA macular oedema grades were classified as "none", "focal leakage", and "diffuse leakage".

Definitions (Table 2): The FAZ area, as measured using early to mid-phase uwFA was divided into "large" (>$0.32mm^2$) and "small" (<$0.32mm^2$) categories. As established in our previous study, a "large" FAZ area corresponds to an Early Treatment Diabetic Retinopathy Study (ETDRS)-defined diabetic macular ischaemia

grade of “moderate” to “severe”.(178) A low peripheral ischaemia/leakage index was defined as less than 50%, and a high peripheral ischaemia/leakage index more than 50% of the total area.

Quantification of retinal vessel calibres: Retinal arteriolar and venular calibres were measured from late phase FFA images (1-2 mins) when the retinal arterioles and venules were clearly outlined with fluorescein dye. FFA images had to have sufficient peripapillary vasculature visible to facilitate grading with a validated semi-automated software which calculated the calibres of arterioles and venules coursing through a region 0.5 to 1 disc diameter from the disc margin.(179, 180) These values were then combined using formulas to derive the central retinal artery and venule calibre equivalent for that eye.(181) Arteriole to venule ratio (AVR) was calculated as the ratio of mean arteriolar to venular calibres **(Figure 2.4)**.

Segmentation protocol for OCT-derived retinal spaces: Boundaries were manually segmented in accordance with standardized OCT grading protocols.(182) The retinal space was defined as the space lying between the inner aspect of the internal limiting membrane and the outer border of the photoreceptor outer segments.(183, 184)

Segmentation protocol for choroidal spaces: The choroid was defined as the space between the outer border of the retinal pigment epithelium and choroidoscleral junction. The choroid was further subdivided into Haller’s large vessel and Sattler’s medium vessel layers **(Figure 2.5)**. Haller’s large vessel layer was defined as the outer choroid consisting large hypo-intense spaces representing large vascular luminal spaces. Sattler’s medium vessel layer consisted of small to medium size hypo-intense spaces, surrounded by hyperintense stroma (increase scattering by high density of melanocytes) giving a mottled appearance on scans.(57) This layer also included the choriocapillaris, which at 10 μm, is not easily distinguished from the Sattler’s medium vessel layer on OCT images. The detailed choroidal segmentation protocol is illustrated in **Figure 2.5**. This protocol was used in the training of graders and was used prior to all grading sessions.

The mean retinal and choroidal thicknesses (μm) and volumes (mm^3) were then calculated for the ETDRS areas 1-9 or the "total macular circle" (TMC), and ETDRS area 9 which corresponds to the foveal central subfield (FCS).

Assessment of repeatability of segmentation: A subset of OCT images (n=20) were segmented three times by a single grader– once before training, and twice after training. This OCT image set was also segmented twice by the experienced grader (S.F.) to assess repeatability. The time-interval between each episode of segmentation was greater than two weeks for both graders.

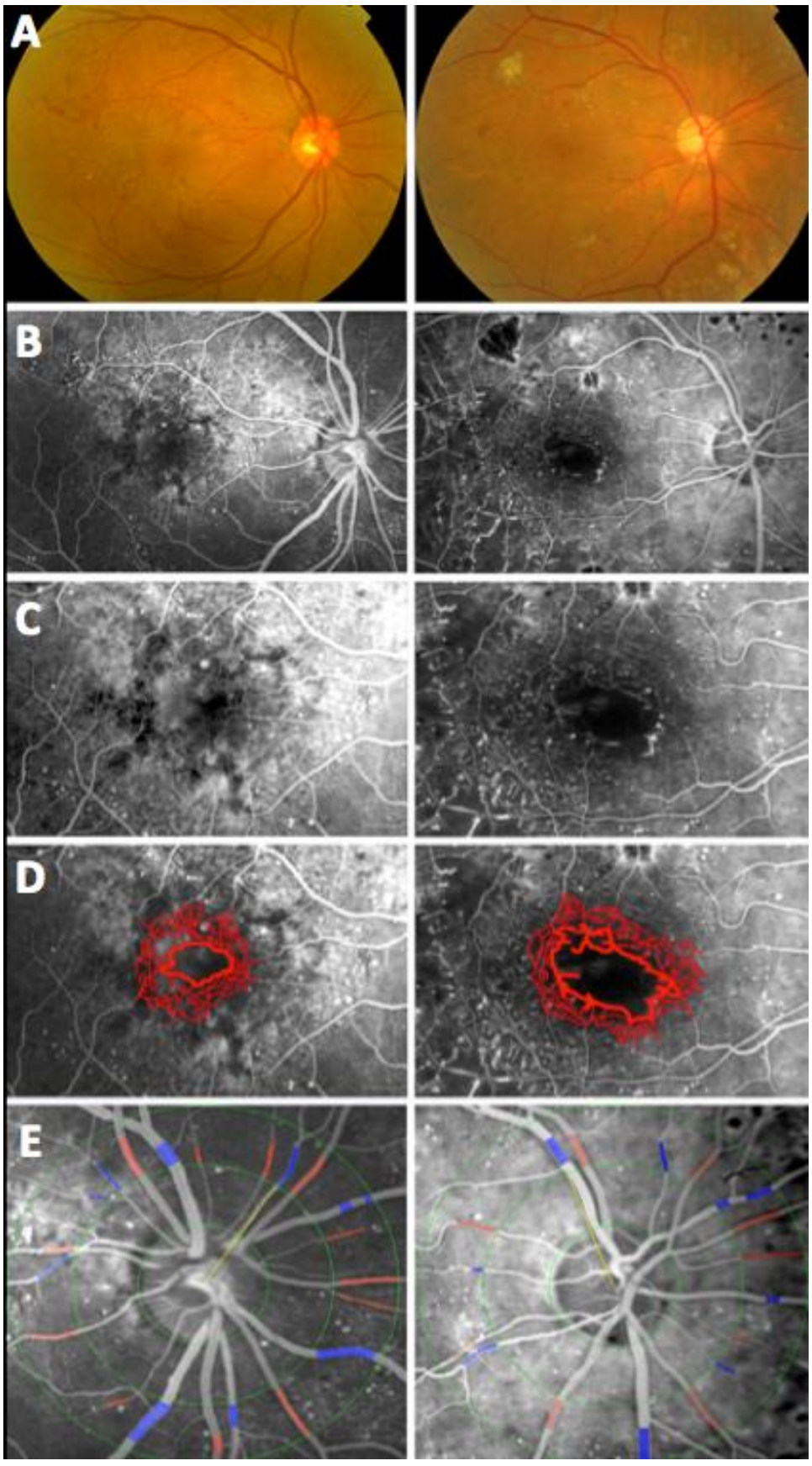
A
B
C
D
E

Figure 2.4. Arteriolar narrowing in persons with different severity grades of diabetic macular ischaemia.

The left panel contains representative images from an eye with no diabetic macular ischaemia, and the right panel representative images from an eye with severe diabetic macular ischaemia. (A) contains colour fundus photographs; (B) early venous phase fundus fluorescein angiograms; the (C) magnified fundus fluorescein angiograms centred at the foveal avascular zone; in (D), macular centered magnified fundus fluorescein angiograms contain annotations of the foveal avascular zone and perifoveal capillaries; the (C) contains examples of how cross-sectional calibre of arterioles (red) and venules (blue) is measured. The boundaries foveal avascular zone is more irregular and its area enlarged in severe diabetic macular ischaemia (D, right panel) compared to no diabetic macular ischaemia (D, left panel). In E, the eye with no diabetic macular ischaemia shows a wider arteriolar calibre (left panel, mean arteriolar calibre 163.5 µm), while the eye with severe diabetic macular ischaemia shows arteriolar narrowing (right panel, mean arteriolar calibre 126.4µm).

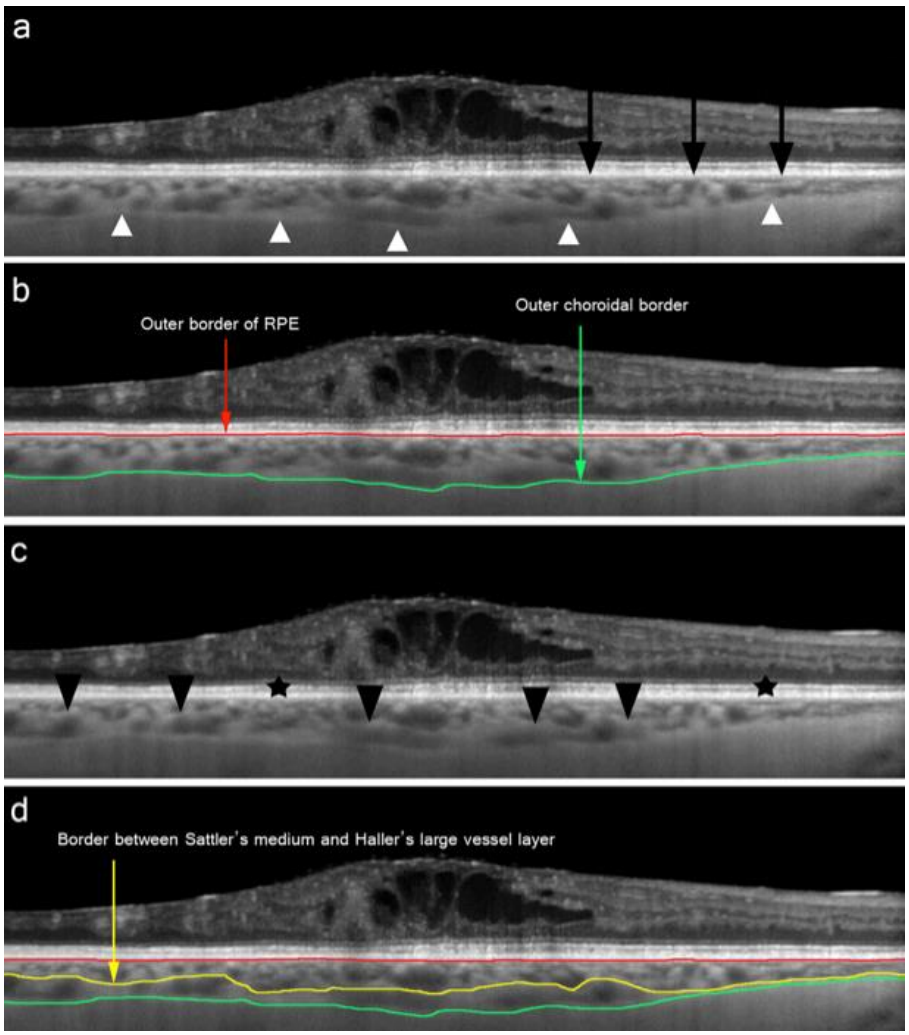

Figure 2.5. Choroidal segmentation on OCT-derived images

An example of a foveal centred B-scan, acquired using the enhanced depth optical coherence tomographic protocol. Annotations illustrate the instructions from the choroidal segmentation protocol, and demonstrate identification and segmentation of choroidal layers by examining changes in light reflectance at the different tissue interfaces. (a) Black arrows indicate the outer border of the retinal pigment epithelium (RPE) and white arrowheads the outer choroidal border (OCB) which represents the choroidoscleral interface. (b) Segmentation lines on the outer border of the RPE (red) and OCB (green) demarcating the total choroidal area / volume. (c) Black arrowheads indicate the junction between Sattler's medium and Haller's large vessel layers. Black stars indicate difficulty areas where the interface between both Sattler's and Haller's layers is ambiguous. Segmentation of these areas may be aided by clues from adjacent B-scans. (d) Segmentation line on the Sattler's and Haller's vessel layer interface (yellow).

2.3.5 Statistical analysis

Patient demographic and imaging data were analysed with frequency and descriptive statistics. Normality of the variables was examined using histograms. As anticipated, distribution of visual acuity and FAZ measurements were negatively skewed and traditional regression analyses could not be applied to the data set. No simple transformation of data redressed the skewness.

The Mann-Whitney U test was used to compare continuous variables, whereas the χ^2 test was used for categorical variables. Spearman's rank correlation was used to test for associations between variables. Snellen visual acuities were converted to LogMAR (logarithm of the minimum angle of resolution) visual acuity for the purposes of statistical analysis.

Multivariable quantile regression analysis was used to test for associations between logMAR visual acuity and each of - age, gender, retinopathy grade, diabetic macular oedema, FAZ measurements, and non-contiguous areas of ischaemia. Quantile regression is a statistical approach to model different sample percentiles or "quantiles" of an outcome variable with respect to predictor variables. It was used to assess for associations in this dataset due to the skewed distribution of parameters measured. An advantage of using this form of regression analysis, was that it allowed us to examine the more complex relationships between variables (such as the VA) which may have unequal variation for different ranges of another variable (ie FAZ), without converting continuous data into dichotomous or categorical fields, which loses information. This approach has been described in more detail elsewhere.(25) Briefly, the interpretation of quantile regression is similar to linear regression, but where linear regression models the mean of the outcome variable, quantile regression models selected percentiles, for example the 0.50 quantile (the median, or 50th percentile). In this study, we analysed the 0.10, 0.25, 0.50, 0.75, and 0.90 quantiles. We developed models for each DMI ischaemia grade, and further adjusted for potential confounders such as age (continuous variable), gender, retinopathy grade, and the presence of diabetic macular oedema (categorical variables). P values < 0.05 were considered statistically significant. Statistical analysis was performed

using the statistical software R 2.15.0 (http://cran.r-project.org, accessed May 24th, 2012), with the addition of the "quantreg" package.

The coefficient of repeatability (CR) of retinal and choroidal thickness measurements was calculated using the within-grader standard deviation (S_w) derived from the intra grader mean square of differences. The CR, as defined by Bland and Altman(185), was calculated as 1.96 times the standard deviation of the differences between two measurements: $CR = 1.96 \times \sqrt{(2S^2_w)}$ or $2.77S_w$. To allow comparison with other studies, we also expressed the CR as a percentage of the mean measurement for all retinal and choroidal layers (CR / Mean), with a lower the CR / Mean percentage representing, greater repeatability within graders. The intraclass correlation coefficient (ICC) was used as a measure of relative reliability of measures within graders.

Reproducibility or inter observer variability was assessed using Bland-Altman plots, using the mean thickness and volume measurements, segmented by each grader.(186) The mean difference and confidence intervals were calculated. Agreement between graders was also examined using Bland-Altman analysis, with the 95% limits of agreement (μm) (LoA) between graders calculated, after confirming that the measurement differences were normally distributed using histograms.

Statistical analyses were performed using statistical software R 2.15.0 (http://cran.r-project.org, accessed May 24th, 2012), with the addition of the "quantreg" package; SPSS software version 16 (SPSS, Inc, Chicago, IL); and MedCalc software version 10.3.2 (MedCalc Software, Mariakerke, Belgium).

2.4 Results:

2.4.1 Diabetic macular ischaemia in type 2 diabetes

2.4.1.1 Baseline Characteristics

Electronic records of 2051 appointments were screened, and 1298 unique attendances identified. 821 patients attended for assessment of diabetic eye disease, of which, 767 patients had Type 2 diabetes. The male to female ratio was 5:4, and mean age was 64.2 years (SD: 12.6). Of the patients with Type 2 diabetes, 488 met the inclusion criteria for fluorescein angiography. In these cases, an attempt was made to grade both eyes for severity of DMI: in 401 patients, FA images were of sufficient quality to allow DMI grading in both eyes; in a further 52 patients, DMI grading was possible in a single eye only. In 35 patients, FA images were of insufficient quality to permit grading of DMI in either eye. Forty-five patients were then excluded due to the presence of ocular co-morbidities. In total, 408 eyes from 408 patients were included in the analysis **(Table 2.1)**. For this assessment of DMI severity, substantial inter-grader agreement was demonstrated, with a weighted kappa of 0.704. (SE: 0.087, 95% CI: 0.535 to 0.874).

2.4.1.2 Symmetry of Disease:

Within the 401 patients where both eyes were gradable, 62.1% had bilaterally symmetrical macular ischaemia. The difference in grade between the asymmetrical eyes was as follows: no more than one grade in 26.7% of patients, two grades in 8%, three grades in 3%, and four grades in 0.2%. Where there was symmetrical disease, one eye was randomized for analysis. In asymmetrical disease (37.9%), the eye with the most severe DMI grade was selected.

2.4.1.3 ***Prevalence of Diabetic Macular Ischaemia:***

Overall prevalence and severity of diabetic macular ischaemia by ETDRS-DMI grade:

In the 408 eyes analysed, 39.7% had none, 18.4% questionable, 25.2% mild, 11% moderate, and 5.6% had severe ETDRS-DMI grades.

Table 2.1: Patient demographics and clinical characteristics of patients (type 2 diabetes) with and without diabetic macular ischaemia.

		No DMI (n=162)	DMI (n=246)	p value
Age, years, Mean (SD)		62 (11.4)	64 (12.2)	0.07
Gender, n, female/male		72 / 90	105 / 141	0.63
Eye, n, right/left		84 / 78	126 / 120	0.94
FAZ area, mm², median (IQR)		0.19 (0.13 to 0.25)	0.29 (0.20 to 0.42)	< 0.001
Retinopathy Grades				**DMI:No DMI (n=408)**
No Diabetic Retinopathy (n=44)	(%)	24 (54.5)	20 (45.5)	0.83
Mild-Moderate NPDR (n=139)	(%)	75 (54.0)	64 (46.0)	0.85
Severe NPDR (n=67)	(%)	27 (40.3)	40 (59.7)	1.48
PDR (n=158)	(%)	36 (22.8)	122 (77.2)	3.39
Maculopathy Grades				
No DME / CSME (n=113)	(%)	55 (48.7)	58 (51.3)	1.05
DME (Non CSME) (n=120)	(%)	53 (44.2)	67 (55.8)	1.44
CSME (n=175)	(%)	54 (30.6)	121 (69.4)	2.24

DMI = Diabetic Macular Ischaemia; NPDR = Non-Proliferative Diabetic Retinopathy; PDR= Proliferative Diabetic Retinopathy; DME = Diabetic Macular Oedema; CSME = Clinically Significant Macular Oedema; SD = Standard Deviation; IQR = Interquartile range

Prevalence of DMI (by ETDRS grade) within different severity grades of retinopathy and maculopathy ***(Table 2.1)****:* In eyes with proliferative diabetic retinopathy (PDR) (both treated and untreated), concurrent DMI was seen in 77.2% of cases (in 22.8% of cases, DMI was not present). The occurrence of DMI was similar across all other grades of non-proliferative diabetic retinopathy (NPDR), and in patients without diabetic retinopathy (i.e., R_0 in the NSC grading system). In eyes with clinically significant macular oedema (CSME), concurrent DMI was seen in 69.4% of cases (in 30.6% of cases, therefore, no DMI was observed). In eyes with DME, but without CSME, concurrent DMI was seen in 55.8% of cases (in 44.2% of cases, DMI was not present). An increase in the proportion of eyes with DMI in relation to eyes with no DMI, expressed as the "DMI : No DMI" ratio, was seen in patients with severe NPDR and PDR, and across all maculopathy grades. Table 2 shows the distribution of eyes between different grades of retinopathy and maculopathy in the presence or absence of DMI.

Increasing FAZ area with ETDRS-DMI severity grades ***(Figure 2.6)****:* As expected, the median FAZ area increased with grade of ETDRS-DMI severity, and ranged from 0.19 mm^2 (interquartile range (IQR): 0.13 to 0.25) in eyes with ETDRS-DMI grade: none, to 0.78 mm^2 (IQR: 0.60 to 1.32) in eyes with ETDRS-DMI grade: severe. **(Figure 2.6)** Highly significant differences in median FAZ area were seen across all subgroups of DMI, with the exception of "questionable" versus "mild" DMI. Median FAZ area was significantly correlated with ETDRS DMI severity grade ($r=0.477$, $p<0.001$). **(Table 2.2)**

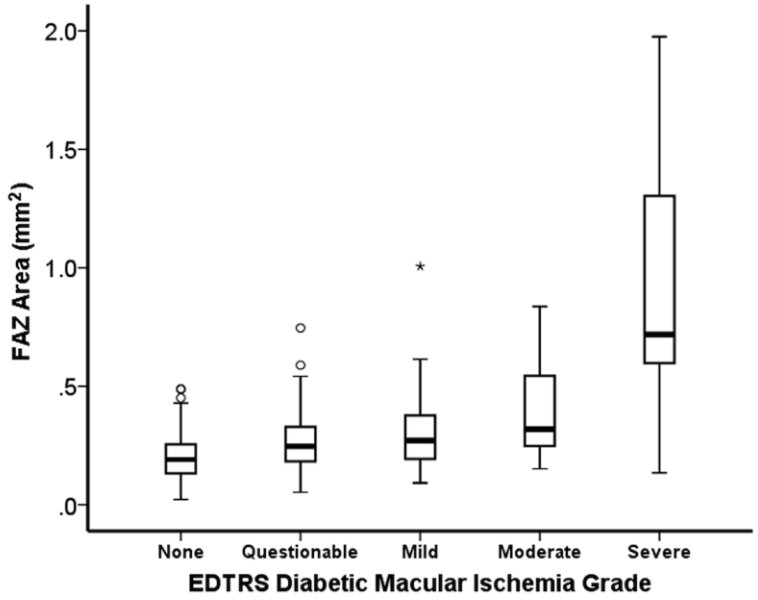

Figure 2.6. Distribution of diabetic macular ischaemia grades

Box-plots of FAZ Area (mm^2) in different Early Diabetic Treatment Retinopathy Study (EDTRS) grades of Diabetic Macula Ischaemia (DMI) – None, Questionable, Mild, Moderate, and Severe. The top of the box represents the 75th percentile, the bottom of the box represents the 25th percentile, and the line in the middle represents the 50th percentile. The whiskers represent the highest and lowest values that are not outliers or extreme values. Outliers and extreme values are represented by circles beyond the whiskers.

Prevalence of temporal and/or papillomacular ischaemia: Temporal ischaemia was seen in 112 eyes (27.5%), while papillomacular ischaemia was seen in 34 eyes (8%). Both temporal and papillomacular ischaemia were most prevalent in higher ETDRS-DMI grades. This was most notable for temporal ischaemia, which was present in 87% of eyes in the severe subgroup, as compared to 6.2% of eyes in without DMI. Papillomacular ischaemia was also more frequently seen in the ETDRS-DMI severe subgroup (34.8% of eyes with severe vs. 10.7% of eyes with mild ETDRS-DMI grade).

2.4.1.4 ***Visual Significance of Macular Ischaemia:***

Relationship between visual acuity and ETDRS-DMI severity Grade ***(Table 2.2)****:*

Median logMAR visual acuity (VA) was 0.2 (IQR: 0 to 0.3) (Snellen 20/32) in eyes with

none, 0.2 (IQR: 0 to 0.5) (Snellen 20/32) in eyes with questionable, 0.2 (IQR: 0.2 to 0.5) (Snellen 20/32) in eyes with mild, 0.5 (IQR: 0.2 to 0.6) (Snellen 20/63) in eyes with moderate, and 0.6 (IQR: 0.3 to 0.8). (Snellen 20/80) in eyes with severe ETDRS-DMI grades. Significant differences in VA were observed between moderate and severe ETDRS-DMI versus all other grades **(Table 2.3)**. Overall, VA showed a weak but highly significant correlation to ETDRS grading of DMI severity (rho=0.22, p<0.001).

Table 2.2: Comparing Median FAZ Area (mm^2) between all Diabetic Macula Ischaemia subgroups.

DMI p-values	None	Questionable	Mild	Moderate	Severe
None					
Questionable	<0.001**				
Mild	<0.001**	0.18			
Moderate	<0.001**	<0.001**	0.002**		
Severe	<0.001**	<0.001**	<0.001**	<0.001**	

*Relationship between FAZ size and visual acuity **(Table 2.3)**:* Overall, we found no evidence any correlation between VA and FAZ area (mm^2) (rho=0.061, p=0.219). However, when the data were stratified by severity of ischaemia, quantile regression models revealed a statistically significant association between VA and FAZ area (mm^2) in all quantiles for eyes with moderate and severe ETDRS-DMI grades **(Table 2.4, Figure 2.7)**. Severe DMI showed the strongest association with quantile regression coefficient, β = 0.406; SE 0.101, (p<0.001), at the 50^{th} percentile. In moderate DMI, the greatest association was also observed at the 50^{th} percentile, β = 0.299; SE 0.108, (p<0.006). The effects of FAZ area on VA on moderate and severe ETDRS-DMI grades for different quantiles are summarized in Table 2.5 and **Figure 2.7A and B**. No relationships were observed between VA and FAZ area for milder grades of ischaemia.

Table 2.3: Comparing Median Visual Acuities (LogMar) between all Diabetic Macula Ischaemia subgroups.

DMI Grade	None	Questionable	Mild	Moderate	Severe
P value for VA					
None					
Questionable	0.651				
Mild	0.143	0.527			
Moderate	<0.001**	0.02*	0.03*		
Severe	<0.001**	<0.001**	<0.001**	0.04*	

Relationship of temporal and papillomacular ischaemia with visual acuity

(Table 2.4)*:* We investigated whether papillomacular and temporal ischaemia had a significant impact on VA after adjustment for FAZ area. A higher than expected association was observed in papillomacular ischaemia at the 25th, 50th, 75th and 90th quantile regression lines **(Table 2.5, Figure 2.7)**. Thus, papillomacular ischaemia has an impact on VA independent of FAZ size. This effect was maintained after adjusting for potential confounders such as DME **(Table 2.6)**. No relationship was observed with temporal ischaemia.

Table 2.4: Association between Visual Acuity and Foveal Avascular Zone area (mm^2) stratified by EDTRS Diabetic Macular Ischaemia severity grades for five different Quantiles.

	10th Quantile			25th Quantile			50th Quantile			75th Quantile			90th Quantile		
	Adjusting for age, (continuous variable) gender, retinopathy grade, and the presence of macular oedema (categorical variable)														
DMI Grade	**β**	**SE**	**p**	**β**	**SE**	**p**	**β**	**SE**	**p**	**β**	**SE**	**p**	**β**	**SE**	**p**
Questionable (n=75)	0.041	0.064	0.530	0.001	0.123	0.994	<0.001	0.030	0.992	0.097	0.142	0.497	0.406	0.186	0.030
Mild (n=103)	0.019	0.063	0.757	0.199	0.123	0.107	0.013	0.044	0.763	0.110	0.081	0.177	0.246	0.122	0.044
Moderate (n=45)	**0.224**	0.083	0.007**	0.199	**0.093**	0.034*	**0.299**	0.108	0.006**	**0.257**	0.099	0.009**	**0.289**	0.117	0.014**
Severe (n=24)	**0.326**	0.083	<0.001**	0.303	**0.142**	0.034*	**0.406**	0.101	<0.001**	**0.359**	0.118	0.002**	**0.299**	0.128	0.020*

Coefficient (**β**) and standard error (SE) are reported for 10%, 25%, 50%, 75%, and 90%. Coefficients that are significant at 5% level are bold, and those at the 1% level are bold and underlined. p values significant at 5% level are indicated with (*), and (**) at 1% level. Standard errors are obtained using 1000 bootstrap replications.

Table 2.5: Association between Visual Acuity and area of Papillomacular or Temporal ischaemia (mm²) for five different Quantiles after adjusting for Foveal Avascular Zone area (mm²) as a co-variate.

	10th Quantile			25th Quantile			50th Quantile			75th Quantile			90th Quantile		
	Adjusting for gender, retinopathy grade, the presence of macular oedema (categorical variables) and age, FAZ area (mm²) (continuous variables)														
Area of ischaemia	**β**	**SE**	**p**	**β**	**SE**	**p**	**β**	**SE**	**p**	**β**	**SE**	**p**	**β**	**SE**	**p**
Papillomacular (n=34)	0.302	0.586	0.612	**1.036**	0.500	0.050*	**1.123**	0.355	0.005**	**1.193**	0.381	0.005**	**0.383**	0.547	0.002**
Temporal (n=112)	0.060	0.017	0.001	0.051	0.015	0.002	**0.056**	0.026	0.039*	0.075	0.001	0.079	0.075	0.054	0.110

Coefficient (**β**) and standard error (SE) are reported for 10%, 25%, 50%, 75%, and 90%. Coefficients that are significant at 5% level are bold, and those at the 1% level are bold and underlined. p values significant at 5% level are indicated with (*), and (**) at 1% level. Standard errors are obtained using 1000 bootstrap replications.

Table 2.6: Multivariable median regression between Visual Acuity and Area of Papillomacular ischaemia (mm^2) adjusting for Foveal Avascular Zone area (mm^2) and other clinical co-variates.

	Median Regression coefficient	Standard Error	p-value
Papillomacular ischaemia	**<u>1.123</u>**	0.341	0.004**
Foveal Avascular Zone Area	0.178	0.259	0.501
Gender	0.17	0.162	0.291
Age	0.01	0.012	0.401
Diabetic Macular Oedema			
No DME	0.193	0.271	0.485
Clinically Significant DME	0.310	0.485	0.530
Treated clinically significant DME	0.106	0.252	0.679

The median regression coefficient is reported with standard errors obtained using 1000 bootstrap replications. Coefficients that are significant at 5% level are bold, and those at the 1% level are bold and underlined. p values significant at 5% level are indicated with (*), and (**) at 1% level.

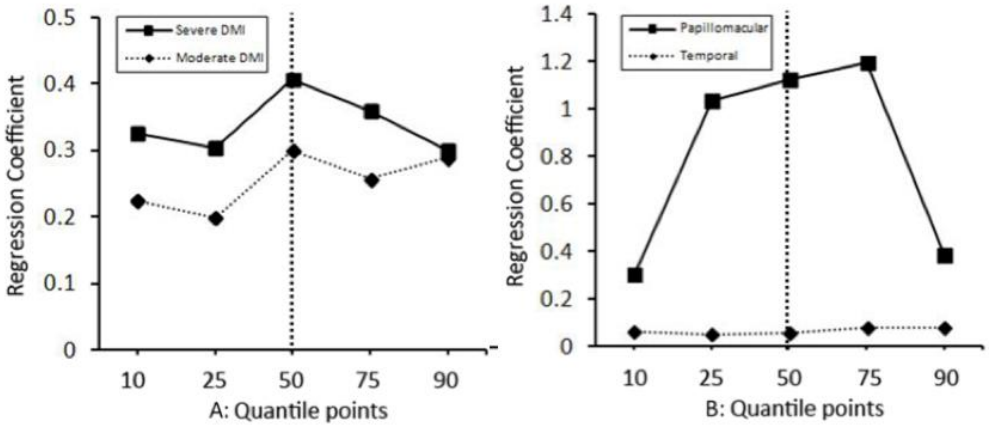

Figure 2.7. Relationship between visual acuity and ischaemia

(a) Line plot of quantile regression coefficients (vertical dotted line represents the median regression coefficient) of Visual Acuity with Foveal Avascular Zone area (mm^2) in the moderate (dotted line) and severe (solid line) subgroups of diabetic macular ischaemia (DMI), after adjustment for age, gender, retinopathy grade and the presence of diabetic macular oedema. (b) Line plot of quantile regression coefficients (vertical dotted line represents the median regression coefficient) of Visual Acuity with Papillomacular and Temporal ischaemia area (mm^2), after adjustment for age, gender, retinopathy grade, the presence of diabetic macular oedema and Foveal Avascular Zone area (mm^2).

2.4.2 Predictive factors for diabetic macular ischaemia in type 2 diabetes

2.4.2.1 Patient Characteristics:

A total of 79 patients were identified, and of these, 61 patients had both eyes, which met the criteria. From the remaining 18 patients, one eye was chosen from each patient using random block permutation, and included in the analysis. Clinical and imaging data from two time points were collected and analysed **(Figure 2.8)**.

There were 24 females and 55 males with a median age of 63 (interquartile range [IQR], 56.5 to 70). At baseline, 44 eyes had both treated, or untreated

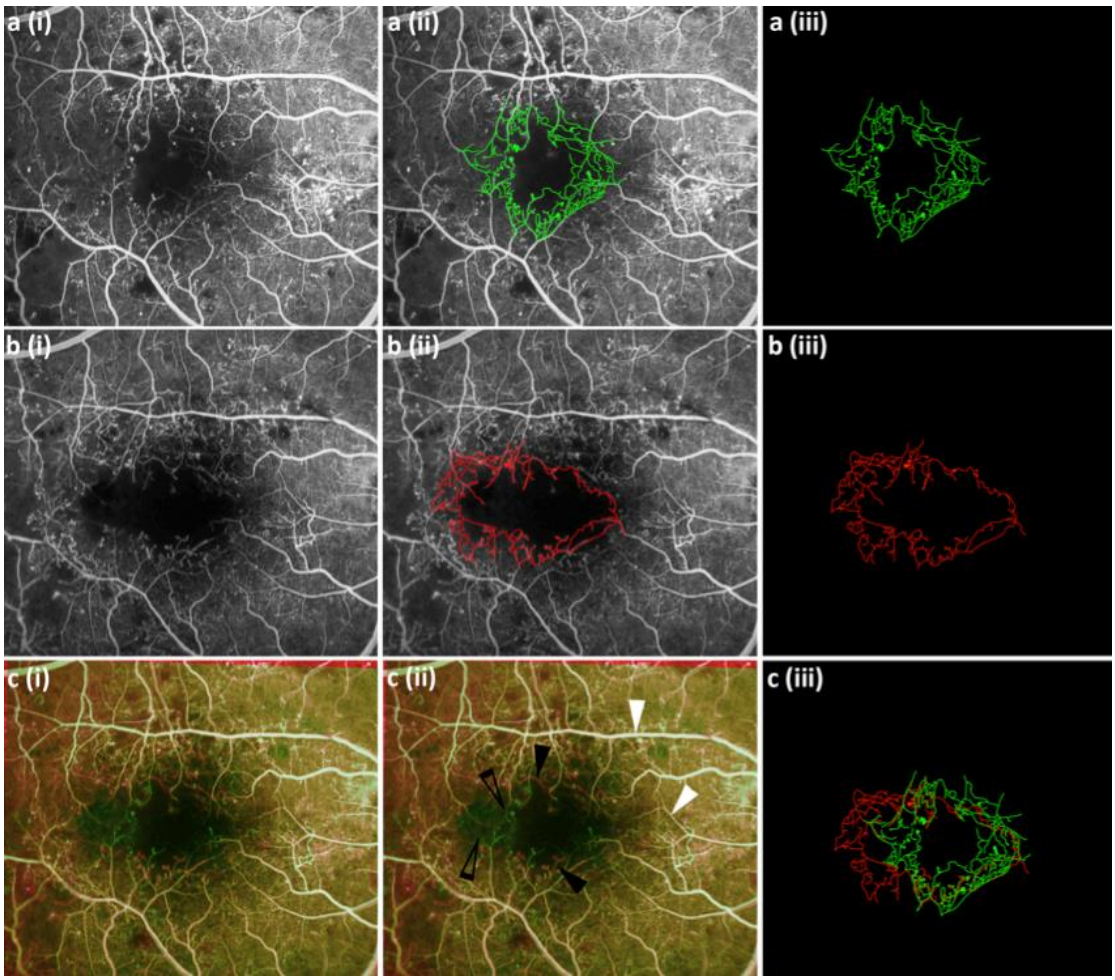

Figure 2.8. Progression of diabetic macular ischaemia

(a)(i) An example of an early phase Fundus Fluorescein Angiography (FA) image centered at the macula demonstrating foveal avascular zone (FAZ). (a)(ii) Annotated solid green lines delineates the boundary of the FAZ and the perifoveal capillaries. (a)(iii) The FAZ boundary (solid green lines) from (a)(ii), with FA image removed. (b)(i) FA image of the same patient after a 2 year time interval. (b)(ii) Annotated solid red lines delineates the boundary of the FAZ and the perifoveal capillaries. (b)(iii) The FAZ boundary (solid red lines) from (b)(ii), with FA image removed. (c)(i) Merged FAs from (a) and (b) with green filters over the baseline FA, and red filters over the FA at 2 years. (c)(ii) A white vessel (solid white arrowheads) represents vasculature that is present at both time points. Green vessels (empty arrowheads) represent vasculature present at the baseline FA, but not at 2 years. Red vessels (solid black arrowheads) represent vasculature present at 2 years but not at the baseline FA. (c)(iii) An overlay of annotated FAZ boundaries from the baseline FA (solid green line), and FA at 2 years (solid red line).

proliferative diabetic retinopathy (DR), 38 eyes had none, or non-proliferative DR. 49 eyes had clinically significant macular oedema (CSME), 18 with non-CSME, and 12 with no macular oedema. In all eyes, the median FAZ area was 0.31 mm^2 (IQR, 0.22 to 0.43) at baseline, and 0.39 mm^2 (IQR, 0.29 to 0.63) at the final FA. The median VA was 0.3 logarithm of the minimum angle of resolution (LogMar) (IQR, 0.2 to 0.5) both at the baseline, and final FA. The median time interval between FAs was 27 months (IQR, 16.5 to 53.5, Range, 7 to 126).

2.4.2.2 Progression of ETDRS-DMI grades:

At the baseline FA, within 79 eyes analysed, there were 42 eyes (53.2%) with "mild", 24 (30.4%) "moderate", and 13 (16.5%) "severe" ETDRS-DMI grades. At the final FA, there were 39 eyes (49.4%) with "mild", 25 (31.6%) "moderate", and 15 (19.0%) "severe" ETDRS-DMI grades. 58 eyes (73.4%) had no change or an improvement of ETDRS-DMI grade between baseline and final FA, of which 31 had baseline ETDRS-DMI grades of "mild", 15 "moderate", and 12 "severe". In 9 eyes (11.4%), there was an improvement in the ETDRS-DMI grade, from "moderate" to "mild" in 8 eyes, and from "severe" to "moderate" in one eye. A total of 12 eyes (15.2%) showed progression in ETDRS-DMI grade, 9 from "mild" to "moderate", 1 from "moderate" to "severe", and 2 from "mild" to "severe". Analysis of the baseline ETDRS-DMI subgroups reveal progression in 11/42 eyes (26.2%) in "mild", 1/30 (3.3%) in "moderate", and 0/7 (0%) in the "severe" grades **(Table 2.7)**.

The median FAZ area was observed to increase from baseline to the final FA, across all ETDRS-DMI grades - with 0.28 mm^2 (IQR, 0.19 to 0.35) to 0.31 mm^2 (IQR, 0.25 to 0.45) in "mild", 0.37 mm^2 (IQR, 0.28 to 0.47) to 0.41 mm^2 (IQR, 0.34 to 0.66) in "moderate", and 0.73 mm^2 (IQR, 0.64 to 1.03) to 1.23 mm^2 (IQR, 0.67 to 1.43) in the "severe" grades **(Figure 2.9)**. This was significantly different within each ETDRS-DMI grade ($p<0.001$); progression observed across all severity grades.

Table 2.7: Foveal avascular zone area (FAZ) (mm²) at the baseline and final fluorescein angiogram and progression rate over time.

	FAZ area (Baseline) (mm2)	FAZ area (Final) (mm2)	Difference in FAZ area (Final - Baseline) (mm2)	p value	Time interval between FA (months)	Change in FAZ area per year (mm² / year)	Change in FAZ area as a percentage of baseline FAZ area per year (% / year)
	Median (Interquartile range)						
All eyes	0.31 (0.22 to 0.43)	0.39 (0.29 to 0.63)	0.06 (0.01 to 0.16)	< 0.001 **	27.0 (16.5 to 53.5)	0.023 (0.001 to 0.060)	7.42
ETDRS-DMI grade (Baseline)							
Mild (n = 42)	0.28 (0.19 to 0.35)	0.31 (0.26 to 0.45)	0.05 (0 to 0.11)	< 0.001 **	27.5 (18.0 to 49.5)	0.021 (0.001 to 0.060)	7.50
Moderate (n = 24)	0.37 (0.28 to 0.43)	0.39 (0.33 to 0.63)	0.05 (0 to 0.14)	< 0.001 **	31.0 (18.5 to 60.8)	0.019 (0.001 to 0.056)	5.13
Severe (n = 13)	0.70 (0.38 to 0.95)	0.82 (0.55 to 1.23)	0.18 (0.08 to 0.40)	< 0.001 **	24.0 (18.0 to 36.0)	0.073 (0.048 to 0.181)	10.4
FAZ area at baseline							
Small (<0.3mm 2) (n = 35)	0.22 (0.16 to 0.27)	0.28 (0.21 to 0.35)	0.06 (0.02 to 0.11)	< 0.001 **	24.0 (14.0 to 42.0)	0.023 (0.007 to 0.056)	10.4
Large (>0.3mm 2) (n = 44)	0.41 (0.36 to 0.59)	0.55 (0.39 to 0.86)	0.06 (0 to 0.20)	< 0.001 **	34.0 (18.0 to 59.8)	0.024 (0 to 0.065)	5.85
Diabetic Retinopathy							
None or NPDR (n = 35)	0.29 (0.22 to 0.35)	0.34 (0.27 to 0.61)	0.06 (0.02 to 0.18)	< 0.001 **	24.0 (16.0 to 35.5)	0.040 (0.007 to 0.068)	13.8
PDR (n = 44)	0.38 (0.27 to 0.55)	0.41 (0.31 to 0.64)	0.05 (0 to 0.14)	< 0.001 **	33.5 (16.8 to 58.3)	0.021 (0 to 0.048)	5.5
Diabetic Maculopathy							
None or Non-CSME (n = 30)	0.31 (0.23 to 0.41)	0.37 (0.29 to 0.61)	0.06 (0.01 to 0.17)	< 0.001 **	28.0 (19.0 to 56.0)	0.022 (0.001 to 0.061)	7.10

CSME (n = 49)	0.34 (0.22 to 0.45)	0.39 (0.30 to 0.70)	0.05 (0.01 to 014)	< 0.001 **	27.0 (15.0 to 50.0)	0.027 (0.001 to 0.057)	7.94
Visual acuity (Baseline) (LogMar)							
Good (< 0.3) (n = 48)	0.31 (0.23 to 0.40)	0.38 (0.29 to 0.56)	0.05 (0.01 to 0.12)	< 0.001 **	28.0 (17.8 to 63.8)	0.019 (0.001 to 0.042)	6.13
Poor (> 0.3) (n = 31)	0.32 (0.22 to 0.80)	0.48 (0.28 to 0.80)	0.10 (0.02 to 0.21)	< 0.001 **	27.0 (14.0 to 47.0)	0.046 (0.003 to 0.141)	14.4
Visual Acuity progression (LogMar/year)							
No progression (<0.05) (n = 56)	0.32 (0.22 to 0.40)	0.39 (0.30 to 0.55)	0.04 (0 to 0.12)	< 0.001 **	34.0 (17.5 to 59.8)	0.018 (0 to 0.042)	5.62
Progression (>0.05) (n = 23)	0.30 (0.22 to 0.45)	0.39 (0.28 to 0.97)	0.10 (0.05 to 0.22)	< 0.001 **	19.0 (15.5 to 29.5)	0.057 (0.026 to 0.124)	19.0

The median and interquartile values of FAZ size, time interval (years), and FAZ progression rate are reported. The Wilcoxon Rank-Sum Test was used for statistical analysis of the difference in FAZ area between FA at baseline and final FA. p values significant at 5% level are indicated with (*), and (**) at 1% level. FA = Fluorescein Angiogram; ETDRS = Early Treatment Diabetic Retinopathy Study; DMI = Diabetic Macular Ischaemia; FAZ = Foveal avascular zone; NPDR = Non-Proliferative Diabetic Retinopathy; PDR= Proliferative Diabetic Retinopathy; DME = Diabetic Macular Oedema; CSME = Clinically Significant Macular Oedema

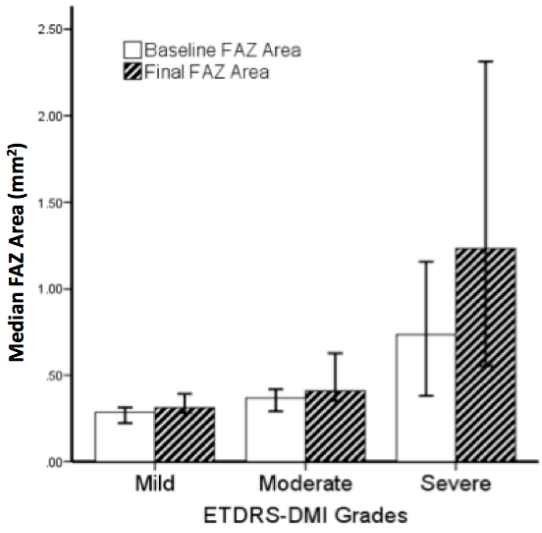

Figure 2.9. Change in foveal avascular zone stratified by diabetic macular ischaemia grade.

Bar chart showing median foveal avascular zone (FAZ) area (mm^2) and interquartile ranges for groups stratified by Early Treatment Diabetic Retinopathy – Diabetic Macular Ischaemia (ETDRS-DMI) grades "mild", "moderate", and "severe". White and black bars denote FAZ area at baseline and final FAs respectively.

2.4.2.2 Rate of FAZ area enlargement:

The overall median enlargement rate of the FAZ area was 0.023 mm^2/year (IQR, 0.001 to 0.060) **(Table 2.7)**. With a median baseline FAZ size of 0.31 mm^2, this represents a FAZ area progression rate of 7.42% per year in all eyes. The enlargement rate was also examined in six categories, according to ETDRS-DMI grade, diabetic retinopathy and maculopathy grade, baseline visual acuity, and rate of visual acuity deterioration (LogMar/year).

Enlargement of FAZ area was significantly higher in ETDRS-DMI grades: severe (0.073mm^2 (10.4%)/year) verses mild (0.021mm^2 (7.50%)/year) (p=0.02), or moderate (0.019mm^2 (5.13%)/year) (p=0.03) **(Figure 2.10)**, and in eyes which showed deterioration in visual acuity: (0.057mm^2 (19.0%)/year), verses eyes which did not (0.018mm^2 (5.62%)/year) (p=0.002). There was no significant difference in the FAZ enlargement rates in the sub categories - diabetic retinopathy (p=0.11) and

maculopathy grades (p=0.88), and baseline visual acuity (p=0.11) **(Table 2.8)**. Though not statistically significant, eyes with poor baseline VA were observed to have more than twice the progression rate (0.046mm^2 (14.4%)/year), compared to eyes with good baseline VA (0.019 mm^2 (6.13%)/year) (p=0.11). There was no significant difference in time interval between baseline and final FA in all groups analysed (p>0.24) **(Table 2.8)**.

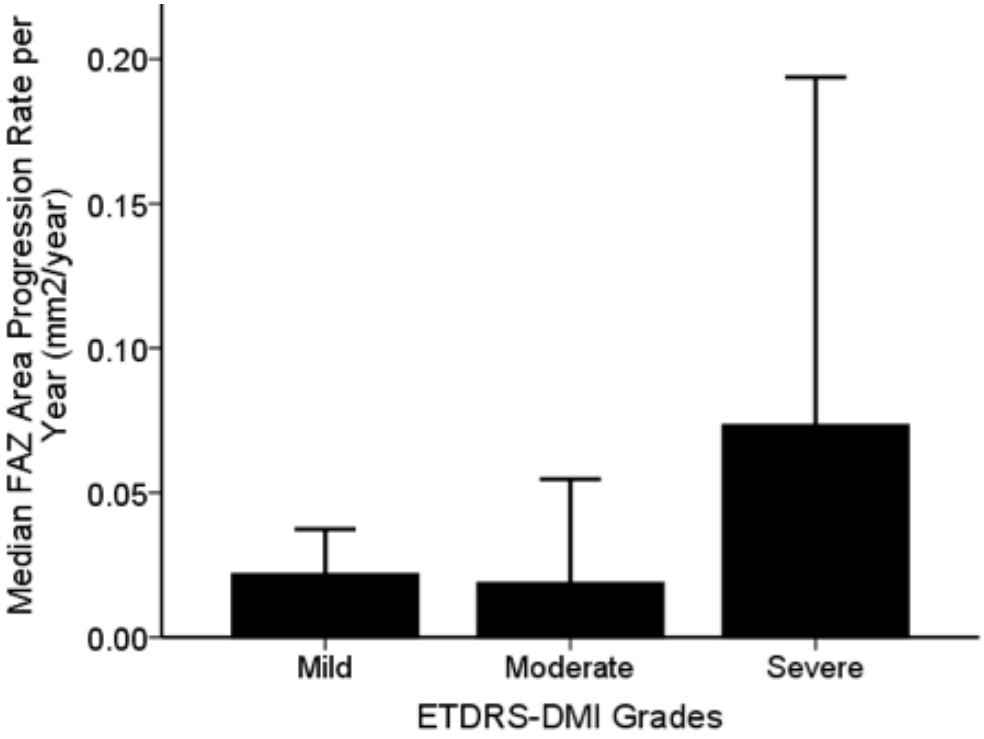

Figure 2.10. Foveal avascular zone growth rate by diabetic macular ischaemia grade.

Bar chart showing median and interquartile ranges for FAZ foveal avascular zone (FAZ) area (mm^2) enlargement or progression rate per year for groups stratified by Early Treatment Diabetic Retinopathy – Diabetic Macular Ischaemia (ETDRS-DMI) grades "mild", "moderate", and "severe".

Table 2.8: Comparison of Foveal Avascular Zone area enlargement rates (mm^2 / year) in different subgroups.

Comparison of FAZ area enlargement rates per year (mm^2 / year)	p-value
ETDRS-DMI Grade (Baseline)	
Mild vs Moderate	0.86
Mild vs Severe	0.02*
Moderate vs Severe	0.03*
Diabetic Retinopathy (Baseline)	
None or NPDR vs PDR	0.11
Diabetic Maculopathy (Baseline)	
None or non-CSME vs CSME	0.88
Visual acuity	
At baseline (LogMar): Good < 0.3 vs Poor > 0.3	0.11
Progression (LogMar/year): Progression > 0.05 vs No progression < 0.05	0.002**

The Mann-Whitney U Test (continuous variables) and χ^2 test (categorical variables) was used the assess the differences in FAZ area progression rate (mm^2 / year) between sub-categories. p values significant at 5% level are indicated with (*), and (**) at 1% level. FA = Fluorescein Angiogram; ETDRS = Early Treatment Diabetic Retinopathy Study; DMI = Diabetic Macular Ischaemia; FAZ = Foveal avascular zone; NPDR = Non-Proliferative Diabetic Retinopathy; PDR= Proliferative Diabetic Retinopathy; DME = Diabetic Macular Oedema; CSME = Clinically Significant Macular Oedema

2.4.2.3 Predictors of FAZ area enlargement:

Multivariable logistic regression models were used to assess the relationship between FAZ enlargement rate (mm^2/year) and its clinical co-variates, namely diabetic retinopathy and maculopathy grades, visual acuity, and the effects of treatment in the follow-up interval (Table 2.9). "DMI progression" was defined as a FAZ enlargement rate of greater than 0.03 mm^2/year, which is approximately represents an increase of more than 10% of the median baseline FAZ area (in all eyes) per year. Model confounders such as age, gender, eye selected, time interval between baseline and final FA (continuous variable), diabetic retinopathy, and maculopathy grades (categorical variable) were adjusted for in the final regression model.

Our multivariable logistic regression models for ETDRS-DMI grade and VA progression rates were good predictors for "DMI progression", with areas under the curve of 0.74 and 0.79 via receiver operating characteristic curve assessment respectively, and a Hosmer-Lemeshow goodness-of-fit χ^2 test of 11.6 (p=0.17), and 10.3 (p=0.24) respectively.

ETDRS-DMI grade, as a categorical measure, was a significant independent risk factor for "DMI progression". (OR=2.47, CI=1.21 to 5.05, p=0.02) This suggests that for every step increase in ETDRS-DMI severity grade, there is an approximately 2:1 OR for "DMI progression". We did not observe any association between DMI progression and the effects of retinal or macular laser treatments. At baseline, 40/79 eyes (50.6%) were treatment-naive for pan-retinal photocoagulation (PRP), and 49/79 (62.0%) for macula laser. 12 eyes had PRP laser, and 16 eyes macula laser treatment over the course of follow-up. There was no association of treatment effects with DMI progression, (OR=1.69, CI=0.51 to 5.57, p=0.39) and (OR=1.31, CI=0.40 to 4.26, p=0.65) respectively **(Table 2.9)**.

Table 2.9: Multivariable logistic regression models of Foveal Avascular Zone area progression rate (mm^2 / year) and other clinical co-variates.

Baseline measurements	Variable	OR	95% CI	p value
ETDRS-DMI Grade	Categorical	2.47	1.21 to 5.05	0.02*
Diabetic Retinopathy	Categorical	0.37	0.14 to 0.98	0.12
Diabetic Maculopathy	Categorical	1.02	0.37 to 2.82	0.12
Visual acuity (LogMar)	Continuous	3.43	0.50 to 23.5	0.10
Treatment effects: PRP	Categorical	1.69	0.51 to 5.57	0.39
Treatment effects: Macular laser	Categorical	1.31	0.40 to 4.26	0.65

Multivariable logistic regression was used for statistical analysis of the relationship between FAZ area progression rate (mm^2 / year) and clinical co-variates. Model confounders include age, gender, eye (right or left), time interval between baseline and final FA, and diabetic retinopathy and maculopathy grades. p values significant at 5% level are indicated with (*), and (**) at 1% level. FA = Fluorescein Angiogram; ETDRS = Early Treatment Diabetic Retinopathy Study; DMI = Diabetic Macular Ischaemia; NPDR = Non-Proliferative Diabetic Retinopathy; PDR= Proliferative Diabetic Retinopathy; DME = Diabetic Macular Oedema; CSME = Clinically Significant Macular Oedema; OR = Odds ratio; CI = Confidence interval.

2.4.2.4 Predictors of VA deterioration:

We also assessed whether DMI progression, was predictive of a deteriorating VA over time. Eyes which showed “DMI progression” - or an increase in FAZ area of more than 10% per year, was associated with a loss of 0.05 LogMar or 1 line of Snellen VA per year (OR=4.60, CI=1.54 to 13.7, p=0.03), independent of age, gender, eye, or retinopathy and maculopathy grade.

2.4.3 Diabetic macular ischaemia in type 1 diabetes

2.4.3.1 Patient Characteristics:

Patient attendances over a period of 24 months were screened, and 105 patients with type 1 diabetes met the inclusion criteria. 12 patients were excluded due to the presence of ocular co-morbidities, and a further 9 had fluorescein angiogram images, which were of insufficient quality to permit grading of macular ischaemia. In total, 86 eyes from 86 patients were included in the analysis. Patient demographics and clinical characteristics are listed in **Table 2.10**, and presented in two categories- eyes with and without diabetic macular ischaemia.

2.4.3.2 Baseline Characteristics:

The mean age of patients with macular ischaemia was significantly greater, 49.5 years (SD = 15.9), compared to those with no macular ischaemia, 41.6 years (SD = 14.6) (p=0.02). Eyes with macular ischaemia were also more likely to have had a vitrectomy (0/26 in eyes with “no macular ischaemia” compared to 6/54 [11.1%] in eyes “with macular ischaemia”, p<0.001). This was similarly observed with eyes that have had cataract surgery **(Table 2.10)**.

There were no eyes with retinopathy grade of “none”, 21 (24.4%) with mild to moderate nonproliferative diabetic retinopathy, 22 (25.6%) with severe nonproliferative diabetic retinopathy, and 43 (50.0%) who had either treated, or untreated proliferative diabetic retinopathy. The proportion of patients with macular ischaemia was highest in eyes with proliferative retinopathy, 35/43 eyes (81.4%), and

Table 2.10: Demographics and clinical characteristics of type 1 diabetes patients, with and without diabetic macular ischaemia.

		No Macular Ischaemia (n=26)	Macular Ischaemia (n=60)	p value
Age, years, Mean (SD)		41.6 (14.6)	49.5 (15.9)	0.02*
Gender, n, female/male		11 / 15	18 / 42	0.39
Eye, n, right/left		10 / 16	37 / 23	0.08
History of Diabetic Vitrectomy, n, yes / no		0 / 26	6 / 54	0.23
History of Cataract Surgery, n, yes / no		1 / 25	6 / 54	0.37
FAZ area, mm², median (IQR)		0.15 (0.10 to 0.19)	0.32 (0.25 to 0.44)	< 0.001**
Visual Acuity (LogMar), median (IQR)		0 (-0.1 to 0.2)	0.2 (0 to 0.5)	0.007**
Retinopathy Grades				
No Diabetic Retinopathy (n=0)	(%)			
Mild-Moderate NPDR (n=21) (24.4%)	(%)	9 (42.9)	12 (57.1)	0.03*
Severe NPDR (n=22) (25.6%)	(%)	9 (40.9)	13 (59.1)	
PDR, treated and untreated (n=43) (50.0%)	(%)	8 (18.6)	35 (81.4)	
Maculopathy Grades				
No DME / CSME (n=44)	(%)	12 (27.3)	32 (72.7)	
DME (Non CSME) (n=23)	(%)	10 (43.5)	13 (56.5)	0.24
CSME, both treated and untreated (n=19)	(%)	4 (21.1)	15 (78.9)	
Paramacular ischaemia				
Papillomacular ischaemia (n=22)	(%)	3 (13.6)	19 (86.4)	0.0001**
Temporal ischaemia (n=45)	(%)	8 (17.8)	37 (82.2)	0.0001**

FAZ= Foveal Avascular Zone; NPDR = Non-Proliferative Diabetic Retinopathy; PDR= Proliferative Diabetic Retinopathy; DME = Diabetic Macular Oedema; CSME = Clinically Significant Macular Oedema; SD = Standard Deviation; IQR = Interquartile range. p values significant at 5% level are indicated with (*), and (**) at 1% level.

was significantly different between all three groups (p=0.03) **(Table 2.10)**. There was no difference in proportion of eyes with macular ischaemia, between diabetic maculopathy grades (p=0.24).

2.4.3.3 Prevalence of Diabetic Macular Ischaemia in type 1 diabetes:

In the 86 eyes analysed, 26 eyes (30.2%) had none, 13 (15.1%) questionable, 28 (32.6%) mild, 10 (11.6%) moderate, and 9 (10.5%) had severe macular ischaemia grades.

Foveal avascular zone areas increased with severity of macular ischaemia: The median foveal avascular zone area was observed to increase with grades of macular ischaemia severity. Median foveal avascular zone areas were 0.15mm^2 (interquartile range [IQR], 0.10 to 0.19) in "none", 0.27mm^2 (IQR, 0.18 to 0.30) in "questionable", 0.30mm^2 (IQR, 0.23 to 0.37) in "mild", 0.40mm^2 (IQR, 0.32 to 0.50) in "moderate", and 0.82mm^2 (IQR: 0.48 to 1.15) in "severe" macular ischaemia grades. Highly significant differences between median foveal avascular zone areas were seen across all grades of macular ischaemia ($p<0.001$).

Prevalence of temporal and papillomacular ischaemia: The area of temporal and PM areas of ischaemia were quantified as previously described. Temporal ischaemia was present in 45/86 eyes (52.3%), and papillomacular ischaemia in 22/86 (25.6%). The median area of temporal ischaemia was 0.60mm^2 (IQR, 0.17 to 1.69), and 0.033 mm^2 (IQR, 0.016 to 0.069) in papillomacular ischaemia. Both temporal and papillomacular ischaemia showed modest correlations to foveal avascular zone area measurements ($\rho=0.38$, $p<0.001$, and $\rho=0.27$, $p=0.013$ respectively), and were more prevalent in establish ischaemia (i.e. ETDRS defined macular ischaemia grades mild, moderate and severe). Temporal ischaemia was present in 31/47 eyes (66.0%), in the "mild to severe" macular ischaemia grades, compared to 14/47 eyes (35.9%) in "none or "questionable". This was similarly observed in papillomacular ischaemia, which

was present in 16/39 eyes (34.0%), in the “mild to severe” macular ischaemia grades, compared to 6/39 eyes (15.4%) in “none or “questionable”.

2.4.3.4 Clinical significance of macular ischaemia in type 1 diabetes:

Multivariable logistic regression models were also used to assess the relationships between age, visual acuity and macular ischaemia. Model confounders such as gender, eye selected, diabetic retinopathy and maculopathy grades (categorical variables), and visual acuity (continuous variable), were adjusted for in the final regression model. The presence of “macular ischaemia” was defined as ETDRS defined grades of questionable, mild, moderate, or severe. Our multivariable logistic regression models for age were good predictors for the presence of “macular ischaemia”, with areas under the curve of 0.87 (standard error [SE]=0.04, 95% confidence interval [CI]=0.78 to 0.93) via receiver operating characteristic curve assessment, and a Hosmer-Lemeshow goodness-of-fit χ^2 test of 7.78 (p=0.46).

Relationship between age and macular ischaemia: The mean age difference between patients with and without macular ischaemia was 7.9 years, and of the patients with macular ischaemia, 51/60 (85.0%) were aged greater than 30 years, compared to 18/26 (69.2%) in those younger than 30 years. (χ^2=4.32, p=0.04) **(Figure 2.11)**. Furthermore, univariate analysis showed that age, per decade increase, was significantly predictive of any grade of macular ischaemia (OR=1.42, 95% CI=1.05 to 1.93, p=0.02). This association remained significant, and was strengthened in multivariate models with severity of concurrent diabetic retinopathy, and visual acuity (OR=2.30, 95% CI=1.27 to 4.16, p=0.006) **(Table 2.11)**.

Relationship between visual acuity, with paramacular and macular ischaemia: We observed a significant difference between the median LogMAR visual acuity in eyes with “no macular ischaemia”, 0 (IQR: -0.1 to 0.2) (Snellen 20/20), compared to eyes with “macular ischaemia” 0.2 (IQR: 0 to 0.5) (Snellen 20/32) (p=0.007) **(Table 2.11)**. In univariate analysis, a loss of visual acuity was associated with macular ischaemia (OR=1.35, 95% CI=1.07 to 1.70, p=0.01). Eyes with a visual acuity of greater

than 0.3 LogMar (6/12 Snellen), were also associated with macular ischaemia (b=2.06, SE=0.71, p=0.004) and diabetic maculopathy (b=0.83, SE=0.34, p=0.01) (Table 3). No associations were observed between visual acuity and foveal avascular zone area (ρ=0.062, p=0.57), temporal (ρ=0.030, p=0.84), or papillomacular ischaemia area (ρ=0.048, p=0.84).

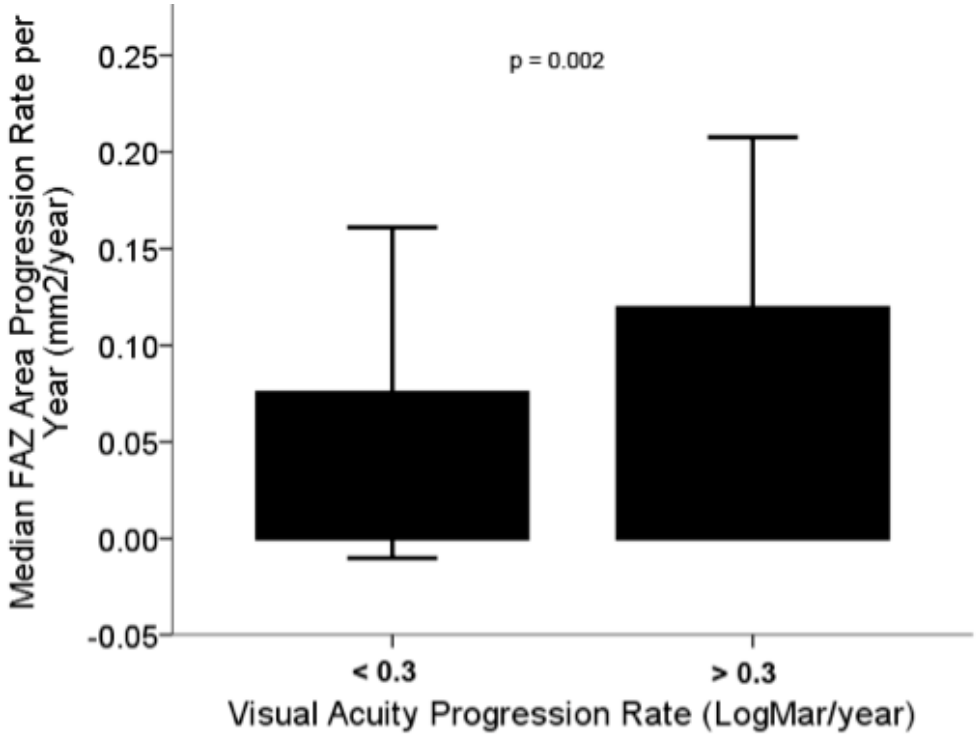

Figure 2.11. Proportion of eyes with diabetic macular ischaemia by age in type 1 diabetes

Bar chart of the number of eyes with and without diabetic macular ischaemia (DMI), in patients aged greater, or less than 30 years. Chi-squared test showed a significantly higher proportion of eyes with "DMI", in those greater than 30 years of age (χ^2=4.32, p=0.04).

Table 2.11: Multivariable logistic regression models for the diagnosis of diabetic macular ischaemia in type 1 diabetes, per decade increase in age, and other clinical co-variates.

	Variable	OR	95% CI	p value
Age (per decade increase)	Categorical	2.30	1.27 to 4.16	0.006**
Visual acuity (LogMAR)	Continuous	1.40	1.06 to 1.83	0.02*
Diabetic Retinopathy	Categorical	2.79	1.13 to 6.89	0.03*
Diabetic Maculopathy	Categorical	0.52	0.23 to 1.20	0.13
Temporal ischaemia	Categorical	3.26	0.84 to 12.6	0.09
Papillomacular ischaemia	Categorical	4.45	0.77 to 25.8	0.10
Gender	Categorical	1.64	0.45 to 5.98	0.46

Multivariable logistic regression was used for statistical analysis of the relationship between eyes with a diagnosis of any grade of diabetic macular ischaemia and it's clinical co-variates. The significance level for the overall model fit was p=0.006. p values significant at 5% level are indicated with (*), and (**) at 1% level. OR=Odds Ratio; 95% CI=95% Confidence Interval.

2.4.4 Retina vessel calibre measurements in diabetic macular ischaemia

Of 53 patients examined, 18 (34%), 18 (34%) and 17 (32%) had none/mild, moderate and severe DMI respectively. There were 23 (38%) females, 10 (19%) with previous PRP, 6 (11%) with NVE, 4 (7%) with NVD) and mean age was 62.3 years (range 27 to 96 years).

Table 2.12 shows that persons with moderate or severe DMI had narrower mean retinal arteriolar calibre than persons with no DMI (140.6 µm 95% Confidence Interval (CI) 134.7, 146.4 vs 150.7 µm, 95% CI 142.5, 158, p=0.04) The association of narrower arterioles with moderate/severe DMI remained after multivariate adjustment for age, gender, previous panretinal photocoagulation and neovascularisation at the disc and elsewhere (adjusted mean retinal arteriolar calibre of 140.7 µm 95% CI 135.5, 146.0 vs 150.4 µm, 95% CI 142.9, 157.8, p=0.04) Increasing severity of DMI was also associated with narrower arterioles, with multivariate adjusted mean arteriolar calibres of 150.6, 142.1 and 139.1 µm in participants with none/mild, moderate and severe DMI respectively.(p trend=0.04) Retinal venular calibre and arteriole to venule ratio (AVR) were not associated with DMI, with venular calibre 240.6 µm 95% CI 227.3, 254.0 and AVR 0.63 95% CI 0.60, 0.66 in persons with no DMI and venular calibre 233.0 µm 95% CI 223.4, 242.6 µm and AVR 0.61 95% CI 0.58, 0.63 in persons with moderate/severe DMI, respectively. Additional adjustment for NSC diabetic retinopathy grade did not change these results. Excluding patients with PRP (n=10) from our analyses attenuated the statistical significance of the results but did not change the direction of effect.(adjusted arteriolar calibres of 153.3, 146.9 and 143.5 µm in participants with none/mild, moderate and severe DMI, respectively.(p trend 0.09)).

Increased FAZ (greatest dimension and area of ischaemia) were also associated with narrower arteriolar calibre **(Table 2.13)**. Each standard deviation decrease in arteriolar calibre was associated with increases of 0.21 mm (95% CI 0.05, 0.38) in diameter and 0.19 mm^2 (95% CI 0.04, 0.33) in area (p=0.01 for both, **Figures 2.12 and 2.13**). **Figure 2.13** shows that in our sample, 77% of persons in the

narrowest quartiles of arteriolar calibre had DMI, compared to 38% in persons in the largest quartiles. Venular calibre and AVR were not associated with FAZ diameter or area.

Table 2.12: Retinal vessel calibres by severity of diabetic macular ischaemia.

Diabetic macular ischaemia severity		Mean arteriolar calibre, µm (95% CI)		Mean venular calibre, µm (95% CI)		Mean arteriole to venule ratio (AVR)	
	N	Unadjusted	Multivariate Adjusted	Unadjusted	Multivariate Adjusted	Unadjusted	Multivariate Adjusted
None	18	150.7 (142.5, 158.9)	150.6 (143.0, 158.1)	240.6 (227.4, 253.9)	243.1 (230.3, 256.0)	0.63 (0.60, 0.66)	0.62 (0.59, 0.66)
Moderate	18	142.4 (134.2, 150.7)	142.1 (134.9, 149.3)	238.8 (225.6, 252.1)	238.8 (226.6, 251.1)	0.60 (0.57, 0.63)	0.60 (0.56, 0.63)
Severe	17	138.6 (130.1, 147.1)	139.1 (131.1, 147.1)	226.8 (213.2, 240.5)	224.2 (210.6, 237.7)	0.61 (0.58, 0.65)	0.62 (0.59, 0.66)
p-trend		0.04	0.04	0.23	0.12	0.25	0.64
None	18	150.7 (142.5, 158.9)	150.4 (142.9, 157.8)	240.6 (227.3, 254.0)	242.1 (229.1, 255.1)	0.63 (0.60, 0.66)	0.63 (0.59, 0.66)
Moderate/Severe	35	140.6 (134.7, 146.4)	140.7 (135.5, 146.0)	233.0 (223.4, 242.6)	232.2 (223.2, 241.3)	0.61 (0.58, 0.63)	0.61 (0.59, 0.63)
Difference		10.1 (0.1, 20.2)	9.6 (0.2, 19.1)	7.6 (-8.8, 24.0)	9.9 (-6.6, 26.3)	0.03 (-0.01, 0.07)	0.02 (-0.03, 0.06)
p-value		0.04	0.04	0.36	0.23	0.18	0.44

Table 2.13: Changes in retinal vessel calibre and size of foveal avascular zone.

Size of foveal avascular zone	Per SD decrease in arteriolar calibre		Per SD decrease in venular calibre		Per SD decrease in arteriole to venule ratio (AVR)	
	Unadjusted	Multivariate adjusted	Unadjusted	Multivariate adjusted	Unadjusted	Multivariate adjusted
Greatest linear dimension (mm)	0.17 (0.04, 0.31)	0.21 (0.05, 0.38)	0.11 (-0.03, 0.26)	0.15 (-0.001, 0.31)	0.08 (-0.06, 0.22)	0.04 (-0.12, 0.19)
p-value	0.01	0.01	0.11	0.06	0.28	0.62
Area of ischaemia (mm^2)	0.15 (0.03, 0.27)	0.19 (0.04, 0.33)	0.09 (-0.04, 0.21)	0.12 (-0.02, 0.26)	0.08 (-0.05, 0.20)	0.04 (-0.09, 0.18)
p-value	0.02	0.01	0.17	0.08	0.22	0.53

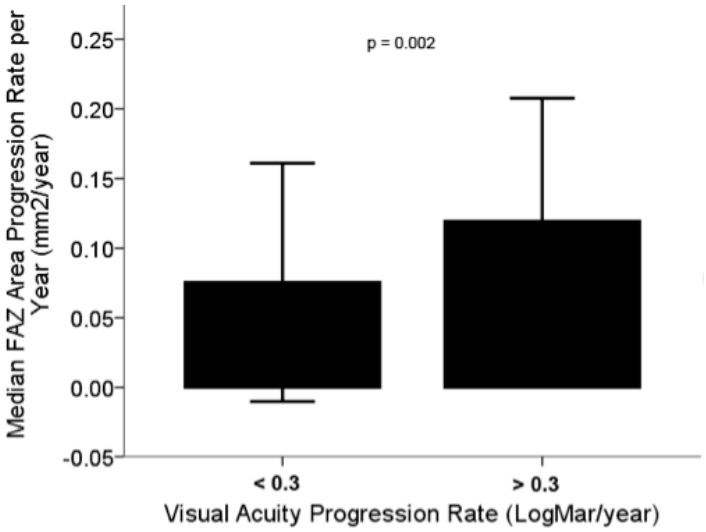

Figure 2.12. Relationship between foveal avascular zone enlargement and visual acuity deterioration in type 1 diabetes.

Bar chart showing median and interquartile ranges for FAZ foveal avascular zone (FAZ) area (mm^2) enlargement or progression rate per year for groups stratified by visual acuity progression rate (LogMar / year) – < 0.3 and > 0.3.

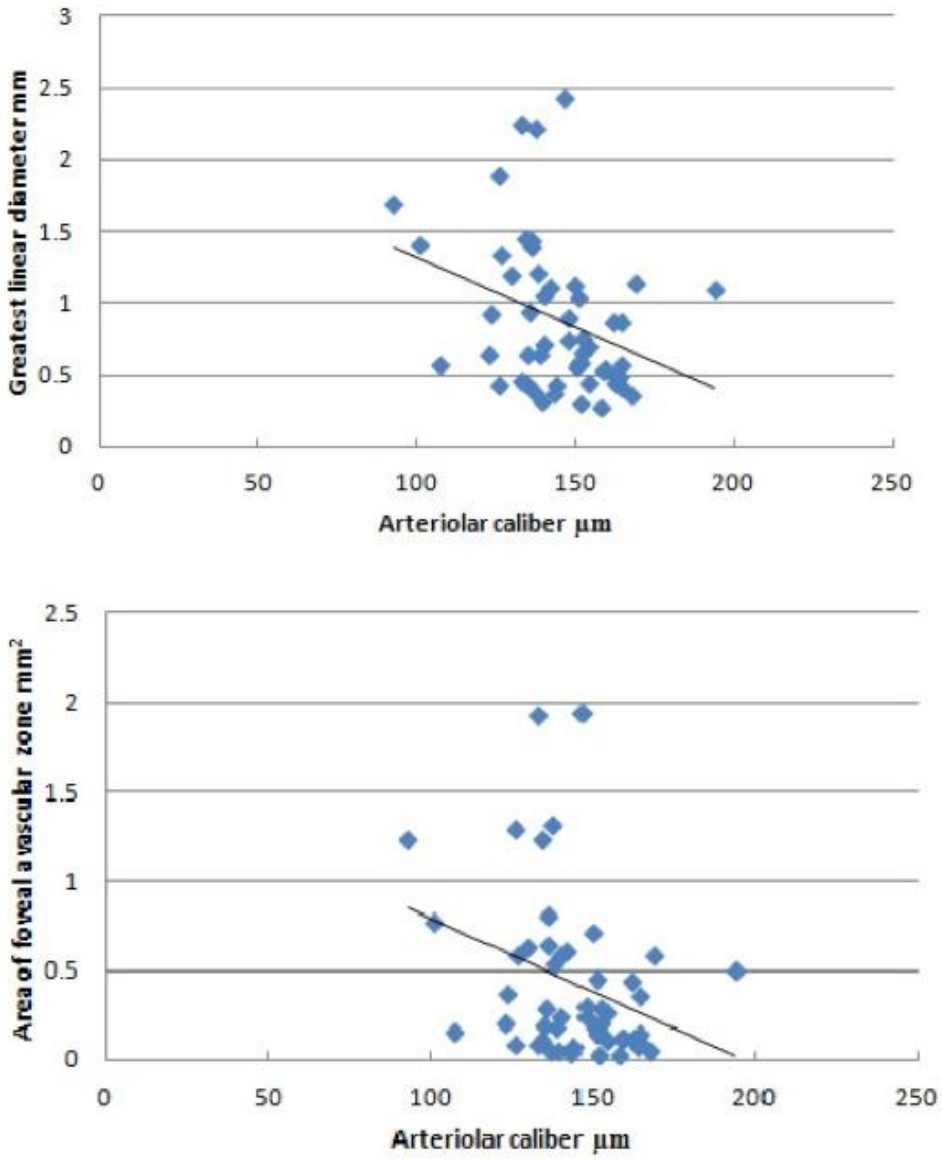

Figure 2.13. Relationship between foveal avascular zone size and retinal arteriolar calibre.

Scatterplots showing the relationship between the foveal avascular zone and arteriolar calibre in eyes with diabetic macular ischaemia. The greatest linear diameter of the foveal avascular zone is plotted against arteriolar calibre in the top figure (Pearsons r=0.34, p=0.01), and in the bottom figure, foveal avascular zone area is plotted against arteriolar calibre (Pearsons r=0.32, p=0.02.)

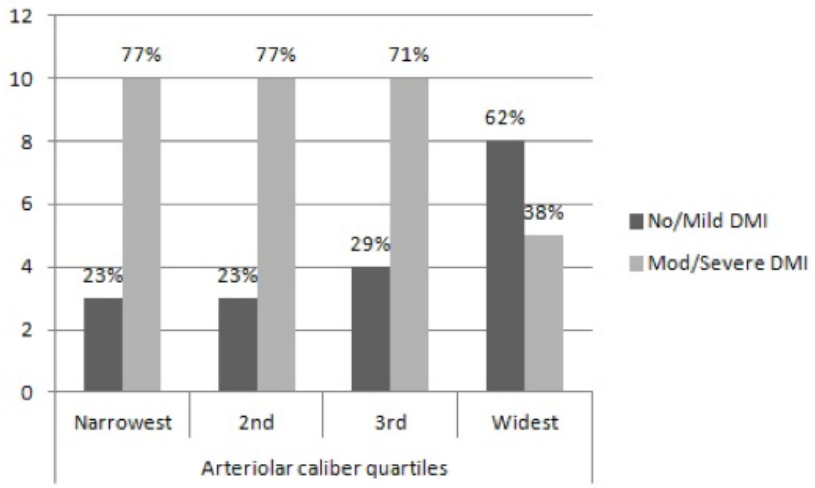

Figure 2.14. Comparing DMI severity grade by retinal arteriolar calibre.

Bar chart comparing the proportion of eyes with different severity grades of diabetic macular ischaemia (DMI) by arteriolar calibre quartiles. Bars represent the number of persons with none/mild (dark grey) compared to moderate/severe diabetic macular ischaemia (light grey).

2.4.5 Repeatability and Reproducibility of OCT-derived measurements in diabetic retinopathy

2.4.5.1 Patient Characteristics:

51 eyes of 51 patients with a diagnosis of type 2 diabetes with a mean age of 60.1 years were included in this study.

2.4.5.2 Repeatability of Measurements:

The repeatability of retinal and choroidal measurements was assessed in subset of 20 eyes randomly selected from the study cohort. Each image set was manually segmented twice by each "trained" grader. (The junior grader received training prior to both episodes of segmentation) The CR (µm or mm^3), CR expressed as a percentage of mean thickness or volume (CR/Mean), and reliability (ICC) for all indices measured in the TMC and FCS are presented in **Tables 2.14, 2.15**.

Repeatability of thickness and volume measurements ***(Tables 2.14, 2.15)***:

Thickness measurements of the TMC showed better repeatability than those at the FCS **(Figure 2.15)**. The CR of both retinal and choroidal thicknesses ranged from 19.2 to 35.2 μm in the TMC, and 26.9 to 49.0 μm in the FCS. TMC thickness measurements were also more reliable in retinal, total choroidal, and Sattler's medium vessel layers. The lowest CR/Mean percentages (greatest repeatability) were observed in the TMC the retina and total choroidal thickness measurements. (6.7 and 11.8 respectively). Segmentation for choroidal sublayers, Haller's large vessel and Sattler's medium vessel layers showed less repeatability, with higher CR / Mean percentages. Repeatability of volume measurements were similar to that of thickness measurements, as observed in the CR / Mean percentages.

The reliability of both thickness and volume measurements, as expressed by the intraclass correlation coefficient (ICC), showed good reliability (ICC > 0.8) across all layers, apart from measurements in Haller's large vessel layer at the FCS (thickness: ICC 0.78, Volume: ICC 0.76).

Table 2.14: Repeatability and Reliability of Retinal and Choriodal Thickness Measurements in Patients with Type 2 Diabetes

Thickness Measurements (μm) (Graders 1 & 2)	CR (μm)	CR / Mean (%)	ICC	95% CI
Retina				
TMC	19.2	6.7	0.98	0.95 to 0.99
FCS	49.0	18.1	0.98	0.95 to 0.99
Choroid				
TMC	26.9	11.8	0.97	0.94 to 0.99
FCS	48.3	19.6	0.93	0.83 to 0.97
Haller's Layer				
TMC	35.2	29.6	0.86	0.68 to 0.94
FCS	38.2	29.7	0.78	0.53 to 0.91
Sattler's Layer				
TMC	29.2	26.0	0.89	0.73 to 0.95
FCS	39.0	32.2	0.88	0.73 to 0.95

TMC = Total macular circle (ETDRS areas 1-9), FCS = Foveal centre subfield (ETDRS area 9), Haller's layer = Haller's large vessel layer of the choroid, Sattler's layer = Sattler's medium vessel layer of the choroid, CR = Coefficient of repeatability, CR/Mean = The coefficient of repeatability, expressed as a percentage of the mean, ICC = Intraclass correlation coefficient, CI = confidence interval.

Table 2.15. Repeatability and Reliability of Retinal and Choriodal Volume Measurements in Patients with Type 2 Diabetes

Volume Measurements (mm^3) (Graders 1 & 2)	CR (mm^3)	CR / Mean (%)	ICC	95% CI
Retina				
TMC	0.64	8.1	0.97	0.94 to 0.99
FCS	0.04	18.7	0.98	0.95 to 0.99
Choroid				
TMC	0.83	13.1	0.97	0.92 to 0.99
FCS	0.04	20.6	0.92	0.80 to 0.97
Haller's Layer				
TMC	1.03	31.4	0.85	0.66 to 0.94
FCS	0.03	29.7	0.76	0.48 to 0.90
Sattler's Layer				
TMC	0.80	25.8	0.89	0.74 to 0.95
FCS	0.03	31.4	0.88	0.71 to 0.95

TMC = Total macular circle (ETDRS areas 1-9), FCS = Foveal centre subfield (ETDRS area 9), Haller's layer = Haller's large vessel layer of the choroid, Sattler's layer = Sattler's medium vessel layer of the choroid, CR = Coefficient of repeatability, CR/Mean = The coefficient of repeatability, expressed as a percentage of the mean, ICC = Intraclass correlation coefficient, CI = confidence interval.

2.4.5.3 Reproducibility of Measurements:

*Reproducibility of retinal and choroidal measurements **(Tables 2.16, 2.17)**:* The reproducibility of thickness and volume measurements between both trained graders are displayed in **Table 2.16** (thickness) and **Table 2.17** (volume) for all retinal and choroidal layers. Bland-Altman plots were used to illustrate agreement between graders **(Figures 2.15, 2.16, 2.17, and 2.18)**. No significant changes were observed with interobserver variability for the range of retinal and choroidal measurements.

To examine whether the 95% limits of agreements were significantly different between observers, the variance of the interobserver measurement differences were calculated and the F statistic (variance ratio) presented **(Table 2.18)**. The variance ratio between graders was not statistically significant in all layers. However, the data showed a trend towards a higher variance ratio in the choroidal sub-layers quantified at the FCS. TMC measurements showed similar variance ratios in all layers.

Factors which may affect agreement were also analysed. A univariate generalised linear model was fitted to the data, with the difference in thickness measurements between graders as the dependent variable, and retinopathy grade, maculopathy grade, age, gender, and visual acuity as co-variates. Visual acuity (VA) was the only factor which showed significant association with retinal and choroidal thickness measurement difference between graders **(Table 2.18)**. There was no significant association in the choroidal sublayers. Scatter plot analysis of VA and LoA did not reveal any association between these two factors **(Figure 2.19)**.

*The effect of training on reproducibility of measurements **(Table 2.19)**:* As expected, the mean intergrader differences were reduced after training. This was most apparent in measurements of the choroid and its sublayers.

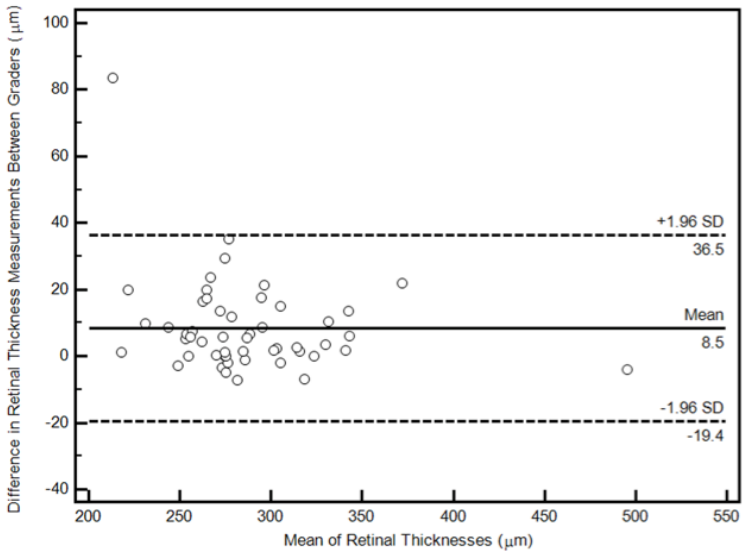

Figure 2.15. Reproducibility of OCT-derived retinal thickness

Bland-Altman plot illustrating the reproducibility of retinal thickness measurements. Mean difference between graders, 8.5 µm; 95% confidence intervals, -19.4 to 36.5 µm. The variance ratio (F statistic) of intergrader differences showed no significant difference between graders. (p=0.91 (TMC), p=0.94 (FCS))

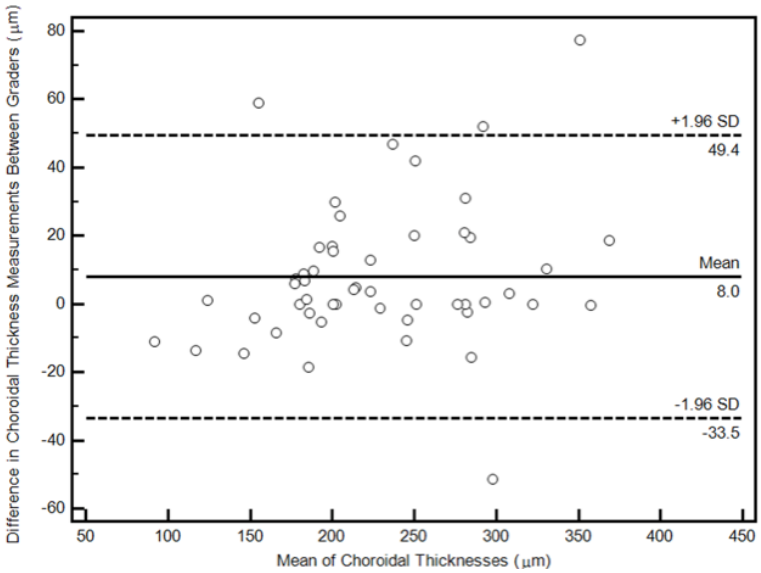

Figure 2.16. Reproducibility of OCT-derived choroidal thickness

Bland-Altman plot illustrating the reproducibility of total choroidal thickness measurements. Mean difference between graders, 8.0 µm; 95% confidence intervals, -33.5 to 49.4 µm. The variance ratio (F statistic) of intergrader differences showed no significant difference between graders. (p=0.94 (TMC), p=0.68 (FCS))

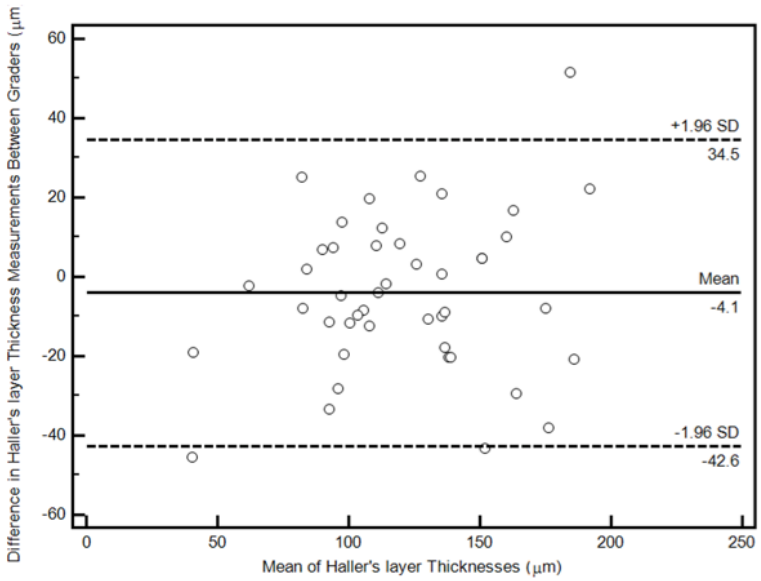

Figure 2.17. Reproducibility of OCT-derived Haller's layer measurements

Bland-Altman plot illustrating the reproducibility of Haller's large vessel layer thickness measurements. Mean difference between graders, -4.1 µm; 95% confidence intervals, -42.6 to 34.5 µm. The variance ratio (F statistic) of intergrader differences showed no significant difference between graders. (p=0.98 (TMC), p=0.49 (FCS)

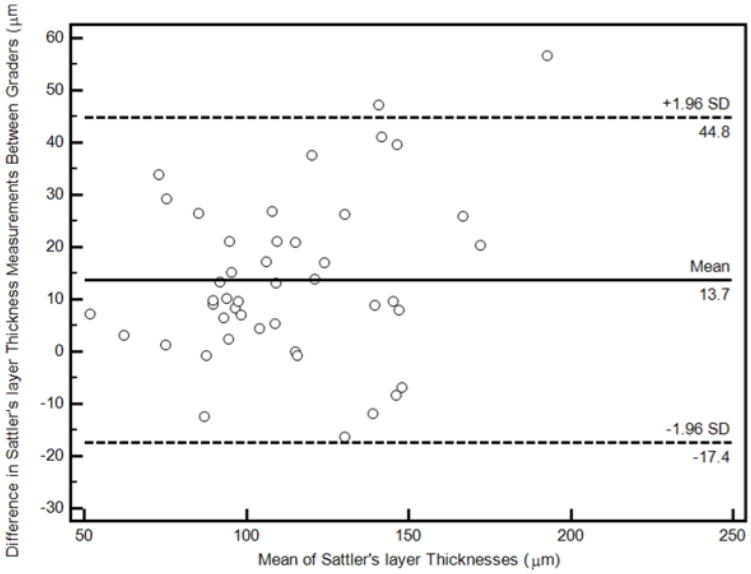

Figure 2.18. Reproducibility of OCT-derived Sattler's layer thickness

Bland-Altman plot illustrating the reproducibility of Sattler's medium vessel layer thickness measurements. Mean difference between graders, 13.7 µm; 95% confidence intervals, -17.4 to 44.8 µm. The variance ratio (F statistic) of intergrader differences showed no significant difference between graders. (p=0.88 (TMC), p=0.45 (FCS))

Table 2.16. Reproducibility of Retinal and Choroidal Thickness Measurements in Patients with Type 2 Diabetes.

Layers Measured (Thickness)	Interobserver Mean Difference (μm)	95% CI (μm)	95% Limits of Agreement (μm)
Retina			
TMC	8.52	4.51 to 12.5	27.9
FCS	2.80	-4.26 to 9.87	48.8
Choroid			
TMC	7.99	2.04 to 13.9	41.5
FCS	9.56	1.85 to 17.3	53.1
Haller's Layer			
TMC	-4.05	-9.96 to 1.86	38.6
FCS	-2.12	-10.9 to 6.63	56.5
Sattler's Layer			
TMC	13.7	8.95 to 18.5	31.1
FCS	14.0	7.16 to 20.8	44.0

TMC = Total macular circle, FCS = Foveal centre, Haller's layer = Haller's large vessel layer of the choroid, Sattler's layer = Sattler's medium vessel layer of the choroid, ICC = Intraclass correlation coefficient, CI = confidence interval.

Table 2.17. Reproducibility of Retinal and Choroidal Volume Measurements in Patients with Type 2 Diabetes.

Layers Measured (Volume) (mm^3)	Interobserver Mean Difference (mm^3)	95% CI (mm^3)	95% Limits of Agreement (mm^3)
Retina			
TMC	0.36	0.18 to 0.54	1.26
FCS	0.00	-0.0035 to 0.0071	0.04
Choroid			
TMC	0.31	0.10 to 0.52	0.43
FCS	0.01	0.0013 to 0.014	0.04
Haller's Layer			
TMC	-0.06	-0.24 to 0.13	1.21
FCS	-0.11	-0.14 to -0.09	0.17
Sattler's Layer			
TMC	0.42	0.28 to 0.56	0.92
FCS	0.01	0.0057 to 0.017	0.03

TMC = Total macular circle, FCS = Foveal centre, Haller's layer = Haller's large vessel layer of the choroid, Sattler's layer = Sattler's medium vessel layer of the choroid, ICC = Intraclass correlation coefficient, CI = confidence interval.

Table 2.18. The Variance Ratio (*F* Statistic) of Intergrader Differences in Retinal and Choroidal Measurements

Layers Measured (Graders 1 & 2)	*F* Test	*p* Value	*F* Test	*p* Value
	Thickness measurements		Volume measurements	
Retina				
TMC	1.18	0.56	1.03	0.91
FCS	1.00	1.00	1.02	0.94
Choroid				
TMC	1.14	0.64	1.02	0.94
FCS	1.15	0.62	1.12	0.68
Haller's Layer				
TMC	1.22	0.50	1.01	0.98
FCS	1.32	0.36	1.23	0.49
Sattler's Layer				
TMC	1.26	0.44	1.05	0.88
FCS	1.32	0.35	1.26	0.45

TMC = Total macular circle (ETDRS areas 1-9), FCS = Foveal centre subfield (ETDRS area 9), Haller's layer = Haller's large vessel layer of the choroid, Sattler's layer = Sattler's medium vessel layer of the choroid, *F* test = variance ratio

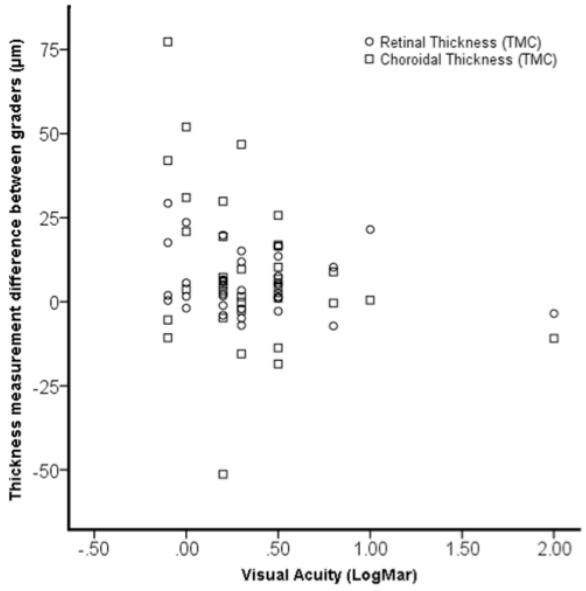

Figure 2.19. Reproducibility of OCT-derived choroidal thickness measurements

Bland-Altman plot illustrating the reproducibility of total choroidal thickness measurements. Mean difference between graders, 8.0 µm; 95% confidence intervals, -33.5 to 49.4 µm. The variance ratio (F statistic) of intergrader differences showed no significant difference between graders. (p=0.94 (TMC), p=0.68 (FCS))

Table 2.19. The Effect of Manual SegmentationTraining on the Reproducibility of Retinal and Choroidal Thickness Measurements.

Layers Measured (Thickness)		Before Training			After Training		
		Intergrader Mean Difference (µm)	95% CI (µm)	95% Limits of Agreement (µm)	Intergrader Mean Difference (µm)	95% CI (µm)	95% Limits of Agreement (µm)
Retina							
	TM	-5.98	-9.13 to -	8.63	4.07	-2.64 to	18.4
	FCS	-4.44	-9.25 to	13.2	-8.96	-32.7 to	65.0
Choroid							
	TM	23.7	11.3 to	34.0	12.3	0.29 to	32.8
	FCS	33.1	9.09 to	65.8	21.3	0.34 to	57.4
Haller's							
	TM	-14.3	-32.4 to	49.6	-4.74	-19.0 to	39.0
	FCS	-6.74	-38.1 to	85.9	5.90	-17.9 to	65.3
Sattler's							
	TM	37.1	24.0 to	35.7	16.7	5.31 to	31.3
	FCS	39.1	23.6 to	42.5	14.7	3.20 to	31.6

TMC = Total macular circle, FCS = Foveal centre subfield, Haller's layer = Haller's large vessel layer of the choroid, Sattler's layer = Sattler's medium vessel layer of the choroid, CI = confidence interval.

2.4.6 Analysis of diabetic macular ischaemia using OCT-derived measurements in diabetic retinopathy

2.4.6.1 **Baseline Characteristics:**

One hundred consecutive patients with Type 2 diabetes mellitus were included in this study. The retinal nerve fibre layer, inner and outer retinal thickness measurements were analysed. **(Figure 2.20)** Of these, 60 patients underwent "enhanced depth imaging" (EDI).(46) In these cases, analysis of the choroid was also performed.

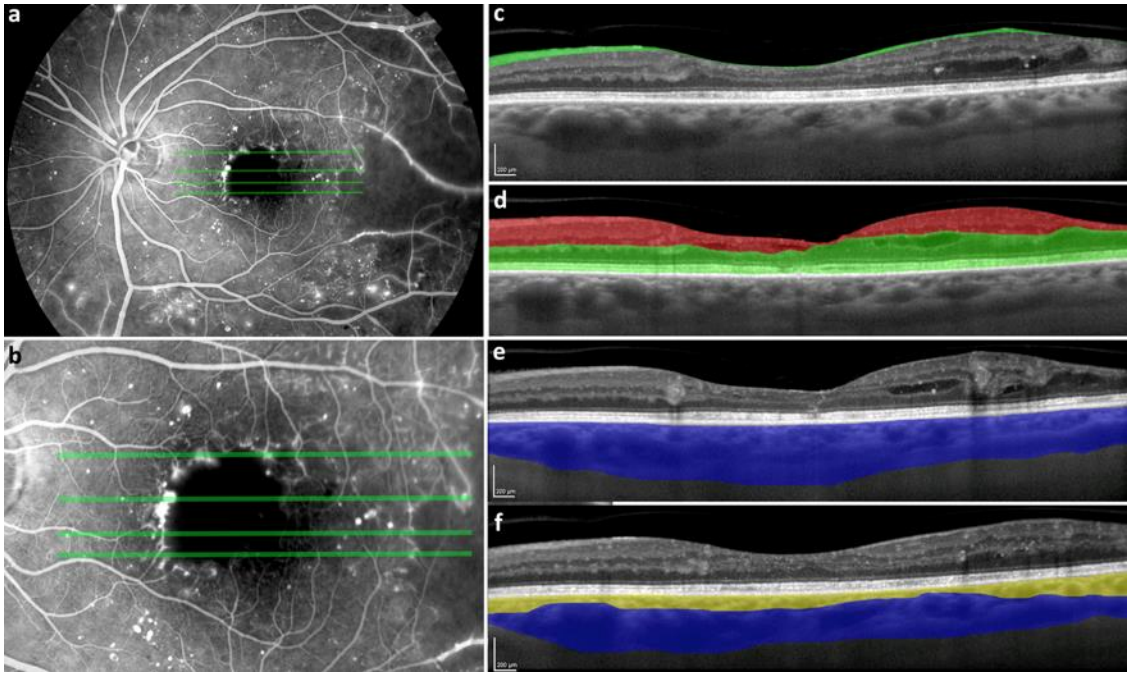

Figure 2.20. Segmentation of retinal and choroidal layers

(a) and (b) are examples of a fluorescein angiograph in an eye with diabetic macular ischaemia. Green horizontal lines represent, optical coherence tomography B-scans (c-f), acquired using the enhanced depth optical coherence tomographic protocol. (c) The retinal nerve fibre layer area (green) was segmented in 13 B-scans acquired over the macular. (d) Similarly, measurements of the inner retina (red), outer retina (green), (e) total choroid (blue), (f) Sattler's medium vessel layer (yellow), and Haller's large vessel layer (blue) were taken.

Twelve patients did not have FA images of sufficient quality to permit grading of macular ischaemia in either eye. These patients were excluded from analysis. From each patient, we selected the eye with the greatest macular ischaemia severity, using permutated block randomization where macular ischaemia severity was symmetrical (n=32). This was to ensure inclusion of patients with a greater diabetic macular ischaemia severity within our patient cohort.

For the 100 eyes that were analysed, the male to female ratio was 1:3, and mean patient age was 62 years (standard deviation (SD): 12). The proportions of eyes with ETDRS defined grades of retinopathy and maculopathy are presented in **Table 2.20**. In the 88 eyes graded for macular ischaemia, 34 eyes (38.6%) had none, 12 (13.6%) questionable, 23 (26.1%) mild, 6 (6.8%) moderate, and 13 (14.8%) severe ETDRS-defined diabetic macular ischaemia grades **(Table 2.20)**.

2.4.6.2 The Effects of Ischaemia on Retinal Morphology:

*Coexistence of diabetic macular oedema with macular ischaemia **(Table 2.21)**:* DME, defined as a foveal retinal thickness of greater than 275µm, was present in 49/100 eyes (49%). The proportions of DME, within different diabetic macular ischaemia grades, are presented in **Table 2.20**. The proportion of eyes with any grade of macular ischaemia was comparable in both DME subgroups (55.6% "with DME" verses 44.4% "without DME"). There were no significance differences in age or gender, between both macular ischaemia or DME subgroups.

*Outer retinal thickness measurements in diabetic macular ischaemia **(Table 2.22)**:* In the analysis of all eyes, a trend towards a negative correlation was observed between FAZ area and retinal thickness measurements (r=-0.19, p=0.07). However, we observed that outer retina measurements significantly thicker at the FCS in eyes "with macular ischaemia" (167.4 ± 18.5 µm) compared to eyes with "no macular ischaemia" (150.4 ± 31.4 µm) (p=0.04). When eyes with DME were excluded, the outer retina was significantly thinner in eyes "with macular ischaemia" (223.1 ± 31.2 µm) compared to eyes with "no macular ischaemia" (244.9 ± 37.2 µm) (p=0.007).

Inner retinal measurements were not significantly different between groups.

Correlation of retinal nerve fibre layer thickness with area of the foveal avascular zone **(Table 2.22)**: We analysed the RNFL thickness measurements in two groups – "all eyes" with FAZ measurements (n=88), and in eyes "without DME" (n=39).

Table 2.20. Baseline demographic and clinical characteristics of patients in OCT-derived measurement in diabetic macular ischaemia study.

Clinical Features		
Age	n (SD)	62 (12)
Gender	M:F	1.3
Diabetic retinopathy grade (n=100)		
No DR	n	5
NPDR	n	54
PDR	n	41
Diabetic maculopathy grade (n=100)		
None	n	32
DME	n	30
CSME	n	38
ETDRS-DMI grade		
None	n (%)	34 (38.6)
Questionable	n (%)	12 (13.6)
Mild	n (%)	23 (26.1)
Moderate	n (%)	6 (6.8)
Severe	n (%)	13 (14.8)

ETDRS = Early treatment diabetic retinopathy study; DMI = Diabetic Macular Ischaemia; NPDR = Non-Proliferative Diabetic Retinopathy; PDR= Proliferative Diabetic Retinopathy; DME = Diabetic Macular Oedema; CSME = Clinically Significant Macular Oedema; SD = Standard Deviation

Table 2.21. Prevalance of diabetic macular oedema in different grades of ETDRS defined grades of diabetic macular ischaemia.

ETDRS-DMI grades		DME (n=49)	No DME (n=39)
None (n=34) (38.6%)	n (%)	19 (55.9%)	15 (44.1%)
Questionable (n=12) (13.6%)	n (%)	4 (33.3%)	8 (66.7%)
Mild (n=23) (26.1%)	n (%)	13 (56.5%)	10 (43.5%)
Moderate (n=6) (6.8%)	n (%)	4 (66.7%)	2 (33.3%)
Severe (n=13) (14.8%)	n (%)	9 (69.2%)	4 (30.8%)
All grades (n=54) (61.4%)	n (%)	30 (55.6%)	24 (44.4%)

ETDRS = Early treatment diabetic retinopathy study; DMI = Diabetic macular ischaemia; DME = Diabetic macular oedema.

Table 2.22. Mean thickness values of the total, inner and outer retina, nerve fibre layer, choroid, and Haller's large vessel layer.

	TMC	p-value	FCS	p-value	PM (inner)	p-value	PM (outer)	p-value	Temporal (inner)	p-value	Temporal (outer)	p-value
Mean total retinal thickness (± SD) (µm)												
No DMI	286.3±34.6	0.37	268.0±80.7	0.45	275.1±31.4	0.03*	307.1±40.1	0.01*	301.4±37.1	0.12	270.1±46.4	0.15
DMI	309.6±58.3		326.6±133.2		297.3±50.3		341.5±80.6		339.7±93.6		285.2±64.3	
Mean outer retinal thickness (± SD) (µm)												
No DMI	134.1±13.0	0.87	150.4±31.4	0.04*	123.9±11.7	0.23	146.9±18.8	0.91	149.3±18.2	0.36	129.4±18.2	0.78
DMI	133.0±25.0		167.4±18.5		132.77±29.1		147.1±35.2		144.3±42.2		122.5±26.3	
Mean inner retinal thickness (± SD) (µm)												
No DMI	142.4±26.1	0.63	71.5±34.0	0.34	138.2±32.6	0.33	147.9±39.5	0.31	146.9±28.1	0.74	133.6±18.3	0.87
DMI	148.9±16.3		107.4±76.8		150.3±23.2		155.4±28.0		152.8±27.2		133.3±25.5	
Mean retinal nerve fibre layer thickness (±SD) (µm)												
No DMI	38.2±4.3	0.84	10.8±5.7	0.87	48.6±13.9	0.75	25.4±4.8	0.77	22.0±4.0	0.88	33.7±15.2	0.88
DMI	30.9±7.1		8.9±2.5		39.0±16.6		21.5±5.8		19.0±3.0		26.9±6.6	
Mean total choroidal thickness (±SD) (µm)												
No DMI	223.5±55.0	0.07	239.3±65.8	0.11	192.3±60.5	0.06	231.5±65.9	0.13	232.7±58.4	0.09	213.5±49.7	0.10
DMI	264.5±66.6		282.6±70.7		240.1±77.3		275.6±75.9		270.2±73.4		245.1±66.3	
Mean Haller's large vessel layer thickness (±SD) (µm)												
No DMI	104.2±30.9	<0.01**	103.5±39.4	<0.01**	89.9±35.7	0.03*	101.2±42.1	0.03*	106.0±31.4	0.23	103.8±26.2	0.13
DMI	138.2±42.6		144.3±51.0		124.8±50.5		141.3±51.1		143.2±48.2		134.0±41.5	

TMC = Total macular circle (ETDRS areas 1-9); FCS = Foveal Central Subfield (ETDRS area 9); PM = Papillomacular (inner: ETDRS area 2) (outer: (ETDRS area 6); Temporal = Temporal to fovea (inner: ETDRS area 9) (outer: ETDRS area 4); DMI = Diabetic macular ischemia

In “all eyes”, the FAZ area showed weak correlation to RNFL thickness at the TMC (r=-0.231, p=0.03), but not at the FCS (r=-0.02, p=0.88), temporal (outer: r=-0.10, p=0.482) (inner: r=-0.11, p=0.43), or papillomacular quadrants (outer: r=-0.21, p=0.482) (inner: r=-0.25, p=0.14).

In eyes “without DME”, the FAZ area showed significant negative correlation with RNFL thickness over the papillomacular quadrant, particularly in the outer quadrant (outer: r=-0.62, p<0.001) (inner: r=-0.38, p=0.04). This was not observed at the TMC (r=-0.12, p=0.44), FCS (r=-0.02, p=0.884), or temporal quadrants (outer: r=-0.12, p=0.54) (inner: r=-0.27, p=0.16).

2.4.6.3 The Effects of Ischaemia on Choroidal Morphology:

Haller’s large vessel layer thickness in diabetic macular ischaemia ***(Table 2.22)****:*

Haller’s large vessel layer was significantly thicker in eyes “with macular ischaemia”, compared to eyes with “no macular ischaemia”, both at the FCS (144.3 ± 51.0 versus 103.5 ± 39.4 µm µm) (p=0.01) respectively and TMC (138.2 ± 42.6 µm versus 104.2 ± 30.9 µm) (p=0.01). There was no significant difference in total choroidal thickness between at the FCS (p=0.11), or TMC (p=0.07). There was also no significant difference in Haller’s layer or choroidal thickness between eyes with, and without DME.

Correlation of Haller’s large vessel layer thickness to FAZ area: In eyes “without DME”, Haller’s layer over the TMC, was correlated to the size of FAZ area (r=0.43, p=0.04). This was not observed in “all eyes” (r=0.22, p=0.16), or eyes “with DME” (r=0.11, p=0.64). Interestingly, there was no correlation between Haller’s layer thickness and retinal thickness measurements. (r=0.16, p=0.31)

2.4.6.4 Relationships between Visual Acuity and Optical Coherence Tomography-Derived Parameters:

Significant correlations were observed between VA, and the FAZ area (r=0.36, p=0.02), papillomacular ischaemia area (r=0.613, p=0.01), but not with the temporal ischaemia area (r=0.22, p=0.29). These relationships are consistent with findings from our previous study.(187)

Retinal thickness and visual acuity: In eyes with both macular ischaemia and oedema, we observed a positive correlation between VA and total retinal thickness, (r=0.52, p=0.001) and outer retinal thickness measurements (r=0.33, p=0.04) at the FCS. Interestingly, in eyes with macular ischaemia but without oedema, we observed the converse, where VA was negatively correlated to total retinal thickness, (r=-0.37, p=0.004) and outer retinal thickness measurements (r=-0.44, p=0.001) at the FCS. There were no significant associations in the analysis of "all eyes", or between VA and inner retinal thicknesses measurements.

Retinal nerve fibre layer and visual acuity: In eyes with macular ischaemia but without oedema, we observed a negative correlation between VA and RNFL thickness over the papillomacular area, (r=-0.37, p=0.004) which was lost in the analysis of "all eyes" (r=0.20, p=0.18), and eyes with both macular ischaemia and oedema (r=0.335, p=0.08). There were no associations between VA and RNFL thickness measurements the analysis of "all eyes".

Subfoveal choroidal thickness and visual acuity: VA was moderately correlated to choroidal thickness measurements at the FCS in macular ischaemia grades "mild" to "severe" (n=42) (r=0.47, p=0.03). This correlation was further strengthened in eyes with macular ischaemia grades "moderate" to "severe" (n=19) (r=0.74, p=0.009).

2.4.7 Relationship of peripheral retinal and central macular ischaemia

2.4.7.1 Baseline Characteristics:

Ultra widefield FA images from 47 patients were assessed. The median age of all patients was 55 years (interquartile range [IQR]=15.0), 21 patients (44.7%) were female, and 12 (25.5%) were diagnosed with Type 1, and 35 (74.5%) Type 2 diabetes. In all patients, the median FAZ area was 0.35mm^2 (IQR=0.28mm^2), median peripheral ischemic index was 31.9% (IQR=38.3%), and median peripheral leakage index was 17.7% (IQR=29.7%). There were no differences with age, gender, and diabetes type, in all 3 categories- "FAZ area", "peripheral ischaemia index", and "peripheral leakage index" **(Table 2.23)**.

Table 2.23. Peripheral ischaemia and leakage index in all patients and in those with a small compared to a large foveal avascular zone area.

	All (n=47)	Small FAZ (n=20)	Large FAZ (n=27)	p-value
Percentage of PRP laser Treated area / Total area visualised, %, (IQR)				
	74.5 (12.4)	74.2 (7.4)	77.6 (19.9)	0.57
Percentage of Peripheral ischaemia to total area visualised, (IQR)				
All eyes	14.6 (40.4)	8.9 (12.7)	33.7 (44.0)	0.004**
PRP laser naive (n=20)	38.8 (38.8)	13.2 (32.3)	45.6 (45.2)	0.04*
PRP laser treated (n=27)	9.2 (10.1)	8.9 (9.3)	9.2 (9.2)	0.97
Percentage of Peripheral FA leakage to total area visualised, (IQR)				
All eyes	11.4 (18.9)	7.1 (19.4)	14.8 (20.4)	0.08
PRP laser naive (n=20)	12.9 (18.0)	6.5 (8.4)	20.6 (22.5)	0.01*
PRP laser treated (n=27)	9.1 (21.7)	7.3 (24.1)	9.3 (8.3)	0.90

IQR = Interquartile range

In our cohort, a large proportion of patients, 35/47 (74.5%), were graded with proliferative diabetic retinopathy. Of these, there were a significantly greater proportion of eyes with of proliferative diabetic retinopathy in the group with a high (> 50%) peripheral leakage index. 27/47 patients (57.4%) were naive to pan-retinal photocoagulation (PRP) laser treatment in our cohort. No significant differences were observed between PRP treatment naive and treated patients across all three categories.

Regarding the presence of macular oedema, 26/47 patients (55.3%) had a UK NSC grade of diabetic macular oedema, compared to 32/47 patients (68.0%), with a uwFA macular oedema grade- defined as central capillary leakage observed on late-phase uwFA images. Of these, 9 patients had "focal leakage" and 23 patients had "diffuse leakage". No significant differences were observed in either the UK NSC maculopathy grades or uwFA macular oedema grades across all three categories **(Table 2.23)**.

2.4.7.2 The Relationship between Peripheral Ischaemia and Peripheral Leakage:

*An association between peripheral ischaemia and peripheral leakage index in laser naive eyes **(Table 2.23)**:* In all eyes, no association was observed between the peripheral ischaemia or leakage index (r=0.20, p=0.19). However, in eyes that were laser naive, a significant association was observed (r=0.56, p=0.004).

2.4.7.3 The Relationship between Peripheral and Macular Ischaemia:

*A high peripheral ischemic index is associated with a large FAZ **(Table 2.24)**:* In all eyes, the median FAZ area was significantly larger in eyes with a high peripheral ischaemia index (0.56mm^2 [IQR=0.86]), compared to eyes with a low peripheral ischaemia index (0.32mm^2 [IQR=0.28]) (p=0.02) **(Figure 2.21)**. A similar trend was observed when only eyes that were PRP laser treatment naive (n=27) were analysed, (0.55mm^2 [IQR=0.55]) versus 0.27mm^2 [IQR=0.05]), though this did not reach

statistical significance (p=0.06). In addition, a moderate correlation was observed between the peripheral ischaemia index and FAZ area, both in all eyes (r=0.49, p=0.0001) and in eyes that were laser naive (r=0.55, p=0.003) **(Figure 2.22)**.

*A high peripheral leakage index was associated with a large FAZ in laser naive eyes **(Table 2.24)**:* When all eyes were included, no difference was observed in the size of the FAZ between eyes with a low or high peripheral leakage index. However, in eyes that were laser naive, there was a moderate correlation between the FAZ area, and the peripheral leakage index (r=0.44, p=0.02) **(Figure 2.22)**.

2.4.7.4 The Effects of Peripheral Ischaemia on Retinal Thickness Measurements:

*No relationship between peripheral ischaemia or leakage was observed with macular oedema **(Table 2.24)**:* In all eyes, no significant difference was observed with NSC maculopathy or uwFA macular oedema grades, for either the peripheral ischaemia or leakage indices. Similarly, there were no differences in OCT-derived retinal thickness measurements of the foveal central subfield (FCS), in eyes with a high or low, ischemic or leakage indices.

The retina is thinner in the presence of macular but not peripheral ischaemia **(Table 2.24)**: The median FCS retinal thickness measurement in eyes with a large FAZ was 217µm (IQR=81.8), compared to 272µm (IQR=36.0) (p=0.02) in eyes with a small FAZ. In the presence of a high peripheral ischaemia index, a thinner retina was also observed at the FCS (226µm [IQR=94.5] compared to 267µm [IQR=75.0]), however, this was not statistically significant (p=0.08). There was no difference in the retinal thickness measurements between eyes with a high or low peripheral leakage index.

Table 2.24. Comparison between patients with a small or large foveal avascular zone area, and low (<20%) or high (>20%) peripheral ischaemia and leakage indexes.

	FAZ area (mm^2)			Peripheral ischaemia index (%)			Peripheral leakage index (%)		
	Small (<0.32 mm^2) (n=20)	Large (>0.32 mm^2) (n=27)	p-value	Low (<50%) (n=33)	High (>50%) (n=14)	p-value	Low (<50%) (n=35)	High (>50%) (n=12)	p-value
Age, Median (IQR)	51 (26.8)	57 (12.5)	0.09	56 (15.0)	51 (9.3)	0.40	55 (14.0)	55 (27.8)	0.17
Female Gender, n (%)	7 (35.0)	14 (51.9)	0.39	15 (45.5)	6 (42.9)	0.88	13 (37.1)	8 (66.7)	0.08
Affected eye – right, n (%)	10 (50.0)	17 (63.0)	0.56	19 (57.6)	8 (57.1)	0.77	20 (57.1)	7 (58.3)	0.87
Diabetes, n (%)									
Type 1	7 (35.0)	5 (18.5)	0.29	9 (27.3)	3 (21.4)	0.94	8 (22.9)	4 (33.3)	0.31
Type 2	13 (65.0)	22 (81.5)		24 (72.7)	11 (78.6)		27 (77.1)	8 (66.7)	
UK NSC Retinopathy grade, n (%)									
Non-proliferative	3 (15.0)	9 (33.3)	0.28	10 (30.3)	2 (14.3)	0.43	10 (28.6)	2 (16.7)	0.04*
Proliferative	17 (85.0)	18 (66.7)		23 (69.7)	12 (85.7)		25 (71.4)	10 (83.3)	
UK NSC Maculopathy grade, n (%)									
No DME	12 (60.0)	14 (51.9)	0.80	18 (54.5)	8 (57.1)	0.88	19 (54.3)	7 (58.3)	0.60
DME	8 (40.0)	13 (48.1)		15 (45.5)	6 (42.9)		16 (45.7)	5 (41.7)	
uwFA Macular oedema grade, n (%)									
None	11 (55.0)	13 (48.1)	0.87	16 (48.5)	8 (57.1)	0.82	19 (54.3)	5 (41.7)	0.94
Focal & Diffuse	9 (45.0)	14 (51.9)		17 (51.5)	6 (42.9)		16 (45.7)	7 (58.3)	
PRP laser									
Naive	8 (40.0)	19 (70.3)	0.07	17 (51.5)	10 (71.4)	0.35	25 (71.4)	2 (16.7)	0.16
Treated	12 (60.0)	8 (29.7)		16 (48.5)	4 (28.6)		10 (28.6)	10 (83.3)	
Retinal thickness, Median µm (IQR)	272 (36.0)	217 (81.8)	0.02*	267 (75.0)	226 (94.5)	0.08	258 (76.3)	276 (68.0)	0.24
Median FAZ area, mm^2, (IQR)	0.24 (0.08)	0.55 (0.54)	0.0001 **	0.32 (0.28)	0.56 (0.86)	0.02*	0.40 (0.41)	0.28 (0.21)	0.12
Visual acuity, Median LogMAR, (IQR)									
Test eye	0 (0.20)	0.2 (0.35)	0.02*	0.2 (0.30)	0.2 (0.60)	0.21	0.2 (0.50)	0.2 (0.23)	0.53
Contralateral eye	0 (0.30)	0.3 (0.60)	0.02*	0.2 (0.50)	0.2 (0.80)	0.43	0.2 (0.75)	0.3 (0.35)	0.97

UK NSC = United Kingdom National Screening Committee; uwFA = ultra widefield fluorescein angiogram; IQR = Interquartile range; DME = Diabetic Macular Oedema; FAZ = Foveal Avascular Zone; Log MAR = Logarithm of the Minimum Angle of Resolution. p values significant at 5% level are indicated with (*), and (**) at 1% level. OR=Odds Ratio; 95% CI=95% Confidence Interval.

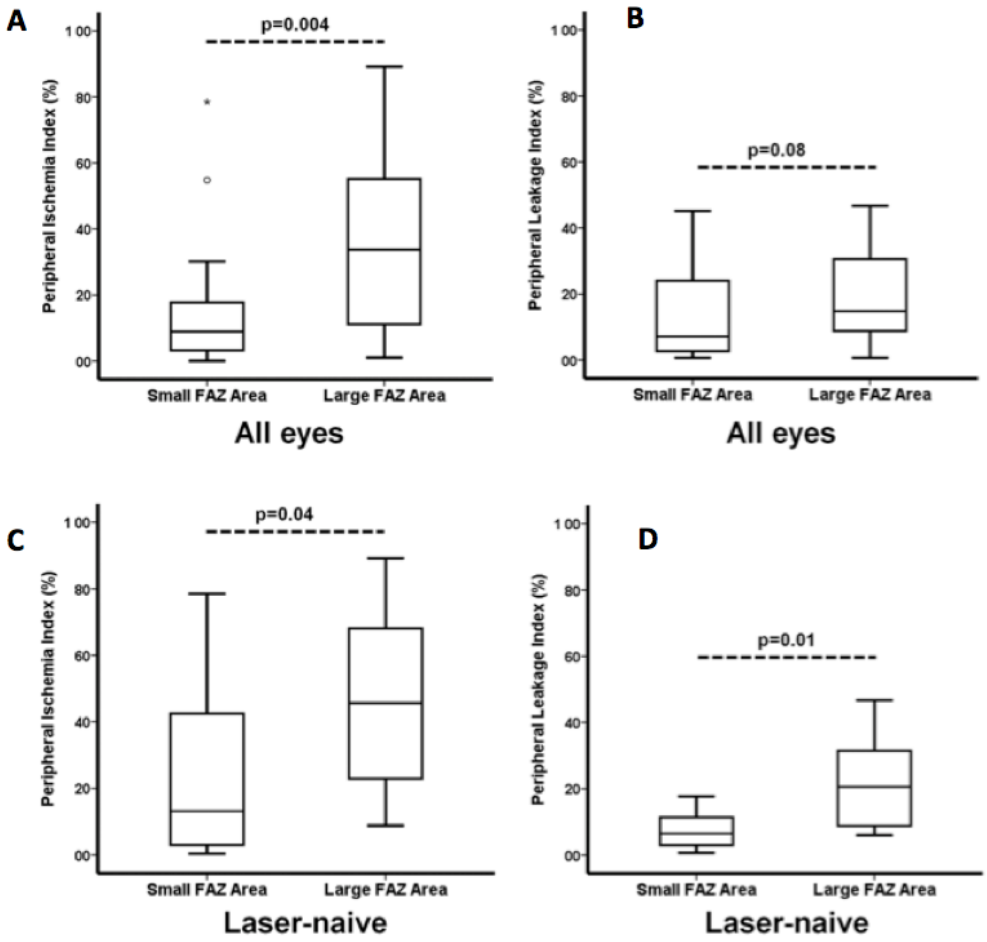

Figure 2.21. Comparison of the Peripheral Ischemic and Leakage Indices

Comparison between indices were made according to foveal avascular zone size categories; small (<0.32mm^2) and large (>0.32mm^2); in all eyes, and in eyes which are laser-naive. Box-plots of the (A), (C) peripheral ischemic index (%), and (B, D) peripheral leakage index (%) in eyes with a small or large foveal avascular zone size. Analysis was performed in (A, B) all eyes, and those which were (C, D) laser-naive. The top of the box represents the 75th percentile, the bottom of the box represents the 25th percentile, and the line in the middle represents the 50th percentile. The whiskers represent the highest and lowest values that are not outliers or extreme values. Outliers and extreme values are represented by circles beyond the whiskers. A significant difference was observed in all categories, except that between (B) the peripheral leakage index and foveal avascular zone in all eyes.

2.4.7.5 Clinical Significance of Peripheral Ischaemia and Leakage in Diabetes:

A poor visual acuity was associated with macular but not peripheral ischaemia: A significant correlation was found between visual acuity and FAZ area (r=0.53, p=0.0002), but not the peripheral ischaemia index (r=0.25, p=0.09), or the peripheral leakage index (r=0.09, p=0.57).

When visual acuity evaluated in a step-wise multivariable regression model, including clinical factors (age, gender, eye analysed, PRP laser treatment), and other ocular parameters measured (FAZ area, OCT-derived central retinal thickness, peripheral ischaemia and leakage index), the variables that remained independently associated were, age (Zero order correlation coefficient [r]=0.33, p=0.03), FAZ area (r=0.45, p=0.02), and OCT-derived central retinal thickness measurements (r=0.38, p=0.01), (R^2-adjusted=0.36) **(Figure 2.22)**.

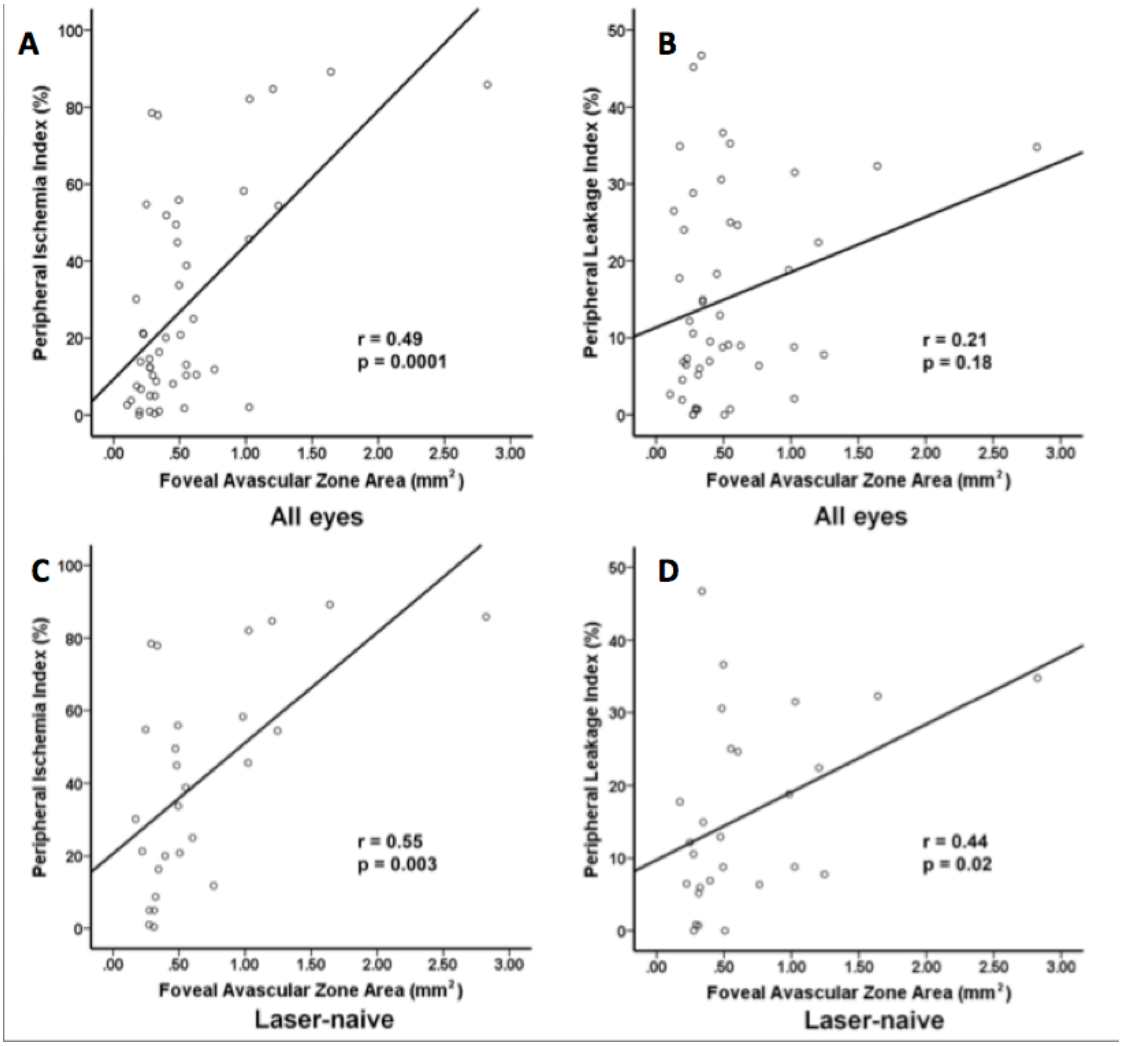

Figure 2.22. Relationship between peripheral ischaemia, leakage and FAZ area

Scatter plots showing the relationships between (A), (C) peripheral ischemic index (%), and (B), (D) peripheral leakage index (%) with the foveal avascular zone area. Analysis was performed in (A, B) all eyes, and those which were (C, D) laser-naive. A significant relationship was observed in all categories, except for (First row, right) the association between the peripheral leakage index and foveal avascular zone in all eyes.

2.5 Discussion:

2.5.1 The impact of DMI on vision, and retinal and choroidal thickness measurements

In this chapter, we were interested in examining the impact of ischaemia, both in the central macula and paramacular areas, on visual function. We examined in detail the prevalence, symmetry, and relationship of diabetic macular ischaemia to the severity of co-existing retinopathy, retinal morphology and visual acuity. DMI and retinal thickness and volumes were manually quantified using custom software, and demonstrated statistically significant correlations between visual acuity, size of FAZ and retinal thickness and volume in type 2 diabetic eyes.

There is a paucity of information regarding the prevalence of DMI due to the rarity of recent large clinical trials using standard fluorescein angiography with the purpose of identifying macular ischaemia. The Early Treatment Diabetic Retinopathy Study (EDTRS), which only included a few cases of severe macular ischaemia (2.3% of eyes at baseline), was limited by attrition (36%), remains as the only large prospective study to grade specifically for DMI.(24) They observed at baseline that 53.4% of eyes had some form of DMI, and 7.2% of eyes with moderate to severe DMI. A more recent, but smaller observational case series of 63 patients, also using the EDTRS grading system for DMI, observed a similar proportion of eyes (50%) with evidence of FAZ damage.(188) In this current study, the prevalence of eyes with any grade of DMI in this was higher (60.3%), and even more so in eyes with moderate to severe DMI (16.6%). This was probably reflective of the study centre as a tertiary referral hospital, and the type of patients who required fluorescein angiography. However, this allowed for more detailed subgroup analysis of larger numbers of patients with a more severe disease phenotype, and comparisons of their retinal morphology and visual function

A high incidence of symmetry was observed in patients with bilateral DMI, with the majority of patients (88.8%) having no greater than one EDTRS DMI grade difference between either eye. To the authors' knowledge, bilaterality or symmetry

of DMI has not been previously described elsewhere. Consistent with previous studies, we observed increasing severity of DMI, as measured by the FAZ size, in more advanced grades of retinopathy.(40, 42, 43, 137) Some studies report that the relationship between FAZ size and DR severity occurs from the earlier stages of NPDR(40, 137) and others only in more advance disease(189, 190). This discrepancy is most likely due to the large inter subject variability of the FAZ; ranging between 0.05 and up to 1.05 mm^2 in non-diseased subjects.(40, 137, 189, 191, 192) In this study, the mean FAZ area of eyes without DMI, fell on the higher side of previously reported normal ranges, consistent with the hypothesis that the FAZ may be affected in early disease. A study which used adaptive optics study scanning laser ophthalmoscopy to assess the FAZ, observed an altered retinal parafoveal capillary network in eyes even before the onset of diabetic retinopathy, suggesting that foveal capillary perfusion may be altered in diabetics without clinically visible disease.(193)

In this study, we chose two areas of non-contiguous capillary perfusion where ischaemia may have a functional significance, and described standardized quantification of those areas. First, temporal ischaemia (TI) – an area that has been observed clinically to be a risk factor for, or a driver of macular oedema, and has been previously associated with angle neovascularisation in proliferative diabetic retinopathy.(194) Second, papillomacular ischaemia (MPI)- an area where the capillary network overlies and supplies the nerve fibres of the papillomacular bundle, originating from the central macula. We hypothesized that ischaemia in these areas may have an impact on visual acuity. Eyes with the presence of concurrent TI or MPI had significantly larger FAZ areas which suggest that these areas of ischaemia tend to occur in more severe DMI phenotypes. Similarly, retinal thickness and volume measurements over EDTRS areas 4&8, which correspond to the MPI area, were significantly higher in eyes with a greater severity of DMI. We observed significant correlations between the area TI and MPI and visual acuity. There are several potential explanations for why this is so. It may simply reflect the severity of diabetic eye disease as a whole, where eyes with larger areas of retinal ischaemia have poor visual acuity, or it could be due to the location in which these capillary network sub-serves. Increased areas of retinal ischaemia in proliferative diabetic retinopathy are

associated poor visual acuity. However, we observed in this study, that the area of temporal ischaemia is independent of FAZ size, which is a surrogate marker for DMI severity. This suggests that the location of ischaemia may be an independent effect on visual function. Interestingly, although retinal capillary network supplies in the inner two-thirds of the retina, 7-40% of normal eyes have an addition supply from the choroidal circulation via the cilioretinal artery(195, 196), which supplies a large proportion of the papillomacular bundle. This incidence has been found to lie between 13.9-38% in diabetic eyes, and may explained the lower numbers of MPI compared to TI observed in our current study.(197, 198) Data from a recent study which analysed retinal blood flow using the Retinal Functional Imager, found that eyes which exhibit cilioretinal-retinal vascular anastomosis were associated with increased arterial and venous retinal blood flow velocities and the increased occurrence diabetic macular oedema. It is possible that the cilioretinal artery confers a protective effect from ischaemia.

Although previous studies have demonstrated the correlation of macular ischaemia with impaired visual acuity(41), this relationship is not always straightforward. Morphological changes do not always correspond with functional change, and visual acuity has been shown to be preserved in the presence of advanced macular ischaemia.(42, 43) Visual acuity, though a crude measure of macular function, remains as the most common parameter used in most studies of diabetic macular disease. More recently, microperimetry has been used to provide more detailed functional assessment of the macular. Most studies that address the relationship of diabetic macular disease and visual function, do so in the field of diabetic macular oedema, assessing ischaemia only as a secondary outcome measure. (199-202) A recent structure-functional correlative study, using the Nidek MP-1 Microperimetry showed correlation of reduced sensitivity with diabetic macular oedema, but no effects on areas of capillary nonperfusion.(203) However, this was a small pilot study of fifteen patients in eyes with non-proliferative diabetic retinopathy, and did not include more severe grades of DMI. Another study on twenty-five patients, which examined the functional outcome of an enlarged FAZ on multifocal electroretinogram, showed correlation between ischaemia areas and a

prolonged implicit time but not in amplitude.(204) In this present study, a low but significant correlation (r=0.26) was observed between FAZ area and visual acuity across all patients which strengthened in the severe DMI group (r=0.6). This correlation was lost in subgroup analysis of all other grades of ischaemia. We also observed that visual acuities were significantly different between eyes with no ischaemia, and the moderate and severe DMI subgroups ($p<0.02$), but not with questionable or mild disease. This suggests that functional impairment secondary to ischaemia may only occur in severe disease. It is possible that a threshold of structural damage has to be reached before vision is affected. Similarly, with OCT measurements of retinal thickness and volume, we found that there was no correlation to vision in eyes with none to mild DMI, and a stronger than expected correlation in eyes with moderate to severe DMI. (r=0.75)

Increases in retinal thickness may be due to macular oedema, ischaemia or both. It is often difficult to determine the degree to which each accounts for decreased visual function. Across all patients, we found a correlation of retinal thickness and visual acuity (r=0.32), which strengthened (r=0.52) when patients with macular oedema were excluded. Though the numbers in this group were small (n=15), it suggests that ischaemia plays an important role in visual function even in the mixed diabetic macular disease where ischaemia and oedema co-exist. Previous studies on diabetic macular oedema, have reported a range of correlations with visual function (r = 0.13 to 0.89), with most showing modest correlations to acuity.(38, 205-209) This wide range of correlations, likely reflects the multiple factors which govern vision that are often not addressed; such as compromised retinal microcirculation, choroidal circulation and duration of disease. These studies on DMO also show consistently, that the location of disease at the foveal point thickness or the EDTRS central subfield has better correlation with visual acuity than the whole macular grid. We found that there was little difference in both the central field in the whole macular grid, for both thickness and volume measurements in DMI. Ischaemia in the wider macular area, unlike oedema, may a distal effect on visual acuity which is mostly dependent on the foveal function(210).

We have observed that both inner and outer retinal thickness increases with DMI severity. However, the inner retina did show thinning, only when taken as a ratio to the outer retinal thickness, to increasing FAZ size. Only in the outer retinal thickness was correlated to visual acuity. This is consistent to earlier studies in which the retinal circulation is compromised, such as retinal vein occlusion, where atrophic changes in the inner retina have been reported.(211, 212) Inner retinal thinning was first observed, in the era of time-domain OCT, to be a finding of DMI.(38, 205) More recent OCT studies have concurred(168, 213, 214), and showed specifically a correlation of ganglion cell layer loss with FFA areas of capillary dropout(168). None of these studies examined the association with VA. We found only one study which examines the relationship of retinal layers and vision where photoreceptor outer segment length was found to correlate to VA in patients with diabetic macular oedema.(206) Interestingly, it was also in the outer retina that the association was observed.

There is a scarcity of studies that examine the relationship of DMI and visual acuity. The main advantages of our study are its large sample size, and the utilization of manual OCTOR and GRADOR grading which allows quantification of any morphological spaces of interest. There are several limitations to this study. First, the retrospective cross-sectional nature of the work carries an inherent limitation of biased selection of patients with a more severe disease requiring FFAs, and does not account for confounders of visual acuity, such as cataracts that were not recorded in the electronic case notes. It also does not examine the way ischaemia and visual acuity changes over time. Second, the number of eyes which had concurrent SD-OCT and FFA were small, as the study was carried out in a single site where patients tended to undergo Topcon OCT scans. These were not included in this study as the amount of speckle noise in the images did not allow repeatable manual segmentation of retinal layers. Finally, visual acuity data was collected as best corrected Snellen acuity in a clinical setting and converted to LogMar for analysis. Ideally, visual acuity should be assessed using ETDRS charts with protocol refraction. The limitations of visual acuity assessment using Snellen charts are well documented.(215)

The presence of macular ischaemia has been reported to impart a poor prognosis after laser(21) or anti-vascular endothelial growth factor (anti-VEGF) therapy(33) for diabetic macular oedema. However, the grade of ischaemia in which this occurs and the extent in which it affects treatment outcomes is unknown. Even in the age of emerging anti-VEGF treatments, there is a lack of evidence from FFA based evaluation of the retinal microcirculation in clinical trials.(216, 217) Moreover, patients with DMI are often excluded from these studies.(218) The BOLT study is the only prospective randomised trial where detailed evaluation of macular ischaemia was before and after laser or anti-VEGF treatment.(39, 219) No statistically significant worsening of macular perfusion was evident at 4, and 12 months. However, as the authors note, patients with severe DMI were not included in the study, and the numbers of patient were too small to detect clinically significant adverse events. Prospective FFA-based evaluation of the effects of anti-VEGF trials on retinal perfusion need to be undertaken. However, before this is done, the natural history of DMI needs to be elucidated with prospective longitudinal studies, which examine the impact of ischaemia on visual function, using reliable and reproducible structure-function correlative indices. This has not been undertaken so far, probably due to the invasive nature of fluorescein angiography and the lack of reproducible functional assessment. Recent rapid advancement of adaptive optics and eye-tracking technology may negate the need for FFAs and allow accurate mapping of macular function over time. The results from such a study would help determine whether a window of opportunity exists, before the onset of diabetic retinal neuropathy, where vascular rescue can occur. This threshold will define the critical therapeutic window for delivery of emerging vascular stem cell treatments.

In summary, diabetic macular ischaemia is present in more than half the diabetic population that attend for assessment of eye disease. It occurs even in early retinal disease, and is symmetrical in a majority of cases. Visual function only tends to be affected in moderate to severe ischaemia, and is associated with the presence and size of non-contiguous capillary dropout in area overlying the papillomacular bundle and temporal to the macula. Retinal thickness as a whole increases with severity, but there is a negative association of the ratio of inner and outer retinal thickness to size

of FAZ. Changes in the outer but not inner retinal morphology has an impact on visual acuity.

2.5.2 Diabetic macular ischaemia progression

A recent paradigm shift in the treatment of diabetic macular oedema - from laser photocoagulation to anti-VEGF pharmacotherapy, has highlighted the importance of a better understanding the natural history of DMI. “Mixed diabetic maculopathy” is often observed in clinical practice, with few patients exhibiting features of either DMI or DME exclusively. In a recent cross-sectional analysis, we observed concurrent DMI (of any severity grade) in up to 70% of cases with clinically significant macular oedema (CSME).(187) In the current study, we performed longitudinal quantitative analyses of FA images obtained in a cohort of patients with Type 2 diabetes mellitus, and an ETDRS-DMI grade of mild, moderate, or severe. Using this approach, we estimate the rate of FAZ enlargement, and evaluate baseline parameters that may be predictive of DMI progression.

In our analysis of EDTRS-defined DMI grade progression - 15% of eyes showed an advancement of at least one severity grade per year. In contrast, the EDTRS demonstrated no change in the distribution of DMI grades over a period of 5-year study period.(24) This may be due to only a few cases of severe macular ischaemia being included in the EDTRS. In our cohort, longitudinal quantification of the FAZ area, detected a significant FAZ enlargement across all EDTRS-DMI severity grades. (median time interval = 27 months) A possible explanation for the discrepancy between ETDRS-DMI grade progression, and FAZ enlargement observed, is that qualitative grading alone may not be sufficiently sensitive for the detection of DMI progression. FAZ enlargement rates were found to be greater in more severe grades of ischaemia, ranging from an increase of approximately 5% (of baseline FAZ area per year) in “mild”, to 7% in “moderate”, and 10% in “severe” EDTRS-DMI grades. Although the increases in FAZ area with advancing stages of diabetic retinopathy is well known, its progression over time has never been assessed.(40, 42, 43, 137, 189, 193) In addition, to assessing the FAZ enlargement rates in different EDTRS-DMI

grades, we also evaluated the effects of baseline diabetic retinopathy and maculopathy severity, FAZ size, and visual acuity. FAZ enlargement rates were found to be more than three-fold higher in eyes that showed a deterioration of VA over the same time-interval, (19%) compared to those which did not. (5.6%) Although previous studies examining the impact of FAZ size on visual acuity have been contradictory,(43, 137, 190) we demonstrate in this study, a clear association between worsening VA and FAZ enlargement rates.

In this report, we also investigated a number of clinical parameters we hypothesized to be of significance to "DMI progression" – defined as a FAZ enlargement rate of greater than 10% baseline FAZ area per year. Moreover, in this process, we developed stratified regression models for baseline FAZ size in order to identify "clinical thresholds" for "DMI progression". A strong association, independent of age, gender, retinopathy and maculopathy severity, was observed between DMI progression and baseline FAZ area at a threshold of 0.6 mm^2. These results have important clinical implications as it provides a practical method that at risk of DMI may identify progression. In practice, this translates to – eyes with a FAZ area, greater than a third of the optic nerve head, has an approximately 6:1 OR of DMI progression. Similarly, we observed a 2:1 OR for DMI progression for every step increase in ETDRS-DMI grade, suggesting that eyes with larger FAZ areas and greater severity of DMI have an increased risk of progression. VA deterioration over time was also an independent predictor of DMI progression. In agreement our previous analyses showing a strong relationship between VA and moderate to severe grades of DMI, we observed a 5:1 OR of DMI progression, in eyes which showed a VA deterioration of greater than 0.05 LogMar units per year. (<1 line Snellen acuity)

Surprisingly, we did not observe any association between the severity of diabetic retinopathy or maculopathy grades, with DMI progression. Previous studies, have shown that DMI is a risk factor for DME and PDR – i.e. the EDTRS, which reported a 1-year risk of development of PDR at 18.2% without DMI, and 41.3% with severe DMI.(24, 43, 220), (35) We speculate that it may be possible that DMI

progression precedes the worsening of retinopathy or maculopathy, though this needs be addressed in larger prospective cohorts.

Our study has a number of strengths, combining longitudinal analysis with standardized qualitative and quantitative assessment of FA images, in an area with a relative paucity of data. For example, the median time interval between FAs analysed was greater than 2 years, allowing for changes in the FAZ area (clinically observed to progress slowly) to be detected. Our use of FA grading software equipped with standard planimetric tools allowed quantification FAZ area, enabling detection of small changes over time. We combined these measurements with multivariate statistical modelling, accounting for known confounders of FAZ measurements, such as age, severity of diabetic retinopathy, and macular oedema, often overlooked in other studies.

Our study also has a number of limitations. Firstly, the retrospective nature of the work results in an inherently biased selection of patients. However, we purposefully identified patients with a diagnosis of established DMI, in order to assess our main outcome measure – rate of FAZ enlargement. However, future prospective studies will be required to validate the thresholds (i.e. baseline FAZ size) established in this study. A further limitation is our reliance on Snellen visual acuities, the limitations of which have been well documented.(221, 222) In prospective clinical trials, VA is now typically assessed using ETDRS vision charts with protocol refraction.

The results of this study provide insight into the natural history of DMI, demonstrating a FAZ enlargement rate of 5 to 10% of baseline FAZ area per year, in eyes with established DMI. We identified prognostic determinants - baseline FAZ size, and a deteriorating VA, which may serve as robust independent predictors of DMI progression in patients with Type 2 diabetes mellitus.

2.5.3 Diabetic macular ischaemia in type 1 diabetes

The prevalence of established ischaemia (i.e., ETDRS defined grades: mild, moderate, and severe), in our cohort of patients with Type 1 diabetes, was 54.7% - higher, than

previously reported in the literature **(Table 2.24)**. A likely explanation, is that our patients comprised of those referred from a national screening program for diabetic eye diseases, and were attending a dedicated tertiary-referral medical retinal clinic with the intention to diagnose or treat.(223) These patients may be more typical of those seen in clinical practice, than those recruited for many clinical trials (for example, in ETDRS, patients with active proliferative and severe non-proliferative retinopathy were excluded). Similarly, more recent clinical trials, such as the RISE/RIDE and RESTORE studies, specifically excluded patients with macular ischaemia.(37, 140) The prevalence of macular ischaemia in Type 1 diabetes (54.7%) was also higher than previously observed in a similar cohort of patients with Type 2 diabetes (41.3%). In fact, a higher prevalence was observed in all ischaemia types quantified in Type 1 compared to Type 2 diabetes, namely, established (54.7% versus 41.3%), advanced (22.2% versus 16.6%), temporal (52.3% versus 27.5%), and papillomacular ischaemia (25.6% versus 8.3%) **(Table 2.24)**. A possible explanation for the increased prevalence in both macular and paramacular ischaemia in Type 1 compared to Type 2 diabetes, may be that central macular capillary nonperfusion mirrors peripheral capillary nonperfusion. In our multivariable regression model, we observed an association between a diagnosis of macular ischaemia and severity of peripheral retinopathy **(Table 2.11)**. Interestingly, a recent study using wide-field angiography has observed an association between peripheral ischaemia and macular oedema.(224) From these findings, we suggest that peripheral and macular ischaemia may also be associated in Type 1 diabetes.

The effect of age, on the development and progression of diabetic retinopathy and macular oedema, has been thoroughly investigated in large epidemiological studies. However, the impact of age on diabetic eye disease appears to be dependent upon the population studied, and the type of retinopathy examined. In Type 2 diabetes, the United Kingdom Prospective Diabetes Study showed that an older age was associated with progression in eyes with established diabetic retinopathy. However, studies in different populations have observed the converse; that an older age was protective of any diabetic retinopathy.(225, 226) The Wisconsin Epidemiologic Study of Diabetic Retinopathy, which followed a cohort of persons

with Type 1 diabetes over 25 years, did not observe any effects of either age at baseline assessment, or age of diagnosis, on the progression of retinopathy.(143) In this study, we hypothesized that age, through its effect on microvascular degeneration and pericyte loss leads to capillary dropout, and increases the risk of developing ischaemia.(227-229) We observed that patients with macular ischaemia were older (mean age 49.5 years), compared to those without ischaemia (mean age 41.6 years) (p=0.02). In fact, age itself, per decade increase, was an independent risk factor for macular ischaemia (OR=2.30, 95% CI=1.27 to 4.16, p=0.006). A possible explanation for this is that older patients in our study, may have had longer duration of disease. Interestingly, our previous study of macular ischaemia in Type 2 diabetes found no significant age differences in patients with (mean age 64.0 years) or without ischaemia (mean age 62 years) (p=0.07).(187)

In addition to assessing the prevalence of macular ischaemia and its relationship to age, we also evaluated its visual significance. We observed that eyes with any grade of macular ischaemia had significantly worse vision, unlike in our related study of patients with Type 2 diabetes, where an association was only observed with advanced macular ischaemia (ETDRS grades moderate and severe).(187) In addition, unlike in Type 2 diabetes, no associations were observed between visual acuity and papillomacular ischaemia despite its higher prevalence. (25.6% in Type 1 compared to 8.3% in Type 2 diabetes) **(Table 2.25)**. One possibility is that a high proportion of patients with papillomacular ischaemia, also

Table 2.25: Comparison of the prevalence of diabetic macular ischaemia between Type 1 and Type 2 diabetes.

Type of ischaemia	ETDRS Grades		Type 1 Diabetes (n=86)	Type 2 Diabetes (n=408)
Established macular ischaemia	Mild, Moderate, Severe	n (%)	47 (54.7)	171 (41.3)
Advanced macular ischaemia	Moderate, Severe	n (%)	19 (22.1)	68 (16.6)
Temporal macular ischaemia	NA	n (%)	45 (52.3)	112 (27.5)
Papillomacular ischaemia	NA	n (%)	22 (25.6)	34 (8.3)

ETDRS = Early Treatment Diabetic Retinopathy Study

had concurrent macular ischaemia (86.4%) **(Table 2.10)**, thereby confounding its effects on visual acuity. However, it may be that in Type 1 diabetes, the location and severity of macular ischaemia impacts less upon visual function than in Type 2 diabetes.

The strengths of this study, include the number of eyes with diabetic macular ischaemia analysed (n=60, **Table 2.10**), a relatively large number for an area where there is relative paucity of data, the use of standardized protocols for qualitative grading of ischaemia, and the use of validated software for quantification of areas of capillary dropout. The limitations to the study include an inherent selection bias due to its inclusion of patients attending a tertiary referral clinic, with an intention to treat, and to its retrospective cross-sectional design. However, the data presented is likely to represent a majority of patients in ophthalmic clinical practice, compared to the clinical trial scenario, where patients with more severe grade of diabetic macular ischaemia are more likely to be excluded. Furthermore, the prevalence reported

more likely reflects patients referred with symptoms or signs of sight-threatening retinopathy, compared to that of a FA-based population survey, and therefore may better reflect a potential future treatment cohort. Secondly, data concerning systemic parameters such as blood pressure, HbA1c, and disease duration were not collected, and are likely to play a role in diabetic macular ischaemia.(9, 139)

In summary, there is a high prevalence of diabetic macular ischaemia (54.7%) in patients with Type 1 diabetes attending a tertiary referral medical retinal clinic. These patients were older, and macular ischaemia of any grade was visually significant. Although no treatment currently exists for diabetic macular ischaemia, this condition often co-exists with, and if severe, may influence the treatment of diabetic macular oedema. A greater understanding of diabetic macular ischaemia, including whom it affects, and its impact on visual acuity, would enable the clinician to better manage diabetic macular disease in patients with Type 1 diabetes.

2.5.4 The relationship of diabetic macular ischaemia to retinal vessel calibre

A narrower retinal arteriolar calibre measured on FFA is associated with DMI. The mean arteriolar calibre was 10.1 μm narrower in moderate/severe DMI compared to none/mild DMI. A narrower arteriolar calibre was also associated with more severe DMI grades, larger FAZ diameter and area. These associations persisted independently, after adjustment for markers of peripheral ischaemia such as NVD, NVE, prior laser therapy, and NSC diabetic retinopathy grading score. Venular calibre and AVR were not associated with DMI. These data suggest that retinal arteriolar calibre may be a quantitative marker of presence and severity of DMI.

The major epidemiological studies on diabetic retinopathy did not perform FFA on participants and hence there are few studies with which to compare our results. However, a narrower arteriolar calibre is associated with lower limb amputation, (230) and peripheral neuropathy, (231) and therefore may be a marker for ischemic diabetic complications. In the absence of diabetes, narrower arterioles

are also associated with small vessel lacunar stroke and reduced myocardial perfusion, and elevated markers of endothelial dysfunction.(232-234) These suggest that retinal arteriolar narrowing may be an ischaemic biomarker marker in both the retinal and systemic microcirculation.

The presence of narrower arterioles, by reducing available blood flow, may contribute to a propensity to DMI. Alternatively, arteriolar narrowing in DMI may occur in response to reduced metabolic needs. These results provide support for both hypotheses and future longitudinal studies may clarify the question of cause or effect.

It was unexpected that venular calibre was not associated with DMI. Other reports have observed that wider retinal venules are strongly associated with increasing retinopathy severity, incidence, and progression.(235-237) However, these well established associations of venular widening were made in peripheral ischaemia, and our study which examined central DMI did not detect any associations. This may be due to the pathogenesis of venular widening, which is dependent upon vascular endothelial growth factors,(VEGF) which may not be raised to the same extent in DMI as in peripheral ischaemia.(238-240) This study suggests that arteriolar and venular calibre may be differentially related to ischaemia that is located in a central or peripheral location.

Strengths of this study include measurement of DMI and vessel calibers from the same series of FFAs, use of validated methods of grading both variables, and multivariable adjustment for retinopathy severity and peripheral ischemia (i.e. PRP, NVE, NVD). Limitations include firstly, the lack of adjustment for blood pressure as this data is not routinely collected from our eye clinic. Nonetheless, as high blood pressure is related to more severe diabetic retinopathy, our adjustment for retinopathy severity may be considered a partial and indirect adjustment for blood pressure. Further, in the event that the association attenuated with adjustment for blood pressure, this in itself would not change our primary finding that narrower arterioles may indicate the presence of DMI. Secondly, we measured vessel calibers from FFAs, rather than color fundus photographs as reported in most epidemiological

and clinical work. We do not believe this would result in significant bias as others have shown high correlation and only very slight differences in caliber measurements from FFA and color photographs.(241) Nevertheless, we will conduct future studies to measure retinal caliber from color photographs in eyes with DMI to determine if retinal calibre from color photographs can be a marker of DMI without the need for FFA. Finally, the number of patients actually analysed (53) is a small sample of the original population of type 2 diabetic patients (408). We do not believe this would bias our findings as we included all the participants with severe and moderate DMI, and a random subsample of controls with none/mild DMI. Poor quality images which could not be graded occurred in similar proportions in these 2 groups, suggesting that this was unlikely to bias our results. Further, including more of the original sample in our study would only increase the number of controls without DMI, and would not change our findings.

In summary, we report that narrower retinal arterioles are associated with the presence and severity of DMI. Narrower arterioles are also associated with larger FAZ diameter and area. These associations were independent of markers of peripheral ischaemia and suggest measurement of retinal arteriolar calibre may be useful to further characterize and understand underlying vascular changes in eyes with DMI.

2.5.5 The relationship of peripheral and central retinal ischaemia

In the current study, our objective was to better understand the relationships between peripheral and central vascular complications of diabetic retinopathy, and how these lesions affect visual function. We performed both qualitative and quantitative analyses of uwFA images obtained in a cohort of patients with diabetes mellitus. Using this approach, we examined the relationships between peripheral capillary non perfusion, peripheral leakage, FAZ size, OCT-derived central macular thickness measurements, and evaluated the visual significance of these parameters.

Retinal capillary non perfusion in diabetes first demonstrated using Indian ink preparations by Norman Ashton in 1953, in series of post mortem retinae from diabetic patients.(242) There, he described a loss of the peripheral capillary bed, predominantly on the side of retinal artery, with narrowing and "corkscrew coiling" in the corresponding pre-capillary arterioles. Subsequently, more recent histological evidence for macular capillary non perfusion was demonstrated by Bresnick et al in 1976, who observed acellularity in perifoveal capillaries.(167) In the early 1990s, these findings were visualized in vivo with fluorescein angiography using a 30 degree-field camera, and classified by the Early Treatment Diabetic Retinopathy Study (ETDRS).(21) The ETDRS approach to the assessment of macular ischaemia consisted of grading of two vascular structures; (1) capillaries and (2) arterioles, using reference photographs. Capillary abnormalities included the loss of perfusion, broadening, or an increase in the size of foveal avascular zone (FAZ). Arteriolar abnormalities, were graded according to descriptions such as "pruning", "staining" and "focal narrowing". Interestingly, and perhaps due to the limitations portended by retinal photography at the time, the ETDRS standard photographs for arteriolar abnormalities were taken only from areas outside the perifovea. In this study, we were able to visualize with good resolution, not only both the capillary and arteriolar features of diabetic macular ischaemia, but also the presence of these features in peripheral, as well as in the central macula locations within a single uwFA image. This allowed, for the first time, simultaneous analysis of both capillary and arteriolar abnormalities in both peripheral and central retina.

In our analyses, we observed that a relationship exists between capillary non perfusion in the peripheral retina and central macula. Eyes with a high peripheral ischaemia index (>50% peripheral capillary non perfusion of total retinal area visualized) had a larger FAZ compared to those with a low peripheral ischaemia index, and there was a modest correlation between peripheral and central ischaemia, both in all eyes examined (r=0.49), and in those that were treatment naïve (r=0.55). A similar trend was also observed with the peripheral leakage index, but only in eyes, which had not received laser photocoagulation therapy, probably representing the regression of neovascular tufts in treated eyes. **Figure 2.23** is an example of a previously laser-treated eye, with leaking neovascular tufts in the mid-peripheral retina. This is in agreement with our previous work, where we observed that a majority of eyes with proliferative diabetic retinopathy (a surrogate marker for peripheral ischaemia) had some evidence of macular ischaemia (77.2%).(178) It is well known that peripheral retinal ischaemia is a primary risk factor for developing proliferative diabetic retinopathy, and for the majority of patients, it probably represents the "ischemic state" of the eyes as a whole. However, it is important to note that there are patients who do not follow this pattern. **Figure 2.24** is an example of such a patient, who has extensive peripheral ischaemia, but a relatively preserved foveal avascular zone and good visual acuity. How and why this occurs is not known. However, with the emergence of uwFA imaging, we now possess the ability to detect this occurrence in patients with diabetes, and future observations in this cohort may lend insight into the pathophysiology governing patterns of ischaemia in the diabetic retina.

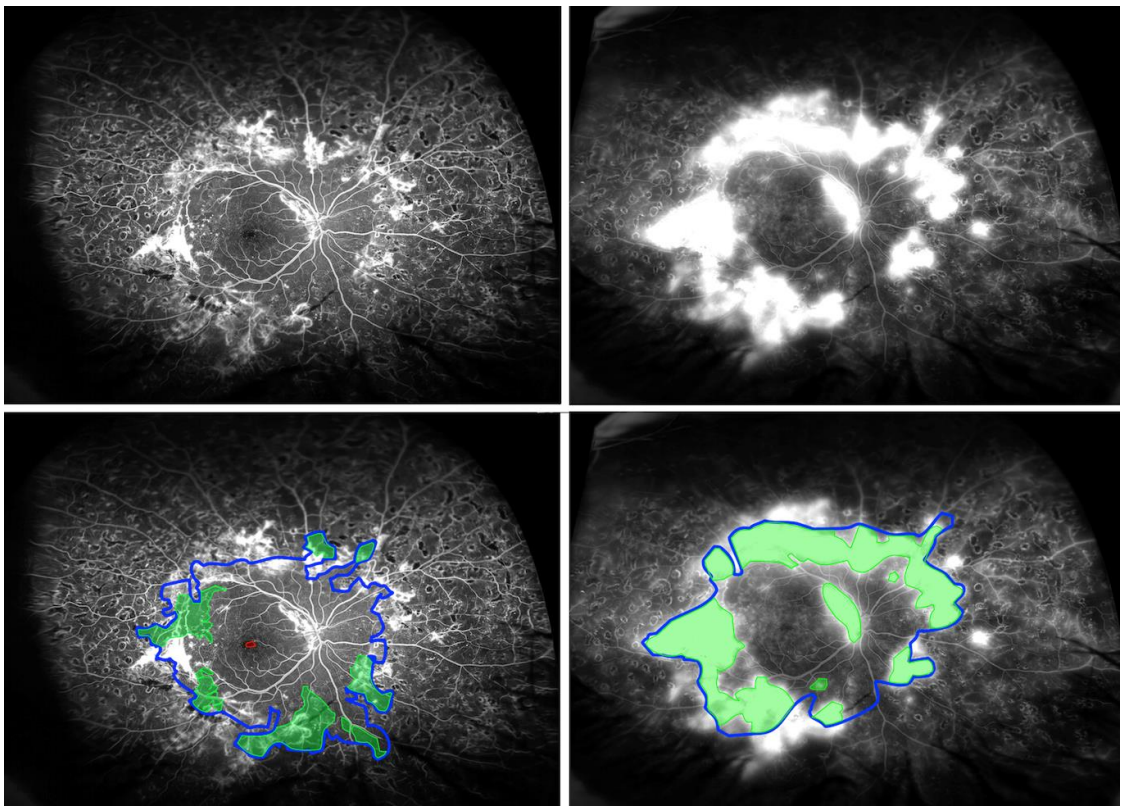

Figure 2.23 An example of an early and late-phase ultra widefield fluorescein angiogram (uwFA) image of a laser-treated diabetic patient, demonstrating peripheral neovascularisation, and leakage.

In eyes that had already received previous laser treatment, the peripheral ischemic and leakage indices were calculated only as a percentage of non-lasered areas of the peripheral retina. (top left) An early-phase uwFA image, acquired at 20 seconds. (top right) Annotated solid blue line delineates the boundary of the non-lasered retina where capillaries are in sharp focus. This area was taken to be the "total retinal area", which was the denominator as the peripheral ischemic index. Annotated solid green lines delineates areas of capillary non perfusion in the non-lasered retinal periphery. Annotated solid red line delineates the boundary of the foveal avascular zone area. (bottom left) A late-phase uwFA image, acquired at 6 minutes. (bottom right) Annotated solid blue line delineates the boundary of the non-lasered retina where capillaries are in sharp focus. Again, this area was taken to be the "total retinal area", which was the denominator as the peripheral leakage index. Annotated solid green lines delineates areas of vascular leakage in the non-lasered retinal periphery.

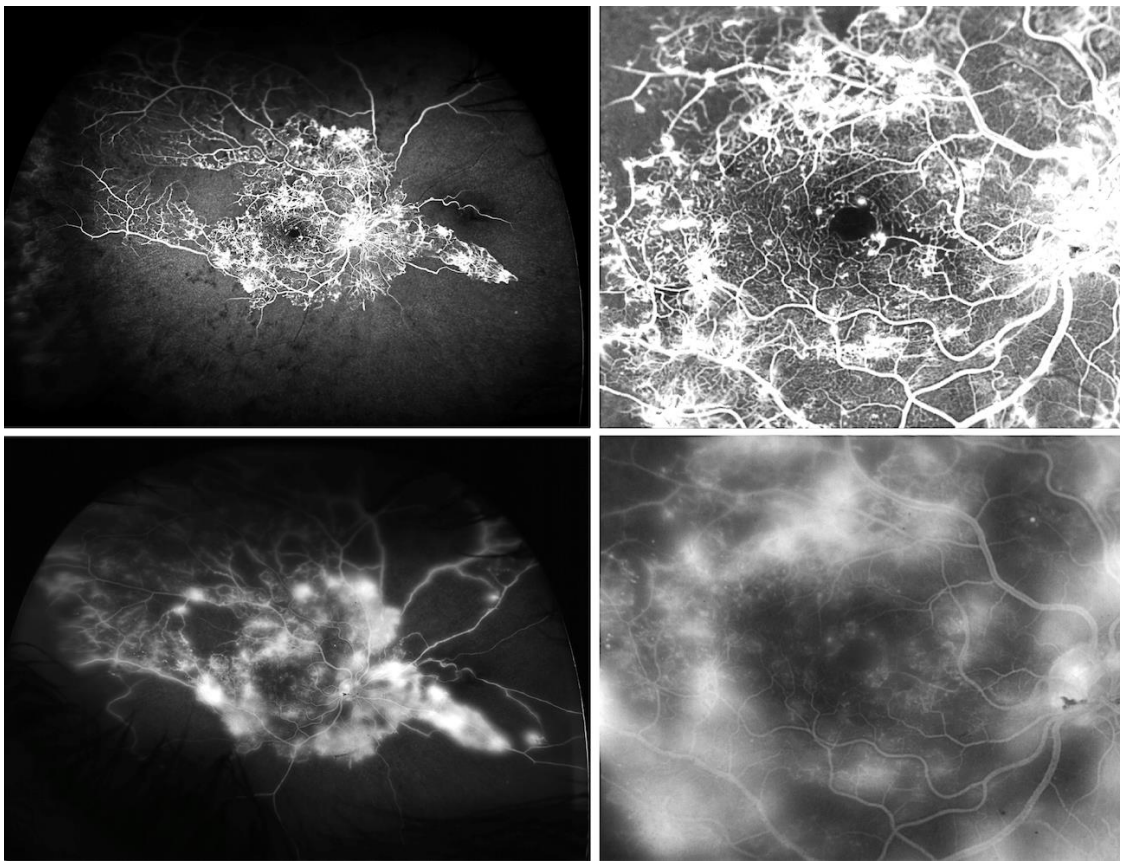

Figure 2.24. An example of an early and late-phase ultra widefield fluorescein angiogram (uwFA) image diabetic patient with severe peripheral capillary non perfusion but only mild macular ischemia.

In this study, the majority of eyes with mild macular ischemia (i.e. a small foveal avascular zone measuring <0.32mm2) had a peripheral ischemia index of less than 50%. However, we observed two outliers with extensive peripheral capillary non perfusion, but a relatively intact foveal avascular zone. The visual acuity of this representative eye was 0.2 LogMAR units. (Top left) An early-phase uwFA image, acquired at 20 seconds. (Top right) 10X magnified early-phase uwFA image, centred on the foveal avascular zone. (Bottom left) A late-phase uwFA image, acquired at 6 minutes. (Bottom right) 10X magnified uwFA image, centred on the foveal avascular zone.

In this study, we also examined the relationships between OCT-derived retinal thickness measurements with peripheral and central retina ischemic indices. We observed that patients with a large FAZ had a significantly thinner retina compared to those with a small FAZ (272 ± 36.0µm versus 217 ± 81.8µm respectively). Conversely, retinal thickness measurements were not different between patients with a high

compared to low peripheral ischaemia index (258 ± 76.3µm versus 276 ± 68.0µm). It appears that thinning of the central macular, i.e. retinal neurodegeneration, occurs with macular but not peripheral ischaemia. This loss of retinal tissue in central ischaemia is in agreement with our previous work, where we observed a reduction of visual function in those with moderate to severe diabetic macular ischaemia (corresponding to the definition of a "large FAZ"= 0.32mm^2 in this study).(178, 243)

Recent uwFA studies utilizing have reported an association between peripheral ischaemia and diabetic macular oedema.(244, 245) This is unsurprising as epidemiological studies have long observed that diabetic retinopathy severity is the major ocular factor associated with diabetic macular oedema. In our study however, although a thicker retina was observed in eyes with a high peripheral leakage index, this did not reach statistically significance (p=0.28). In eyes with a high peripheral ischemic index, the opposite was observed (a thinner retina), but again, this was not statistically significant (p=0.08). A possible explanation for this discrepancy may be the difference in study populations between studies. In this study, a large proportion of our patients (27/47 [57.4%]) had concurrent diabetic macular ischaemia; compared to previous uwFA studies which may have examined population of patients with macular oedema, but minimal or no macular ischaemia.

In light of the relationships observed in this study, we hypothesize that the pattern distribution of ischaemia and vascular leakage in diabetic eyes, may be suggestive of how any functional loss may be reversible or amenable to treatment. In **Figure 2.25**, the relationships observed in this study are represented diagrammatically, with solid arrows representing statistically significant relationships, and dashed arrows trends. From our observations, we suggest two patterns of diabetic retinopathy phenotypes exist; which we have represented as either a "therapeutic triangle" or a "degenerative triangle". For example, in the "degenerative triangle" a patient may present with central vision loss, macular ischaemia, and retinal thinning. Conversely, in the "therapeutic triangle" a pattern of visual loss and macular ischaemia may occur with retina thickening. If it is confirmed in future prospective studies, that these patterns of capillary non perfusion and leakage are

indeed indicative of the treatability of the disease, they may be useful in forming algorithms to identify a window of opportunity for treatment where irreversible visual loss has not occurred, or be used to prognosticate a patients' response to treatment.

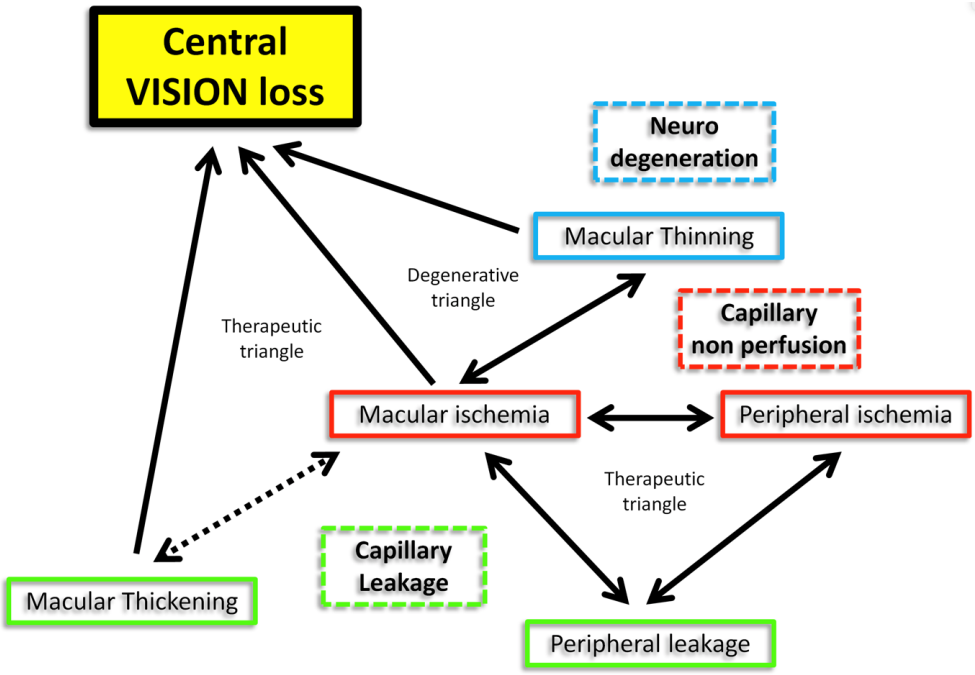

Figure 2.25. Flowchart of the relationships of the two parameters quantified in this study- capillary non perfusion, and vascular leakage, in the peripheral retina, and central macula.

The strengths of this study include, combining a previously validated technique for quantifying macular ischaemia in order to calculate the peripheral ischaemia and leakage indices, and its novel application to examine different patterns disease in the peripheral and central retina. The limitations of this study are inherent to its retrospective, cross-sectional design, and analysis of uwFA images sets from a small number of patients. However, uwFA imaging is a relatively new imaging modality, therefore, though the data we present is exploratory in nature, there are no existing prospective data which examines the relationships between the macular and retinal periphery, and our observations may serve to guide larger prospective studies.

The results of this study, obtained from uwFA images, provide an insight into the relationships between diabetic vascular complications in the retinal periphery and central macular. Although a relationship exists between ischaemia in the center and periphery, it was only macular ischaemia that was associated with a reduced visual function that was further accompanied by retinal thinning. uwFA enables the clinician, for the first time, to observe simultaneously, different patterns capillary leakage and non perfusion. These patterns may be of clinical significance and warrant future evaluation in prospective studies.

2.6 Chapter summary:

In this chapter, DMI was examined in large clinical population of patients with diabetes, attending a tertiary eye referral hospital. DMI was observed to be more prevalent than previously thought but only impacted on visual function when present in moderate to severe severity. Furthermore, a papillomacular location had a greater impact on visual acuity. A relationship between peripheral and central ischaemia was also observed. However, it was only central macular ischaemia that was associated with reduced visual function.The progression rate was calculated at about 7% per year, and progression of DMI itself was predictive of visual loss. DMI was more prevalent in type 1 diabetes, and associated with narrower retinal arterioles, neurodegeneration (thinner retinal nerve fibre layer and outer retinal layers), and thicker Haller's large vessel layer of choroid. No effective treatment currently exists for patients with visual loss attributable to DMI – such a patient group may be an appropriate first target for the development of cellular therapies in diabetic retinopathy. Increasing our understanding of DMI is crucial in developing therapeutic strategies for this disease entity.

3. Clinical imaging in inflammatory eye disease

3.1 Introduction:

Uveitis comprises of a group of diseases characterized by intraocular inflammation, and is an important cause of blindness worldwide.(246) The annual incidence of uveitis is between 17 and 52 per 100,000 of the population, with up to 35% of patients reported to suffer significant visual impairment or legal blindness.(247-250) One of the greatest challenges in caring for patients with sight-threatening uveitis is the lack of objective markers of disease activity. This applies in context of routine clinical practice, where patients receive direct treatment for ocular inflammation, or in clinical trials where these markers are important in order to establish efficacy of new therapies and ensure standardization of care.(251)

Panuveitis is a subtype of uveitis and represents a generalized inflammation of the entirety of the uveal tract as well as the retina and vitreous. This occurs to 15%-25% of patients with uveitis.(252-254) There are numerous causes of panuveitis and can be broadly classified into infectious or autoimmune categories. It is noteworthy that in clinical practice, despite advances ophthalmic imaging capabilities and the availability of laboratory-based diagnostic tests, it is common that a definitive cause of panuveitis is not established. In this chapter, relatively common uveitic conditions such as idiopathic panuveitis, sarcoid- and tuberculosis (TB)-associated uveitis, and punctate inner choroidopathy (PIC) are covered, with respect to the imaging modalities used to detect, diagnose, and monitor these conditions in the vitreous, retina and choroid.

In this chapter, enhanced depth imaging (EDI) protocols were used to acquire OCT-derived images of the choroid in eyes with idiopathic, sarcoid and TB-associated granulomatous uveitis, and punctate inner choroidopathy. Quantitative analysis of these images was performed in an effort to identify parameters, which may potentially be applied in the clinical arena, for example to aid diagnosis and measure disease activity. A further exploratory study was performed to obtain measurements of vitreous signal intensity from OCT image sets obtained in cohorts of patients with intermediate and posterior uveitis. These findings were correlated with standard

assessments of vitreous haze in an effort to develop an improved marker of inflammatory activity in patients with this disease. Objective quantification of ocular inflammation using these techniques, if validated for inflammatory eye disease, may in future be applied in the context of diabetic eye disease.

3.1.1 Idiopathic panuveitis

Idiopathic panuveitis represents this diagnosis of exclusion, and describes cases of panuveitis in which a diagnosis cannot be assigned, despite thorough clinical, imaging and laboratory investigation. For this reason, it has been under represented in clinical and laboratory research. Akin to an orphan disease, idiopathic panuveitis has not received attention due to its lack of a diagnostic label.

Imaging modalities used for the assessment of panuveitis has traditionally been fluorescein angiography (FA); for evaluation of the neuroretina, retina vessels, and retinal pigment epithelium (RPE), and indocyanine green angiography (ICGA); for assessment of inflammatory lesions in the choroid and the choroidal vasculature. Although the patterns of fluorescence, leakage and staining observed on FA and ICGA provide useful information for diagnosis and monitoring of disease activity, they do not provide any information regarding ultra-structural changes. Optical coherence tomography (OCT), which provides excellent cross-sectional images of the retina and the RPE had limited use previously in patients with panuveitis, due to the presence of anterior synechiae, cataracts, or vitritis, (poor media clarity) precluding the acquisition of images. The advances of spectral-domain OCT however, and adaptation of its software for ‘‘enhanced depth imaging’’ (EDI) (46) has allowed in vivo evaluation of the choroid – which by definition, is implicated in “panuveitis”.

The term “Idiopathic” panuveitis may be, in fact, a misnomer. Although the aetiology of this disease entity is unknown, as with many of the “white dot syndromes”, it is the absence of distinguishing features on more traditional modes of imaging, such as FA and ICGA that defines this disease. The ability of EDI OCT to

examine the choroid in detail may provide clues to better describe the disease process in these patients.

3.1.2 Sarcoid and TB- associated panuveitis

Granulomatous uveitis is a chronic inflammatory process that can involve both the anterior and posterior segments of the eye.(255) It is characterized by clinical features such as “mutton-fat” keratic precipitates in the cornea, cells within the anterior chamber and vitreous, retinal vasculitis, and focal or diffuse choroidal lesions.(256-259) Granulomatous disease may result from either an autoimmune process, most commonly sarcoidosis,(256, 257) or a systemic infection, usually tuberculosis (TB),(256, 260, 261) occurring either as an isolated ocular condition or as part of a wider systemic disease.(262)

Sarcoid and TB-associated granulomatous uveitis can cause visual disability from inflammatory sequelae such as cystoid macula oedema, glaucoma, or chorioretinal ischaemia.(263) Fortunately, the majority of patients with sarcoid and TB-associated uveitis are responsive to immunosuppressive treatment and/or the appropriate antimicrobial therapy.(264) However, these treatments can have potential side effects, causing significant ocular and systemic morbidity linked to duration and dosage of treatment and even a possible increase in mortality rates with biologics such as TNFα.(265, 266) And so, the clinician faces the constant challenge of balancing the risk of uncontrolled inflammation on visual outcome with the potentially devastating side effects of immunosuppressive therapy. It is therefore important that the level of treatment for each individual patient is closely titrated against disease activity. In current practice, methods for assessing disease activity are largely reliant on clinical examination - grading the number of cells and intensity of flare in anterior chamber or vitreous by manual or automated means, or measuring the size of retinal or choroidal lesions.(267) Although fluorescein and indocyanine green angiography offers additional information regarding disease activity, it is an invasive procedure, and not suitable for the frequent testing required to closely titrate treatment to disease activity in the patient.(268)

In recent years, the rapid advancement of optical coherence tomography (OCT) technology has allowed non-invasive imaging of the choroid in addition to the retina in cross-section.(46, 269, 270) Several early studies have indicated how OCT-derived choroidal images can be useful in uveitic disorders. For example, OCT has been used (1) to describe characteristic features of specific uveitis entities, including thinning of Haller's large vessel layer of the choroid in idiopathic panuveitis and extra-macular choroidal changes in birdshot chorioretinopathy;(271, 272) to identify distinct stages of a disease process as illustrated by punctate inner choroidopathy;(273, 274) (3) objective measurement of vitreous inflammation(275), and (4) to monitor response to therapy, exemplified by a reduction of subfoveal choroidal thickening with corticosteroid therapy in Vogt-Koyanagi-Harada disease.(276) However, the full potential of OCT in uveitic diseases has yet to be realised.

3.1.3 Punctate inner choroidopathy

Punctate inner choroidopathy (PIC), a disease that typically affects young myopic women, is characterized by the development of multiple, small, yellow-white spots in the posterior pole of each eye.(277-279) These "PIC lesions" are thought to occur at the level of the inner choroid and retinal pigment epithelium (RPE), and develop in the absence of clinically apparent intraocular inflammation. After a few weeks, these acute PIC lesions resolve, leaving atrophic spots with variable pigmentation. In many patients, such resolution leads to improvement or resolution of visual symptoms. However, in about 40%, more severe visual loss subsequently occurs, primarily due to development of choroidal neovascularisation (CNV).(277-280)

In recent years, the advent of intravitreal anti-angiogenic therapies has greatly improved the treatment options for patients with PIC who develop CNV.(280-285) Despite this, the underlying pathophysiology of the disorder remains little understood. For example, during the acute phase, patients often complain of photopsia and visual field defects out of proportion to lesion size and extent,(277,

286) thus suggesting the presence of more widespread disease than is clinically evident (in fact, widespread focal areas of choroidal hypofluorescence may be seen on indocyanine green (ICG) angiography).(287) Furthermore, in the continued absence of clinicopathologic correlative studies, the nature of the acute PIC lesions – and their role in CNV development – remains unclear (on fluorescein angiography (FA), these lesions show early hyperfluorescence with late staining).(279) Fortunately however, recent advances in optical coherence tomography (OCT) imaging offer some exciting opportunities to address these issues.

In patients with uveitic disease, OCT is most commonly used for the evaluation of cystoid macular oedema (CME),(288, 289) although its use for diagnosis and phenotyping has increased in recent years.(290) A recent case report described the evolution of an acute multifocal choroiditis without inflammation that was PIC-like (291) Despite this, the OCT features of PIC have not been extensively evaluated. For the most part, the use of OCT in PIC studies has been restricted to assessment of treatment response in patients with CNV.(281, 283, 292) More recently, a small number of studies have attempted to evaluate PIC lesion characteristics in the absence of CNV.(293-295) Although these studies have utilized the latest generation of “spectral domain” OCT technology, the rarity of the disease means that their patient numbers are small (i.e., case reports or small case series). Furthermore, as a result of limitations with conventional OCT scanning, these studies have been unable to comprehensively evaluate disease features of the choroid. Given that PIC has long been regarded as a disease of the inner choroid – and hence the name – this represents a significant shortcoming. In 2008 however, Spaide et al., described a method by which OCT scanning protocols could be modified to permit direct visualization of the choroid (EDI-OCT).(46) Since this seminal work, EDI-OCT has been used to evaluate the choroid in a variety of conditions, with examples including high myopia and Vogt-Koyanagi-Harada (VKH) disease.(296, 297)

3.1.4 Novel methods for quantification of vitreous inflammation

The current gold standard for assessing vitreous inflammation in patients with intermediate and posterior uveitis is the National Eye Institute (NEI) system for grading of vitreous haze.(298, 299) In this system, often referred to as the Nussenblatt scale, the patient's eye is examined with an indirect ophthalmoscope and the appearance compared to a series of photographs representing various degrees of fundal vitreous haze. This assessment is recognised as a surrogate endpoint by the FDA and has been adopted as a primary outcome in almost all recent studies of uveitis. Despite this, the technique has a number of limitations, notably that it is: 1) subjective, with only moderate inter-observer agreement; 2) non-continuous, leading to very large steps in disease activity between categories; 3) poorly discriminatory at lower levels of vitreous haze, with most cases of active uveitis being scored at 0.5+ or 1+; 4) limiting of sensitivity in a clinical trial context (where a two point change is required to be counted as significant).(300, 301)

In recent years, ophthalmology has been revolutionized by the introduction of a new imaging modality, optical coherence tomography (OCT).(26) OCT provides high-resolution, cross-sectional images of ocular tissues in a non-invasive manner. From an early stage in its development, OCT has also been pioneering in its attempts to provide automated measurements of disease morphology and thus objective markers for clinical care.(302) Until recently, OCT imaging has focused in large part on the neurosensory retina, allowing qualitative assessment of disease features such as cystoid macular oedema (CME) and providing automated measurements of retinal thickness.(205, 303) Lately however, the use of OCT for direct visualization of vitreous inflammatory cells in patients with uveitis has been described.(304) In addition, quantitative assessment of OCT image sets has begun to evolve, from simple measurements of thickness or volume, to the assessment of more novel parameters such as optical density/signal intensity.(305-311) Taken together, these advances present an opportunity to derive objective, OCT-derived measurements of inflammation in patients with uveitis.

3.2 Aim:

To investigate recent and novel imaging techniques for quantifying inflammation in the human vitreous, retina and choroid using OCT-derived images in patients with uveitis. The rationale for including patients with uveitis is to identify retinal inflammation imaging biomarkers that may be applied to diabetic retinopathy, where inflammation is hypothesized to play a role in the pathogenesis and prognosis of disease.

3.3 Materials and Methods:

3.3.1 Inclusion criteria and data collection

Clinical and imaging data were retrospectively collected from consecutive patients diagnosed with idiopathic panuveitis, sarcoid and TB-associated panuveitis, and punctate inner choroidopathy attending a specialist uveitis clinic over a period of six-months. Patient notes were also checked 12 months later to confirm diagnoses. Approval for data collection and analysis was obtained from a UK National Health Service (NHS) research ethics committee and adhered to the tenets set forth in the Declaration of Helsinki.

Patients included in this study had the following assessments: physical examination for features of systemic inflammatory or autoimmune disease; complete ophthalmic examination including best corrected visual acuity (BCVA), disease activity and duration, treatment, and presence of cystoid macular oedema (CMO) or epiretinal membrane (ERM); a standard laboratory work-up for panuveitis, including full blood count with differential analysis, angiotensin-converting enzyme, autoantibody screen, C-reactive protein, erythrocyte sedimentation rate, liver and kidney function tests, treponemal EIA, and quantiFERON TB-Gold test; chest X-ray, FA and ICGA. Patients with myopia or hypermetropia of greater than 6 diopters were excluded. The right eye was included in patients with bilateral disease.

The First International Workshop on Ocular Sarcoidosis (FIWOS) recommended four levels of certainty for diagnosis in patients in whom other possible causes of uveitis had been excluded:(312) (1) biopsy-supported diagnosis with a compatible uveitis was labelled as definite ocular sarcoidosis; (2) if biopsy was not done but chest x-ray was positive showing bilateral hilar lymphadenopathy associated with a compatible uveitis, the condition was labelled as presumed ocular sarcoidosis; (3) if biopsy was not done and the chest x-ray did not show bihilar lymphadenopathy but there were three of the classic intraocular signs and two positive laboratory tests, the condition was labelled as probable ocular sarcoidosis; and (4) if lung biopsy was done and the result was negative but at least four classic intraocular signs and two positive laboratory investigations were present, the

condition was labelled as possible ocular sarcoidosis. Only patients with definite, presumed or probable sarcoidosis were included in this study. The combination of clinical signs and laboratory tests proposed by the FIWOS has been validated to be highly specific and sensitive for the diagnosis of ocular sarcoidosis.(313)

With TB associated uveitis the large variations in clinical presentation and the lack of uniformity in diagnostic criteria makes diagnosis difficult.(314) Most patients have no evidence of *Mycobacterium tuberculosis* in their ocular biopsies.(315) Patients with clinical ocular signs suggestive of TB,(259) and positive microscopy or culture of *Mycobacterium tuberculosis* from any bodily fluid, in the absence of another identifiable cause for their uveitis were labelled as definite ocular TB. In the absence of confirmatory microbiology, when other identifiable causes of uveitis had been excluded, patients were labelled as presumed ocular TB only if they met all of the following 3 published criteria: (1) Ocular signs suggestive of TB(259); (2) Positive QuantiFERON-TB Gold test(316-320); (3) Positive response to anti-tuberculous therapy(321).

In patients with granulomatous uveitis, disease activity was recorded from notes based on clinical examination and investigations including macula OCT, fundus fluorescein and indocyanine green angiography. Anterior chamber activity was graded by measuring the number of cells and intensity of flare. Posterior segment activity was based on the clinician's impression of significant vitritis, vasculitis, chorioretinitis, papillitis. Cases of intermediate uveitis, posterior uveitis and panuveitis were recorded as 'posterior uveitis'. Only cases of isolated anterior chamber activity with or without cystoid macula oedema were recorded as 'anterior uveitis'.

3.3.2 Optical coherence tomography image acquisition and analysis

3.3.2.1 Acquisition of EDI OCT-derived images

Spectral domain OCT images were acquired on the Spectralis imaging system. (Heidelberg Engineering, Germany). This system acquires 40,000 A-scans per second with an axial resolution, in tissue, of 7 μm, and a transverse resolution of 14 μm. All images were acquired using a custom EDI scanning protocol (each image set consisted of 7 OCT B-scans obtained in a 20 x 15 degree horizontal raster pattern, and with each individual B-scan generated from 50 averaged scans). No image manipulation was performed prior to analysis.

For the assessment of vitreous inflammation, volume scans centered on the fovea were obtained. The EDI mode was not used in any case and the zero delay line, or the point of maximum sensitivity, was maintained on the vitreous side.(322)

3.3.2.1 Analysis of EDI OCT-derived images

For the generation of retinal and choroidal thickness maps, raw OCT data were exported from the Heidelberg Spectralis OCT system and imported into validated custom grading software (OCTOR) developed by Doheny Image Reading Center, Los Angeles, California.(173, 323) All OCT image sets contained a minimum of 13 B-scans distributed in a horizontal raster pattern overlying the area covered by the nine subfields of the Early Treatment Diabetic Retinopathy Study (ETDRS) grid. For each OCT image set, the inner and outer boundaries of both the retina and the choroid were manually segmented. All boundaries were drawn in accordance with a standard OCT grading protocol by a grader masked to patient identity, underlying diagnosis and disease activity.(324)

The retinal space was defined as the space lying between the inner aspect of the internal limiting membrane and the outer border of the photoreceptor outer segments. The choroid was defined as the space between the outer border of the retinal pigment epithelium and choroidoscleral junction. The choroid was further

subdivided into Haller's large vessel and Sattler's medium vessel layers. On OCT, the walls of blood vessels appear hyperreflective, and their lumens appear hyporeflective. Haller's large vessel layer was defined as the outer choroid, consisting of large hypointense spaces representing large vascular luminal spaces (with luminal-to-vessel wall ratio ≥50%).(325) Sattler's medium vessel layer consisted of small- to medium-sized hypointense spaces, surrounded by hyperintense stroma (with a lumen-to-vessel wall ratio <50%), giving a mottled appearance on scans. This layer also included the choriocapillaris, which is not easily distinguishable with the current resolution of OCT images.(326, 327) The foveal central subfield (FCS) in micrometers (μm), corresponds to the Early Treatment Diabetic Retinopathy Study (ETDRS) central subfield (area 9), and the total macular circle (TMC), corresponds to ETDRS areas 1-9.

In cases of PIC, the number of visible PIC lesions was then counted using macula-centered NIR fundal images (55° field of view). Only those lesions that were included in the 7 raster OCT scans covering the 20x5º scanned area were selected for analysis. OCT lesions that could be interpreted as CNV were classified as "definitely CNV" or "questionably CNV" were correlated with previous clinical records, colour fundus photographs and fluorescein angiography images and were excluded from qualitative analysis. Location of definite CNV lesions was addressed with these clinical data as subfoveal, juxtafoveal and extrafoveal for subgroup analysis purposes. Each PIC lesion included in OCT image sets was then evaluated for the following changes in retinal morphology: 1) focal elevation of the RPE (with underlying hyporeflective space between RPE and Bruch´s membrane and increased penetration of light through the inner choroid), 2) focal atrophy of the outer retina/RPE, and 3) presence of sub-RPE deposits (with hyperreflective signal within the lesion). Choroidal morphology was then assessed, including: 1) presence of focal hyperreflective dots in the inner choroid, and 2) focal thinning of the choroid adjacent to PIC lesions. Examples of each retinal and choroidal morphologic feature are illustrated in **Figure 3.1**

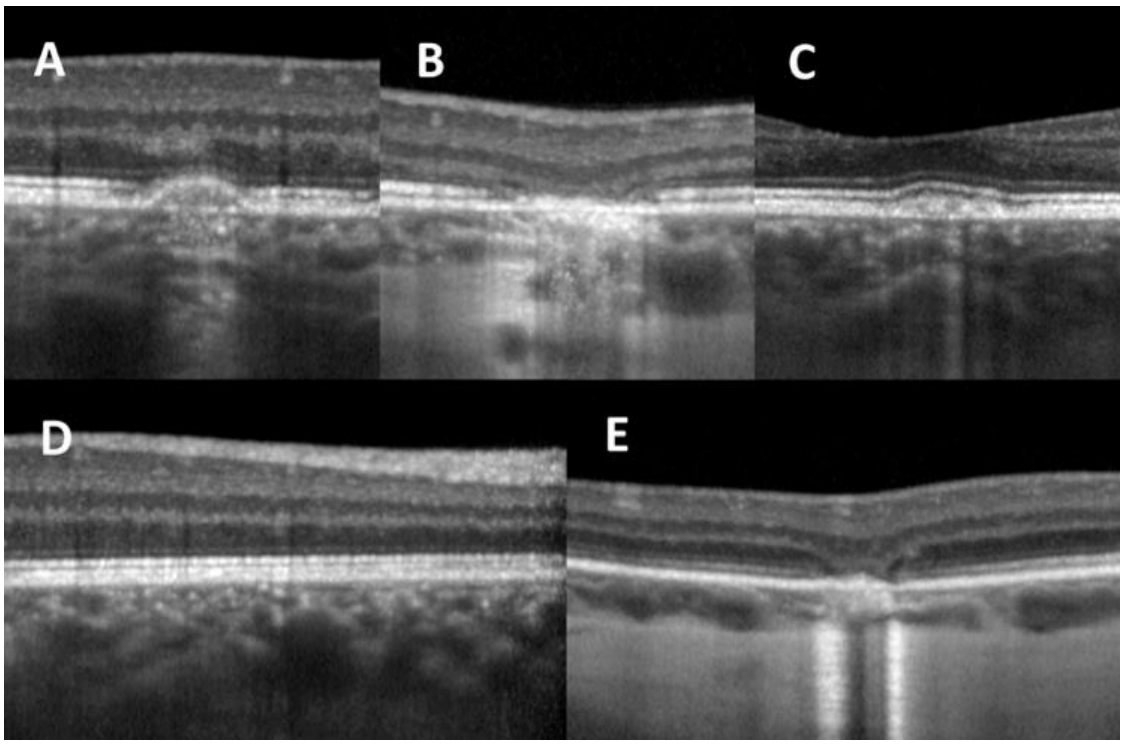

Figure 3.1. Qualitative analysis of punctate inner choroidopathy (PIC) lesions by optical coherence tomography (OCT).

[A] Retinal pigment epithelium (RPE) elevation with sub-RPE hyporeflective signal. **[B]** Focal disruption of outer retinal layers and RPE atrophy, with window defect resulting in increased signal transmission from inner choroid. **[C]** Sub-RPE deposit with hyperreflective signal. **[D]** Multiple hyperreflective dots in the inner choroid. **[E]** Focal choroidal thinning localized beneath atrophic PIC lesion.

In the qualitative Analysis of the Vitreous using OCT, the presence or absence of intravitreal cellular infiltrates was noted each OCT image set. These were defined as hyperreflective dots in the vitreous that were larger and of greater density than background speckle noise.(304) These were differentiated from the larger, non-punctate, irregular condensations within the vitreous cavity, which appeared to reflect normal age-related vitreous syneretic changes. Examples of vitreous cells and flare, as seen on OCT, are presented for a variety of uveitic aetiologies in **Figure 3.2**.

In the quantitative Analysis of the Vitreous using OCT: Raw OCT data were exported from the Heidelberg Spectralis OCT system and imported into validated custom grading software OCTOR.(328, 329) This software enables easy navigation of

spectral domain OCT volume scans and manual boundary annotation of each B-scan, or a subset of B-scans. Based on these boundaries, the intensity of all pixels in a morphologic compartment of interest (e.g., vitreous) can be summed, and mean OCT intensity values generated.(170, 330) Image contrast was not adjusted either before or after export from the OCT system. For each OCT image set, boundaries were manually segmented in accordance with standardized OCT grading protocols **(Figures 3.3 and 3.4)**.(330, 331) These boundaries consisted of: 1) "vitreous top", the uppermost extent of the vitreous space as visualized on OCT, 2) internal limiting membrane (ILM), the inner boundary of the neurosensory retina, 3) retinal pigment epithelium (RPE)-inner, the inner boundary of the RPE, and 4) RPE-outer, the outer boundary of the RPE. The "vitreous" was defined as the space lying between the vitreous top and the ILM. The "RPE" was defined as the space lying between the inner and outer boundaries of the RPE.

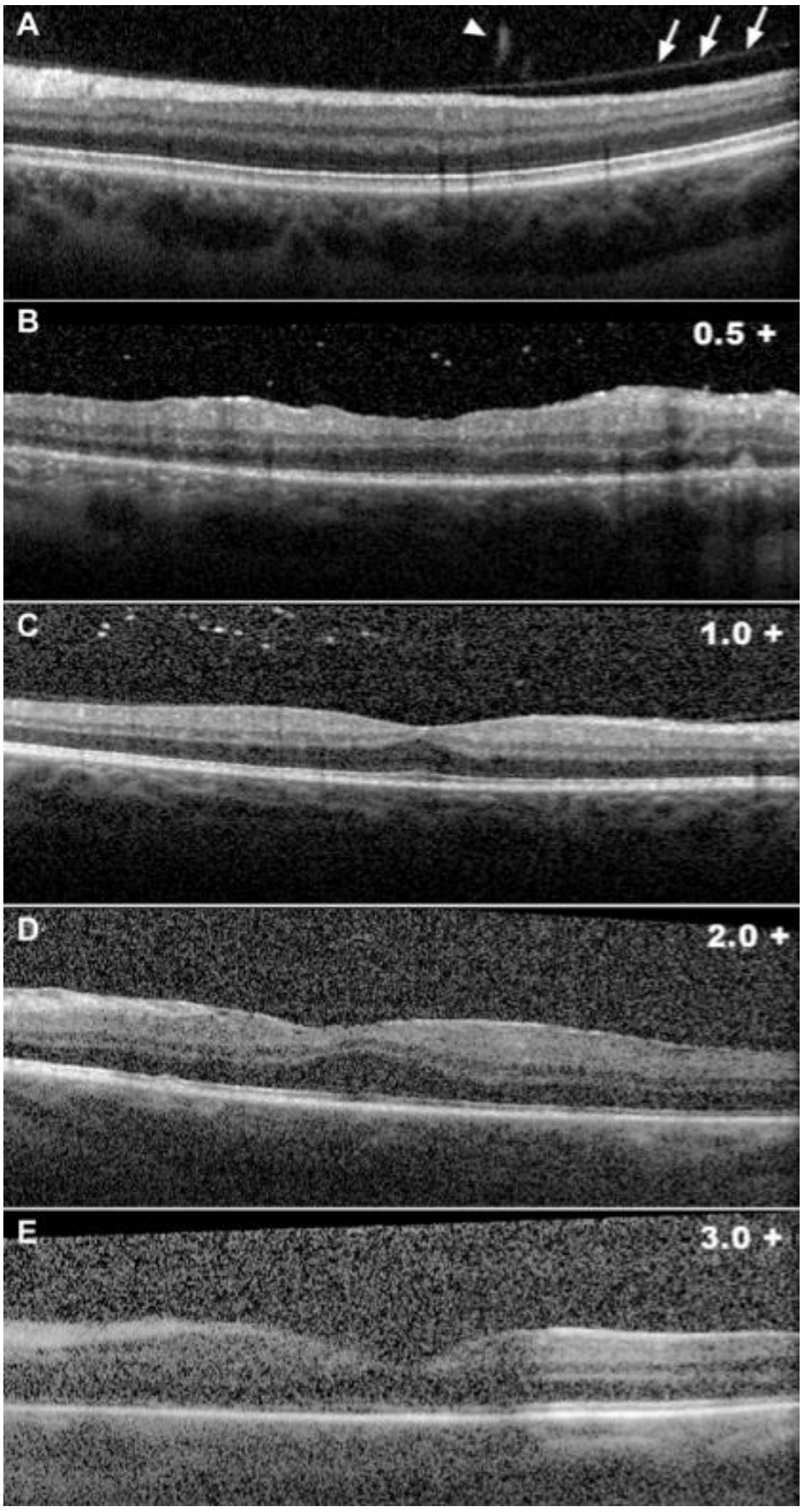
A
B
0.5 +
C
1.0 +
D
2.0 +
E
3.0 +

Figure 3.2. Optical coherence tomography images of vitreous haze

Visualization of age-related and inflammatory changes in the vitreous using spectral-domain optical coherence tomography (SD-OCT). A, An OCT B-scan obtained from a 74-year-old woman without uveitis demonstrating detachment of the posterior hyaloid face (arrows) and age-related vitreous condensation (arrowhead). B, An OCT B-scan obtained from a patient with birdshot chorioretinopathy demonstrating vitreous cells with minimal vitreous haze (clinical vitreous haze score .0.5, vitreous signal intensity/retinal pigment epithelium [VIT/RPE]-relative intensity 0.0783). C, An OCT B-scan obtained from a patient with sarcoid-related panuveitis demonstrating vitreous cells in combination with moderate vitreous haze (clinical vitreous haze score .1.0, VIT/RPErelative intensity 0.2222). D, An OCT B-scan obtained from a patient with idiopathic panuveitis demonstrating vitreous cells in combination with moderate to severe vitreous haze (clinical vitreous haze score .2.0, VIT/RPE-relative intensity 0.2701). E, An OCT B-scan obtained from a patient with idiopathic panuveitis demonstrating vitreous cells in combination with more severe vitreous haze (clinical vitreous haze score .3.0, VIT/RPE-relative intensity 0.3818).

After completion of grading, mean intensity values were calculated for the vitreous space (termed “VIT-Absolute Intensity”) and the RPE space (termed “RPE-Absolute Intensity”) in the foveal central subfield (i.e., the 1 mm in diameter central subfield of the ETDRS grid). Intensity values for the vitreous and RPE spaces were then expressed as a ratio (termed “VIT/RPE-Relative Intensity”). To assess reproducibility, a second, experienced OCT grader, also in a masked fashion, also segmented the OCT image sets.

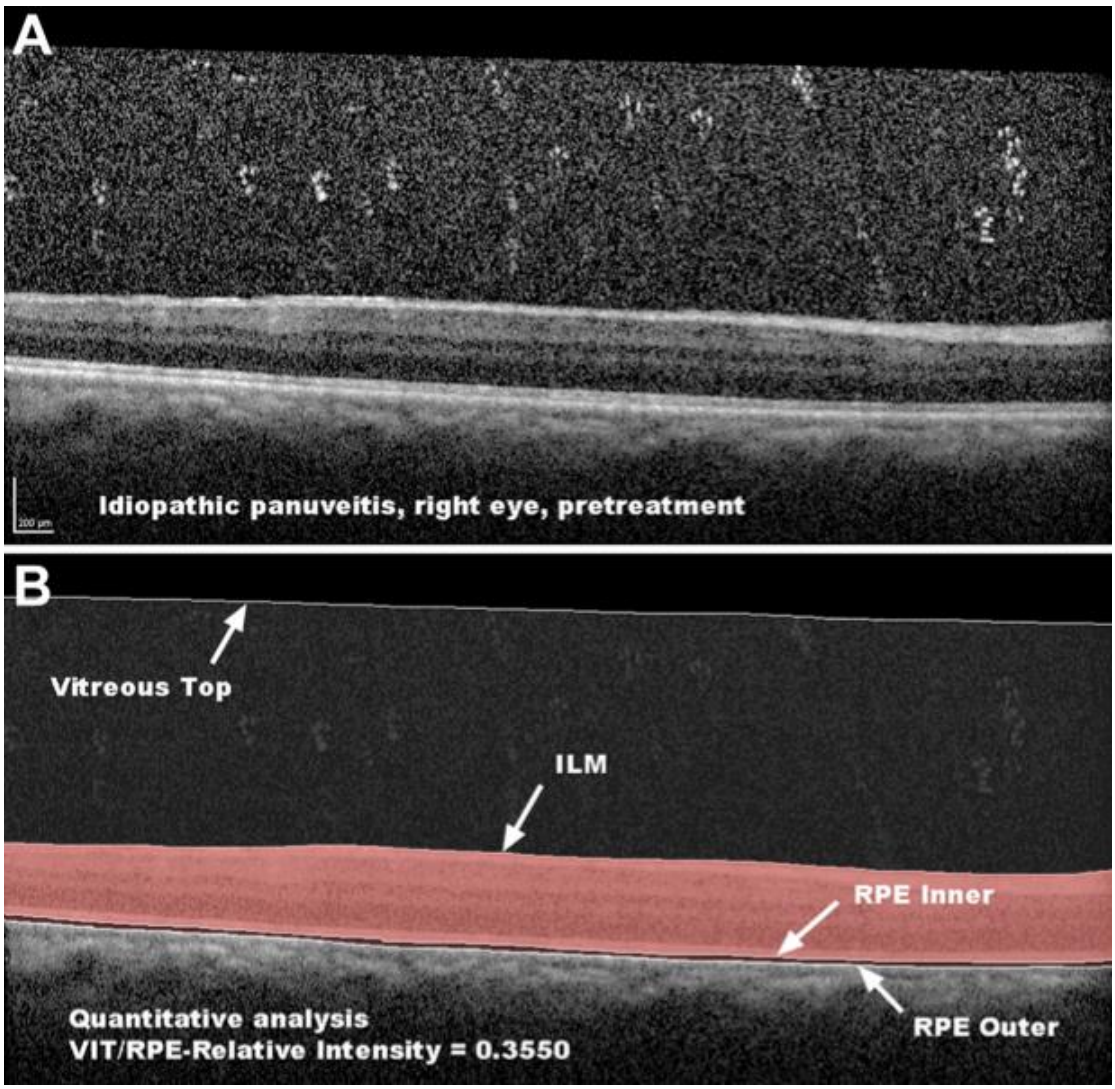

Figure 3.3. Quantitative assessment optical coherence tomography images of vitreous haze

Quantitative assessment of the vitreous using spectral-domain optical coherence tomography (SD-OCT) at initial presentation in a 57- year-old patient with idiopathic panuveitis (clinical vitreous haze score 2.). A, An OCT B-scan revealing widespread intravitreal cellular infiltrates and diffusely increased vitreous signal intensity. B, An OCT B-scan after manual segmentation of the vitreous compartment (boundaries: vitreous top to internal limiting membrane) and the retinal pigment epithelium (RPE) (boundaries: RPE-inner to RPE-outer), with a resulting vitreous signal intensity/retinal pigment epithelium (VIT/RPE)-relative intensity of 0.3550. ILM. internal limiting membrane.

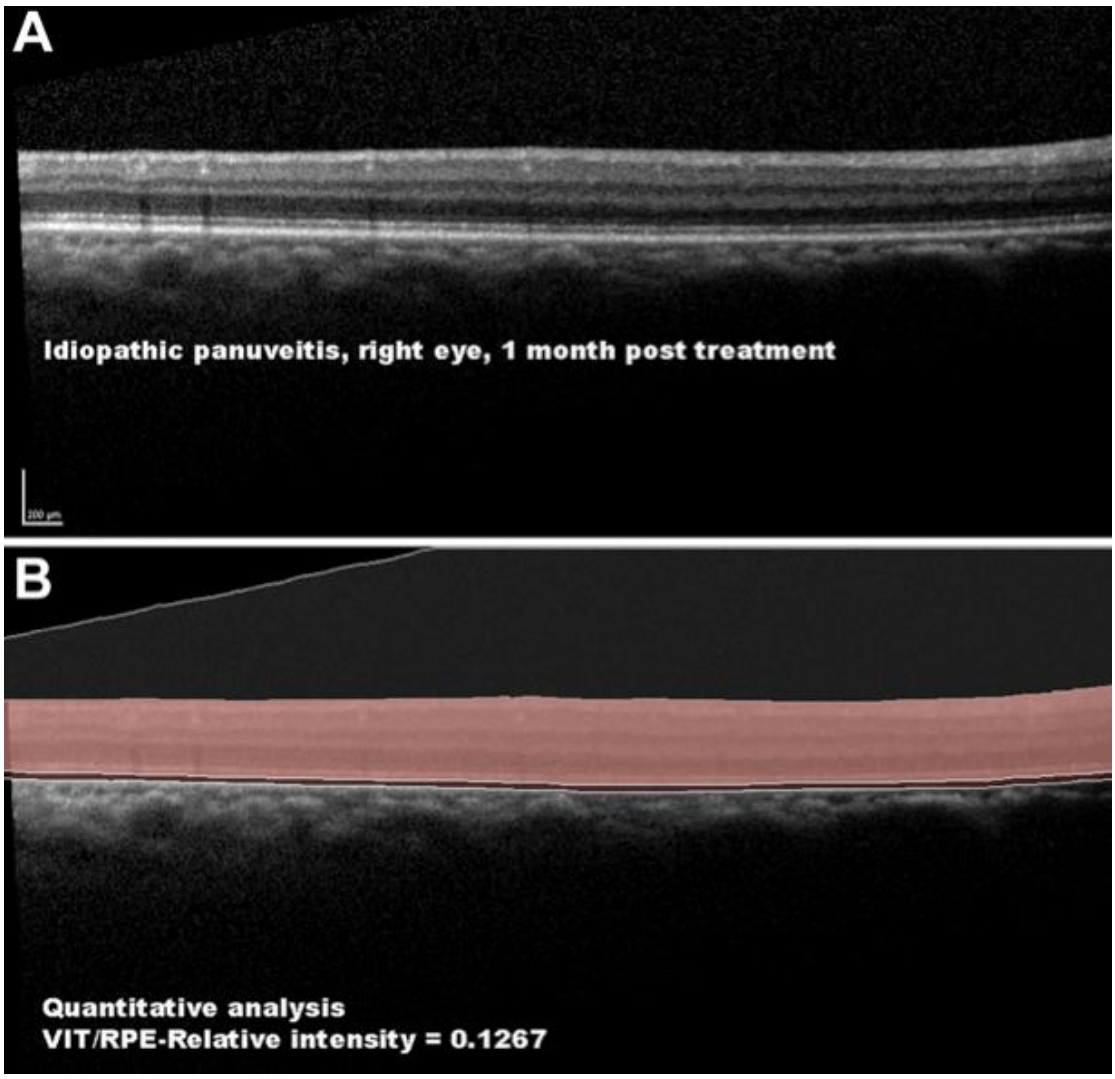

Figure 3.4. Quantitative assessment of the vitreous using spectral-domain optical coherence after corticosteroid treatment.

1 month after treatment with oral corticosteroids, this 57-year-old patient with idiopathic panuveitis had an OCT B-scan (A) revealing a significant reduction in both vitreous haze and inflammatory cells. (B) An OCT B-scan after manual segmentation of the vitreous compartment, with a resulting vitreous signal intensity/retinal pigment epithelium (VIT/RPE)-relative intensity of 0.1267.

3.3.2 Statistical analysis

Non-parametric analyses were used as histograms reveal that the distribution of data was skewed to the left. The Chi-squared test was used to assess categorical variables and, Mann-Whitney U test and Spearman's rank correlation coefficient were applied to continuous variables. Multivariable regression was then used to model the effects of clinical characteristics on mean OCT intensity values. Snellen BCVA was converted to logarithm of the minimum angle of resolution (LogMAR) equivalents for the purposes of statistical analysis. Reproducibility, or inter observer variability, was assessed using Bland-Altman plots, using the mean OCT intensity values obtained by each grader. The mean difference and confidence intervals were calculated. Agreement between graders was also examined using Bland-Altman analysis, with the 95% limits of agreement (LoA) between graders calculated after confirming that the measurement differences were normally distributed using histograms.

Due to multiple statistical comparisons, we applied a Sidak correction to adjust p values to a more stringent value of $p \leq 0.004$, to allow for an experimental wide type 1 error of 10%. Less stringent $p<0.05$ were also presented. Statistical analyses were performed using SPSS software version 16 (SPSS, Inc, Chicago, IL).

3.4 Results:

3.4.1 Idiopathic panuveitis

3.4.1.1 Baseline characteristics

Twenty-one eyes from 21 patients were analysed. The mean age was 47.7 years (range: 23-88), and male to female ratio was 1:2. The mean VA was 0.29 logMAR (range: -0.08 to 1.78) (6/12 Snellen). Seventeen patients (80.9%) had bilateral and 4 unilateral (19.1%) disease. All patients had clinically inactive disease at the time of data acquisition. Patient demographics and clinical characteristics are summarized in **Table 3.1**.

3.4.1.2 Visual Significance of Clinical Parameters

Poor visual acuity is associated with longer duration of disease: The mean disease duration of all eyes was 78.4 months with a wide range: 1 to 240 months. Approximately half or 10 eyes (47.6%) had disease duration of greater than 24 months, and 11 eyes (52.4%) less than 24 months. The mean VA was significantly worse in patients with longer disease duration (>24 months) ($p=0.05$), and was negatively correlated with the duration of disease. ($\rho=-0.49$, $p=0.03$)

Treatment modality has no effect on visual acuity: The majority of eyes (90.5%) were on some form of immunosuppressive treatment. Four eyes (19.1%) were on systemic steroids, 7 (33.3%) were on systemic steroids with a second-line immunosuppressive agent, 7 (33.3%) were on topical steroids, 1 (4.7%) had periocular steroids, and 2 (9.5%) were not on any treatment. There was no significant difference in VA between any of the treatment subgroups. ($p>0.40$)

The presence of concurrent CMO and ERM is associated with poor visual acuity: The proportion of eyes with CMO and ERM were 14.3% and 28.6% respectively. VA in these eyes was significantly lower compared to the rest of the patients ($p=0.007$).

Table 3.1. Demographics and clinical characteristics of patients with idiopathic panuveitis.

Patient	Age	Sex	Eye	Type	Duration (months	Treatment	CMO	Activity	ERM	BCVA logMAR
1	53	M	RE	Bilateral	168	Systemic steroids	No	Inactive	No	0.60 (6/24)
2	75	F	RE	Bilateral	132	Systemic steroids	No	Inactive	Yes	0.78 (6/36)
3	50	F	LE	Unilateral	144	Topical steroids	Yes	Inactive	No	1.30 (3/60)
4	41	F	RE	Bilateral	108	Systemic steroids and mycophenolate mofetil	Yes	Inactive	No	1.78 (1/60)
5	48	M	RE	Bilateral	48	Topical steroids	No	Inactive	No	-0.08 (6/5)
6	27	M	RE	Bilateral	100	Systemic steroids and mycophenolate mofetil	No	Inactive	Yes	0.30 (6/12)
7	33	F	RE	Unilateral	12	No treatment	No	Inactive	No	-0.08 (6/5)
8	35	F	RE	Unilateral	5	No treatment	No	Inactive	Yes	0 (6/6)
9	55	M	RE	Bilateral	144	Periocular steroids	No	Inactive	No	0 (6/6)
10	74	F	RE	Bilateral	144	Topical steroids	No	Inactive	Yes	0.30 (6/12)
11	57	F	RE	Bilateral	132	Systemic steroids	No	Inactive	No	-0.08 (6/5)
12	88	F	RE	Bilateral	120	Topical steroids	No	Inactive	Yes	0.30 (6/12)
13	79	F	RE	Bilateral	36	Systemic steroids and mycophenolate mofetil	Yes	Inactive	No	0.48 (6/18)
14	26	M	RE	Bilateral	36	Systemic steroids and mycophenolate mofetil	No	Inactive	No	0.18 (6/9)
15	39	F	RE	Bilateral	32	Systemic steroids and mycophenolate mofetil	No	Inactive	No	-0.08 (6/5)
16	23	F	RE	Bilateral	24	Systemic steroids and mycophenolate mofetil	No	Inactive	No	0 (6/6)
17	37	M	RE	Bilateral	240	Systemic steroids	No	Inactive	No	0.18 (6/9)
18	39	M	RE	Bilateral	1	Topical steroids	No	Inactive	No	-0.08 (6/5)
19	26	F	RE	Bilateral	1	Topical steroids	No	Inactive	No	0.18 (6/9)
20	43	F	RE	Unilateral	15	Topical steroids	No	Inactive	Yes	0.18 (6/9)
21	53	F	RE	Bilateral	5	Systemic steroids and azathioprine	No	Inactive	No	0 (6/6)

(CMO: cystoid macular oedema, ERM: epiretinal membrane, BCVA: best corrected visual acuity)

3.4.1.3 Qualitative features of EDI OCT:

As expected, there was a lack of distinctive features in the EDI OCT of this patient cohort. We did not observe any evidence of inflammatory masses in any of the 147 B-scans from 21 eyes. In the 4 patients with unilateral disease, we also reviewed OCT images from the unaffected eye as a basis of comparison to the affected eyes, paying particular attention to the choroidal vasculature. We observed a qualitative difference in the vascular pattern of Haller's large vessel layer (HLVL) in "affected" compared to "unaffected" eyes. There was a decrease in hypo reflective areas, corresponding to the vessel lumen, in "affected" eyes. A similar pattern was observed in 13/17 remaining eyes. **(Figure 3.5)**

3.4.1.4 Clinical Significance of Retinal and Choroidal OCT parameters:

Retinal and choroidal thickness measurements: The mean retinal thickness was 342.1 µm ± 110.3 and ranged from 218 to 686 µm. The mean choroidal thickness was 233.7 µm ± 73.3 and ranged from 103 to 319.8 µm. Its sublayers – Sattler's medium vessel layer (SMVL) and HLVL were 66.1 µm ± 36.7 and 167.8 µm ± 53.7 respectively. A summary of thickness and volume measurements are listed in **Table 3.2**.

Ratio of choroidal layers to retinal thickness measurements: There were no significant correlations between retinal and choroidal parameters with duration of disease, treatment modality, and VA. However, when thickness of the choroidal layers were expressed as a ratio of the retina **(Table 3.2)**, the "choroid: retina ratio" (C:R) showed significant correlation to VA. ($r=0.58$, $p=0.006$) This correlation was maintained in HLVL to retinal thickness ratio (H:R) ($r=0.56$, $p=0.009$), but not in the SMVL to retinal thickness ratio (S:R). ($r=0.352$, $p=0.12$)

Comparing eyes with and without CMO, the C:R and H:R ratio was significantly different between the two groups ($p=0.01$). There was no difference in the S:R ratio. ($p=0.155$) with age. This correlation was maintained in the C:R ($r=-0.60$, $p=0.004$) and S:R ($r=-0.705$, $p<0.001$) ratios, but not in the H:R ratio ($r=-0.39$, $p=0.08$).

Table 3.2. OCT-derived measurements of the retinal, choroidal layers and ratios for all patients with idiopathic panuveitis.

Patient	Retinal thickness (μm)	Retinal volume (mm^3)	Choroidal thickness (μm)	Choroidal volume (mm^3)	Sattler's thickness (μm)	Sattler's volume (mm^3)	Haller's thickness (μm)	Haller's volume (mm^3)	Sattler's/ Choroid ratio	Haller's/ Choroid ratio	Sattler's/ Retina ratio	Haller's/ Retina ratio	Chroid/ Retina ratio
1	287.60	9.80	192.70	6.56	52.10	1.78	140.60	4.79	0.27	0.73	0.18	0.49	0.67
2	279.10	10.18	103.00	3.76	34.20	1.25	68.90	2.51	0.33	0.67	0.12	0.25	0.37
3	686.30	24.21	239.40	8.43	77.00	2.71	162.40	5.73	0.32	0.68	0.11	0.24	0.35
4	595.60	16.89	310.00	8.80	106.30	3.01	204.10	5.78	0.34	0.66	0.18	0.34	0.52
5	303.40	10.34	284.80	9.70	52.10	3.49	182.30	6.18	0.36	0.64	0.34	0.60	0.94
6	471.40	16.07	256.00	8.72	105.90	3.61	150.20	5.11	0.41	0.59	0.22	0.32	0.54
7	299.00	9.83	319.80	10.52	128.60	4.23	191.60	6.29	0.40	0.60	0.43	0.64	1.07
8	328.80	10.44	310.60	9.86	159.40	5.05	151.60	4.81	0.51	0.49	0.48	0.46	0.94
9	284.20	10.37	203.60	7.40	27.10	.99	176.50	6.42	0.13	0.87	0.10	0.62	0.72
10	328.90	10.82	181.00	5.94	52.80	1.73	128.30	4.21	0.29	0.71	0.16	0.39	0.55
11	218.90	7.22	171.40	6.04	37.00	1.30	134.40	4.73	0.22	0.78	0.17	0.61	0.78
12	272.70	8.96	138.90	4.56	30.30	.99	108.60	3.57	0.22	0.78	0.11	0.40	0.51
13	333.60	11.34	147.30	5.01	30.80	1.05	116.50	3.97	0.21	0.79	0.09	0.35	0.44
14	340.80	13.73	357.60	14.40	87.60	3.52	270.10	10.84	0.24	0.76	0.26	0.79	1.05
15	293.00	10.31	297.10	10.47	61.50	2.15	235.90	8.26	0.21	0.79	0.21	0.81	1.01
16	329.10	11.21	259.40	8.79	66.00	2.24	193.70	6.58	0.25	0.75	0.20	0.59	0.79
17	328.60	11.60	279.00	9.80	61.00	2.13	218.60	7.65	0.22	0.78	0.19	0.67	0.85
18	296.10	13.93	144.20	6.77	33.10	1.56	111.10	5.22	0.23	0.77	0.11	0.38	0.49
19	304.80	10.39	269.70	9.18	60.00	2.04	210.00	7.15	0.22	0.78	0.20	0.69	0.88
20	312.80	10.65	294.30	10.03	33.70	1.15	260.80	8.87	0.11	0.89	0.11	0.83	0.94
21	290.30	10.59	148.00	5.38	40.30	1.45	108.30	3.90	0.27	0.73	0.14	0.37	0.51
Mean ±SD	342.1 ± 110.3	11.8 ± 3.6	233.7 ± 73.3	8.1 ± 2.5	66.1 ± 36.7	2.25 ±1.1	167.8 ± 53.7	5.8 ± 1.9	0.27±0.1	0.72 ± 0.1	0.19 ± 0.1	0.51 ± 0.1	0.71 ± 0.2

3.4.2 Granulomatous panuveitis

3.4.2.1 Baseline characteristics

Over a six-month period, 36 patients with a diagnosis of granulomatous uveitis suspected to be secondary to sarcoidosis or tuberculosis were imaged according to the protocol above. Nine patients were excluded as diagnoses were later reclassified (1 syphilis, 1 Lyme disease, 7 idiopathic panuveitis). Patient demographics and clinical characteristics of the 27 patients included are listed in **Table 3.3**.

Table 3.3. Baseline demographic and clinical characteristics of all patients, and in those with a diagnosis of sarcoid or tuberculosis.

	All	Sarcoid	Tuberculosis	p-value
Age, Median (IQR)	51 (25.5)	52 (18.0)	46 (22.0)	0.20
Female Gender, n	16 (59.3)	3 (23.1)	8 (57.1)	0.16
Affected eye – right,	17 (63.0)	8 (61.5)	9 (64.3)	0.80
Visual acuity -	0.18 (0.30)	0.18 (0.26)	0.24 (0.30)	0.53
Diagnosis type, n (%)				
Presumed	11 (40.7)	4 (30.8)	7 (50.0)	0.08
Probable	4 (14.8)	4 (30.8)	0 (0.0)	
Definitive	12 (44.4	5 (38.4)	7(50.0)	
Disease Activity				
Active	10 (37.0)	5 (38.5)	5 (35.7)	0.80
Quiescent	17 (63.0)	8 (61.5)	9 (64.3)	
Uveitis				
Anterior	5 (18.5)	3 (23.1)	2 (12.3)	0.93
Posterior	22 (81.5)	10 (76.9)	12 (85.7)	
Topical Steroid, n (%)	21 (77.7)	10 (76.9)	11 (78.6)	0.88
Oral Steroids, n (%)	11 (40.7)	4 (30.8)	7 (50.0)	0.81
2nd line agent, n (%)	3 (11.1)	2 (15.4)	1 (7.1)	0.88

3.4.2.2 The effects of granulomatous uveitis on choroidal morphology

Haller's large vessel layer of the choroid is thicker in eyes diagnosed with TB: The ratio of median Haller's large vessel to median Sattler's medium vessel layer was significantly greater in eyes diagnosed with tuberculosis (1.47 [=140.71µm/95.72µm] compared to eyes diagnosed with sarcoidosis (1.07 [=137.70µm/128.69µm]) at the TMC (p=0.001), but did not achieve statistical significance at the FCS (1.38 [=162.85 µm/118.01µm] versus 1.15 [=166.09µm/144.43µm]) (p=0.02) **(Figures 3.5, 3.6, and 3.7)**. No significant differences were observed in the choroidal sublayers between active or quiescent, or anterior or posterior disease. Although total choroidal thickness measurements were correlated with age at the TMC (r=-0.51, p=0.007) and FCS (r=-0.50, p=0.007), no associations between the ratio of median Haller's to median Sattler's vessel layers were observed at the TMC [(r=-0.23, p=0.25) and FCS (r=-0.16, p=0.44)].

Visual acuity and choroidal thickness measurements: The median VA of all patients was 0.18 LogMAR (IQR=0.00 to 0.30 LogMAR) and there was no difference between eyes diagnosed with tuberculosis or sarcoid **(Table 3.3)**. However, in the TMC, eyes with a VA equal to, or worse than 0.3 LogMAR, had a significantly thinner choroid (198.1µm [IQR=147.0µm to 253.4µm]), compared to eyes with a VA better than 0.3 LogMAR (292.4µm [IQR=240.1µm to 347.6µm]) (p=0.004) with factors including age and disease activity well matched between these sub-groups. However, at the FCS this did not reach statistical significance (p=0.02). Choroidal thickness measurements, showed a modest correlation with LogMAR VA (R^2=-0.17, p=0.04) at the TMC and FCS (R^2=-0.10, p=0.10), but did not reach statistical significance. There was no significant difference in age of the good VA (<0.3 LogMAR) group versus the poor VA (≥0.3 LogMAR) group (p=0.27).

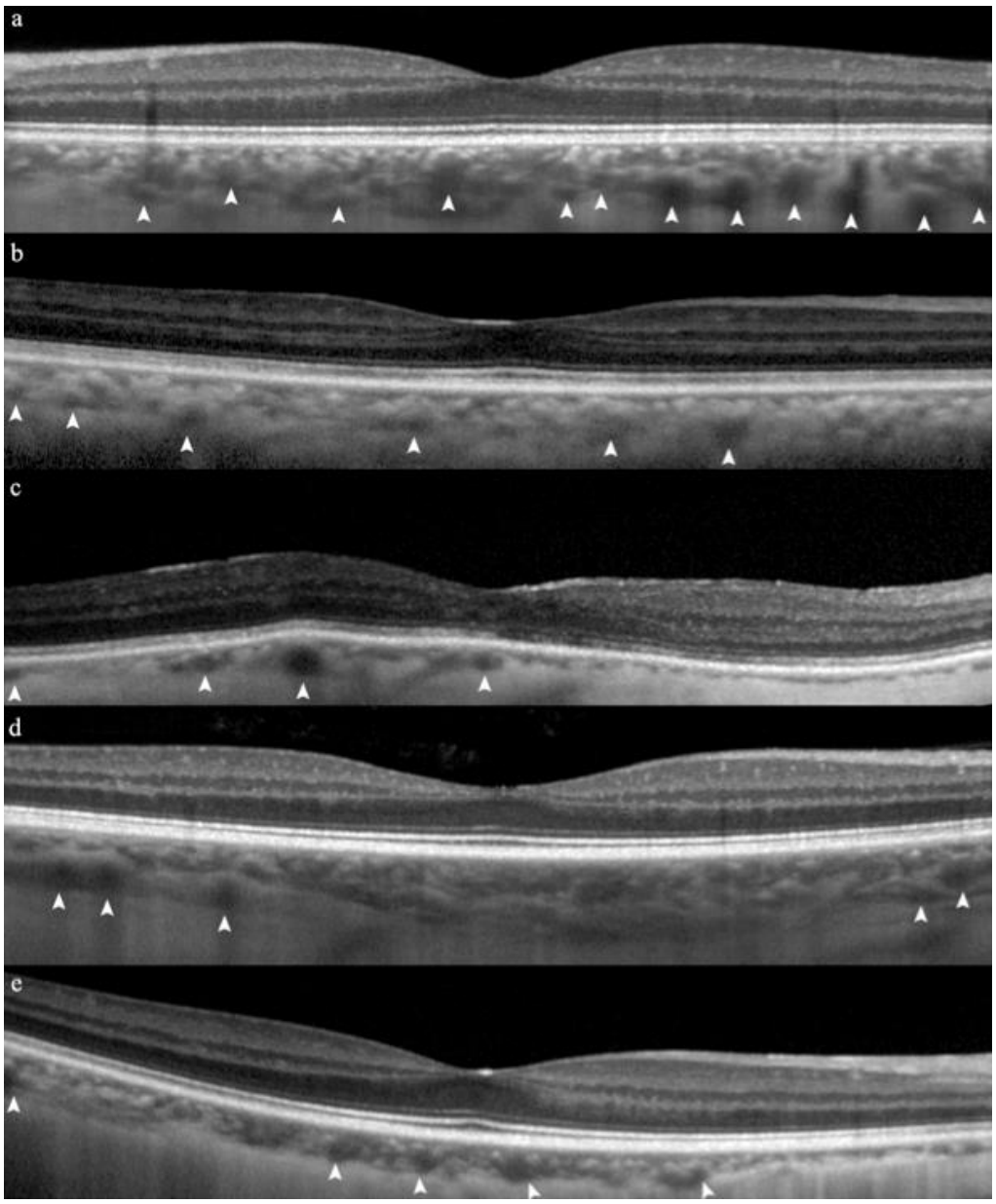

Figure 3.5. Decreased hypo reflective areas in the choroidal vasculature in idiopathic panuveitis.

Spectral domain optical coherence tomography using enhanced depth imaging. Arrowheads denote the hypo-reflective areas in Haller's layer that correspond to choroidal vessels. a) Normal eye showing multiple hypo-reflective areas. Loss of these areas was evident in the majority of our study eyes, as illustrated in these examples: b) Right eye of patient No 1, c) Right eye of patient No 2, d) Right eye of patient No 5, e) Right eye of patient No 18.

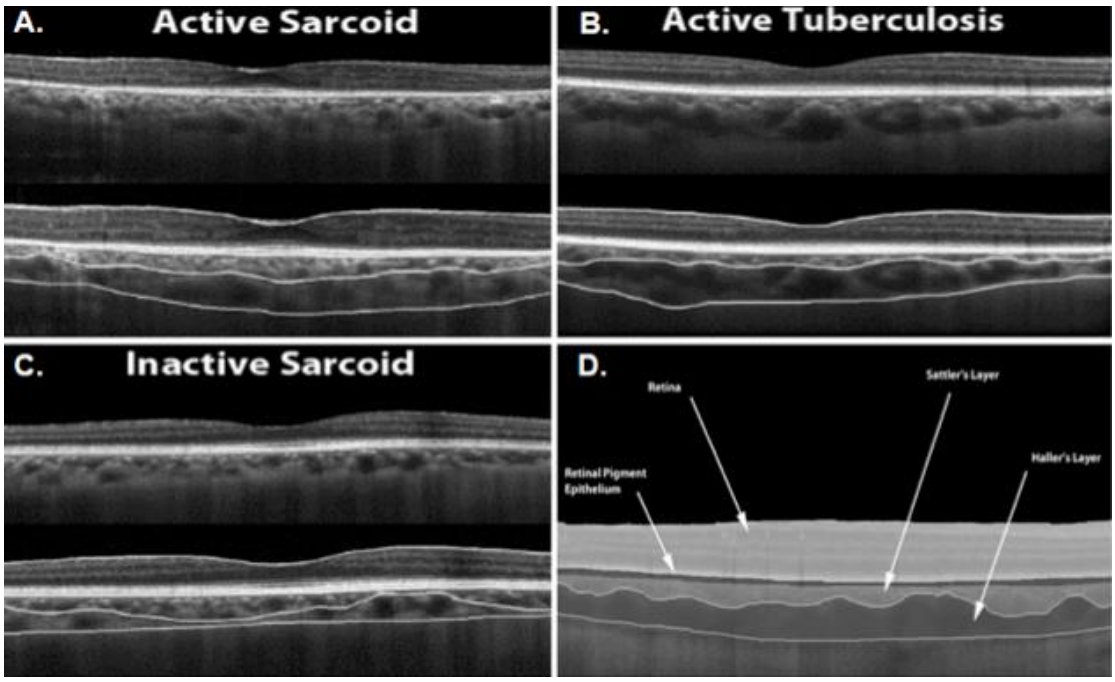

Figure 3.6. EDI OCT images of the choroid in A) Active sarcoidosis B) Active tuberculosis C) Inactive sarcoidosis and D) Normal eye

Manual segmentation delineates Haller's large vessel layer of the choroid from Sattler's medium vessel layer. Figure 1A is from a patient with active sarcoid uveitis and Figure 1B is from a patient with active TB uveitis. Although the median total choroidal thickness measurements were not different between sarcoid and TB uveitis groups, the ratio of median Haller's large to median Sattler's medium vessel layers at the Total Macula Circle was significantly higher in eyes diagnosed with TB (1.47 [=140.71µm/95.72µm] compared to eyes diagnosed with sarcoidosis (1.07 [=137.70µm/128.69µm]) (p=0.001). Figure 1C is from a patient with inactive sarcoid uveitis. At the Foveal Central Subfield, the choroid was thicker in eyes with active (336.8µm [IQR=272.3µm to 375.4µm]) compared to inactive granulomatous uveitis (239.3µm [IQR=195.3µm to 330.9µm]) but this failed to reach statistical significance at the stringent 0.004 level (p=0.04). Figure 1D is from a normal control eye to demonstrate the retina, retinal pigment epithelium, Haller's large and Sattler's medium vessel choroidal layers.

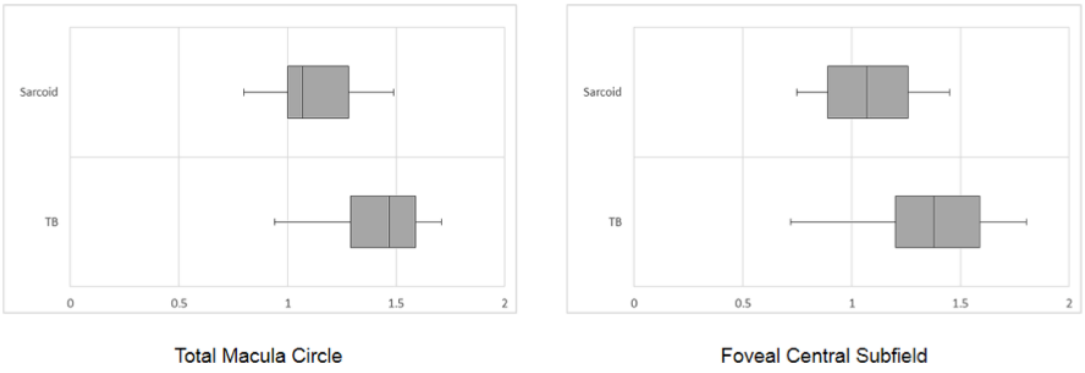

Figure 3.7. Box plot of ratio of Haller's to Sattler's vessel layers in eyes diagnosed with tuberculosis compared to sarcoid uveitis.

This box plot demonstrates that the ratio of median Haller's large to median Sattler's medium vessel layers at the Total Macula Circle was significantly higher in eyes diagnosed with TB (1.47 [=140.71µm/95.72µm] compared to eyes diagnosed with sarcoidosis (1.07 [=137.70µm/128.69µm]) (p=0.001). This did not achieve statistical significant at the Foveal Central Subfield (1.38 [=162.85 µm/118.01µm] for TB versus 1.15 [=166.09µm/144.43µm] for sarcoid) (p=0.02). There was also no distinct cut-off in the ratio of these layers to reliably distinguish between the diseases. Quartiles 1 and 3 are delineated by the borders of the box. The median is represented by the solid line within the box. The whiskers extend from quartile 1 to the minimum value and from quartile 3 to the maximum value. Because of the skew of the data, medians and interquartile ranges were presented.

3.4.2.3 The effects of granulomatous uveitis on retinal morphology:

In the 27 eyes analysed, the median retinal thickness measurement was 286.5µm (IQR=271.2µm to 309.1µm)) at the TMC and 235.9µm (IQR=216.6µm to 261.7µm) at the FCS. Retinal thickness measurements at the TMC and FCS showed good correlation within patients (R^2=0.56, p=0.0001). There were no significant differences in retinal thickness measurements between the type of granulomatous uveitis – sarcoid or tuberculosis, disease activity, or anatomical site of uveitis.

3.4.3 Punctate inner choroidopathy

3.4.3.1 Baseline Characteristics and Clinical Features

46 patients with a clinical diagnosis of PIC were included. Thirty-five eyes, from 35 patients, had EDI-OCT images, which met the inclusion criteria. The mean age was 40.1 ± 9.4 years (mean ± standard deviation, range 21-60 years), with an 8:1 female to male ratio (82.8%). The mean refractive error was -4.5 ± 4.1 diopters, BCVA was 0.33 ± 0.47 logMAR units (Snellen: 20/47 ± 4.7 lines) and mean duration of disease 61.0 ± 48.6 months. Twenty-four patients presented with bilateral disease (68.5%), and 11 had unilateral disease (31.4%). Of the total cohort, 29 patients (82.8%) had a history of choroidal neovascular membranes (CNV). 22 had unilateral and 7 patients bilateral CNV. No differences were observed in CNV characteristics or location among the study groups. In the current study, no patients had active CNV at EDI-OCT acquisition, or in the preceding three months. Eighteen patients (51.4%) were on immunosuppressive therapies (14 on oral steroids (40.0%), 3 on oral steroids plus second-line agents (8.6%), 1 on second-line agents (2.8%)), and 17 patients (48.6%) were no longer on treatment. No significant differences between typical and atypical disease were seen for baseline characteristics, CNV frequency, CNV location or treatment modality. (**Table 3.4**)

3.4.3.2 Qualitative Analysis of Retinal and Choroidal Morphology

In total, 142 PIC lesions were counted from the NIR fundal images. Of these, 90 lesions (63%) were also captured by the 20° x 5° OCT scanning protocol and included in the qualitative analysis. Among the three lesion patterns analysed, 46.6% of all PIC lesions (42/90) showed focal atrophy of the outer retina, in particular the photoreceptor inner segment/outer segment (IS/OS) junction, and RPE (**Figure 3.1**). This focal disruption was also associated with atrophic changes affecting the overlying outer nuclear and outer plexiform layers. 34.4% of PIC lesions (31/90) were seen to consist of sub-RPE deposits **(Figure 3.1C)**, and 18.8% (17/90) consisted of localized RPE elevations

Table 3.4. Baseline demographic and clinical characteristics of all patients, and in those with a diagnosis of punctate inner choroidopathy.

		TOTAL	TYPICAL	ATYPICAL	p value
n		35 (100%)	16 (45.7%)	19 (54.28%)	
Age (years)		40.1+/-9.4	37.7+/-8.8	42.1+/-9.7	0.17
Gender (M:F ; %Female)		6:29 (82.9%)	3:13 (81.3%)	3:16 (84.2%)	0.82
Refraction (diopters)	**Total**	-4.5+/-4.1	-3.2+/-2.7	-5.6+/-4.9	0.09
	No HM	-2.1+/-2.4	-2.3+/-1.8	-1.9+/-3.1	0.65
	HM	-9.5+/-2.1	-8.0+/-1.4	-9.8+/-2.1	0.29
BCVA(LogMAR)		0.33+/-0.47	0.17+/-0.27	0.45+/-0.52	0.06
Duration of Disease (months)		61.0+/-48.6	43.6+/44.5	75.7+/-50.1	0.06
Disease Inactive		35	NA	NA	NA
Laterality	**Unilateral**	11 (31.4%)	5 (31.2%)	6 (31.5%)	0.98
	Bilateral	24 (68.5%)	11 (68.7%)	13 (68.4%)	
CNV	**Total**	29 (82.8%)	14 (87.5%)	15 (78.9%)	0.50
	Unilateral	22 (75.8%)	10 (71.4%)	12 (80.0%)	0.11
	Bilateral	7 (24.1%)	4 (28.5%)	2 (20.0%)	
CNV location	**Extrafoveal**	7 (24.1%)	3 (21.4%)	4 (26.6%)	0.86
	Juxtafoveal	13 (44.8%)	6 (42.8%)	7 (46.6%)	
	Subfoveal	9 (31.0%)	5 (37.5%)	4 (26.6)	
Treatment[A]	**No**	17 (48.6%)	7 (43.7%)	10 (52.6%)	0.65
	Steroid	14 (40.0%)	6 (37.5%)	8 (42.1%)	
	Steroid + Immunosup[B]	3 (8.6%)	2 (12.5%)	1 (5.3%)	
	Immunosup	1 (2.8%)	1 (6.2%)	0 (0.0%)	
	Anti-VEGF[C]	16 (45.7%)	9 (56.3%)	7 (36.8%)	0.25

(PIC= punctate inner choroidopathy, M= male, F= female, HM= high myopia, defined as refraction ≥-6 diopters, BCVA= best corrected visual acuity, logMAR=logarithm of the minimum angle of resolution, CNV= choroidal neovascularization; [A] Treatment refers to systemic treatment at the moment of the scan (steroids/immunosuppresives) and previous intravitreal treatments with Anti-VEGF drugs; [B] combined treatment with systemic steroids + immunosuppressants; [C]>3 months free-of-injections before OCT scan date). Significance level: $p<0.05$. (NS: Not significant).

(Figure 3.1A). In the subgroup analyses, untreated eyes had a trend towards a greater number of sub-RPE deposits (47.0% [16/34] untreated vs 26.7% [15/56] treated, p=0.05). Conversely, a trend towards a greater presence of outer retinal atrophy was observed in treated eyes (35.3% [12/34]) compared to untreated eyes (53.6% [30/56], p=0.09).

Focal hyperreflective dots were seen in Sattler's medium vessel layer in 68.5% (24/35) of patients (**Figure 3.1 D**). They were most commonly located directly beneath, or adjacent to, PIC lesions, but were also observed in areas distant to lesions (**Figure 3.1 A to C**). These hyperreflective dots appear to be located adjacent to vessel walls or on the luminal surface, and were not observed within the hyporeflective luminal vascular spaces (**Figure 3.1 B**). No hyperreflective dots were noted in Haller's large vessel layer. This feature was more common in eyes with typical PIC (87.5% [14/16]) compared to atypical PIC (57.9% [11/19]) but this difference did not reach statistical significance level (p=0.05). Focal areas of thinning, spanning large and medium vessel layers of the choroid, were observed in 17.1% (6/35) of the eyes (**Figure 3.1 E**). In all cases, these areas were associated with PIC lesions containing outer retinal layer disruption and atrophy.

3.4.3.3 Quantitative Analysis of Retinal and Choroidal Morphology:

The mean retinal thickness was 256.04 ± 32.9 µm, whereas the mean choroidal thickness was 210.52 ± 103.44 µm. Mean retinal volume was 10.16 ± 1.41 mm^3, and mean choroidal volume was 8.13 ± 3.60 mm^3.

The retina was significantly thinner in eyes with atypical (243.73 ± 35.36 µm) compared to typical PIC (270.66 ± 23.22 µm)(p=0.01). When high myopic eyes were excluded from analysis, this difference remained significant (246.65 ± 30.2 vs 270.05 ± 24.6 µm; p=0.04). In the subgroup analysis by refractive status, the retinal volume was significantly lower in low myopic than high myopic eyes (9.86 ± 1.20 mm^3 vs 10.90 ± 1.67 mm^3 respectively, p=0.04).

The choroid was significantly thinner in eyes with atypical PIC (177.77 ± 100.98 µm) versus eyes with typical PIC (249.42 ± 95.10 µm) (p=0.03). This difference was maintained in Haller´s large vessel layer (114.96 ± 61.93 µm in atypical PIC versus 167.68 ± 65.92 µm in typical PIC, p=0.02). However, when high myopic eyes were excluded from analysis, this difference was not significant (229.09 ± 98.96 vs 268.85 ± 84.75 µm, p=0.29). In eyes with high myopia, the choroid, Haller's, and Sattler's layers thickness and volume were significantly lower compared to eyes with low myopia (p<0.001).

3.4.3.4 Clinical Significance of OCT-derived Parameters:

A highly significant correlation was observed between the refractive state of eyes with PIC and both foveal and macular choroidal thickness (r= 0.72, p<0.001; r= 0.73, p<0.001) This correlation was also maintained with the choroidal volume measurements (r= 0.72, p<0.001; r= 0.60, p<0.001). After excluding high myopic eyes, disease duration showed a significant negative correlation between retinal thickness and volume measurements when controlling by age and refraction (r=-0.53, p=0.01; r=-0.47, p=0.04). A significant negative correlation was observed between foveal retinal thickness and BCVA (r=-0.40, p=0.03) and volume (r=-0.40, p=0.02).

3.4.4 Vitreous inflammation

3.4.4.1 Baseline Characteristics

In the main study group (patients with uveitis and evidence of vitreous haze), 30 patients (30 eyes) were evaluated in our study. In the control group, 30 patients (30 eyes) were also evaluated, consisting of 12 patient (12 eyes) with uveitis but without vitreous haze, and 18 patients (18 eyes) without any evidence of uveitis or vitreoretinal disease. Clinical details of patients included are summarized in **Table 3.5**.

Table 3.5. Baseline demographic and clinical characteristics of all patients, and in those assessed for vitreous inflammation.

	Uveitis with vitreous haze (n=30)	Uveitis without vitreous haze (n= 12)	Healthy controls (n=18)
Age, mean ± SD (years)	49 ± 18	44 ± 14	67 ± 8
Visual acuity, mean ± SD			
Etiology, no. (%)			
Idiopathic	17 (57)	6 (50)	N/A
Birdshot	5 (17)	2 (17)	
Toxoplasma	2 (7)	0 (0)	
Sarcoidosis	2 (7)	0 (0)	
Other	4 (12)	4 (33)	
Anatomic type of uveitis, no. (%)			
Anterior	3 (10)	4 (33)	N/A
Intermediate	5 (17)	1 (8)	
Posterior	7 (23)	2 (17)	
Panuveitis	15 (50)	5 (42)	
Keratic precipitates, no. (%)			N/A
Posterior synechiae, no. (%)			N/A
Cataract, no. (%)			
Posterior capsular opacification, no. (%)			
Anterior chamber cells, no. (%)			N/A
0			
0.5+			
1+			
2+			
3+			
4+			
Anterior chamber flare, no. (%)			N/A
0			
1+			
2+			
3+			
4+			
Vitreous haze, no. (%)			N/A
0	0 (0)	12 (100)	
0.5+	4 (13)	0	
1+	13 (43)	0	
2+	10 (33)	0	
3+	3 (10)	0	
4+	0	0	

3.4.4.2 OCT-derived Measurements of Vitreous Intensity:

OCT-derived measurements of vitreous intensity for each group ("uveitis with vitreous haze" versus "uveitis with no vitreous haze" versus "normal eyes"), and for each grade of vitreous haze are summarized in **Figure 3.8**. A significant difference in VIT/RPE-Relative intensity was found between those eyes with "uveitis with no vitreous haze" or "normal eyes" (median=0.0767, interquartile range (IQR)=0.0478), when compared those with "uveitis with vitreous haze" (median=0.150, IQR=0.135) (p=0.0001), and between each grade of vitreous haze (p=0.001).

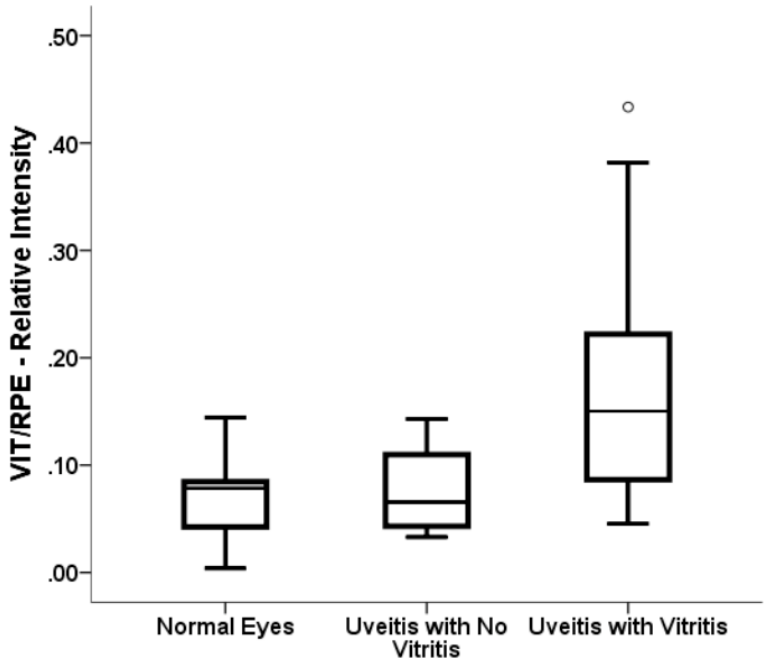

Figure 3.8. Box plots illustrating Vitreous (VIT)/Retinal Pigment Epithelium (RPE)

Relative Intensity measurements in "uveitis with vitreous haze" versus "uveitis with no vitreous haze" versus "normal eyes". The horizontal lines within each box represent the median for each group; the ends of the boxes are the upper and lower quartiles, and the whiskers represent minimum and maximum values.

A significant correlation was found between VIT/RPE-Relative Intensity and clinical vitreous haze scores (r=0.566, p=0.0001, Spearman non-parametric testing), VA (r=0.573, p=0.0001), and clinical AC cells (r=0.613, p=0.0001) and AC flare scores (r=0.385, p=0.003). Of note, as the strength of the relationship between variables increases, so does the value of the correlation coefficient (r), with a value of 1 showing a perfect relationship. When evaluated in a step-wise multivariable model examining factors governing media clarity (i.e. AC cells and flare) and other ocular characteristics such as VA and disease etiology (i.e. birdshot chorioretinopathy, Behçet's disease, and idiopathic panuveitis), location of inflammation (i.e. anterior, intermediate, posterior, and panuveitis), VIT/RPE-Relative Intensity remained independently associated with clinical vitreous haze scores (R^2-adjusted=0.292, p=0.0001).

3.4.4.3 Reproducibility of Vitreous Grading:

Bland-Altman plots were used to illustrate the agreement between graders and 95% LoA are presented in **Table 3.6** and **Figure 3.9**. It is expected that the 95% LoA include 95% of differences between the two graders and this is represented for visual judgment in the Bland-Altman plot. The smaller the range between these two limits the better the agreement is.

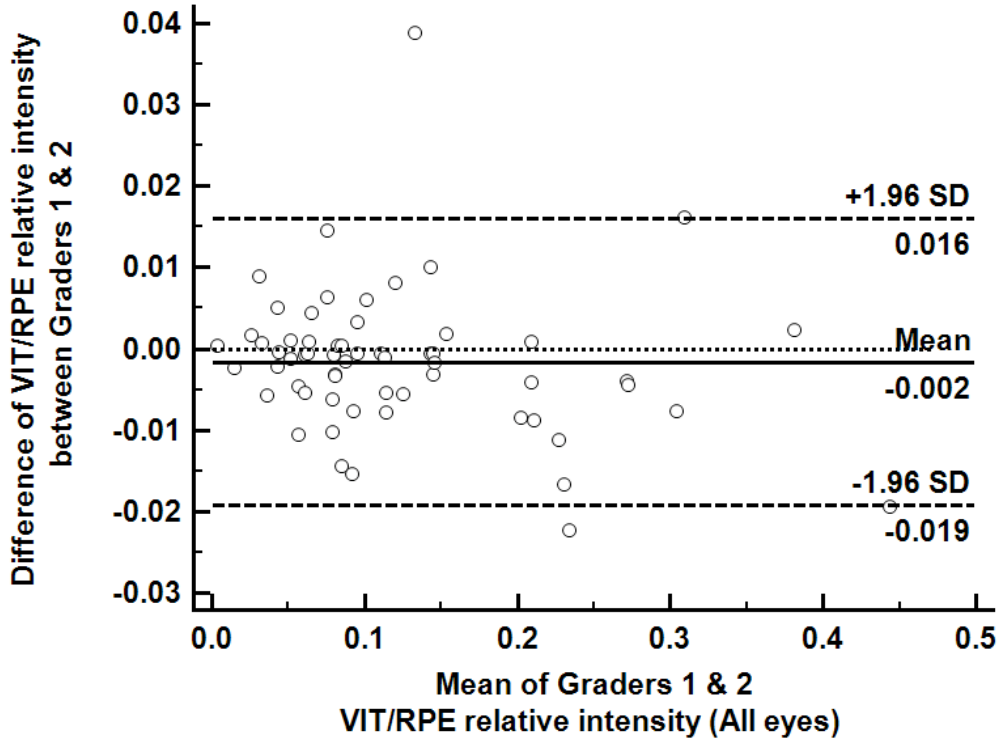

Figure 3.8. Bland-Altman plot of difference in VIT-RPE-Relative Intensity

Measurements obtained by Graders 1 and 2, versus the mean VIT/RPE-Relative Intensity score obtained by Graders 1 and 2. The solid horizontal line corresponds to the mean difference (−0.002 arbitrary units) while the dashed horizontal lines correspond to the 95% limits of agreement (−0.019 to 0.016 arbitrary units).

Table 3.6. Reproducibility of VIT/RPE-Relative Intensity values in Patients with Vitritis and Controls as assessed by Bland-Altman plots.

	Interobserver	95% CI	95% Limits
	VIT/RPE - Relative intensity		
Vitritis (n=30)	-0.00164	-0.00593 to	0.0450
All Controls (n=30)	-0.00158	-0.00373 to	0.0226
Normal Eyes (n=12)	0.00301	-0.00193 to	0.0305
Uveitis without vitritis	0.000633	-0.00129 to	0.0151
ALL (n=60)	-0.00161	-0.00394 to	0.0353

To examine whether the 95% LoA were significantly different between observers in controls and uveitic eyes, with and without vitritis, the variance of the interobserver measurement differences were calculated and the *F* statistic (variance ratio) presented (**Table 3.7**). The variance ratios between graders were not statistically significant in all groups, which suggest that VIT/RPE relative intensity measurements were reproducible in both controls as well as in eyes with vitritis. However, there was a trend towards a higher 95% LoA in eyes with vitritis compared to controls (0.0450 versus 0.0226 respectively).

Table 3.7. The Variance Ratio (F Statistic) of Intergrader Differences in VIT/RPE-Relative Intensity Measurements in Eyes with Vitritis and Controls.

	F Test	*p* value
Vitritis (n=30)	1.06	0.88
Controls (n=30)	1.07	0.86
Normal Eyes	1.00	1.00
Uveitis without vitritis	1.07	0.90
ALL (n=60)	1.04	0.87

3.5 Discussion:

3.5.1 Retinal and choroidal morphology in idiopathic panuveitis

In this cross-sectional study, OCT images obtained from patients with idiopathic panuveitis were examined along with the effects of co-pathology, duration of disease and different treatment regimes. Their impact on visual acuity as well as OCT-derived parameters of the retina and choroid were analysed. Novel segmentation protocols for the choroidal sub layers were also described, which if confirmed in future longitudinal studies, may be a useful tool for the diagnosis and monitoring of inflammatory retinal disease.

Choroidal thickness at the posterior pole, based on histopathological studies, has been historically reported as 220 µm.(332) However, it has been noted that fixation techniques can cause tissue shrinkage and underestimate the true thickness of the choroid. OCT-derived measurements of choroidal thickness, overcomes these artefacts, and has been reported to range from 262 to 332 µm.(270, 333, 334) **Table 3.2** summarises the normative values for normal eyes and those with panuveitis. The mean choroidal thickness in our patient cohort was 234 µm, thinner than that observed in normal subjects. In the current study, we found a thinner mean Haller's layer thickness, (168 µm) and a lower ratio of Haller's to total choroidal thickness, (0.72 ± 0.09) suggesting that the reduction of choroidal thickness observed in eyes with idiopathic panuveitis, occurs mainly in this layer.

Recent publications on small patient cohorts of posterior uveitis, include, Vogt-Koynagi Harada (VKH) disease (6 and 8 cases respectively), (296, 335) and multiple evanescent white dot syndrome (MEWDS) in 2 patients. (336) Both studies observed an increase choroidal thickness measurements, ranging from 273 µm to 805 µm. (**Table 3.2**) This is likely because 12 of the 16 reported cases had active disease, compared to our patients who were all clinically inactive. Alternatively it might reflect different pathological mechanisms between diseases.

Choroidal ischaemia has been suggested as a common pathophysiological pathway in different uveitic entities, and may be an explanation for the thinning of Haller's large vessel layer observed in our study. The evidence for choroidal hypoperfusion, has been historically derived from studies using ICGA. In VKH, the choroidal stroma is thought to be the locus of inflammation. The associated ICGA features include delayed filling, loss of definition of stromal choroidal vessels, and a generalised disturbance of the choroidal vasculature.(337, 338) Similar features have been described in multiple inflammatory ocular conditions such as MEWDS, acute posterior multifocal placoid pigment epitheliopathy, sarcoid, Behçet's related uveitis, birdshot chorioretinopathy, and multifocal choroiditis.(339-344)

There has been limited evidence from OCT studies, with only two reports implicating choroidal vessel damage in eyes with uveitis. The first study described a changes in Sattler's medium vessel layer in 12 patients with VKH, and attributed this to structural changes in choroidal vessels.(296) The second study described a reduction of choroidal hyper-reflectivity using a longer wavelength swept source OCT (better penetration to the choroid) in a patient with multifocal choroiditis and panuveitis.(345) In our patient cohort, we similarly found reduced hypo reflective spaces and thinning occurring in Haller's layer. We hypothesize that this reflects a loss of luminal spaces in the choroidal vasculature, and suggest Haller's large vessel layer may be implicated in the pathophysiology of idiopathic panuveitis. These findings will need to be confirmed by immunohistopathological studies, which will be able to pinpoint the location of vessel wall damage, identify the nature of inflammatory infiltrate, and visualise vessel wall hypertrophy or fibrosis may shed some light into the aetiology of this disease.

We observed no relationship between retinal or choroidal thickness with visual acuity. This is similar to previous studies in patients with posterior uveitis secondary to Behçet's disease also found no correlation between choroidal thickness and visual acuity.(346) We did, however, observe a lower mean visual acuity in eyes with co-pathology such as cystoid macular oedema or epiretinal membrane. Furthermore, a relationship with visual acuity was identified when choroidal

thickness measurements were expressed as a ratio to retinal thickness. This suggests that the interplay between the retina and choroid, may be an important feature of uveitis-related visual loss.

Limitations of our study include its retrospective nature and small sample size. Refractive error, a well-known confounder in studies of choroidal thickness, was not included in our data. However, we excluded eyes with greater than 6 diopters of ametropia from our study. Our cross-sectional study also does not provide any data regarding temporal changes, useful in a disease like Idiopathic panuveitis, which usually follows a chronic clinical course. Nevertheless, this study does provide novel analysis on OCT-derived parameters about a clinical entity that is poorly described in literature.

In conclusion, patients with idiopathic uveitis were observed to have a loss of hypo reflectivity in Haller's large vessel layer, and thinning of both Haller's and the choroid as a whole. The ratio of Haller's to retinal thickness was observed to correlate to visual acuity.

3.5.2 Retinal and choroidal morphology in granulomatous panuveitis

In this cross-sectional study, we assessed OCT-derived measurements of choroidal thickness, and its component Haller's large and Sattler's medium vessel layers, in eyes with sarcoid and TB-associated granulomatous uveitis.

The ratio of Haller's large to Sattler's medium vessel layer was different in eyes with sarcoid compared to TB-associated uveitis. Although the median total choroidal thickness measurements were not different between both entities, the ratio of Haller's to Sattler's layers was significantly higher (37%) in TB (1.47 versus 1.07 at the TMC). We speculate that this may reflect their different underlying pathogenesis. In 1976, Gass *et al.* in a clinicopathological correlative study of a patient with sarcoid posterior uveitis, found that lesions labelled as "focal choroiditis" were actually below the retinal pigment epithelium and not within the choroid.(347) Other studies have since confirmed these findings, observing that in sarcoid-

associated uveitis, choroidal involvement is infrequent.(348, 349) This is in contrast to TB-associated uveitis where choroidal tubercles are commonly observed.(258, 350) Furthermore, in a recent clinical study, it was observed that ocular TB in the posterior segment presents as a retinal vasculitis that not only predominantly affects venous structures, but also chorioretinal structures adjacent to involved vessels. In comparison, the classic feature of sarcoid-associated posterior uveitis, 'candle wax drippings', was found to be a periphlebitis primarily located in the inferior retinal periphery without adjacent vascular or choroidal involvement.(262) If future prospective studies confirm that the ratio of the sublayers of the choroid are indeed characteristic for either disease, EDI-OCT may prove a useful aid in the diagnosis of these granulomatous diseases. It should be noted that TB associated uveitis can have disparate retinal and choroidal manifestations and this study, with the relatively few cases available, cannot distinguish whether there are differences in choroidal thickness measurements according to the type of presentation.

In this study, we observed an association between a thin choroid and poor VA at the TMC ($p=0.004$) but interestingly not the same degree of significance at the FCS ($p=0.02$). A possible explanation is that OCT images over the TMC cover a larger area compared to the FCS, and therefore more representative of the total choroidal thickness of the eye. It may be that occurrence of choroidal inflammation over extended periods ultimately leads to generalised choroidal atrophy and thinning, and it is this, rather than focal choroidal atrophy under the fovea which affects visual function. This raises the question as to whether choroidal thinning in chronic granulomatous disease is localised to the macula region or more widespread, especially since granulomatous uveitis can present with diffuse posterior segment signs.(259, 349, 351) In a recent study, extra-macular scans performed in eyes diagnosed with birdshot chorioretinitis demonstrated generalised choroidal thinning outside the macula.(271) Whilst factors including age and disease activity were well matched between the good (<0.3 LogMAR) and poor (≥0.3 LogMAR) visual acuity groups, other confounders are possible.

EDI OCT studies into other uveitic conditions such as Vogt-Koyanagi-Harada disease(276) and Behçet's disease(352) have observed a thicker choroid in active compared to quiescent disease. A possible explanation for this observation is that in the presence of inflammation, the release of mediators such as prostaglandins causes blood vessels to dilate leading to increases in OCT-derived measurements of choroidal thickness.(353) This does not occur in the vessels of the retina as autoregulation maintains a constant perfusion pressure to the corresponding vascular tree.(354) However, in the highly vascular choroid no such autoregulatory mechanism is present.(355),(356) We hypothesize that the "spongiform" choroidal vasculature is highly reactive to changes in the inflammatory state of the immediate environment, with consequent changes to choroidal thickness measurements. Measuring choroidal thickness could therefore provide a non-invasive method to monitor disease activity within an individual over time. This would be important in addressing the difficult therapeutic question encountered in clinical practice - when and how quickly to taper immunosuppressive therapy, thereby allowing treatment to be better tailored to the individual patient.

In this cross-sectional study, we observed a trend of a thicker choroid in active (median 336.8µm [IQR=272.3µm to 375.4µm]) compared to quiescent (median 239.3µm [IQR=195.3µm to 330.9µm]) granulomatous uveitis (p=0.04) but this did not reach statistical significance at the stringent p≤0.004 level set to avoid the chance of type 1 errors. This might be explained by the observation that choroidal thickness is highly variable between individuals and is significantly dependent on variables such as age and sex which were recorded in this study and factors such as refractive error and axial length which were not recorded. However, looking for longitudinal changes *within* an individual may allow some of the natural choroidal variation *between* individuals to be accounted for.(357-360)

Strengths of the study included the use of a validated segmentation protocol to analyse OCT images from patients with a relatively rare disease entity.(324) To the authors' knowledge, this is the largest EDI-OCT study in granulomatous uveitis to

date. There are a number of limitations. Firstly, it included patients from a single tertiary referral centre that has a bias towards a more severe spectrum of disease. However, the data presented is likely to represent the patient cohort more likely to require immunosuppressive therapy and hence close monitoring. Secondly, the retrospective cross-sectional design carries inherent bias and longitudinal prospective studies involving larger patient cohorts will be required to confirm our findings. Thirdly, diagnoses were not all based on biopsy-proven cases. This reflects real world clinical practice. The clinical and laboratory diagnostic criteria, detailed in the methods section, have high specificity and sensitivity reported in the published literature.(313, 316) Fourthly, imaging with current OCT equipment was limited to the macula region, and as discussed above preliminary evidence suggests that extra-macular scans may be more discriminatory for disease activity and visual function. It is likely that next generation OCT devices, with faster acquisition times will allow larger areas of the choroid to be assessed.(361) Lastly, we employed manual segmentation using custom software that is not currently available in the clinical arena. However, efforts are underway to provide automated choroidal thickness maps, similar to automated retinal thickness maps currently available, particularly with the coming next-generation OCT systems.(362)

In conclusion, we observed that the ratio of Haller's large to Sattler's medium vessel layers was significantly higher in TB compared to sarcoid related uveitis, and there is a trend for the choroid to be thicker in active granulomatous uveitis. In addition, choroidal thinning was observed to be associated with reduced VA. These OCT-derived parameters of the choroid, if validated in larger prospective studies, may not only offer insights into diagnosis and visual prognosis for eyes with granulomatous uveitis, but also potentially be used to monitor disease activity within an individual over time or as an objective measure for clinical trials.

3.5.3 Retinal and choroidal morphology in punctate inner choroidopathy

The aetiology of PIC is poorly understood. Although a genetic predisposition is thought to play a role (363), as with other white dot syndromes, the prevailing hypothesis is that of initial insult triggering an autoimmune response towards antigens in the outer retina and inner choroid. (364)(366)(354)(354)(356)(349) Previous studies have identified PIC lesions, located in the RPE, choriocapillaris, and in the inner choroid.(277, 279, 293, 365) The natural history of the PIC lesions has been described as pale yellow spots, which evolve into deep, cylindrical, punched out scars with corresponding loss of tissue in the inner choroid, RPE and outer retina.(366) This is consistent with results obtained in the current study, where we observed that 46.6% of PIC lesions consisted of focal atrophy of the outer retina and RPE. In addition, 34.4% of PIC lesions consisted of sub-RPE hyperreflective deposits, and 18.8% of lesions presented as focal RPE elevations with underlying hyporeflective space. Other studies have suggested that this focal RPE elevation occurs in active disease.(294, 295) In our cohort of stable/inactive patients, this focal RPE elevation may be the presence of subclinical inflammation or reflect another pathophysiological process affecting the outer retina-RPE-inner choroid complex.

In this study, we further examined choroidal morphology using EDI-OCT. In 68.5% of patients, discrete hyperreflective dots were observed to be confined within the inner choroid. Previous studies using ICG have also shown involvement of this layer.(287, 365) It has been suggested that changes observed were indicative of choroidal vasculitis. It is possible that the inner choroidal hyperreflective clusters observed in our study reflect inflammatory changes in the choroidal vessel wall. This may include aggregation of inflammatory cells or pigment in the choroidal stroma. Histopathological studies will be required to confirm these speculations. In addition, focal thinning of the choroid (underlying PIC lesions) was also observed in our study. Studies carried out in other uveitic entities such as VKH disease have shown similar thinning during quiescent phase.(296, 367) Lastly, we observed that patients with

greater duration of disease were found to have thinner retinas. This may reflect repeated inflammatory episodes or long-standing subclinical inflammations.

In summary, the clinical value of OCT in evaluating patients with PIC was assessed. We suggest OCT may be used as a non-invasive tool for both qualitative and quantitative analysis of inflammatory lesions in these patients.

3.5.3 Objective measurement of vitreous inflammation

In patients with uveitis, the onset of inflammation commonly leads to permeation of the vitreous with inflammatory cells and protein-rich exudate.(368) These changes typically reflect the degree, and to an extent the location and character, of the underlying uveal inflammation. Vitreous inflammatory cells can be directly visualized using slit-lamp biomicroscopy and, more recently, using OCT.(304) However, in many cases of uveitis (e.g., pars planitis), vitreous cells may persist for extended periods even after resolution of their initiating inflammatory episode.(298) In contrast, protein-rich exudate is only seen in the presence of active inflammation. This exudate may also be seen on clinical examination in the form of vitreous "flare" (i.e., the scattering of light by fine particles suspended in solution as described by the Tyndall effect).(369, 370) As OCT is fundamentally a light scattering-based imaging modality, it is well suited to the visualization of this feature. Although OCT does not provide the exact composition of the vitreous compartment, higher vitreous signal intensity will be indicative of increased scattering of light and thus increased density of particles within the space. Conversely, lower vitreous signal intensity will reflect a relatively clearer vitreous composition with fewer suspended particles.

In this report, we first obtained an "absolute" measurement of vitreous signal intensity ("VIT-Absolute Intensity"), reflecting the mean intensity value for all image pixels contained within the vitreous compartment. In order to reduce the effects of OCT signal strength, anterior media opacities, and other confounding factors, we then compared this to a reference value ("RPE-Absolute Intensity"), and generated an optical density ratio with arbitrary units ("VIT/RPE-Relative Intensity"). The use of

OCT-derived optical density ratios has previously been described for the assessment of intra- and subretinal fluid.(305-310) In eyes with intraretinal fluid, increased signal intensity of cystoid spaces has been reported in diseases with active exudation (e.g., diabetic retinopathy) versus those without (e.g., cone dystrophies and idiopathic perifoveal telangiectasia).(306, 307) Similarly, subretinal fluid in eyes with neovascular age-related macular degeneration (AMD) shows an increased OCT signal intensity relative to that seen in central serous chorioretinopathy (a finding the authors hypothesize is related to increased breakdown of the outer blood-retinal-barrier in the former condition).(308)

In the current study, we demonstrate that: 1) VIT/RPE-Relative Intensity is significantly higher in uveitic eyes with known vitreous haze than in uveitic eyes without haze or in healthy controls, 2) VIT/RPE-Relative Intensity values are higher with each incremental increase in clinical vitreous haze score, 3) VIT/RPE-Relative intensity values show a significant, positive correlation with clinical vitreous haze scores, and 4) VIT/RPE-Relative Intensity scores can be calculated with a high degree of inter-grader reproducibility. These results are a preliminary, proof-of-concept, step in the validation of this OCT-derived biomarker as an outcome measure in uveitis. This OCT-derived biomarker has important theoretical advantages over the current gold standard in that it is objective (vs subjective), continuous (vs ordinal) and has a high level of inter-grader reproducibility. If validated in future studies, OCT-derived measures of vitreous inflammation may prove useful as an objective, quantitative, disease activity endpoint in clinical trials of posterior segment uveitis. One of the key limitations in such trials currently is the relatively poor 'signal:noise ratio' which renders a positive result unlikely except in the context of a highly effective treatment in a large-scale (and expensive) clinical trial. The reasons for this have been summarized elsewhere,(251) but include the lack of an objective outcome measure with a high degree of discrimination. If the OCT-derived measures described here are validated, and are demonstrated to robustly predict visual function and clinical benefit in patients with uveitis, it may be possible for trialists and regulatory bodies to adopt such a marker as a surrogate endpoint in clinical trials of this disease.(371, 372) In this manner, OCT-derived measurements of vitreous inflammation may be

used to improve the sensitivity and efficiency with reductions in sample-size and cost for clinical trials in posterior segment uveitis.

It should be noted that whilst this study demonstrated a statistically significant association of VIT/RPE-Relative Intensity with the NEI Vitreous Haze score, the correlation was relatively weak at r=0.566. It should be recognised that both these tools are imperfect surrogate measures for the 'true' gold standard of intraocular inflammation as manifest in the vitreous cavity, and thus discordance between the two indices may reflect the limitations of either. Limitations in this OCT-derived vitreous reflectivity index will be explored further in subsequent studies and may be amenable to refinements in protocol, standardization in acquisition technique, and technical advances (discussed later). Some of the limitations in the NEI Vitreous Haze score have been assessed by Kempen et al.,(373) who noted an inter-observer agreement of k=0.53 (for exact agreement) and k=0.75 (for within 1 grade) and by Davis et al.(301) Indeed, Davis et al., have addressed some of these issues by utilizing an extended nine-point graded photograph-to-photograph technique which was assessed in the MUST trial.(301) Similarly to our study, whilst they note excellent interobserver and intraobserver intraclass correlations (correlation coefficients 0.84 - 0.93), the correlation between the photographic and the NEI vitreous haze scores was much weaker (r=0.51; P<0.001).

Our study has a number of strengths, combining detailed clinical assessments of ocular characteristics by uveitis specialists with novel, standardized qualitative and quantitative assessments of OCT images by a senior grader certified for image interpretation in clinical trials. Of note, our study was performed using standard volume scans obtained from the current generation of commercially available spectral domain OCT systems (i.e., without the need for specialized hardware). Although our study required the use of custom image analysis software employed at the Doheny Image Reading Center, similar forms of analysis are possible using free, publically available, image analysis tools (e.g., ImageJ, National Institutes of Health, Bethesda, MD; available at http://rsb.info.nih.gov/ij/index.html), or commercial software (Photoshop, Adobe Systems, San Jose, CA).(304, 310) As such, this form of

analysis may be applied retrospectively to any large-scale clinical trial of uveitic conditions where spectral domain OCT was employed. Although our study required manual segmentation of the vitreous boundaries on OCT images, development of automated segmentation solutions are unlikely to prove challenging (especially given the progress in recent years of automated analysis of more challenging morphology on OCT, such as choroidal neovascularisation (CNV)).(374-376)

Our study also has a number of limitations. In particular, it involves cross-sectional analysis of OCT image sets obtained from a small number of patients. In the future, longitudinal studies involving larger patient cohorts will be required to validate the clinical significance of our findings. Of note, no image sets were acquired using the EDI mode of the device – i.e., in all cases, the point of maximum imaging sensitivity was at the vitreoretinal interface rather than at the choroid, and only minimal B-scan averaging was performed.(322) In future studies, it will be interesting to examine the effects of increased B-scan averaging on VIT/RPE-Relative Intensity levels, and to determine whether the associated reductions in image speckle noise will result in increased accuracy of measurements.

The design of the study was pragmatic in utilizing scans conducted under normal macular scanning conditions, rather than attempting to optimize for vitreous – for example, it is possible for the operator to increase the amount of vitreous imaged by pulling back on the joystick during image acquisition.(377) Even employing this technique, the depth of vitreous that can be imaged is still limited to the scanning range of the Spectralis OCT system (1.9 mm).(378) As a result, only the posterior aspect of the vitreous is directly visualized. Although this is a significant shortcoming for the assessment of vitreous cells, it may be less of a disadvantage when assessment is of diffuse vitreous permeation with protein-rich exudate. Moreover, the next generation of “swept source” OCT technology will allow for greatly increased scanning ranges.(379) In fact, the introduction of vertical cavity surface-emitting lasers (VCSEL) already allows “whole eye” OCT image sets with visualization of the vitreous in its entirety.(380) To date, these systems have only been used for simple applications such as ocular biometry;(381) their potential for

vitreous imaging in uveitic disease is intriguing, particularly if combined with measures such as VIT/RPE-Relative Intensity.

In conclusion, in this pilot study, we describe a method for quantitative analysis of vitreous signal intensity on OCT. We apply this method to a cohort of patients with uveitis, both with and without vitreous haze, and to healthy controls. As a result, we describe a new OCT-derived biomarker: “VIT/RPE-Relative Intensity” with potential for use as an objective marker of disease activity in patients with uveitis. Measurements of this biomarker can be made using existing, commercially available OCT devices, both prospectively, and in image sets that have already been collected. The incorporation of automated vitreous measurements in commercial OCT software would allow use of this parameter in routine clinical practice. Moreover, assessment of the vitreous in patients with uveitis may be an important clinical application of the next generation of “whole eye” swept source OCT systems.

3.6 Chapter summary:

In this chapter, novel methods for the assessment of inflammatory eye disease, in a clinical setting were examined. OCT-derived images from four uveitic entities; idiopathic panuveitis, granulomatous uveitis, punctate inner choroidopathy, and vitritis, were qualitatively and quantitatively analysed. It was observed that by slight alterations in the way OCT images were acquired on commercially available devices; for example enhance depth imaging, extramacular scans, or vitreous imaging, it was possible in a clinical setting, to visualise ocular inflammation in far greater detail compared to conventional imaging techniques. Direct, in vivo visualisation of the loci of inflammation could be examined in the vitreous, retina, choroid, and furthermore, OCT images could be acquired across specific loci of inflammation. The non-invasive, rapid acquisition nature of OCT imaging lends itself to repeated scans and therefore longitudinal monitoring of inflammation. If confirmed and larger, prospective studies, these techniques may be used for not only the diagnosis of specific uveitic entities, but the assessment and monitoring of disease activity, and may be useful in individualising treatment strategies in the future. It may also be applied in the wider context, to visualise and assess inflammation in diabetic eye disease.

4. In vivo detection and monitoring of retinal inflammation

4.1 Introduction:

Resident and infiltrating leukocytes have an important role in sight-threatening diseases of the eye. Substantial evidence exists that activated or altered immune responses are not only present in uveitic syndromes (382), but also prevail in the form of parainflammation during age-related macular degeneration and diabetic retinopathy (383, 384), the two main causes of blindness in Western industrialised countries. In these diseases the cellular components of inflammation can drive pathological angiogenesis causing sight threatening complications (385-388). A better understanding of the role of inflammation in pathological angiogenesis is not only essential for the development of disease modifying strategies but also for monitoring disease progression and assessing efficacy of treatments.

The development of clinically viable imaging tools for *in vivo* visualisation of inflammation is a crucial step in this process. To date, live imaging of inflammation has been restricted to experimental animal models, with examples such as, magnetic particles - iron oxide and gadolinium chelates for magnetic resonance imaging, fluorescent nanoparticles which can be tagged with aptamers or peptides targeted against cell surface biomarkers, circulating factors or nucleic acid structures, or dyes such as Acridine orange - a known human carcinogen (389-393). The only application that is currently used to image inflammatory cells in humans is based on *in vitro* radionucleotide labelling of leukocytes from the patient's own blood. Although this allows direct visualization of cell migration patterns, current imaging techniques do not allow sufficient resolution to track single cells (394).

Here, we present the use of indocyanine green (ICG) for *in vivo* visualisation of myeloid cells in the mouse. ICG is a near infrared (NIR) fluorescence tricarbocyanine dye with a peak spectral absorption of 800-810 nm (in blood) that is approved by the US Food and Drug Administration (FDA) for clinical use. The introduction of ICG in ophthalmic angiography in the late 1960s was largely due to its minimal toxicity and favourable optical and biophysical properties (395). NIR light could penetrate the

ocular pigments of the eye such as melanin and xanthophyll, thereby allowing visualisation of the deep choroidal vasculature (not possible with conventional fluorescein angiography). In addition, its tendency for conjugation to plasma proteins meant that the dye did not readily leak from the fenestrated choriocapillaris (396).

Despite the wide use of intravenous (iv) ICG, U.S. Food and Drug Administration approval, and good safety profile, there is limited evidence for its use in cellular imaging. This is probably due to its pharmacokinetic properties – ICG is rapidly removed from the circulation via hepatic clearance, and has a half-life of approximately 3-4 minutes, which precludes *in vivo* labelling of cells. However, we observed that by administering ICG as a depot injection, we could obtain reproducible labelling of peripheral CD11b+ circulating myeloid cells, establishing a novel method for *in vivo* tracking of these cells, at near single cell resolution as they invade the eye in response to inflammation and injury. Furthermore, we show *in vitro* evidence that human myeloid cells stain similarly which strongly supports the translation of this promising technique into clinical practice.

Techniques for in vivo cellular imaging requires a biocompatible, non toxic agent, that is able to distinguish the resident macrophage population from invading circulating monocytes, allowing reproducible quantification of these cells. Our results clearly demonstrate that this can be achieved in mouse models by using a depot injection of ICG. Translation of ICG, which has been used clinically for over 50 years as an intravenous dye, to that of a depot preparation for use in humans, may be useful not only for monitoring ocular inflammation and pathological angiogenesis, but may also have applications further afield, for example, the detection of an immune response to more novel treatment strategies such as stem cell therapies or retinal implants.

4.2 Aim:

To develop a method to label and image myeloid cells infiltrating the mouse retina and choroid *in vivo*, using a Indocyanine green dye (ICG). The rationale for this

chapter is to develop a imaging biomarker for inflammation in murine models of where inflammation is well-established to play a role of disease pathology, in order to apply it to models of disease where the role of inflammation is less well understood.

4.3 Materials and Methods:

Technical acknowledgements: I would like to thank Dr Colin Chu, University College London for his assistance with Flow cytometry of murine splenic and blood cells.

4.3.1 In vitro labelling of peripheral blood mononuclear cells and splenocytes with ICG.

Mouse blood was drawn via cardiac puncture with a 0.5M EDTA-coated 23G needle, before either red cell lysis or Ficoll-gradient separation using Histopaque-1077 (Sigma Aldrich, UK) according to manufacturer's guidelines. PBMCs were isolated from murine whole blood using Percoll-gradient separation. Mouse spleens were dissected and mechanical cell dissociation was performed in order to create single cell suspensions. The whole sample was passed through a 60µm cell strainer (Merck Millipore, Watford, UK) and washed with 1mL of PBS. The Eppendorf was centrifuged at 300g for 5 minutes and remaining cell pellet suspended in 6.25µg/mL ICG for 30 minutes at room temperature. After the cells were stained with ICG, they were incubated with Fc-block (BD Biosciences, UK) before primary antibody staining at manufacturer's recommended concentrations at 4°C for 20 minutes. PBMCs and splenocytes were washed and co-stained with CD45, CD11b, CD3 fluorescent antibodies. All antibodies were from BD Biosciences. Human PBMCs were isolated from 20mL whole blood using Ficoll-gradient. PBMCs washed and co-stained with CD45, CD11b, CD3 fluorescent antibodies (Miltenyi Biotech, Bisley, UK).

4.3.1.1 Optimisation of invitro ICG-labelling of peripheral blood mononuclear cells and splenocytes

Human PBMCs were used for optimisation initially, in order to assess the concentration, timing of exposure, number of washes in phosphate-buffer saline, pH 7.4 (PBS) that were required for cellular labelling with ICG. Serial dilutions of ICG were used and the most reproducible concentration, with the least indiscriminate labelling, was observed to be 6.25µg/mL. Cells were also labelled in room temperature and at 4 degrees Celsius with the former achieving optimal labelling and paradoxically minimal cell death. This was likely due to the length of time required for ICG-labelling at 4 degrees Celsius (60-90 min). Figure 4.1 showed a clear difference between control (Figure 4.1c') compared to those incubated in 6.25µg/mL ICG for 30 minutes at room temperature (Figure 4.1c). 99.4% of CD11b monocytes were stained with ICG using this protocol with 2 washes with PBS. In vitro staining of mouse PBMC yielded a lower percentage of monocytes stained with ICG. (Figure 4.2) After optimization, the largest proportion (43.3%) of CD45+ CD11b+ CD3+ cells staining was also achieved with 6.25µg/mL ICG for 30 minutes at room temperature. A similar protocol achieved optimal ICG-staining with splenocytes and reduction in proportion of cells labelled with serial dilutions of ICG. (Figure 4.3)

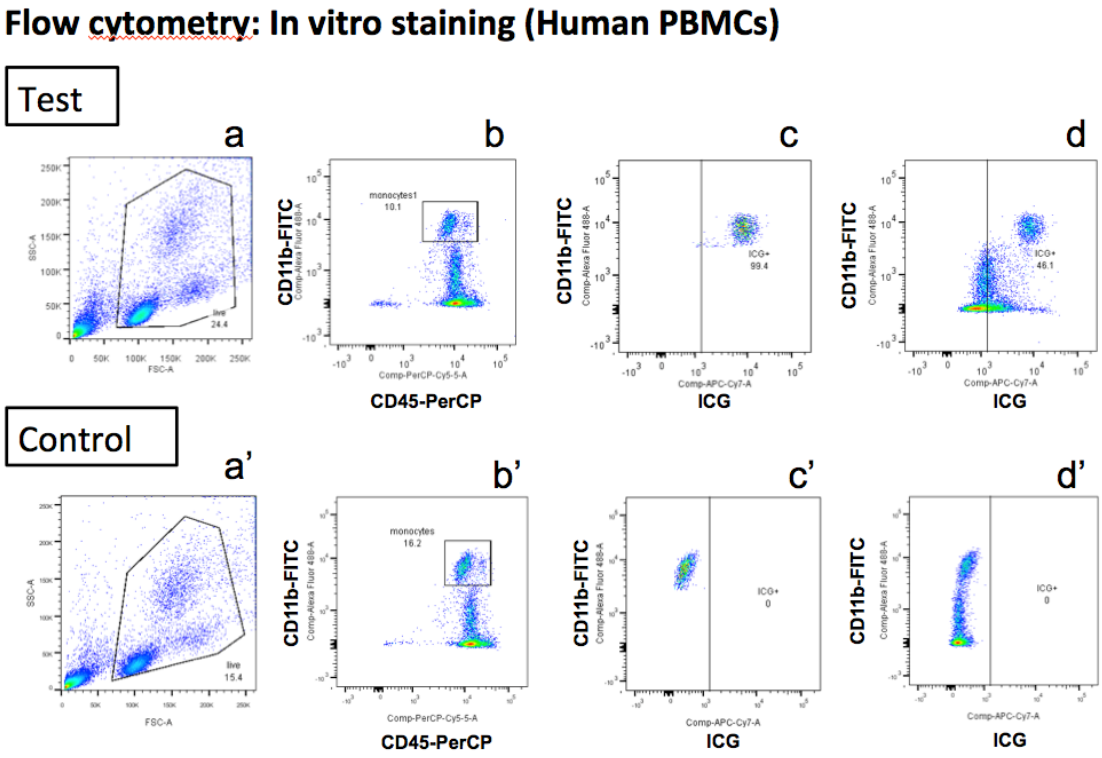

Figure 4.1. Gating strategy for in vitro labelling of human peripheral blood mononuclear cells (PBMCs).

(a-d) Gating strategy to assess the proportion of CD11b-FITC+ CD45-PerCP+ cells stained by a concentration of 6.25µg/mL indocyanine green dye (ICG) when incubated for 30 minutes at room temperature. (a'-d') represent the control sample where cells were incubated in phosphate-buffer saline, pH 7.4 (PBS) under the same conditions. (c, c') shows the proportion of CD11b-FITC+ CD45-PerCP+ cells stained by ICG, and (d, d') shows the proportion of all live cells stained by ICG.

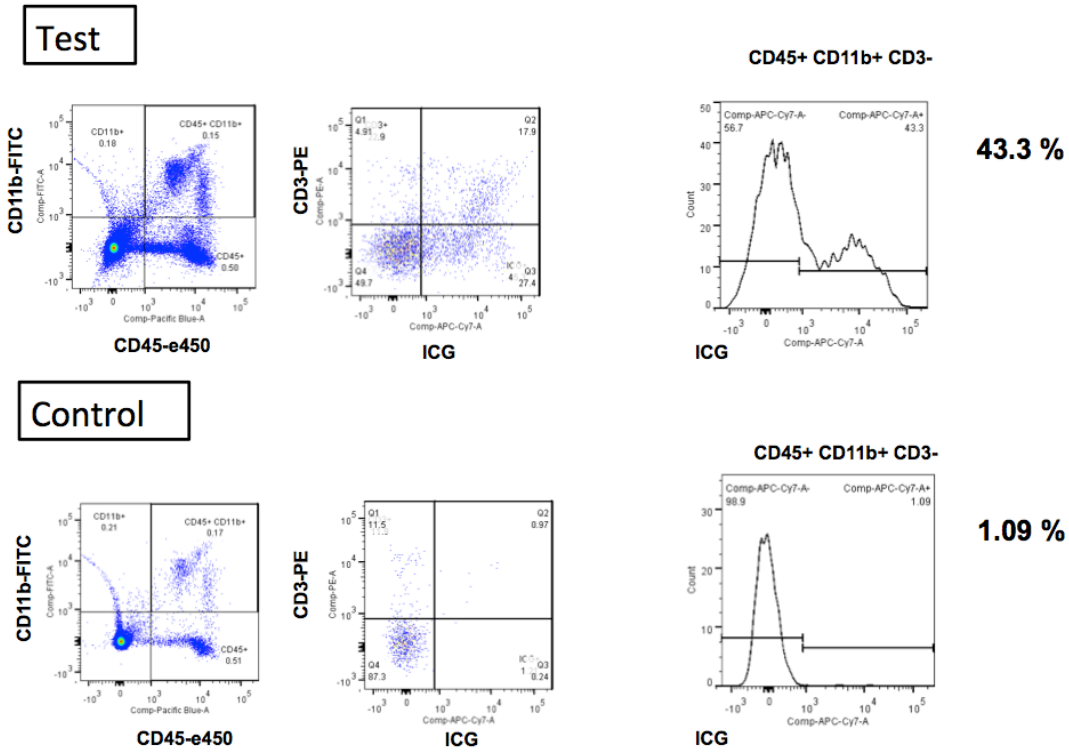

Figure 4.2. Gating strategy for in vitro labelling of murine peripheral blood mononuclear cells (PBMCs).

Gating strategy to assess the proportion of CD11b-FITC+ CD45-e450+ CD3- cells stained by a concentration of 6.25µg/mL indocyanine green dye (ICG) when incubated for 30 minutes at room temperature. The bottom panel represent the control sample where cells were incubated in phosphate-buffer saline, pH 7.4 (PBS) under the same conditions. Histograms on the right show the proportion of CD11b-FITC+ CD45-e450+ CD3- cells stained by ICG compared to controls.

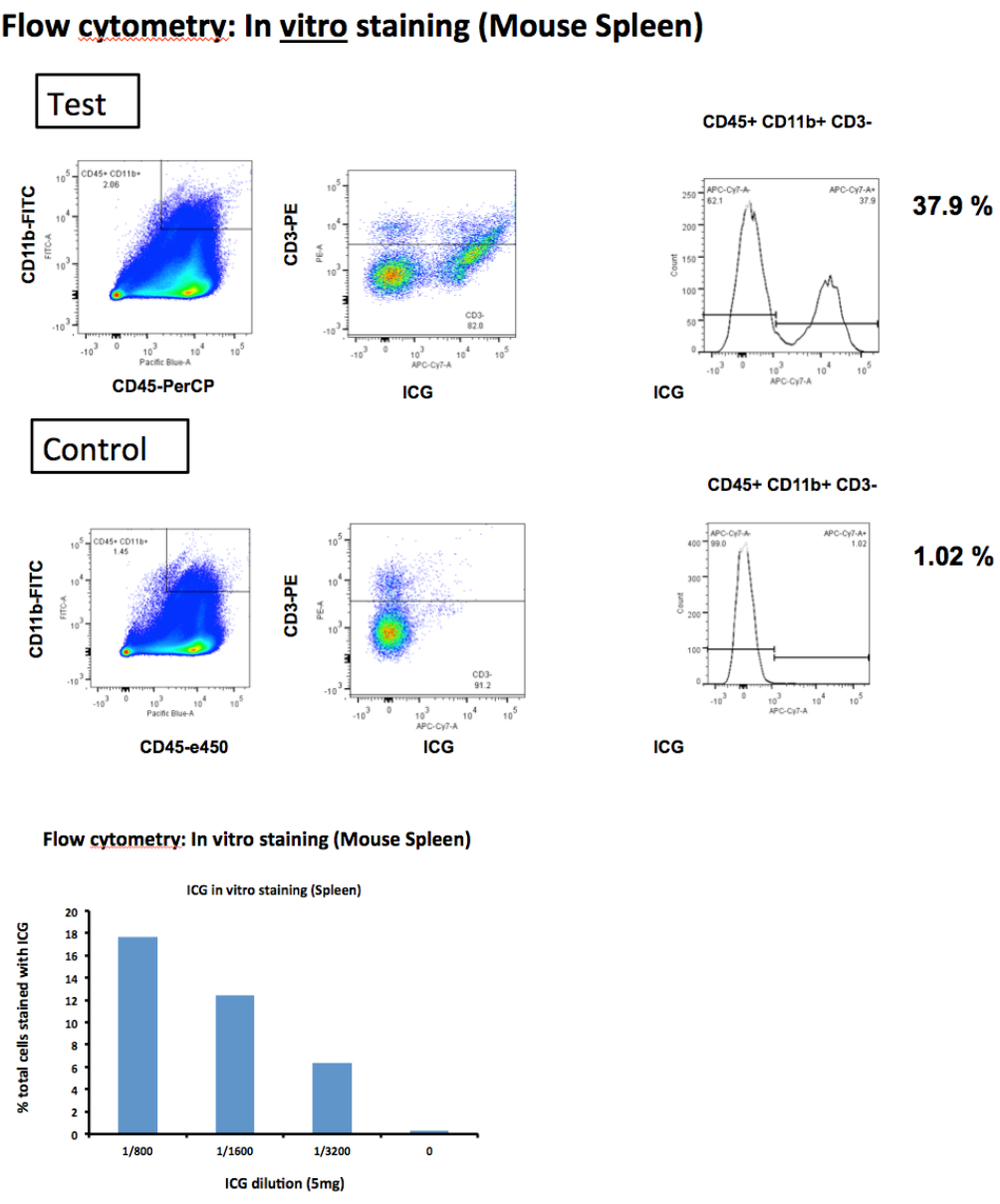

Figure 4.3. Gating strategy for in vitro labelling of murine splenoscytes

Gating strategy to assess the proportion of CD11b-FITC+ CD45-e450+ CD3- splenocytes stained by a concentration of 6.25µg/mL indocyanine green dye (ICG) when incubated for 30 minutes at room temperature. The bottom panel represent the control sample where cells were incubated in phosphate-buffer saline, pH 7.4 (PBS) under the same conditions. Histograms on the right show the proportion of CD11b-FITC+ CD45-e450+ CD3- cells stained by ICG compared to controls. Bar chart showing the percentage of ICG-labelled cells with serial dilutions of ICG.

4.3.2 Flow cytometric analysis of ICG labelled cells

ICG stained PBMCs, whole blood and splenocytes were analysed using a BD Bioscience LSRII flow cytometer as no commercial machine was available with a near infra-red laser for ideal excitation of ICG. Sub-optimal excitation by the 633nm red laser nonetheless still resulted in a reliable signal using a 780/60 bandpass filter. A minimum of 10,000 events was collected for each sample and fluorescence-minus-one controls were used to determine the placement of gates. Medium or High flow rates were used. Compensation was performed using OneComp eBeads (eBioscience, San Diego, USA, 01-1111-42) and an ArC Amine reactive Compensation bead kit (Invitrogen Life Sciences, A10346) for the live-dead stain. Data was processed using FlowJo v10.1 (TreeStar. Ashton, Oregon, USA)

4.3.3 Animal procedures

All animals were handled in accordance with the UK Animals (Scientific Procedures) Act 1986. Female C57BL/6J mice (Harlan, UK) at seven to eight-weeks of age were used. For in vivo procedures, the mice were anesthetized with an ip injection of medetomindine hydrochloride (1 mg/kg body weight; Domitor; Pfizer Animal Health, New York, NU), and ketamine (60mg/kg body weight) in water. Post-procedure, anaesthesia was reversed by peritoneal injection of an equal volume of AntiSedan (Pfizer pharmaceuticals, USA). Mice were recovered overnight on heat mats and supplied with hydrated chow. Pupillary dilation was achieved with 1 drop of 1% Tropicamide (Bausch and Lomb, Surrey, UK).

4.3.3.1 Induction of Endotoxin Induced Uveitis

Female C57BL/6J mice (Harlan, UK) at eight-weeks of age received a single ip injection of 0.2mg of lipopolysaccharide (LPS) from *Escherichia coli* (Sigma-Aldrich, St Louis, MO, USA) in phosphate-buffered saline (PBS). 1mg ip bolus injection of ICG was given 24 hours prior to LPS treatment. Imaging was performed 48 hours later, at a previously determined time point where these is peak infiltration by myeloid cells.

4.3.3.2 Induction of laser choroidal neovascularisation

In Female C57BL/6J mice (Harlan, UK) at seven to eight-weeks of age laser CNV was induced using a slit-lamp-mounted diode laser system (wavelength 680nm; Keeler, Windsor, UK). Laser settings used: 200 mW power, 100 ms duration, and 100µm spot diameter. Laser CNV lesions were applied at a distance of 3 disc diameters from the optic nerve avoiding any blood vessels.

4.3.3.3 In vivo imaging

Ocular imaging was performed using a scanning laser ophthalmoscope (Spectralis™ HRA, Heidelberg Engineering, Heidelberg, Germany). A 55° field of view lens was used and a mean of 100 consecutive frames was taken for each image. In order to visualize ICG-labelled cells, a near-infrared filter (790 nm diode excitation laser and 800 nm long-pass filter) was used. Cell labelling was achieved with various doses (1mg to 0.0125mg) **(Figure 4.6)** of 5mg ICG (Pulsion Medical Systems AG) dissolved in 5mL of water and administered 3 days prior to laser induction of CNV, ip injection of LPS, imaging of the EIU model. The different routes of administration are summarized in **Figure 4.7**. To assist the identification of laser CNV lesions, infrared-reflectance imaging was performed with a 820 diode excitation laser and no barrier filter. For autofluorescence imaging and fluorescein angiography, a blue-light filter (488 nm solid state excitation laser and 500 nm long-pass filter) was used. Fluorescein angiography was performed 1 week after laser CNV induction with an ip injection of 0.2 mL fluorescein sodium (2%). Images were acquired at 90 seconds and 7 minutes after injection.

4.3.3.4 Quantification of ICG positive cells in the retina

Images were exported from the Heidelberg eye explorer version 1.7.1.0. and processed in Adobe Photoshop CS5 (Adobe Systems Incorporated, San Jose, USA).

Details of image processing and quantification can be found in the results section and **Figures 4.4, 4.5**.

4.4 Results:

4.4.1. In vitro labelling of peripheral blood mononuclear cells (PBMCs) and splenocytes with ICG.

To establish whether ICG can label circulating leukocytes we incubated whole blood with the dye *in vitro* for 30 minutes at room temperature. Visual inspection of a blood smear from human blood by fluorescent microscopy revealed a small population of fluorescent cells in the NIR channel **(Figure 4.4, A, B)**. Next we exposed PBMCs isolated from human and mouse blood, and mouse splenocytes to ICG (30 minutes at room temperature) and then analysed dye uptake and cell identity by flow cytometry. In human PBMCs, whilst many cells stained slightly with the dye, 6.5% (SD +/- 1.3%) of all cells were strongly stained with ICG **(Figure 4.4, C, D)**. In this strongly stained population 90% were CD45+ CD11b+, suggesting ICG is primarily taken up by myeloid cells. Similarly, incubating mouse PBMCs with ICG strongly labelled 1% (SD +/- 0.3%) of cells and 64% of ICG+ cells were CD45+ CD11b+ **(Figure 4.4, E, F)**. When mouse splenocytes were used for the same experiment 10.3% (SD 0.7%) of cells were labelled by ICG, of which 58% were CD45+ CD11b+ **(Figure 4.4, G, H)**.

We observed that although the proportion of ICG-stained cells increased when incubated in higher temperatures and concentrations of ICG, there was an increase in non-specific staining. We identified that a 30-minute incubation of ICG at a concentration of 6.25µg/mL at room temperature achieved reproducible staining of cells. Furthermore, we identified that the minimum dose in which some stained cells could be detected was 1.6µg/mL, although 5µg/mL was required for reliable and reproducible staining. For comparison, the 5mg ICG dose used in ophthalmic clinic equates to a plasma concentration of roughly 1.5µg/mL in an adult human. In

summary, the specificity of ICG-binding to PBMCs *in vitro* was dependent on concentration, ambient temperature, and period of incubation.

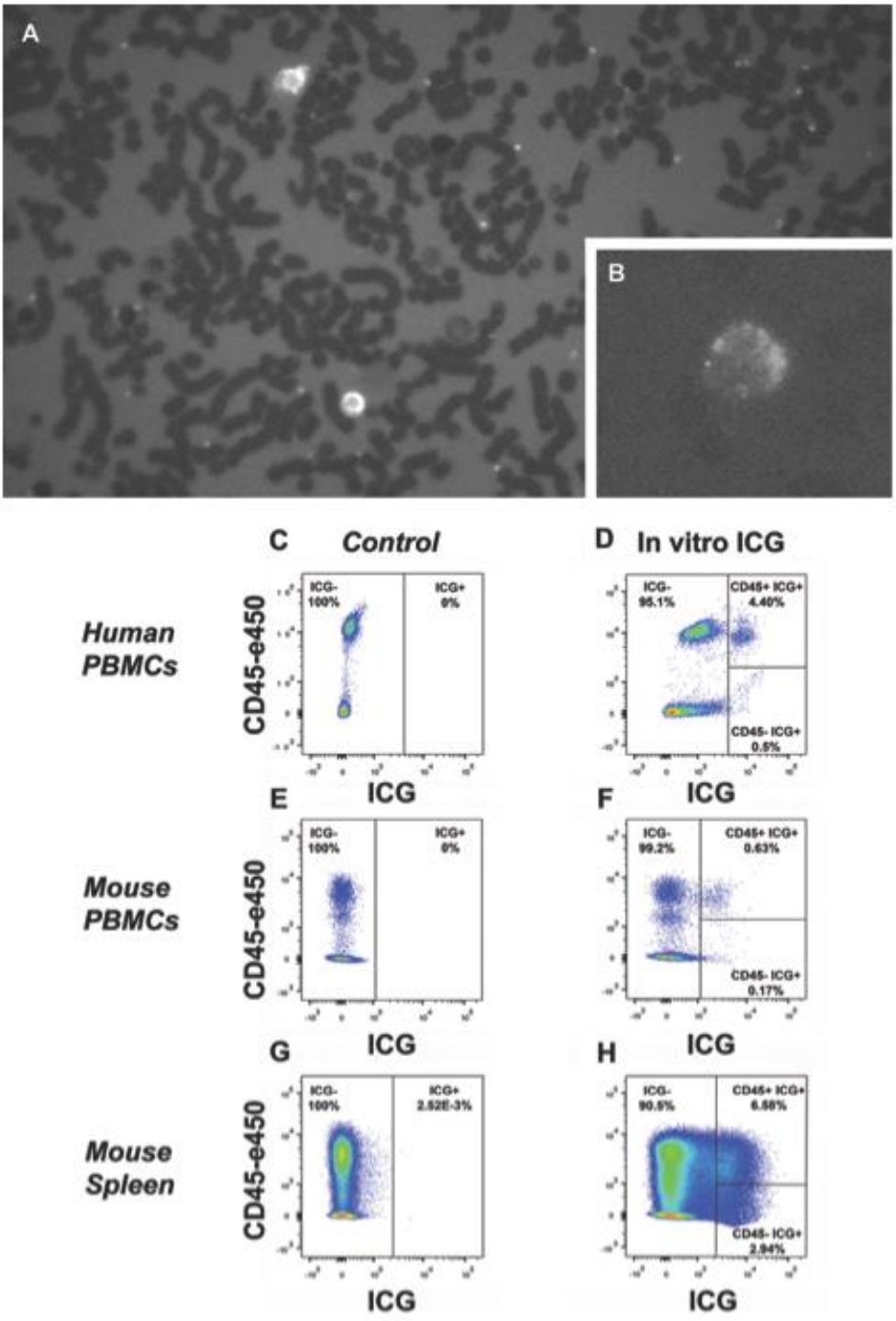

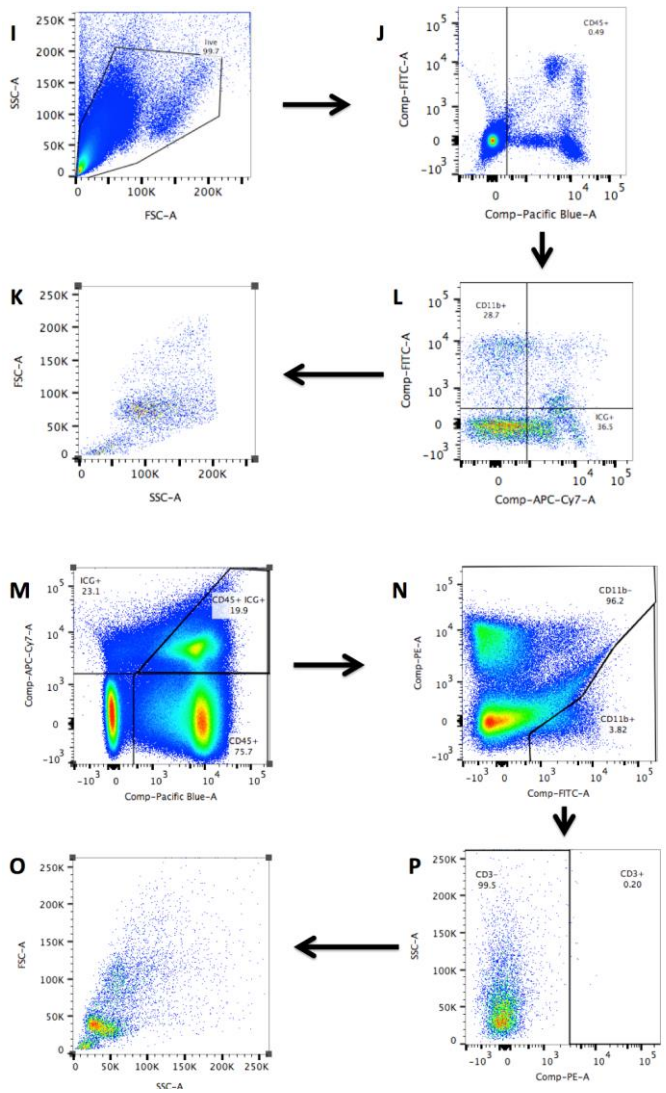

Figure 4.4. In vitro labelling of peripheral blood mononuclear cells (PBMCs) and splenocytes in human and mouse.

(A) Blood smear of human blood incubated in a concentration of 6.25µg/mL indocyanine green dye (ICG) for 30 minutes at room temperature. A small proportion of cells stained with ICG were visualized on the near-infrared channel at 10X magnification and (B) 20X magnification. (C, D) An example of detecting ICG-stained human PBMCs by flow cytometry reveals labelling in around 5% of cells (mean 6.5%, SD +/- 1.3%, N=4). (E, F) In mouse PBMCs a smaller proportion of ICG-labelled cells were detected (mean 1%, SD +/- 0.3%, N=4), (G, H) whereas mouse splenocytes labelled more readily with ICG (mean 10.3%, SD +/- 0.7%, N=4). (I to K) show the gating strategy used to identify ICG-stained CD45+ CD11b+ murine PBMCs, and (M-O) ICG-stained CD45+ CD11b+ CD3- murine splenocytes. (K, O) represent the forward and side scatter back gates.

4.4.2 In vivo labelling of infiltrating leukocytes by ICG.

After establishing that ICG can label myeloid cells *in vitro*, we proceeded to test whether these cells can be labelled by ICG *in vivo*. We administered ICG to C57BL/6 mice that were used in three different retinal disease models, known to have substantial leukocytic (including monocyte/macrophage) infiltration into the retina.

The first model was endotoxin-induced uveitis (EIU), induced by systemic delivery of lipopolysaccharide (LPS) from *Escherichia coli*. A previous study has detected acridine orange labelled leukocytes in the subretinal space/deep retina, 2 days after LPS injection (187). In our study, animals were first injected with ICG (1mg) by intraperitoneal (ip) injection and after 3 days with LPS. In the subsequent days we found that ICG labelled cells were detectable in the retina *in vivo* using a fluorescence scanning laser ophthalmoscope in the ICG channel (near infrared). The number of labelled cells peaked at 2 days after LPS administration (5 days after ip ICG, **Figure 4.5, A, B**), with a weaker signal at 1 day and 4 days after LPS (not shown). No signal was seen in the fluorescein channel (FA), indicating that the ICG signal did not derive from autofluorescence. Control animals that were only injected with ICG but not with LPS showed only a few sporadic ICG positive cells **(Figure 4.5, C, D)**. This suggests low levels of peripheral cells trafficking in the normal retina, as previously inferred via flow cytometric analysis (397, 398), which dramatically increases after LPS stimulation.

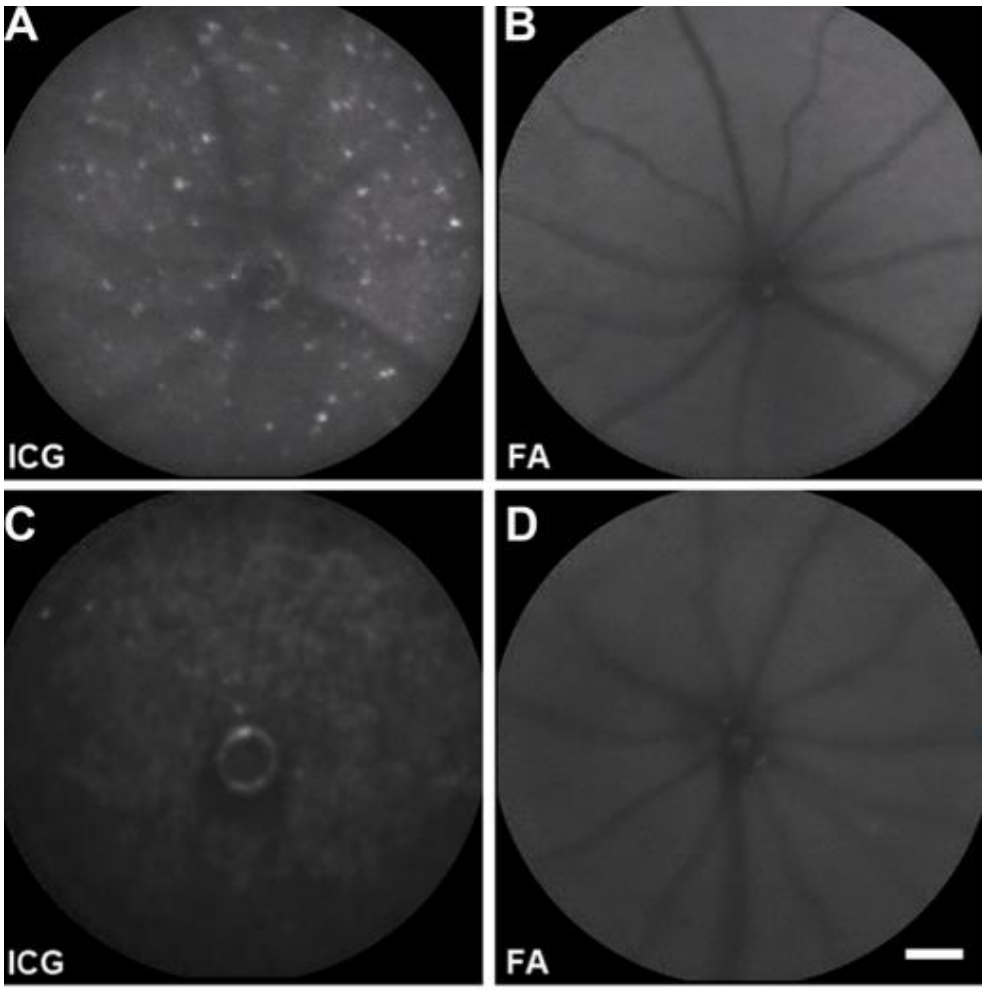

Figure 4.5. In vivo labelling of infiltrating leukocytes in a murine model of ocular inflammation.

(**A**) Inflammatory infiltration into the deep retina/choroid in an endotoxin-induced uveitis (EIU) eye, imaged with a scanning laser ophthalmoscope. In the ICG channel (ICG) white dots were visualized after ip injection of ICG (5 days prior to imaging), and induction of systemic inflammation (ip LPS injection 2 days prior to imaging). (**B**) Image of the same eye taken in the fluorescein channel (FA) shows no white dots. (**C**) A control mouse that only received ip ICG (3 days prior to imaging) but no LPS. Imaging in the ICG channel showed only a few sporadic ICG-labelled cells suggesting low level circulation of myeloid cells into the retina. (**D**) The same eye shows no signal in the FA channel.

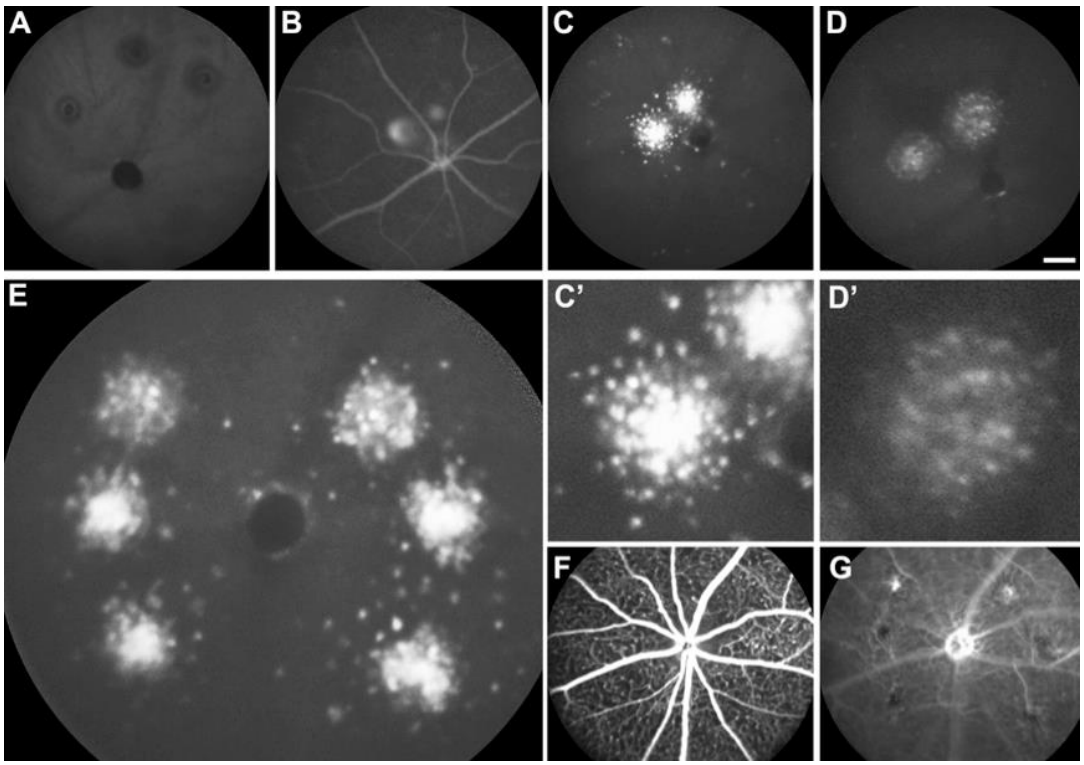

Figure 4.6. In vivo labelling of infiltrating leukocytes in a laser-induced choroidal neovascularisation (CNV) murine model.

(**A**) Scanning laser ophthalmoscopy in the ICG channel showed no signal in an animal that received laser burns but no ICG. (**B**) In an animal which received ip ICG and laser simultaneously fluorescence is observed in retinal vessels and laser lesions, without obvious leakage of ICG into the surrounding retinal tissues. (**C**) An animal which received ip ICG (10 days prior to imaging) and laser burns (7 days prior to imaging) shows accumulation of ICG-labelled cells in and around laser lesions. (**C'**) Magnified image of laser lesion and surrounding cells shown in C. (**D**) 3 days later, in the same eye (as shown in C) ICG intensity was reduced (13 days after ip ICG) (**D'**) Magnified image of laser lesion and surrounding cells shown in D. (**E**) In an animal that received six laser lesions (7 days prior to imaging) and ip ICG (10 days prior to imaging) ICG-labelled cells accumulated in and around all six laser lesions. (**F, G**) Corresponding fluorescein angiography (FA channel) of the superficial retina (F) and deep retina/choroid (G) taken 10 minutes after ip injection with fluorescein shows that only 2 of six laser lesions had developed choroidal neovascularisation, and none of these lesions display obvious fluorescein dye leakage, suggesting that inflammatory cellular infiltration occurs independently of neovascularisation.

The second model was the laser-induced choroidal neovascularisation (CNV) model, a widely used model to study pathological angiogenesis in the retina (399). The vascular response in this model is accompanied by an accumulation of infiltrating leukocytes in the laser lesion from the circulation and from within the retina (400, 401). We hypothesised that the infiltrating leukocytes can be visualised by first labelling cells with ICG in the periphery and then inducing the lesion. Since laser injury can induce autofluorescence we first imaged laser-lesioned animals without ICG. In the ICG channel, no fluorescence was detected in the lesion **(Figure 4.6, A)**. Next, we tested whether administration (ip) of ICG immediately after laser would result in ICG leakage into the retina. Although ICG could be visualised inside the retinal vasculature and laser lesions, overt leakage of ICG into the retina was not apparent **(Figure 4.6, B)**. Since ICG is rapidly cleared from the circulation (within minutes in humans) we reasoned that administering ICG 3 days before laser should be sufficient for minimizing any ICG in the circulation that may directly leak into the retina from the blood stream and label resident retinal macrophages. Consistent with this, ICG could no longer be detected inside blood vessels 3 days after ICG injection (not shown). 7 days after laser (10 days after ICG) we observed a marked aggregation of clearly labelled cells in and around the laser lesions **(Figure 4.6, C, C')**. After a further 3 days (10 days after laser) the signal started to subside **(Figure 4.6, D, D')**. The invasion of ICG positive cells was a general response to laser injury and independent of neovascularisation. This is illustrated by an example shown in **Figure 4.6, E**. Here 6 laser lesions were applied. Although all of them accumulated ICG positive cells, only 2 lesions showed signs of neovascularisation based on fluorescein angiography **(Figure 4.6, F, G)**.

We further tested whether cellular infiltration around the laser-induced CNV lesion could be monitored over time. As before, ICG was administered ip 3 days prior to laser, and animals were imaged sequentially 2, 5 and 8 days after laser **(Figure 4.7)**. The number of ICG-labelled cells in and surrounding the CNV lesion could be observed qualitatively to increase over time **(Figure 4.7, C, D, E)**. We attempted to quantify these changes by using image analysis software (ImageJ) to count cells in thresholded images of CNV lesions **(Figure 4.8)**; a method we have used successfully

for quantifying ICG-labelled cells in the EIU model. However, due to the narrow range of intensity values and the high number of cells within each lesion, it was not possible to visualize individual cells overlying CNV lesion. We therefore assessed the mean intensity values for a given pixel area using histograms in order to reproducibly quantify cellular infiltration in CNV lesions **(Figure 4.8, G)**. Using this method, we demonstrate that ICG-labelled cellular infiltration can be quantified and monitored over time **(Figure 4.7, B, C', D', E')**.

Because ICG is routinely used in clinical practice, we compared the dosage and delivery routes normally used in humans (5mg iv bolus injection) with our mouse protocol (1mg ip bolus injection). We reduced the ICG in a stepwise fashion from 1mg to 0.0125mg per mouse (the latter roughly equates to the human dose in current ophthalmic use). Invading cells could still be readily detected after administration of 0.5mg ICG ip but at 0.25mg they were fainter. With progressively reduced amounts of ICG (0.125mg, 0.05mg, 0.025mg and 0.0125mg), the lesions were faintly fluorescent but individual cells could no longer be detected **(Figure 4.9)**. We also tested different delivery routes and found that ip injection was most efficient at labelling cells. A subcutaneous depot (1mg) produced weaker labelling, but individual cells could still be detected, whereas iv (1mg) delivery produced only very faint staining. Oral administration (by gavage or in drinking water) (n=6) did not lead to any labelling **(Figure 4.10)**.

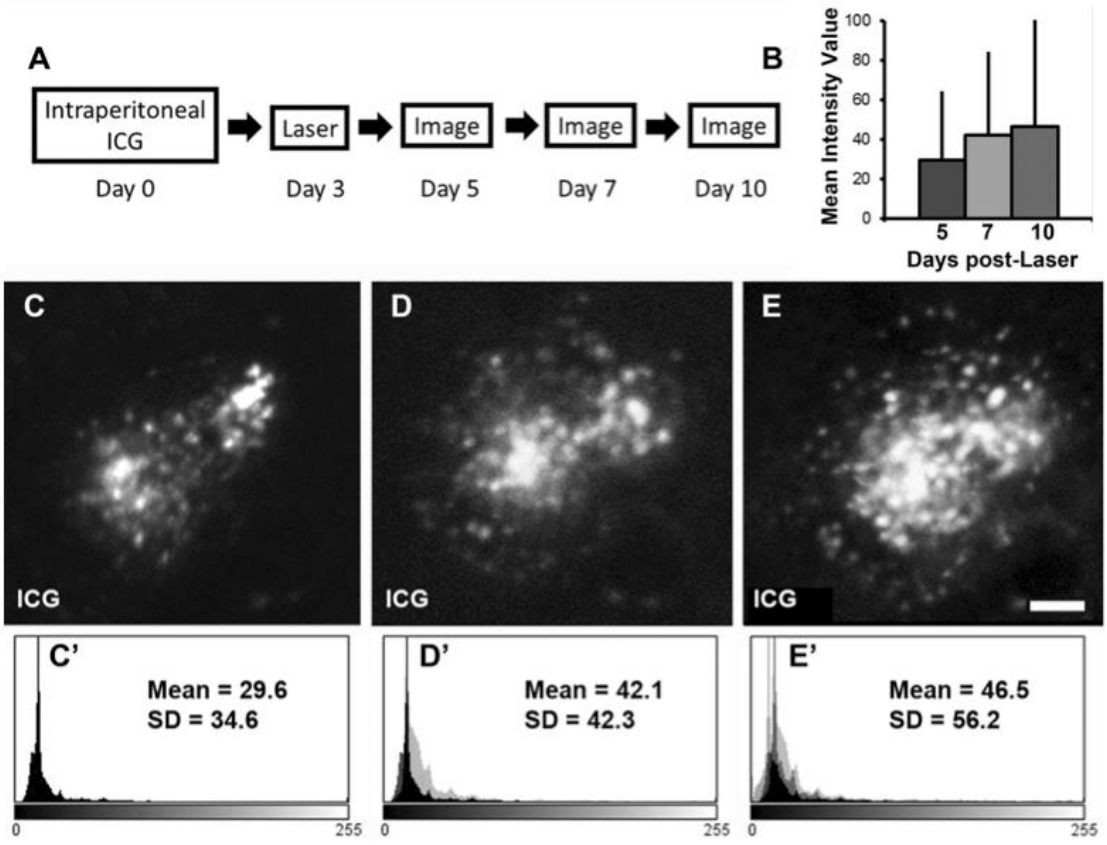

Figure 4.7. In vivo quantification of laser-induced CNV related infiltration.

(**A**) ICG was injected intraperitoneally at day 0 before laser-CNV induction at day 3 in C57BL/6 mice. Imaging in the ICG channel was performed on day 5, 7 and 10, (**C-E**) visualising increasing cellular infiltration in and surrounding the laser-CNV lesion. (**B, C'-E'**) We demonstrate that the mean intensity values and standard deviations can be quantified over a given area and show an increase in inflammation over time. The mean intensity value of the lesion at day 5 is represented by the black histogram (C'), day 7 the superimposed light grey histogram (D') and day 10 the superimposed medium grey histogram (E').

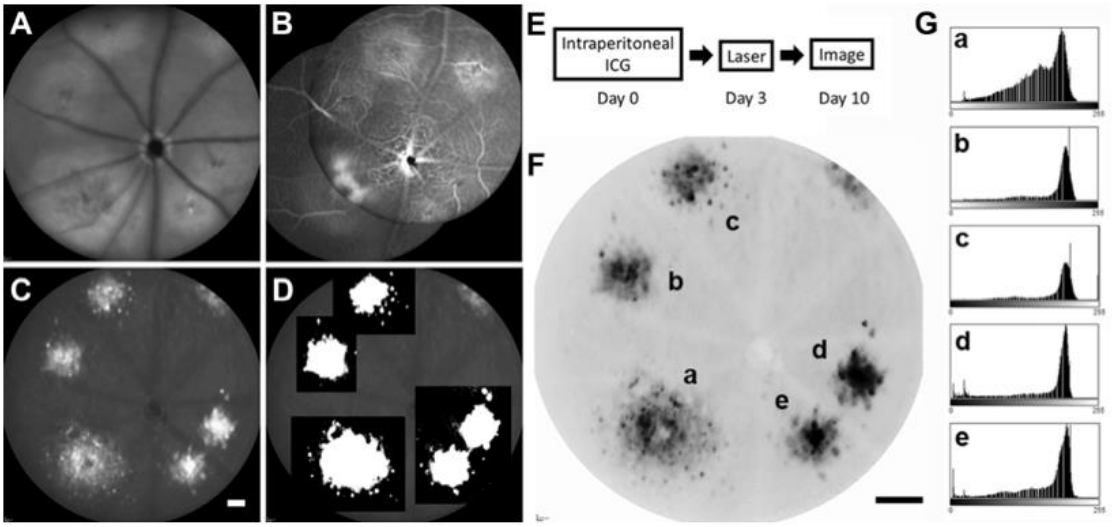

Figure 4.8. Quantification of ICG-labelled cells.

Methods for the quantification of indocyanine green (ICG)-labelled cells in the laser induced choroidal neovascularisation (CNV) murine model were assessed 10 days after ip ICG and 7 days after laser (schedule shown in E). (**A**) Autofluorescence imaging in the FA channel shows the laser-induced CNV lesions, and (**B**) fluorescein angiography shows the vascular response. (**C**) Images of ICG-labelled cells in and around CNV lesions were acquired in the ICG channel. (**D**) An example of grey level thresholding demonstrates that individual cell counts are not possible with this approach. (**F**) An inverted image of (C) was used to quantifying (**G a-e**) ICG-labelled cellular infiltration by the use of histograms. This method could reproducibly quantify the mean intensity of each lesion for the purpose of tracking changes over time. Scale-bars = 1.5mm.

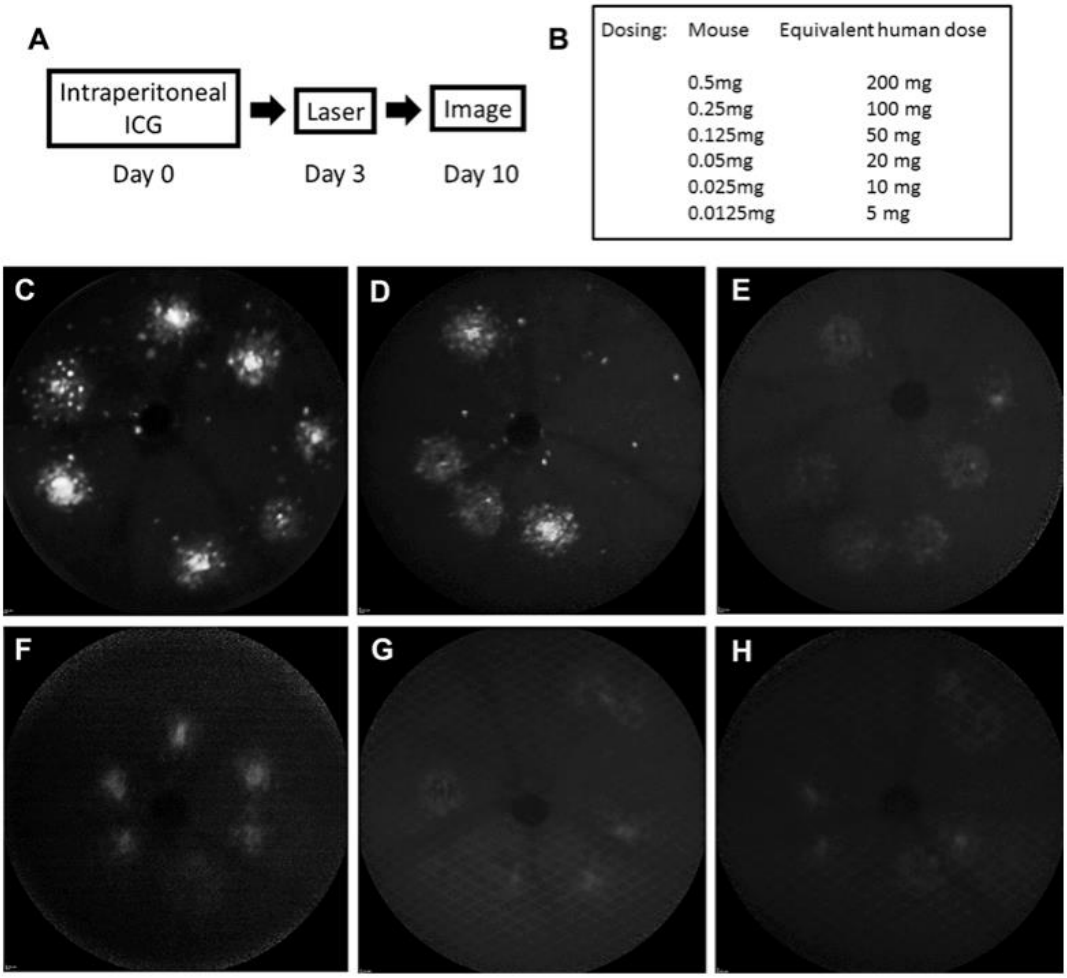

Figure 4.9. ICG dosing for the purpose of cellular labelling.

The doses required for cellular labelling were tested in the laser induced choroidal neovascularisation (CNV) murine model. (**A**) The experimental protocol is shown diagrammatically with intraperitoneal (ip) indocyanine green (ICG) administered at day 0, laser-CNV induction at day 3, and subsequent imaging at day 10. (**B**) Table showing ICG doses in a stepwise reduction in mice from 0.5mg to 0.0125mg in the left column, and the estimated equivalent human dose in the right column. (**C, D**) A deep retinal/choroidal image of animals that received 0.5mg and 0.25mg of ip ICG respectively. Although ICG-labelled cells can be detected, they were fainter compared to the higher dose of 1mg used in previous experiments (not shown). (**E-H**) A deep retinal/choroidal image of animals that received 0.125mg, 0.05mg, 0.025mg, 0.0125mg of ip ICG respectively. In these further dose reductions, CNV lesions were faintly fluorescent but individual cells could no longer be detected.

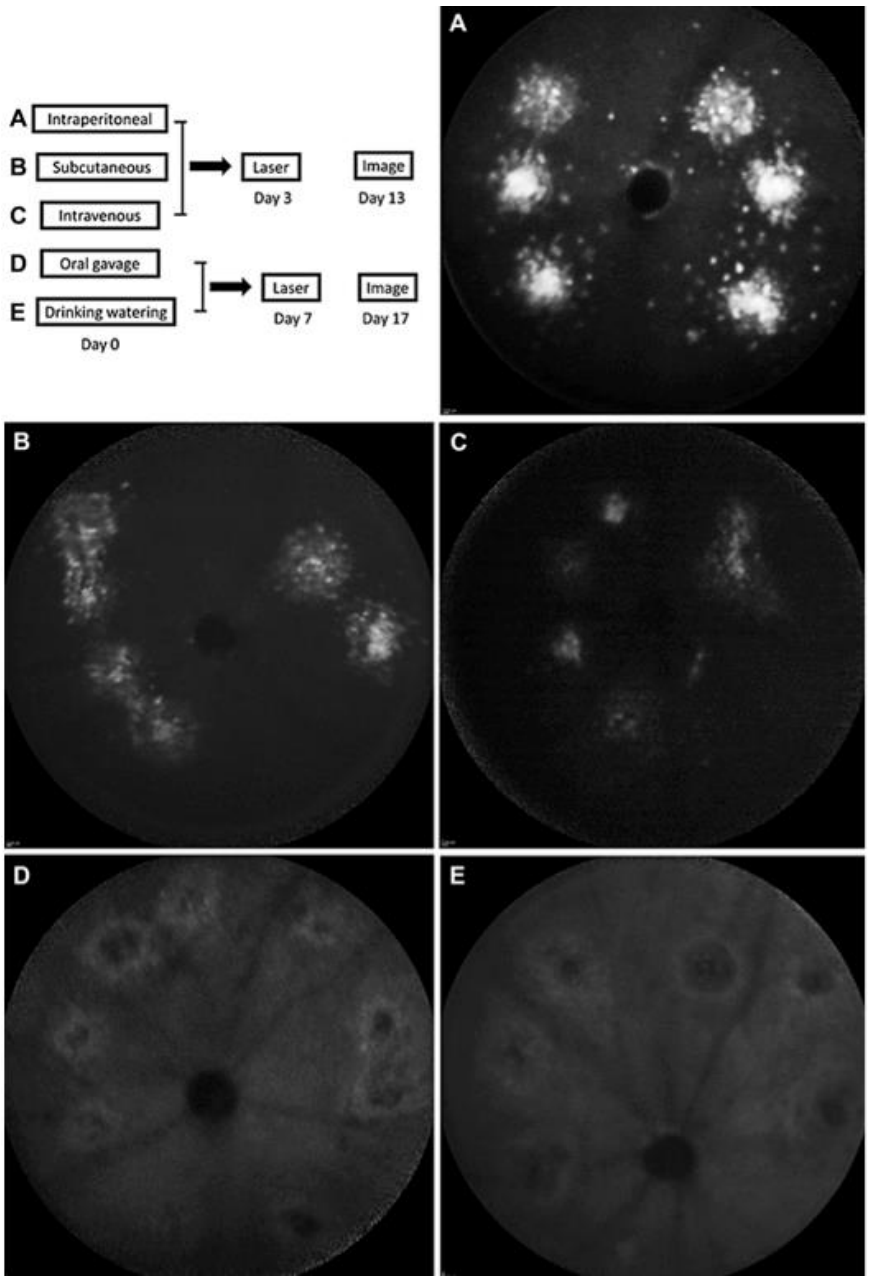

Figure 4.10. ICG dosing for the purpose of cellular labelling.

Route of administration of ICG for the purpose of cellular labelling. Different delivery routes for ICG were tested in the CNV model. (**A-C**) 1mg of ICG was administered via the intraperitoneal, subcutaneous, and intravenous (tail vein) route at day 0 before laser-CNV induction at day 3 and imaging at day 13 respectively. (**D, E**) 1mg of ICG was given by daily oral gavage and the equivalent added to the drinking water for 7 days respectively, before laser-CNV induction, and subsequent imaging 10 days later. The intraperitoneal route of administration (**A**) was the most effective for cellular labelling. Faint labelling could be detected with the subcutaneous route (**B**) but not with the intravenous (**C**), or oral routes of administration (**D, E**).

4.4.3 Characterizing in vivo ICG-labelled cells

In order to identify what cell types are labelled by ICG we analysed PBMCs and dissociated spleen by flow cytometry 72 hours after ICG administration (1mg ip). In control animals isolated PBMCs did not show any ICG signal, whereas PBMCs from ICG injected animals contained a small population (mean=0.74%, SD=0.31%, range 0.47 to 1.01%) of strongly labelled ICG+ cells **(Figure 4.11, A)**. Of these, a mean of 75.9% (SD=9.64%) also stained for CD45+ CD11b+ (not shown). Similarly, the spleen, which is known for its role as a reservoir for circulating monocytes, contained a larger population of ICG-labelled cells (mean=2.42%%, SD=1.22%, range=0.86 to 3.48%), compared to circulating PBMCs **(Figure 4.11, B)**. We observed that a mean of 70.1% (SD=6.66%) of the CD45+ CD11b+ splenocytes were stained with ICG.

These findings reinforce our *in vitro* data showing that ICG is predominantly taken up by CD45+CD11b+ monocytes/macrophages. However, it also highlights that ICG may stain other inflammatory cells. We observed in our in vivo experiments that a very small proportion of CD4, CD8, and CD20+ cells which we included in our exclusion 'dump' channel (R-Phycoerythrin) were also stained with ICG. Furthermore, dissection of the mice 7 days after ICG ip revealed "green" staining of lymphatic tissue in the thoracic cavity **(Figure 4.12, A, B)**, mediastinal lymph nodes **(Figure 4.12, C)**, thymus (not shown) and the greater omentum in the abdominal cavity **(Figure 4.12, D, E, F)**. This suggests that inflammatory cells in the circulation, most likely both monocytes and lymphocytes that continuously circulate between the bloodstream and lymphoid organs can be labelled with ICG.

To further test the identity of ICG positive cells invading the retina in the laser-induced CNV model we used an *in vivo* staining protocol. 7 days after laser (and 10 days after ip ICG) the retina was imaged **(Figure 4.13, A, B, C)**. Immediately after imaging a fluorescently labelled (FITC) antibody against CD11b was injected (iv). Over the course of 30 minutes this labelled a population of cells that spatially matched the ICG labelled cells **(Figure 4.13, D, E, F)**. The CD11b signal was weaker than the ICG

signal and there was not a perfect overlap. Nevertheless, all CD11b positive cells were also ICG positive. The same approach was also taken with an anti CD45 antibody with the same outcome. This further supports that the identity of most of the ICG labelled cells in the retina as infiltrating myeloid cells.

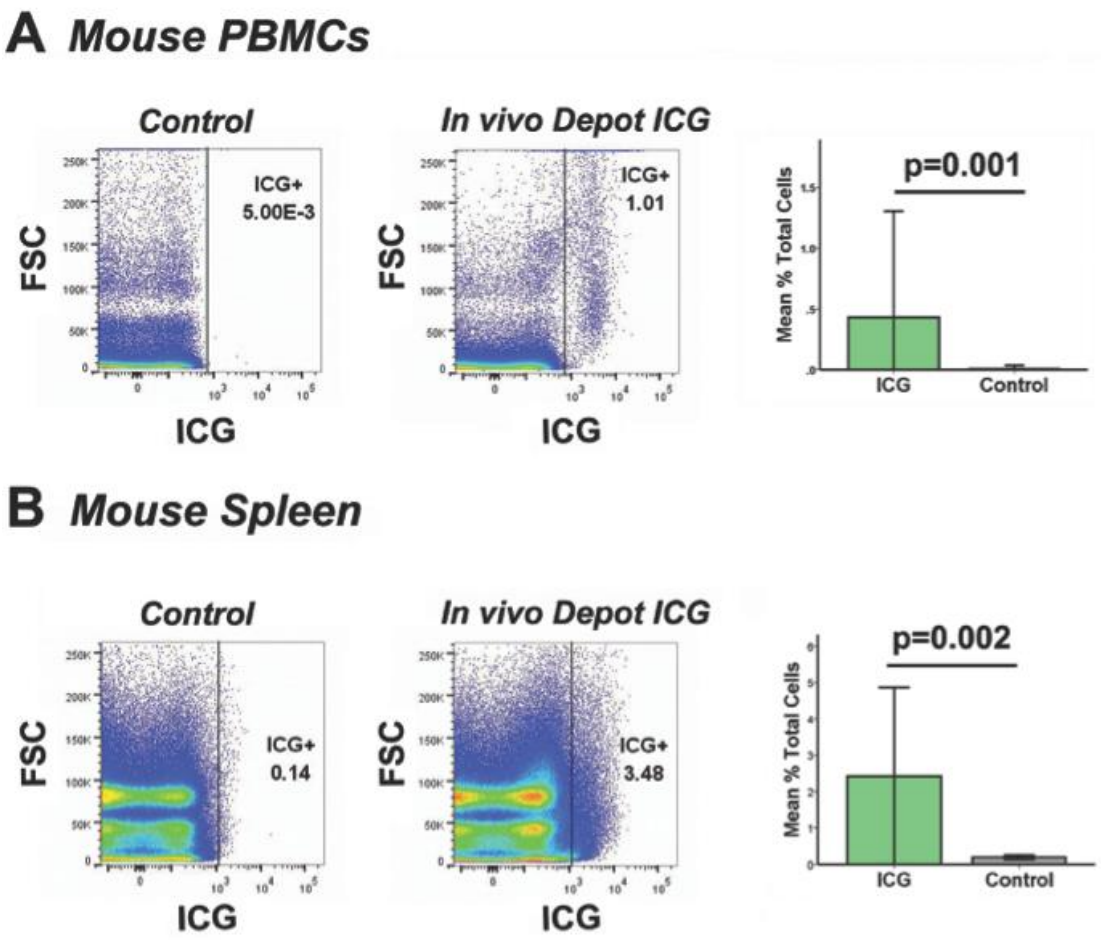

Figure 4.11. Detection of in vivo ICG-labelled cells by flow cytometry.

24 hours after ip injection of ICG dye, PBMCs and splenocytes were isolated from C57B6 mice in order to assess the proportion of cells labelled by ICG. (**A**) 1.01% of circulating mouse PBMCs were stained with ICG. This was statistically significant from control animals (p=0.001). (Mean=0.74%, SD=0.31%, range 0.47 to 1.01%). (**B**) A higher proportion of splenocytes (3.48%) were stained with ICG. This was also statistically significant from control animals (p=0.002). (Mean=2.42%%, SD=1.22%, range=0.86 to 3.48%). [Mann-Whitney U test, n=5]

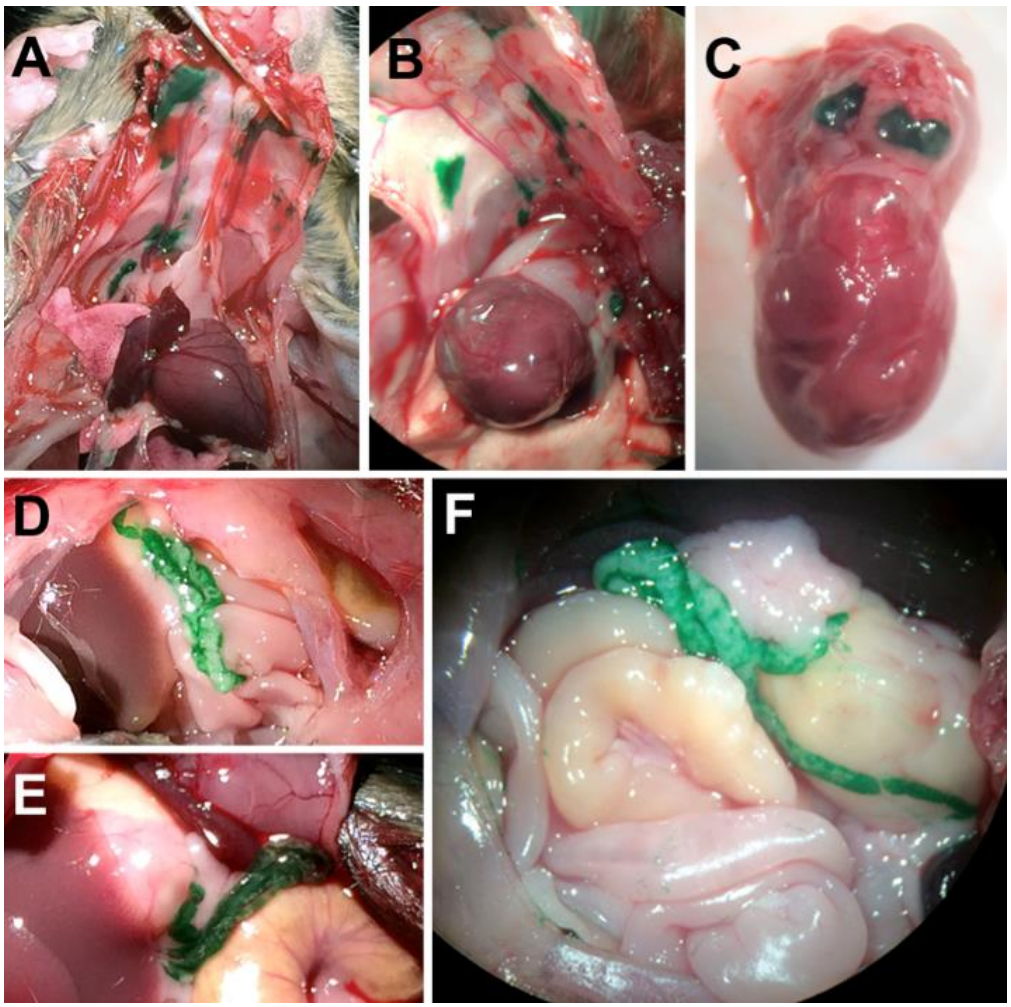

Figure 4.12. Distribution of ICG within the abdominal and thoracic cavity after intraperitoneal administration.

We performed dissection of mice 7 days after intraperitoneal administration of 1mg of indocyanine green (ICG). (**A, B**) In the thorasic cavity we observed green staining of lymphatic tissue along the thorasic wall and (**C**) mediastinal lymph nodes. (**D-F**) In the abdominal cavity, we observed a strong green stain of the greater omentum.

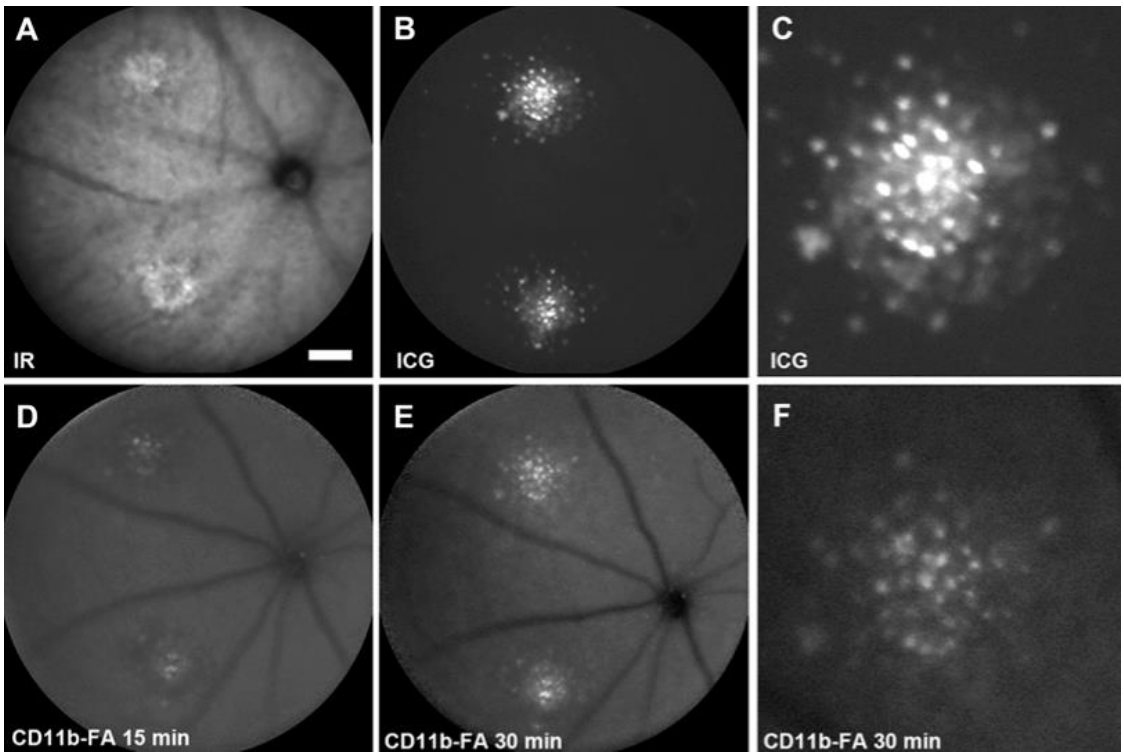

Figure 4.13. Characterization of in vivo ICG-labelled cells in the CNV model.

Animals received laser 7 days prior, and ip ICG 10 days prior to imaging. (**A**) Infrared-reflectance imaging (IR) demonstrates the presence of laser-induced CNV lesions in the deep retina/choroid, and (**B**) a deep retinal/choroidal image taken in the ICG channel shows ICG-labelled cells surrounding two laser-induced CNV lesions. (**C**) A magnified view of ICG-labelled cells surrounding the CNV lesion from the upper lesion in (B). Immediately after IR and ICG imaging FITC-conjugated anti CD11b antibody was injected (iv) and imaged in the FA channel at 15 (**D**) and 30 minutes (**E, F**) post-injection. (**F**) A magnified view of CD11b-FITC-labelled cells demonstrates good correlation with ICG-labelled cells (C).

4.5 Discussion:

We describe a novel technique for in vivo labelling of circulating cells with ICG dye. We found that in order to label these cells reproducibly *in vivo*, ICG must be administered as a depot preparation. Using this approach, we showed in three disease models of retinal inflammation that infiltrating leukocytes can be detected, tracked over time, and quantified in the murine retina.

We found that the commonly used intravenous route of administration of ICG failed to label infiltrating leukocytes. However, by administering ICG as a depot, we have shown that infiltrating cells were clearly labelled in our disease models. A possible explanation for this is the increase period of ICG exposure that circulating cells have, in order to be labelled. In keeping with this, we observed *in vitro*, that an increased time of exposure to ICG resulted in increased cell labelling. Furthermore, we observed that *in vivo* and *in vivo* the majority of these labelled cells were of myeloid origin.

Our technique will be useful in the above mentioned mouse models. In particular the laser-induced neovascularisation model is widely used to study pathological vessel growth in the retina. This model also contains an important inflammatory component, which so far has been mainly assessed by immunohistochemistry on postmortem tissue. With our ICG technique it will be possible to monitor inflammatory cell invasion longitudinally in these animals in parallel with vascular changes.

More generally, in the field of inflammation the ability to monitor a sequence of events over time is particularly important in order to elicit cause-and-effect relationships. As such, recent developments have been focused on the ability to visualize inflammation in vivo using molecular imaging techniques such as intravital microscopy using fluorescent antibodies, nanoparticles and transgenic animals that express fluorescent proteins.(402, 403) Although our ICG method does not target specific cell types or epitopes as specifically as transgenic animals or antibodies, we have nevertheless found that ICG is mainly taken up by CD45+CD11b+ monocytes/macrophages. Moreover, our approach has the advantage that it can be

carried out very easily, does not depend on specific mouse strains and, most importantly, has the potential for immediate translation to human use.

Current strategies for in vivo molecular imaging in humans include conjugation of NIR dyes, such as ICG, with ligands such as small molecules, antibodies, peptides, DNA and nanoparticles. Nevertheless, none of these probes have been approved for human use because of their so far insufficiently characterized safety profiles. In particular nanoparticles suffer from poorly characterized distribution, accumulation and clearance from the human body, and potential cytotoxicity of heavy metal ingredients (382, 404).

In contrast, ICG an inert, water-soluble organic dye, is rapidly bound to plasma proteins and solely removed from the circulation through the liver via a specific carrier-mediated transport system (405, 406). Furthermore, ICG is known not to provoke inflammation even when injected directly into tissues. The ICG dye was first developed in the mid-1950s to determine cardiac output and hepatic function. The dye is rapidly cleared, low in toxicity and well tolerated by patients; even at doses which exceed what is now routinely given by 10-fold (407, 408). This led to its application to a variety of clinical uses; with examples including sentinel node biopsy, tumour demarcation surgery, lymphatic vessel assessment and choroidal vasculature imaging in the eye. Thus, ICG has a well-documented safety and tolerance track record of more than 60 years in clinical practice. Furthermore, instruments that are needed to visualize ICG are readily available in most ophthalmic clinics.

In conclusion, we have demonstrated cellular imaging of circulating monocytes invading the retina by using a depot injection of ICG. Translating this insight into clinic will involve the development of a formulation suitable for depot ICG application in humans. This may be useful not only for monitoring ocular inflammation, but may also have applications further afield, for example, the detection of an immune response to novel treatment strategies such as stem cell therapies or retinal implants, or serve as an imaging biomarker for predicting the onset of angiogenesis in age-related macular degeneration or diabetic retinopathy.

4.6 Chapter summary:

We have developed a method to label and image myeloid cells infiltrating the mouse retina and choroid *in vivo*, using a single depot injection of Indocyanine green dye (ICG). This was demonstrated using different ocular mouse models of inflammation and angiogenesis – endotoxin-induced uveitis (EIU) and laser-induced choroidal neovascularisation (CNV). A near-infrared scanning laser ophthalmoscope was used for *in vivo* imaging of the eye and flow cytometry was used on blood and spleen to assess the number and phenotype of labelled cells. We found that *in vivo* intravenous administration failed to label any leukocytes, whereas depot injection, either intraperitoneal or subcutaneous, was successful in labelling CD11b+ myeloid cells. Progression of inflammation in the retina could be traced over a period of 14 days following a single depot injection of ICG. Additionally, flow cytometric analysis revealed that the predominant population of cells stained by ICG are circulating and splenic reservoir CD11b+ myeloid cells. The translation of this approach into clinical practice would enable visualisation of immune cells in situ. This will not only provide a greater understanding of pathogenesis, monitoring and assessment of therapy in many human ocular diseases but also open the ability to image immunity live for neurodegenerative disorders, cardiovascular disease and systemic immune mediated disorders.

5. The relationship between endothelial progenitor cells, circulatory monocytes, and diabetic eye disease

5.1 Introduction:

CD34+ EPCs derived from the peripheral circulation have the capacity to migrate, proliferate, and differentiate into mature endothelial cells.(59) Their potential for use in the treatment of ischaemic diseases lie in the ability of these cells to repair damaged blood vessels. However, the translation of EPC therapy into clinical practice has been limited by the ambiguity of its definition, relative rarity in the peripheral circulation, and duplicitous behaviour in cell culture. Established cell surface markers for EPCs, albeit inconsistently, have included CD34+; a stem cell marker, CD309+ (also known as KDR/VEGFR2); a marker for endothelial cells, CD133+; an early stem cell marker, and CD31; a mature endothelial cell marker.(70, 409, 410) There is increasing evidence that at least some of the cultured EPCs are derived from CD14+ monocytes, and furthermore, CD14+ monocytes themselves can give rise and behave functionally as endothelial cells.(74) It is therefore important to understand the relationships between these cells in both health and disease states. In this chapter, clinical evidence for the therapeutic efficacy of both EPCs and CD14+ monocytes is summarized and their relationship with diabetic eye disease examined.

5.1.1. EPCs in clinical practice

Clinical studies that explored the potential of EPC numbers as a biomarker have reported conflicting results. In cardiovascular disease, most studies demonstrate a reduced number of circulating EPCs.(411-413) However, reports have indicated that shifts in EPC levels were associated with disease severity; i.e. elevated levels in early, and lower levels in severe and late stages of coronary and peripheral arterial disease, and stroke.(414-418) These studies have also shown that low levels predict a poorer outcome of disease and response to treatment. In diabetes, reduced numbers of circulating EPCs with functional impairment have been observed, relative to age-

matched healthy controls.(62-64, 419). Conversely, elevated levels have been reported to correlate with the presence and/or severity of diabetes-associated complications.(415, 420)

The clinical relevance of the identity of EPCs lies in their relative rarity in bone marrow sample and even more so in the peripheral circulation. Ex-vivo expansion of these cells for the purpose of regenerative therapy is essential in order to obtain sufficient numbers for therapy. Moreover, the intermediate step “in culture” provides an opportunity to intervene; i.e. repair deficits or restore the regenerative potential of these cells, as observed in disease.(63) Strategies to enhance EPC function have included exposing these cells (both in vivo and in vitro) to numerous agents such as, tissue kallikrein (421), statins (a lipid lowering drug) (422, 423), losartan (an angiotensin II receptor antagonist drug used in hypertension) (424), and thymosin β4 (an actin sequestering protein) (425). In a diabetic mouse model, topical Sonic hedgehog gene therapy has been shown to improve wound healing by enhancing EPC function.(426) This was similarly observed with AMD3100, a CXCR4 antagonist, in a mouse model of myocardial infarction.(427) Combination therapy of both Sonic hedgehog gene transfer and AMD3100 has also been observed to further enhanced EPC mobilisation from the bone marrow.(428)

Pioneering clinical studies have shown that administration of EPCs can restore tissue vascularisation after ischaemic events in other parts of the body e.g. ischaemic limbs (60, 429), chronic ischaemic heart disease and heart failure (430), refractory angina (431), and stable angina (418). Pre-clinical studies in rat models have shown that transfusion of autologous peripheral blood derived EPCs can improve neurological functional outcome in stroke.(432) In diabetes, mobilisation of EPCs with negative-pressure wound therapy have shown efficacy in patients with foot infections or skin wounds (419), and a feasibility study using autologous G-CSF-mobilised peripheral blood CD34+ for non healing diabetic foot ulcers shows promising results in 5 patients (433). The long-term efficacy of EPC therapy has yet to be demonstrated in randomised controlled clinical trials.

5.1.2. The identity of the EPC

The identity of the EPC remains unknown. During embryonic development, it is thought that the both endothelial and haematopoietic cells arise from a common progenitor- the haemangioblast.(116, 434) In 1997, Asahara et al were the first to demonstrate the existence of circulating bone marrow derived cells that were able to form primitive vascular structures in culture. These cells displayed cell surface markers of early progenitor cells such as CD34 (59, 435), CD133 (69), and formed colonies of cells, which resembled endothelial cells; expressing CD31, CD309, and eNOS. These colonies were described by Hill et al (436), whom cultured circulating EPCs by pre-plating peripheral blood mononuclear cells (PBMCs) to first remove circulating mature endothelial cells. The resultant colonies; called "CFU-Hill" colonies, were found to be reduced in those at greater risk of cardiovascular disease. However, it has since been shown that these CFU-Hill colonies are made up of not just EPCs but a mixed phenotype of cells, including monocyte and lymphocytes.(437-439) Many studies have also observed a large heterogeneity in cultured EPCs.(76, 440, 441) Two main phenotypes arose from short-term (less than 7 days), and long-term culture (more than 3 weeks) and were called early- and late-outgrowth EPCs respectively.(70, 442, 443)

The nomenclature surrounding these cells is confused; the early-outgrowth EPCs are more commonly known as circulating angiogenic cells (CACs) and late-outgrowth EPCs termed endothelial colony forming cells (ECFCs). Both cultured EPCs subtypes differed in their proliferative and secretory behaviour, and their ability to integrate into existing vascular networks. CACs have low proliferative capacity but secrete growth factors in a paracrine fashion (70, 443, 444), and ECFCs are highly proliferative, producing cobblestone shaped monolayers resembling endothelial cells.(70, 76, 410). The sub-type of "cultured EPC" which most resembles the circulating EPC were thought to be CACs as they expressed surface markers of a haematopoietic lineage; CD34 and VEGFR2/KDR .(437, 445-447) Interestingly, myeloid lineage markers such as CD45 and CD14 have been found on CACs and these cells further express phagocytic ability (443, 448). Transcriptome analysis have further observed that CACs closely resemble myeloid cells showing similarity to

CD14+ monocytes.(449, 450) In contrast ECFCs expressed genes that are typically expressed by endothelial cells, such as Tie2 and eNOS.(449)

5.1.3. The relevance of Monocytes

Clinical studies utilising autologous EPCs to date, have been therefore been transfusing CACs, i.e. monocytes, with success in restoring perfusion to ischaemic tissue (74, 451), whereas direct transfusion of CD14+ monocytes do not show the same effect.(452) This suggests that a subset of CD14+ monocytes is enriched in the process of culture. The difference between an unselected population of circulating CD14+ monocytes and CACs (selected by culture) has been observed to be the upregulation of antioxidant genes such as superoxide dismutase, glutathione peroxidase, and catalase.(453) CACs have further been observed to be more resistant to hydrogen peroxide induced oxidative stress than unselected CD14+ monocytes and endothelial cells.(453) Schirmer et al observed in a patient population with coronary artery disease that the transcriptomes of monocytes and CD34+ cells differed in those that responded to treatment compared to non-responders.(454) This was most marked when the cells were stimulated with LPS with cells from non-responders showing inhibited arteriogenesis. It is therefore important to consider changes in the circulating monocyte population in conjunction with EPC status when examining their differences in health and disease.

Changes in monocyte subsets have been discussed in the **Chapter 1.3.2**. In this chapter, we further examine the co-expression of CD309+ and CD163+ in an effort to elucidate their differential expression in different diabetic eye disease phenotypes. CD309 is expressed in monocytes and have been observed to be upregulated as a response to pro-angiogenic stimuli such as tissue injury, or ischaemia in the context of myocardial infarction and heart failure.(455, 456) CD163 is a member of the scavenger receptor cysteine-rich superfamily, whose expression is restricted to the monocyte/macrophage lineage.(457, 458) CD163 expression is also upregulated in response inflammatory stimuli but only in the latter “resolution phase” of the insult. (459, 460) Monocytes that express CD163 are therefore

considered an anti-inflammatory, akin to medics in a battlefield tending to injured soldiers when the gunfire has slowed.

5.2 Aim:

In this study, therefore, we propose to characterise circulating EPCs in conjunction with CD14+ monocyte subtypes, in cohorts of patients with different phenotypes of diabetic retinopathy. The rationale for this chapter is to identify biomarkers in the peripheral circulation that may increase the understanding of the pathogenesis of diabetic eye disease and its relationship with ocular phenotypes.

5.3 Materials and Methods:

5.3.1 Patient recruitment, image analysis, and blood collection

Peripheral blood samples were collected from 20 healthy adult donors and 18 patients with diabetic eye disease. Collection of samples was approved by the institutional Health Research Ethics Authority and signed informed consent obtained from all donors. Inclusion criteria included patients with Type 2 Diabetes aged 18 years or more. Exclusion criteria included 1) coexisting retinal or optic nerve pathology (e.g. age-related macular degeneration (AMD), glaucoma), 2) media opacities precluding accurate retinal imaging (e.g. dense cataract). Patient demographics and clinical information were collected from electronic and paper records, including age, sex, body-mass index, HbA1c, history of hypertension and hypercholesterolemia, diabetic retinopathy and maculopathy severity grade, and visual acuity. Progression data regarding diabetic retinopathy and maculopathy severity grades were collected in 2011 and 2015 from electronic patient records. Retinal imaging, including fluorescein angiography and optical coherence tomography scans were analysed as previously described in **chapter 2.3.** Between 40 to 60mL of blood was obtained from each donor using glass BD Vacutainer system containing Sodium Heparin (BD Biosciences, 366480).

5.3.2 Isolation of Peripheral blood mononuclear cells (PBMCs)

PBMCs were isolated from the peripheral blood samples using Ficoll-Paque (PAA laboratories, LSM1077), a long established method for depleting red blood cells (RBC), and platelets.(461-463). Briefly, 50 mL conical tubes were used and blood samples were diluted with an equal volume phosphate-buffer saline, pH 7.4 (PBS) prior to layering over 20 mL of Ficoll-Paque. This was centrifuged at 800 X g for 30 minutes in a swinging-bucket rota without the brake applied and the top layer of plasma removed. The PBMC layer was carefully removed by pipetting and washed with PBC by centrifugation at 250 x g for 10 minutes. PBMC pellets were re-suspended in ammonium chloride potassium lysis buffer (Invitrogen) for 10 minutes

at room temperature with gentle mixing to lyse remaining red blood cells before a final wash with PBS. Cell numbers were recorded using a cell counter under a light microscope and trypan blue used to determine proportions of cell viability. PBMCs were cryopreserved in liquid nitrogen using fetal calf serum (FCS) (Invitrogen) containing 10% dimethyl suloxide (DMSO) (Thermo Fisher Scientific) and stored until analyses.

5.3.2.1 Optimisation protocols for PBMC isolation

Red cell lysis was used initially to isolate leukocytes from whole blood. Although this yielded a high number of cells and therefore reduced the volume of blood draw required for each patient, cell death with this technique alone was much higher than when combined with Ficoll separation, which yielded an average of 1 x 10^6 cells/mL of whole blood. (Figure 5.1)

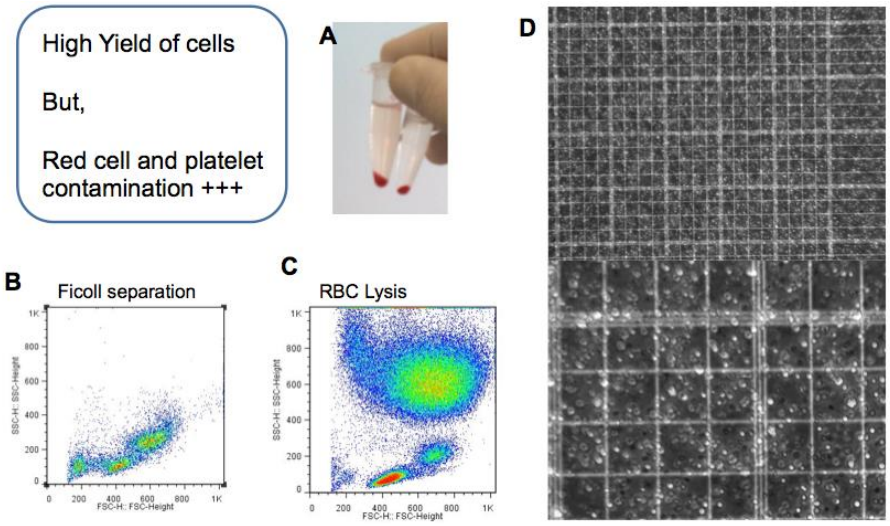

Figure 5.1. Red cell lysis to isolate leukocytes from human whole peripheral blood.

(A) Colour photograph demonstrating red cell contamination despite red cell lysis. (B,C) Forward and side scatter flow cytometry plots using Ficoll separation and red blood cell (RBC) lysis protocols showing reduced contamination in the former. (D) light microscopy after RBC lysis demonstrating red cell contamination.

5.3.3 Primary antibodies

Directly conjugated monoclonal antibodies were selected to minimise the risk of non-specific binding and to increase experimental efficiency. Surface markers were selected with the aim of defining EPC proportions and monocyte subsets of in the PBMC samples in normal and patients with diabetic eye disease.

At the time of when these experiments were conducted, the accepted definition of an EPC, albeit controversial, was CD45, CD34, CD133, and CD309.(69) These markers were therefore selected for the EPCs. Surface markers CD45, CD14, CD16 were selected to define for the monocyte population and were divided into three subtypes according to surface expression; classical monocytes (CD14++ CD16-), intermediate (CD14++ CD16+) and non-classical/inflammatory (CD16++ CD14 low). Of note percentages of these subsets have been reported as 83-85%, 4-5%, and 7-11% in healthy human PBMC samples.(464, 465)

In addition, co-expression of CD309 (a pro-angiogenic marker)(456, 466, 467) and CD163 (an "anti-inflammatory" marker) (468-470) were assessed on monocyte subsets. The inclusion of other markers was limited by the availability of suitable fluorophores for conjugation at the time of experimental design and the 4 channels possible on the FACScalibur. The PE fluorochrome, with a high quantum yield, was reserved for CD133 staining, as the CD133 antigen was known to be weakly expressed in human PBMCs.

5.3.3.1 Titration assay of primary conjugated antibodies used for flow cytometry

Titration assays were performed for all antibodies to identify the antibody amount and concentration that resulted in the highest signal of the positive population and the lowest signal of the negative population. Titration assays were performed using frozen cells derived from blood cones due to the lack of fresh blood cells available. As such, this was a high proportion of non specific binding in dead cells. Figure 5.1 is illustrative a titration assay performed on CD34-FITC, an important marker for this

thesis that was used to identify a relatively rare cell population. Enriched samples for CD34+ should have been used for titration. However, at the time of these experiments, the cost of enrichment for CD34+ was deem to high for use for antibody titration.

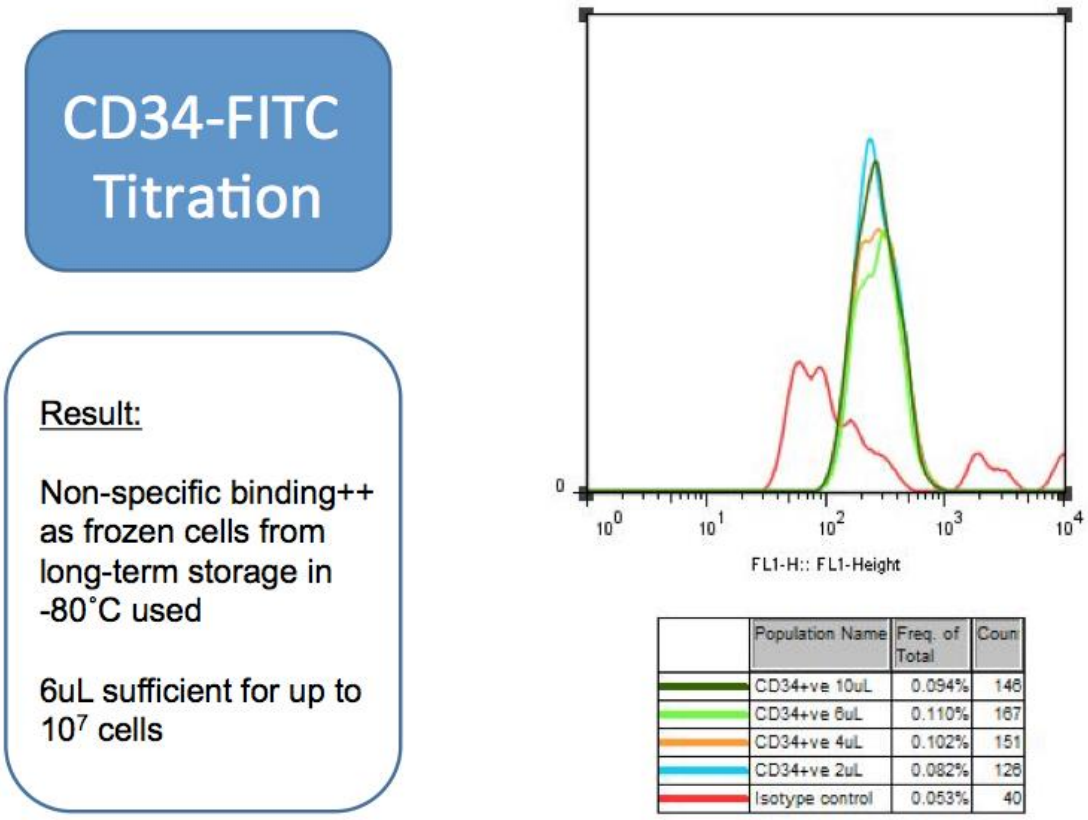

Figure 5.2. CD34-FITA titration assay

Histograms showing the fluorescence intensity for CD34-FITC antibody on frozen peripheral blood mononuclear cells with 10, 6, 4, 2, and isotype control.

Table 5.1. Primary conjugated antibodies used for flow cytometry. Unless stated otherwise, all antibodies were raised against human tissues.

Reactivity	Clone	Conjugate	Company	Volume used (μL)	Catalogue number
CD34	AC136	FITC	Miltenyi Biotec	6	130-081-001
CD34	AC136	PE	Miltenyi Biotec	4	130-081-002
CD133	AC133	PE	Miltenyi Biotec	10	130-105-225
CD309/KDR/VEGFR2	ES8-20E6)	APC	Miltenyi Biotec	10	130-093-601
CD45	5B1	PerCP	Miltenyi Biotec	6	130-094-975
CD14	TÜK4)	FITC	Miltenyi Biotec	6	130-098-063
CD14	TÜK4)	PerCP	Miltenyi Biotec	10	130-094-969
CD16	REA423	FITC	Miltenyi Biotec	10	130-106-703
CD163	GHI/61.1	PE	Miltenyi Biotec	10	130-097-628

5.3.4 Flow cytometry

PBMCs were removed from liquid nitrogen storage and thawed in a water baths. Cells were transferred into 15 mL conical tubes and incubated in RMPI-1640 medium (Invitrogen) and 10% FCS for an hour to allow recovery of the cells. PBMC counts and cell viability were assessed as above.

The flow cytometer used for all experiments was FACScalibur (BD Biosciences), which was regularly maintained and used according to manufacturer's instructions. Low flow rates were used for EPC analyses and 1,000,000 events collected for each sample. Medium flow rates for monocyte analyses with a minimum of 100 000 event collected. Compensation was performed using single-stain samples and Propidium Iodide (PI) (eBioscience, 00-6990) used as a live-dead stain. Fluorescence-minus-one (FMO) controls were used to determine gate position. Analysis was performed using FlowJo (Treestar, Ashland, OR, USA).

5.3.4.1 Optimisation protocols for CD34+ cell analysis

Positive selection for CD34+ with magnetic –activated cell sorting (MACS) (MACS CD34 MicroBead Kit, human, Mitenyi Biotech) was used to enrichment this rare cell population from PBMCs. **Figure 5.3** shows an increase in CD34+ fraction from 0.203% to 9.88% using MACS with freshly isolated PBMCs, with no cell loss observed in the MACS negative fraction and minimal contamination. With frozen PBMCs, the enrichment was less effective, with an increase from 0.155% to 2.75%. **(Figure 5.4)** Although this was a good protocol for the enumeration for CD34+ cells, it was ideally performed with freshly isolated PBMCs. In addition, an important technical constraint was the protocol from recruiting patients to sample preparation exceeded the working hours of the host institution. Therefore samples could not be process on the same day and PBMCs had to be frozen. It was for this reason that MACs was not used for the enumeration of CD34+ cells.

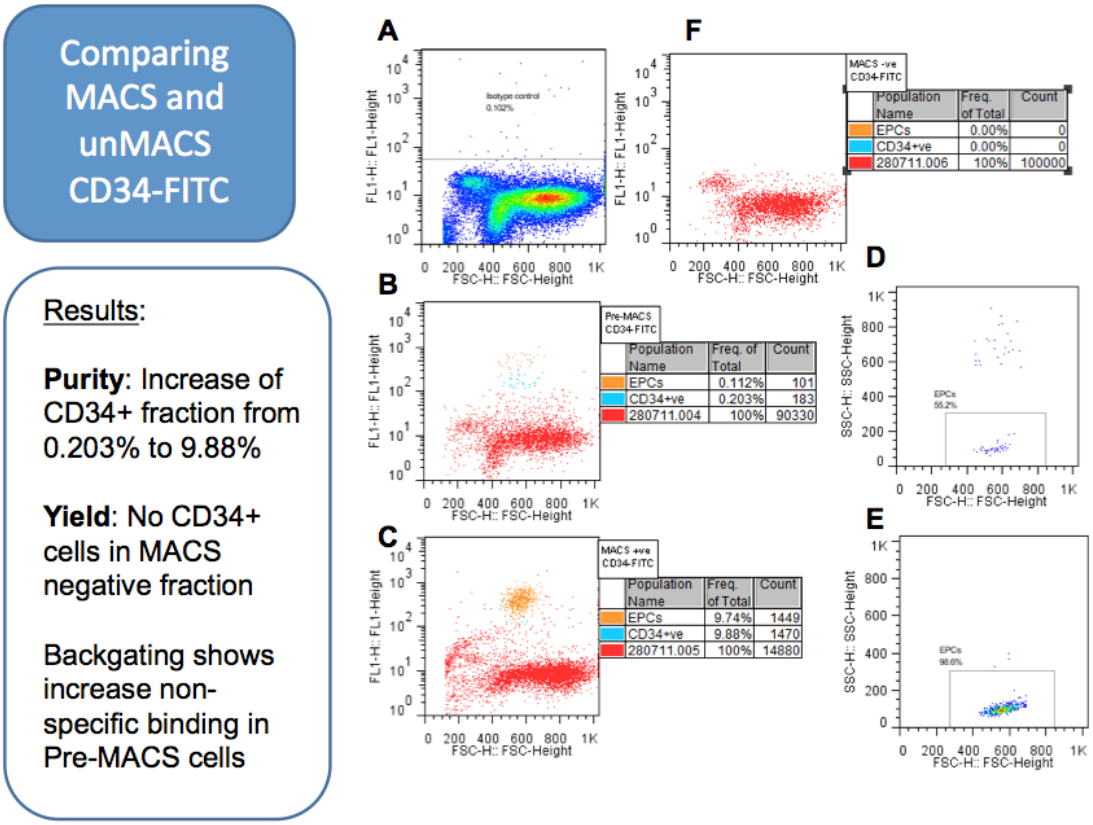

Figure 5.3. Optimisation experiment using magnetic-activated cell sorting in freshly isolated human peripheral blood mononuclear cells.

(A,F) Scatter plot of isotype control (B,C) CD34-FITC plotted again forward scatter showing CD34+ cells in light blue, and back gated endothelial progenitor cells (EPCs) from (D, E). (B, D) represent PBMC samples analysed with flow cytometry without MACS enrichment (unMACS), and (C,E) after MACS enrichment.

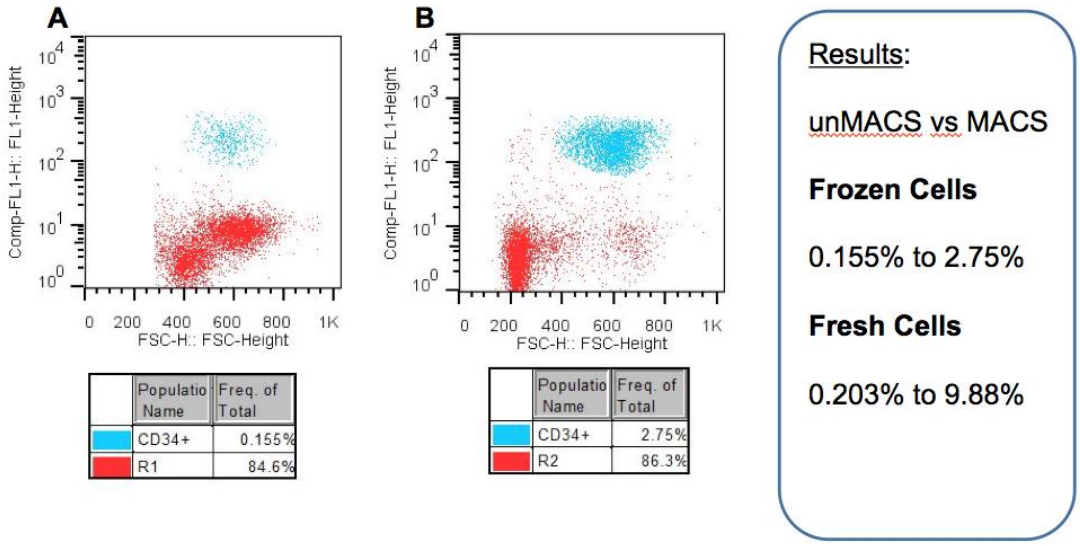

Figure 5.4. Optimisation experiment using magnetic-activated cell sorting in frozen human peripheral blood mononuclear cells.

Scatter plot of CD34-FITC plotted again forward scatter showing CD34+ cells in light blue. (A) No MACS enrichment was carried out prior to flow cytometry (unMACS) and (B) MACS enrichment was carried out prior to flow cytometric analysis of PBMCs.

5.3.4.2 Introduction of a cell culture step prior to for flow cytometric analysis of cells

Hill et al in 2003 observed that the colony forming potential of peripheral blood mononuclear cells were strongly correlated to the subjects' Framingham cardiovascular risk factor score.(436) We therefore explored the possible use of this pre-culture step prior to flow cytometric analysis of PBMCs in our patient cohort.

20mL of whole blood was collected from five healthy volunteers and cultured according to the methods described by Hill et al. Briefly, a n initial pre-plating step step in a fibronectin-coated six-well plate using 5 million PBMCs per well was performed, which the author reasoned as to remove mature circulating endothelial cells. After 48 hours, the nonadherent cells were collected and 1 million cells were replated onto fibronectin-coated 24-well plates for a final assessment of the number of colonies. Growth medium consisting of consisting of Medium 199 (GIBCO BRL Life Technologies) supplemented with 20 percent fetal-calf serum, penicillin (100 U per

milliliter), and streptomycin (100 µg per milliliter). was changed every three days, and cells analysed at seven days. Cells were dissociated using trypsin for 3 minutes at room temperature. Both adherent and nonadherent cells were analysed by flow cytometry both immediately after plating and at 7 days respectively.

Figure 5.5 shows the proportion of CD34+ cells present in the initial PBMC sample, adherent, and nonadherent cells. The pre-plating and culture step failed to enrich the PBMC sample for CD34+ cells. Interestingly, monocytes were greatly enriched by this culture step, with an expansion of the intermediate and non-classical populations. **(Figure 5.6)** The shift in monocyte characteristics and volume of whole blood required for this experiment made this culture step unsuitable for this project, which sort to analyse EPC as well as Monocyte phenotypes in diabetic eye disease.

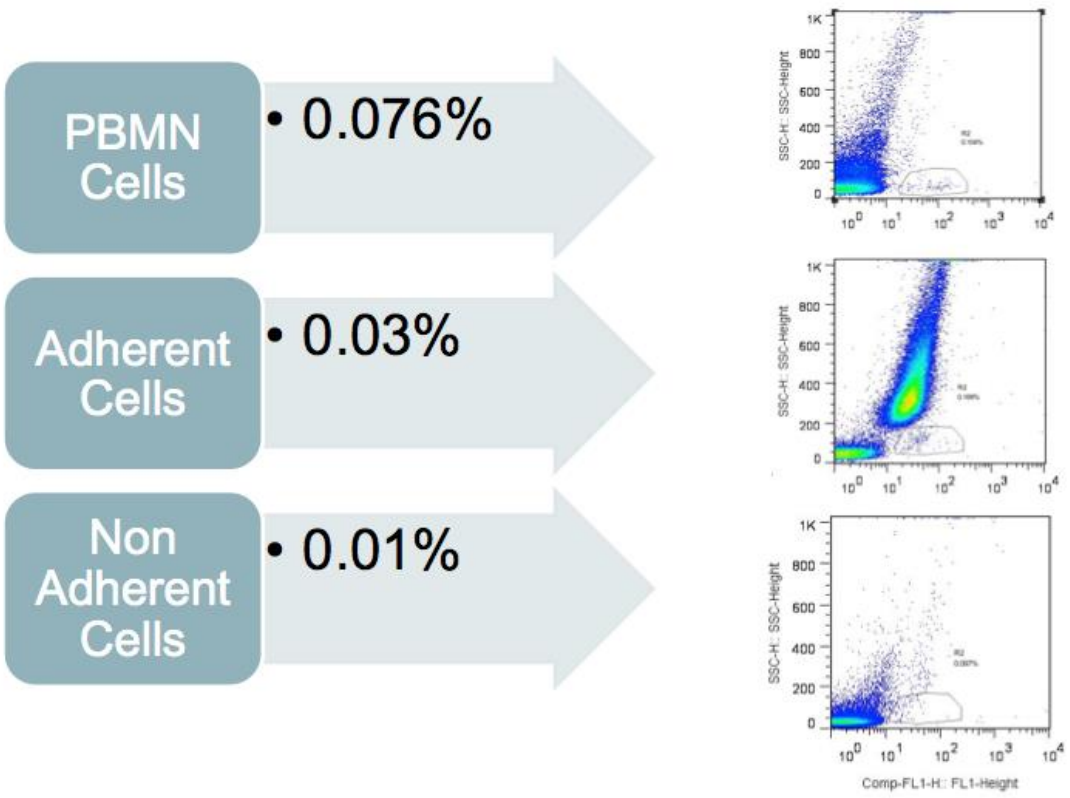

Figure 5.5. Optimisation experiment: flow cytometric analysis CD34+ cells from peripheral blood mononuclear cells (PBMCs) cultured for seven days.
The left panel shows CD34+ cells expressed as a percentage of PBMCs 7 days after culture. The right panel are representative scatter plots showing CD34+ cells plotted against side scatter.

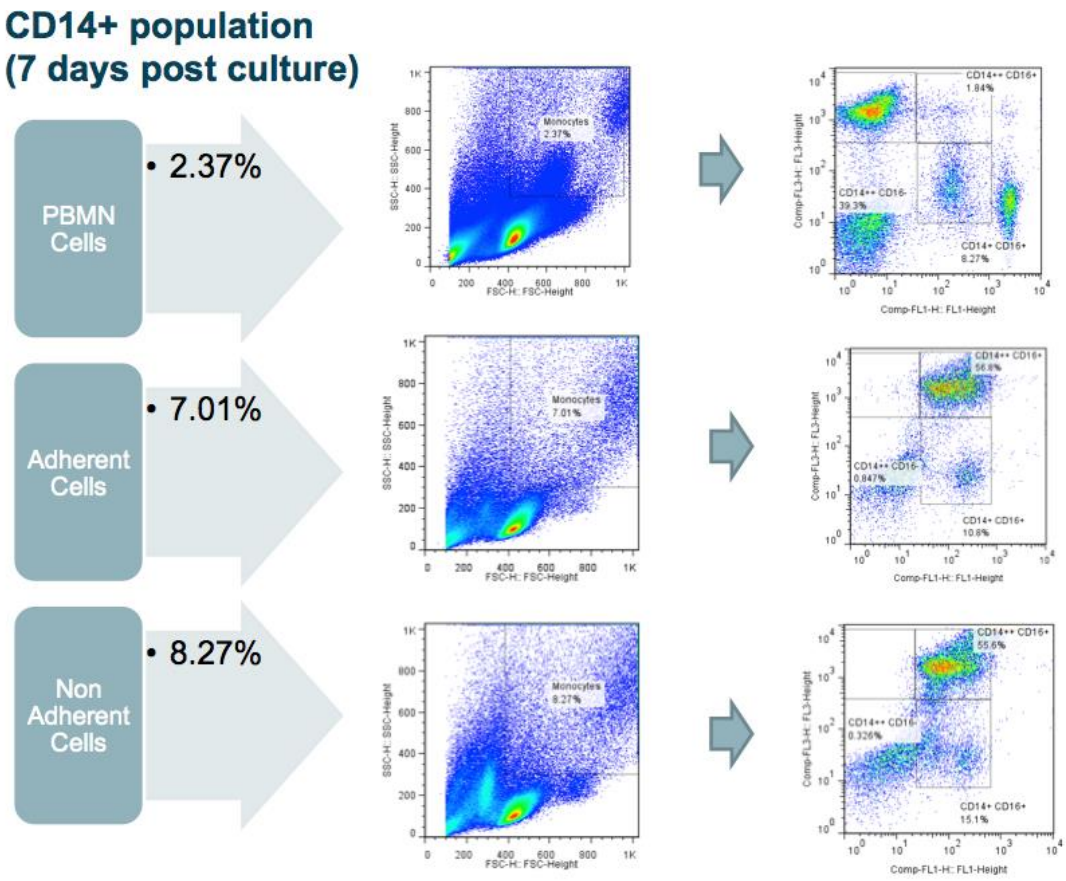

Figure 5.6. Optimisation experiment: flow cytometric analysis CD14+ cells from peripheral blood monocyte cells cultured for seven days.

The left panel shows CD14+ cells expressed as a percentage of PBMCs. The middle panel are representative scatter plots showing a monocyte gate place on a forward and side scatter plot. The right panel shows scatter plots with CD14-PerCP on the Y-axis and CD16-FITC on the X-axis, and relative proportions of classical monocytes (CD14+ CD16-), intermediate monocytes (CD14+ CD16+), and non classical monocytes (CD14+ CD16++).

5.3.5 Statistical Analysis

Patient demographic and imaging data were analysed with frequency and descriptive statistics. Normality of the variables was examined using histograms. The Mann-Whitney U test was used to compare continuous variables, whereas the χ^2 test was used for categorical variables. Spearman's rank correlation was used to test for associations between variables. Snellen visual acuities were converted to LogMAR (logarithm of the minimum angle of resolution) visual acuity for the purposes of statistical analysis. Statistical analyses were performed using statistical software SPSS software version 16 (SPSS, Inc, Chicago, IL).

5.4 Results:

5.4.1 Patient Demographic and Clinical Characteristics

The mean age of patient included was 50 years (SD=13.3) with a male to female ratio of 1.5. The mean body mass index was 29 (SD=8.8), mean diabetes duration was 20 years (SD=9.1), and mean HbA1c 7.6 (SD=1.59). 15/20 patients (75%) had a history of treated hypertension and 15/20 treated hypercholestrolaemia.

Regarding diabetic retinopathy and maculopathy severity grades (assessed during clinical examination), the eye with greater severity was included. 6 patients had mild non-proliferative diabetic retinopathy, 7 moderate to severe non-proliferative diabetic retinopathy, and 7 treated proliferative diabetic retinopathy in the more severely affected eye. 6 patients had no evidence of diabetic maculopathy in either eye, and 14 clinical evidence of diabetic maculopathy in one or more eyes. There was a wide range of visual acuity measurements in all patients, with a mean of 0.41 logMar (or 6/15 Snellen equivalent) (SD=0.49). 10 patients had fluorescein angiograms at the time of this study, and of these, 3 patients had none to mild, 2 moderate, and 5 severe diabetic macular ischaemia. All patients had OCT scans, and these were used to assess for the presence of diabetic macular oedema (7/20 patients [35%]).

5.4.2 EPCs and monocytes in diabetes and in healthy controls

5.4.2.1. EPCs

FMOs were used along with a published gating strategy in order to ascertain the percentage of CD34+ cells and their subsets.(471) These were compared between patients with type 2 diabetes and healthy controls. No difference was observed between groups with mean of 0.34% of live cells (SD=0.32) in control compared to 0.28% of live cells (SD=0.16) in diabetes. (**Table 5.1, Figure 5.7**) However, when subsets of CD34+ cells were analysed, a significant difference was observed in the

CD34+ CD309+ subset between those with controls (2.14% of CD34+ cells [SD=2.00]) compared to diabetes (5.77% of CD34+ cells [SD=2.15]). (**Table 5.1**) No difference was observed in CD34+ subsets with CD133+ surface marker. (**Figure 5.1**)

Table 5.2. Comparing the proportions of EPCs in patients with type 2 diabetes and normal controls

EPC (CD34+) analysis		Control		Diabetic		
		Mean	SD	Mean	SD	p-value
	%					
CD34+	Live cells	0.34	0.32	0.28	0.16	0.87
CD34+ CD133+	CD34+	32.71	22.41	24.25	17.37	0.41
CD34+ CD 309+	CD34+	2.14	2.00	5.77	2.15	0.001**
CD34+ CD309+ CD133+	CD34+	2.47	1.86	1.69	2.02	0.15
p values significant at 5% level are indicated with (*), and (**) at 1% level.						

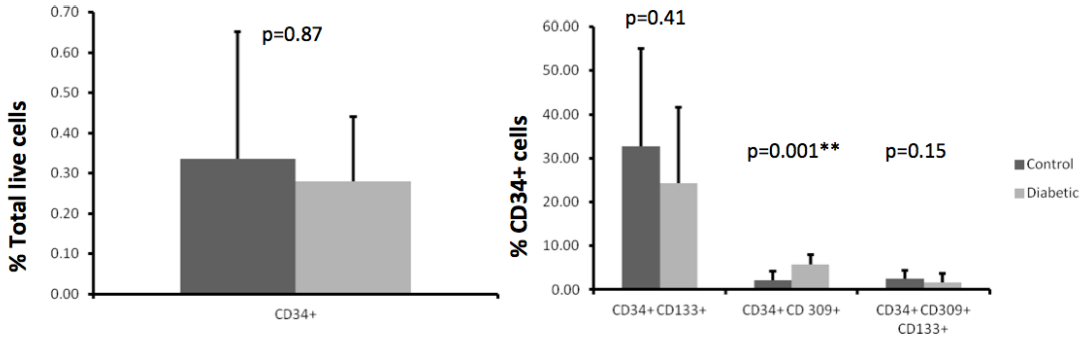

Figure 5.7. Comparing the proportions of EPCs in patients with type 2 diabetes and normal controls

Table 5.3. Comparing circulating monocytes and their subsets in patients with type 2 diabetes and normal controls

		Control		Diabetic		
		Mean	SD	Mean	SD	p-value
Monocyte analysis	%					
All Monocytes CD45+ CD14++	Live cells	13.63	3.46	18.19	8.06	0.15
Classical Monocyte (M2)						
CD14++ CD16-	Live cells	71.47	8.38	63.00	12.59	0.12
CD14++ CD16- CD309+	M2	20.32	21.35	1.98	1.17	0.001**
CD14++ CD16- CD163+	M2	29.75	27.13	50.18	10.23	0.14
CD14++ CD16- CD309+ CD163+	M2	37.74	17.73	37.01	11.46	0.49
Intermediate Monocyte (iM)						
CD14+ CD16+	Live cells	4.75	0.69	6.75	3.85	0.58
CD14+ CD16+ CD309+	iM	29.34	29.68	0.57	0.68	0.03*
CD14+ CD16+ CD163+	iM	42.60	44.94	77.61	13.61	0.38
CD14+ CD16+ CD309+ CD163+	iM	16.54	10.62	15.76	13.87	0.72
Non-Classical Monocyte (M1)						
CD16+ CD14 low	Live cells	7.71	3.38	10.71	5.18	0.31
CD16+ CD14 low CD163+	M1	1.65	1.67	0.16	0.26	0.28
CD16+ CD14 low CD309+	M1	31.99	19.64	43.66	15.43	0.15
CD16+ CD14 low CD309+ CD163+	M1	1.16	1.13	3.09	11.82	0.06

p values significant at 5% level are indicated with (*), and (**) at 1% level.

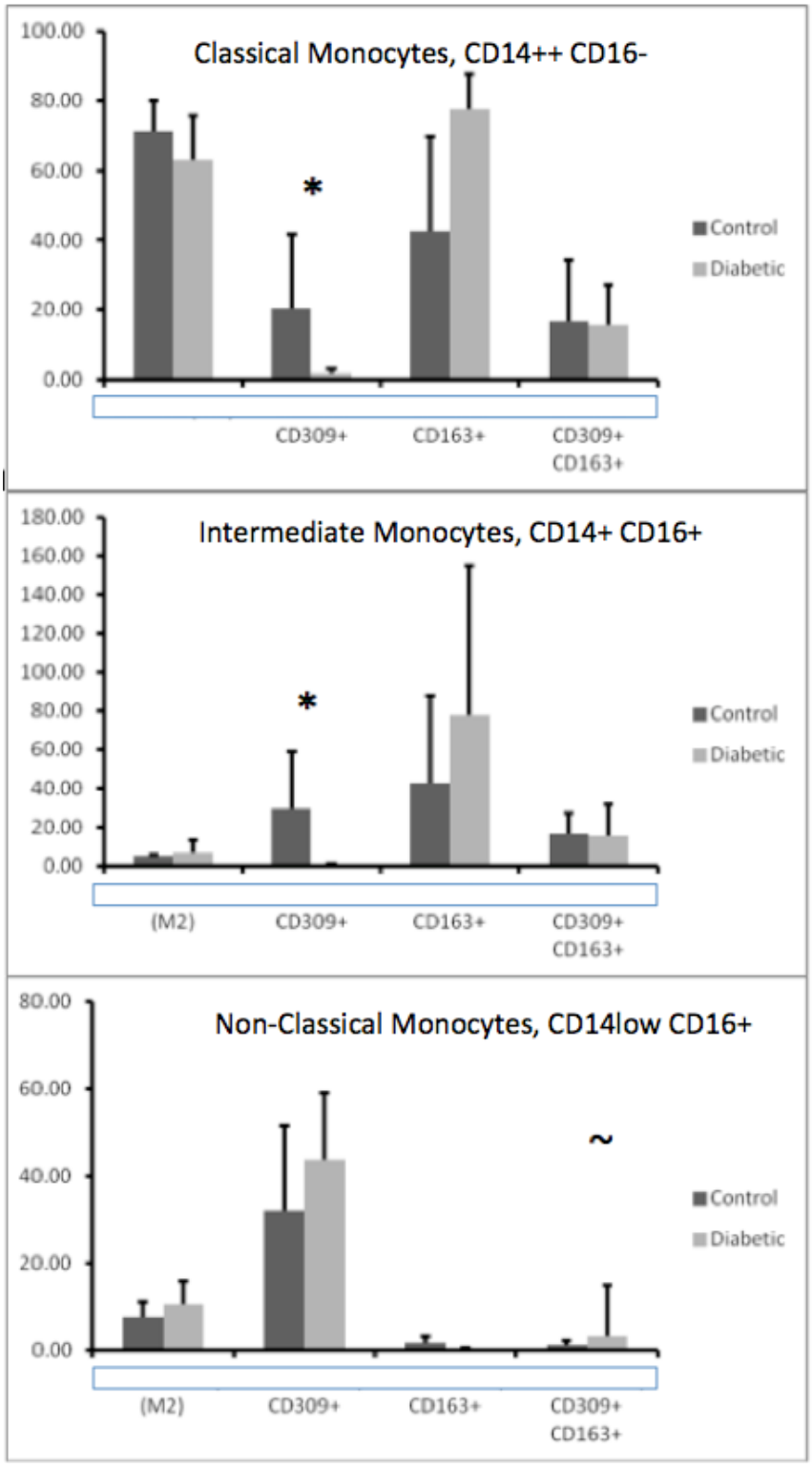

Figure 5.8. Comparing the proportions of monocyte subsets in patients with type 2 diabetes and normal controls.

* denotes a p-value of <0.05, and ~ denotes a p-value=0.06

5.4.2.2. Monocyte Subtypes

Published gating strategies were used to identify the proportion of circulating monocytes and their subsets in PBMCs from patients with type 2 diabetes and controls.(472) In this study, the "rectangular" gating strategy was used. Monocytes were defined by cell surface markers CD45 and CD14 and subsets further categorised using CD16. (**Table 5.3**) No statistically significant difference was observed in all monocytes, or their subsets as described above in diabetes compared to controls. (**Table 5.3**) However, the trends observed in the proportion of these subsets in diabetes (compared to controls) were (1) reduced classical monocytes (63.0% vs 71.5%) (p=0.12), (2) increased intermediate monocytes (6.8% vs 4.8%) (p=0.58), (3) increased non-classical monocytes (10.7% vs 7.7%) (p=0.31). (**Figure 5.8**) Interestingly, the total proportion of monocytes in the live cell population was greater in diabetes (18.2%) compared to controls (13.6%) however, this was not statistically significant (p=0.15). (**Table 5.3**) Co-expression of CD309 on all three subsets were further analysed and a statistically significant reduced expression was observed in diabetes compared to controls; classical monocyte population; controls (mean=20.3% of M2 cells [SD=21.4]) and diabetes (mean=1.98% of M2 cells [SD=1.17]) (p=0.001), and intermediate monocyte population; controls (mean=29.3% of iM cells [SD=29.7]) and diabetes (mean=0.57% of iM cells [SD=0.68]) (p=0.03). (**Table 5.3, Figure 5.8**)

Co-expression of CD163 on all three subsets was also analysed. No significant difference in expression was observed all monocyte subsets. A trend of increased expression was observed in classical monocyte population in patients with diabetes (mean=50.2% of M2 cells [SD=10.2]) compared to controls (mean=29.8% of M2 cells [SD=27.1]), (p=0.14). (**Table 5.3, Figure 5.8**)

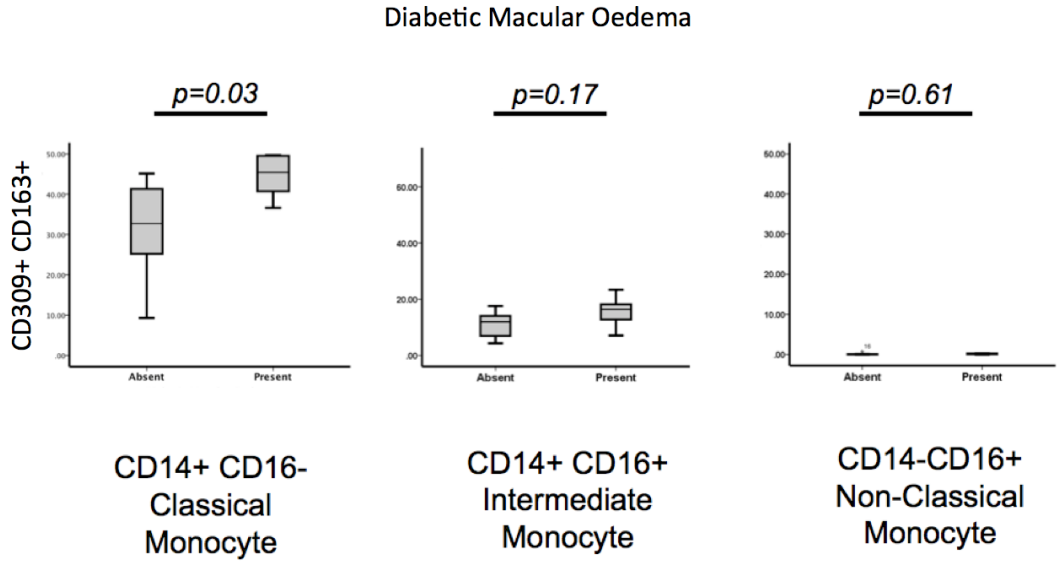

Figure 5.9. Comparing the co-expression of CD309 and CD163 on monocyte subsets in patients with and without diabetic macular oedema.

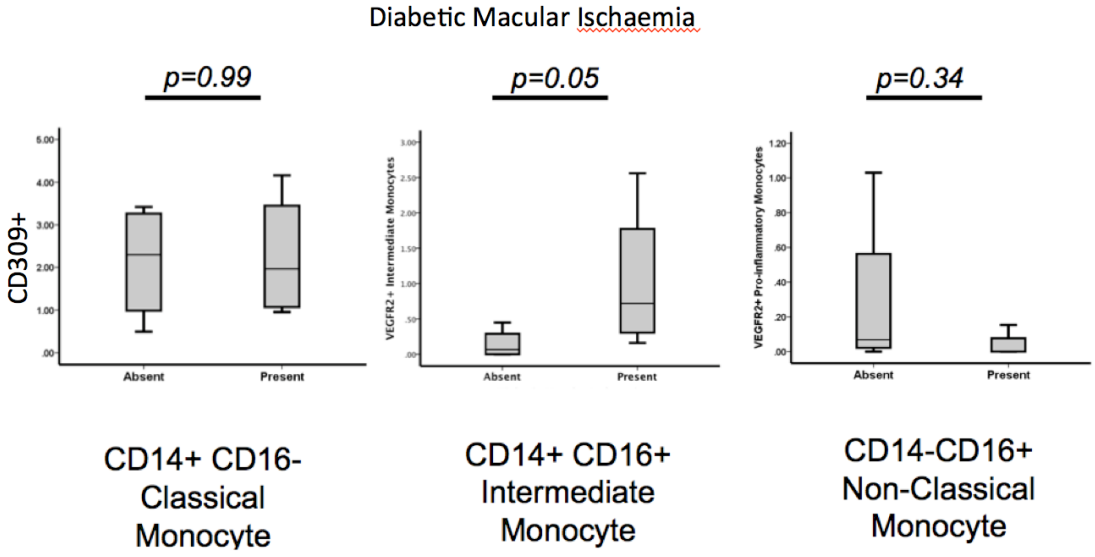

Figure 5.10. Comparing the co-expression of CD309 on monocyte subsets in patients with and without diabetic macular ischaemia.

5.4.3 The effects of diabetic macular disease

No difference was observed in EPCs or their subpopulations in either phenotype of diabetic macular disease or retinopathy severity levels.

Monocyte subsets and co-expression of CD309 and CD163 were assessed in patients with diabetic macular oedema (DMO) and diabetic macular ischaemia (DMI). In DMO, a significant increase was observed in classical monocytes which co-expressed both CD309 and CD163 in patients (mean=43.0% of M2 cells [SD=9.0]) compared to controls (mean=32.4% of M2 cells [SD=11.4]), (p=0.03). (**Figure 5.9**)

In DMI, a significant increase was observed in intermediate monocytes, which co-expressed CD309 in patients (mean=1.04% of iM cells [SD=1.07]) compared to controls (mean=0.15% of iM cells [SD=0.21]), (p=0.05). (**Figure 5.10**)

5.4.3 The effects of age and body mass index (BMI)

No relationships were observed between EPCs or their subpopulations with age or body mass index or retinopathy severity levels. In addition, no relationship was observed between both age and BMI with monocytes subsets in different retinopathy severity levels.

Monocyte subsets and co-expression of CD309 and CD163 were assessed in patients 60 years and older and those with a BMI of greater than 30. In patients 60 years and older, a significant increase was observed in classical monocytes which co-expressed both CD309 and CD163 (mean=41.9% of M2 cells [SD=8.8]) compared to those younger than 60 years (mean=30.2% of M2 cells [SD=11.8]), (p=0.04). (**Figure 5.11**) In addition, there was a positive correlation with age and classical monocytes that expressed both CD309 and CD163. (r=0.56, p=0.03).

In patients whose BMI was greater than 30, a significant increase was observed in non-classical monocytes, which co-expressed CD309 in patients (mean=31.7% of M1 cells [SD=5.08]) compared to those with a BMI less than 30 (mean=51.9% of M1 cells [SD=8.6]), (p=0.036). (**Figure 5.11**)

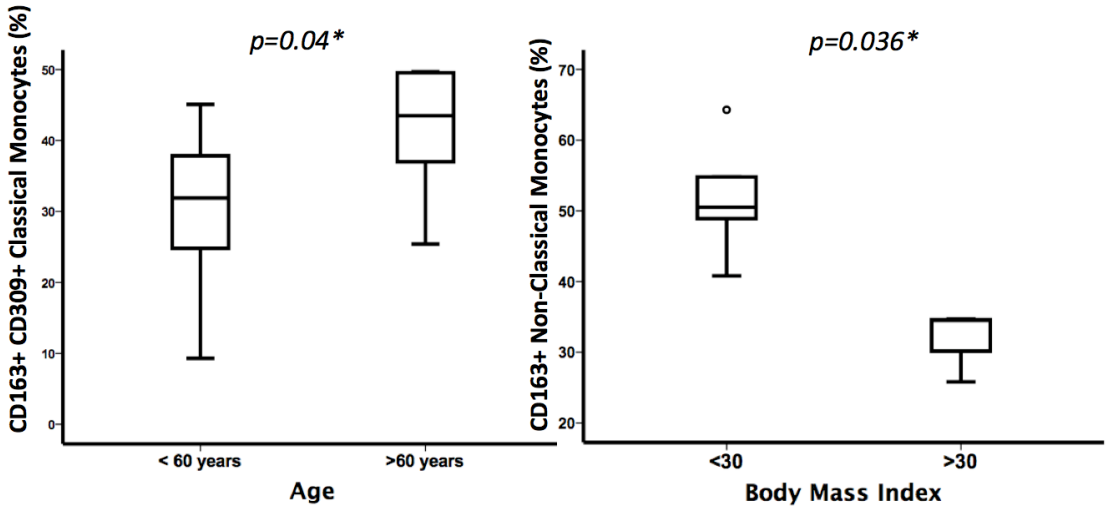

Figure 5.11. The effect of age and body mass index on classical monocytes.

Comparing the co-expression of CD309 +/- CD163 on monocyte subsets in patients aged greater or less than 60 (left), and with a BMI of greater or less than 30 (right).

5.4.4 Biomarkers for progression of diabetic eye disease

In the 4-year intervening period, one patient died in 2014. 9/17 (52.9%) patients showed progression over the 4 year intervening period of either retinopathy or maculopathy severity; 9/17 (52.9%) retinopathy only, and 8/17 (47.1%) maculopathy only. Patients had progression in either phenotype had a significantly smaller proportion of classical monocytes (mean=58.4% of all monocytes [SD=9.96]) vs stable (mean=73.3% of all monocytes [SD=8.35]), (p=0.02); a larger proportion of intermediate monocytes (mean=8.25% of all monocytes [SD=3.98]) vs stable (mean=4.95% of all monocytes [SD=3.11]), (p=0.05) and a larger proportion of non-classical monocytes (mean=13.0% of all monocytes [SD=5.38]) vs (mean=6.83% of all monocytes [SD=2.31]), (p=0.04). (**Figure 5.12**) Binary multivariable logistic regression was performed, and the changes observed in classical and non-classical monocytes remain significant, independent of age.

No significant differences were observed with maculopathy progression alone. However, in retinopathy progression alone, the proportion of non-classical monocytes was double that of those who were stable. (mean=14.3% of all monocytes

[SD=5.33]) compared to those who were stable (mean=7.25% of all monocytes [SD=2.39]), (p=0.02).

There were no differences in the EPC profiles between patients who had stable or progressive diabetic eye disease in all groups.

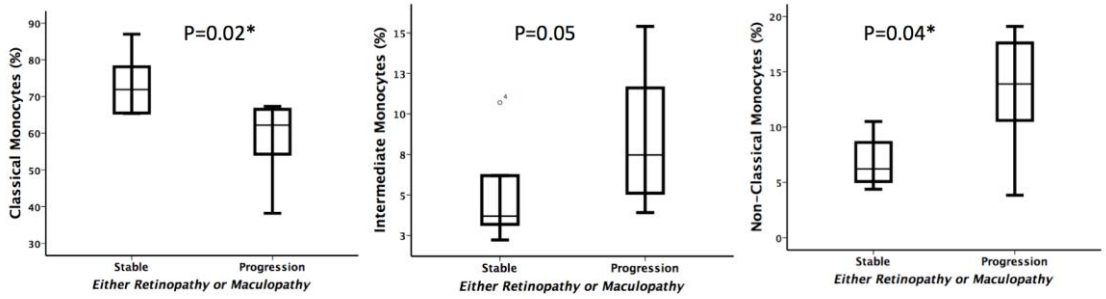

Figure 5.12. Monocyte subsets and diabetic eye disease progression.

Comparing monocyte profiles in patients who had progression in either diabetic retinopathy or maculopathy to those that remained stable over a 4 year period. Classical monocytes (Left); Intermediate monocytes (Middle); Non-classical monocytes (Right).

5.5 Discussion:

In this chapter, we examined the relationships between EPCs, monocytes and their respective subpopulations, with clinical phenotypes of diabetic eye disease and clinical demographics such as age, BMI, and glycaemic control. No difference was observed with both cells type in diabetic retinopathy severity levels but in different phenotypes of macular disease. Additionally, age and BMI were the only parameters in which a significant difference was observed in monocyte populations.

5.5.1 EPCs in diabetic eye disease

The concept of EPC therapy for repairing blood vessels in the adult has continuously received attention since its discovery by Asahara et al. (59) Previous studies have observed reduced numbers and decreased function of circulating EPCs in diabetes. (62-64) In our cohort, we observed no difference between CD34+ or CD34+ CD133+ cells between patients with type 2 diabetes and healthy controls. However, we did observe more than double in the proportion of CD34+ CD309+ cells in diabetes.

In 2005, Fadini et al found in 24 patients with type 2 diabetes, a significant reduction in circulating CD34+ cells (33%) as well as CD34+ CD309+ cells (40%). A possible explanation for this difference may lie in dissimilarity between the cohorts of patients examined. There were a sizable number of patients (8/24 [33%]) in that cohort with peripheral vascular disease compared to none in our study. Loomans et al in 2004 similarly observed a 44% reduction in cells in 20 patients with type 1 diabetes. However, this study was not comparable as “EPCs” were quantified after PBMCs from 60 mL of whole blood were cultured for 4 days, and mature endothelial cells markers CD31, DiI-labeled acLDL, and UEA-1 were used. It is now well known that cell culture conditions create an artificial phenotype in EPCs, and it is not even known whether this culture phenotype correlates with any cells actually existing in the bloodstream.(473) Tepper et al, examined 20 patients with type 2 diabetes (63) and also observed a 48% reduction of “EPCs” that were defined by CD34+ surface marker. Here, mature endothelial cell markers such as vascular endothelial (VE)-

Cadherin, CD31 (474) were used again. It is likely these cells represented circulating endothelial cells (CECs) rather than EPCs.

Recent evidence from polychromatic flow cytometry with rigorous gating protocols have observed that CD34+ CD309+ cells were not detectable in peripheral blood samples from healthy volunteers.(475) This comes against much of the published literature to date, which though controversial, established a widely accepted the EPC marker combination; (CD34+CD133+CD309+) in the bone marrow. These cells also expressed CD31 at bright levels, suggesting that they were at an early stage of endothelial differentiation. To add to the controversy, there have also been inconsistent reports of CD133 as an identifier for EPCs that are able to differentiate both in vitro and in vivo along the endothelial lineage.(409, 410, 476) The identity of the EPC remains controversial, even after a decade of examination. It is noteworthy that these observations were made on healthy volunteers. The diversity of EPCs numbers and phenotype observed in the literature may simply reflect different disease states. Elevation levels of EPCs, as defined by CD34+ CD309+, have been reported in head and neck cancer, hepatocellular carcinoma, haemangioma, and small cell lung cancer; suggesting their involvement in tumour vasculogenesis and tumour growth.(477-480) We similarly observed increased levels of CD34+ CD309+ cells in diabetes compared to controls. This may reflect the possible pro-angiogenic, pro-inflammatory role played by these cells in the development of diabetic eye disease, be it impaired vasculogenesis (retinal ischaemia) or neovascularisation (proliferative diabetic retinopathy.(477) Our results however, did not identify any difference in EPC profiles between different clinical phenotypes of diabetic eye disease, nor served as a biomarker for predicting the progression of disease severity.

A potential confounder in this study was the use of statins in 75% of our patients. A recent systematic review of both preclinical and clinical studies has shown that statins improve the number and function of both mesenchymal stromal cells and EPCs in cell-based regenerative therapy.(481) Of relevance to this thesis, the 13 preclinical studies reviewed that involved the administration of stains alone to animals, an increase in the number and function of EPCs and improved organ

function was observed in 85% and 92% respectively. In the 7 clinical studies that used statins alone (without cell therapy), all similarly described an increase in EPC numbers and function and improved organ function. The concurrent use of statins in patients recruited to this study may therefore mask differences between disease and normal in our cohort.

5.5.2 Monocytes in diabetic eye disease

In this chapter, we observed no difference in monocytes proportions or their subsets in diabetes compared to controls. This is consistent with a study which examined a larger cohort of patients with type 2 diabetes (n=53) (111), but converse to another study in Type 1 diabetes that observed elevated levels of non-classical and intermediate monocytes.(110) This may reflect the pathophysiological differences between type 1 and type 2 diabetes and the role of the autoimmune response in former. CD16+ subsets of monocytes have been observed to be elevated in other autoimmune diseases, and thought to be involved in the induction of an inflammatory autoimmune response.(104, 482, 483) Of note, in type 1 diabetes, CD16+ monocytes (both non-classical and intermediate) were further associated with an increased risk of developing diabetic retinopathy. (110)

We found significantly decreased CD309+ expression on classical (**Figure 5.8** top) and intermediate monocytes (**Figure 5.8** middle), and a trend toward increased CD309+ expression in non-classical monocytes (**Figure 5.8** bottom) in diabetes compared to controls. We propose that this reflects the reduced angiogenic capacity and pro-inflammatory state of patients with type2 diabetes. Under physiological conditions, CD309+ (also known as VEGFR2) expression is mostly limited to endothelial cells. It acts by binding (with greatest affinity) to VEGF-A to transduce a signal for angiogenesis via a tyrosine kinases pathway.(484) However, many reports have indicated that bone marrow derived “EPCs” are mostly of myeloid origin.(485) Moreover, in the peripheral circulation, CD309 expression has been mainly observed in monocytes, not CECs or EPCs (475), and is upregulated after tissue injury.(455) Also, it is these CD309+ monocytes that have been observed to contribute to re-

endothelialisation of balloon-injured femoral arteries in mice.(486). Monocytes have angiogenic properties and participate in both physiological and pathological angiogenesis (485), either by orchestrating the process through it secretory activity or directly incorporating into blood vessels.(74, 487-489) Circulating monocytes have further been reported to express the mature endothelial marker CD31 in tumour angiogenesis.(490) Therefore, in this study, it is possible that reduced expression of CD309 observed in the classical and intermediate monocytes of patients with type 2 diabetes, reflect the impaired reparative process in the microvasculature of the retina.

This theory is supported by our findings that in DMI (retinal capillary loss) we observed a significant increase in intermediate monocytes that co-expressed CD309. (**Figure 5.10**) This may be a dynamic alteration of the monocytic phenotype in response to tissue injury in the retina (up regulation of pro-angiogenic monocytes), or it may reflect an impaired physiological homeostatic repair of the retinal microvasculature resulting in retinal capillary loss. It has been suggested that intermediate monocytes may represent a journey of transition from classical to non-classical monocytes (103), and increased in different disease states. (104-106) It is therefore more likely that the increase in pro-angiogenic intermediate monocytes observed in this study, is a response rather than the cause of macular ischaemia.

Interestingly, in DMO (leaking retinal capillaries), we observed a significant increase in classical monocytes which co-expressed both CD309 and CD163. (**Figure 5.9**) Classical monocytes are known to direct pro-inflammatory responses to injury. CD163 is a member of the scavenger receptor cysteine-rich superfamily, whose expression is restricted to the monocyte/macrophage lineage.(457, 458) CD163+ monocytes have been observed to develop in the “healing phase” of an acute inflammatory reaction (459, 460), and shown to produce both anti-inflammatory and angiogenic factors (491, 492). In addition, IL-6 and IL-10 (anti-inflammatory cytokines) and dexamethasone have been shown to induce CD163 mRNA expression in monocytes.(470) CD163 expression has therefore been associated with an anti-inflammatory response. The differential expression CD163+ monocytes may be one

of the explanations as to why different phenotypes of diabetic eye disease occur. In DMO, it may be a response to chronic low-grade inflammation caused by the gradual accumulation of fluid in the intra-retinal and sub-retinal spaces of the macula. Furthermore, CD163+ cells have been observed in significant numbers in both dry and neovascular age-related macular degeneration (AMD).(493) In dry AMD, CD163+ cells were restricted to the inner retina, whereas in neovascular AMD (where neovascularisation from the choroid is present and leakage of fluid occurs into the retina), CD163+ cells were markedly increased in all layers of the retina. This suggests that CD163+ cells are recruited from the peripheral circulation into the retina and confirms the association between pathological fluid accumulation in the retina and these cells. These support the hypothesis that CD163+ cells play a role in the pathophysiology of DMO.

We observed that older patients (>60 years) also had a significantly higher co-expression of both CD309 and CD163 classical monocytes. Although frequency of total monocyte counts in PBMC has been observed to increase with age (494), the relationship of CD163+ monocytes with age has not been previously described in diabetes. This difference may also reflect the chronicity of disease in the older patients. In the United Kingdom, obesity is defined by a BMI of greater than 30. In these patients, we observed a significant increase in non-classical monocytes, which co-expressed CD309. Increased proportions of the “pro-inflammatory” non-classical monocytes have been observed in previous studies, though the expression of CD309 in these cells have not been previously described. The increased expression of CD309 in obese patients may contribute to their severity levels of diabetic eye disease. This study was not powered to assess this question, but large population-based studies have observed an association between BMI and the presence and severity of diabetic eye disease.(495-497)

Perhaps our most clinically relevant results were the differences observed in monocyte subsets when we compared patients who progressed in diabetic eye disease severity with those who remained stable over a period of 4 years. (**Figure 5.12**) The proportion of classical monocytes was depressed and non-classical

elevated in those who progressed in diabetic eye disease severity independent of age. Differences in the relative proportions of monocytes subsets have been reported in a myriad of other chronic conditions such as coronary artery disease, liver cirrhosis, and obesity.(498-500) If validated in a larger cohort of patients, relative proportions of monocytes subsets may be used as a biomarker for diabetic eye disease.

5.6 Chapter summary:

In this chapter, EPC and monocyte profiles were examined in patients with type 2 diabetes and compared to controls. Associations between these, and clinical demographic information and diabetic eye disease phenotype were compared. Although no difference between EPC and monocyte subsets was detected between groups, a greater proportion of EPCs that co-expressed the pro-angiogenic marker CD309+ was observed in diabetes compared to controls. Conversely, in monocytes (classical and intermediate), the proportion of cells expressing CD309+ was reduced in diabetes compared to controls. CD309+ expression was raised however, in patients with macular ischaemia (on intermediate monocytes), and those who were greater than 60 years of age (on classical monocytes). In DMO, elevated co-expression of CD309+ and the anti-inflammatory CD163+ surface marker was observed on classical monocytes, similar to those with a BMI greater than 30 (M1). Finally, a low proportion of classical monocytes and a high non-classical monocytes were both associated with progression of diabetic eye disease, independent of age.

6. Final discussion and Outlook

6.1. Final Discussion:

The aim of this work was to better understand diabetic macular ischaemia (DMI); identify novel methods of quantifying this disease entity and explore its relationship to circulating of cellular mediators of angiogenesis and inflammation, with the view to developing therapy in the longer term. The reasons behind this goal were the paucity of literature in the area, largely due to the lack of treatment for this condition, and the devastating effects observed in some patients in clinical practice. Not only were retinal specialists unable to offer treatment, there was no knowledge of prognosis for these often working-age patients. At the time of conception of this thesis, there were promising early results from clinical trials using EPCs for the treatment of ischaemic conditions. There was also evidence to show EPC dysfunction in diabetes, arguing against the feasibility of autologous cell therapy, and indications that inflammation played a vital role in impairment angiogenesis observed in diabetic microvascular disease. For these reasons, novel methods of retinal imaging analyses were performed on data collected from human and animal models of vascular and inflammatory disease. Circulating EPCs and monocytes were further examined for associations with severity and progression of diabetic eye disease.

In the second chapter, data regarding the visual impact of diabetic ischaemia was presented. Visual loss was observed to occur only in moderate to severe disease, and preserved in questionable and mild ischaemia. (**Table 2.4**) Capillary non perfusion of the nerve fibre layer of the papillomacular bundle was also found to be a strong independent risk factor for visual loss. The natural history of the disease was further described; with the foveal avascular zone expansion rate of 5-10% increase in area per year. (**Figure 2.10**) This data allows identification of a window of opportunity for therapy; ideally before visual acuity is affected, but where disease can be detected. The limitations of this study were inherent to its retrospective design. Data collection was dependent on the frequency with which patients had fluorescein angiography - the main retinal imaging modality used to assess diabetic macular

ischaemia. This procedure requires an intravenous injection of a fluorescein dye, and takes approximately 20-30 minutes to complete. It further carries a small risk of anaphylaxis thus precluding its frequent use in patients. Since the commencement of this work, the first commercially available OCT angiography device, since its first description in 1991(26), has become available (in the latter half of 2014). OCT angiography allows for a rapid (~6 seconds), non-invasive (dye injection not required) means to visualise not only the superficial retinal capillary plexus, but also the deeper layers down to the choriocapillaris.(501) (**Figure 6.1**) The ease with which these images can be acquired will enable patients with DMI to be monitored more closely and will further provide information regarding deep retinal capillary perfusion, and nerve fibre layer perfusion (**Figure 6.2**) not possible conventional fluorescein angiography. Moreover, quantification of capillary density has been automated (**Figure 6.3**) unlike the manual delineation performed in this study, which will make it more amenable to clinical use. In future, data generated from this study will inform assessment performed in patients using OCT angiography, will be useful in identifying patients with progressive macular ischaemia who may be ideal candidates for regenerative therapy.

In chapters 3 and 4, novel methods for quantifying inflammation in the vitreous and retina were described. For the purposes of monitoring inflammation in clinical practice, techniques used much fulfil the following criteria; it must be safe, efficient, and sufficiently comfortable for the patients for the purpose of repeated, longitudinal imaging, and it must not alter the behaviour of cells being measured (i.e. incite inflammation). Current methods for measuring inflammation include indirect analyses such as levels of CRP in blood, visualising the leakiness of a vessel or swelling of the retina. Cellular imaging has also been limited to ex-vivo labelling that has inherent limitations such as phenotypic and genotypic alterations that occur when cells are taken out of the circulation, and being only able to observe cells that are

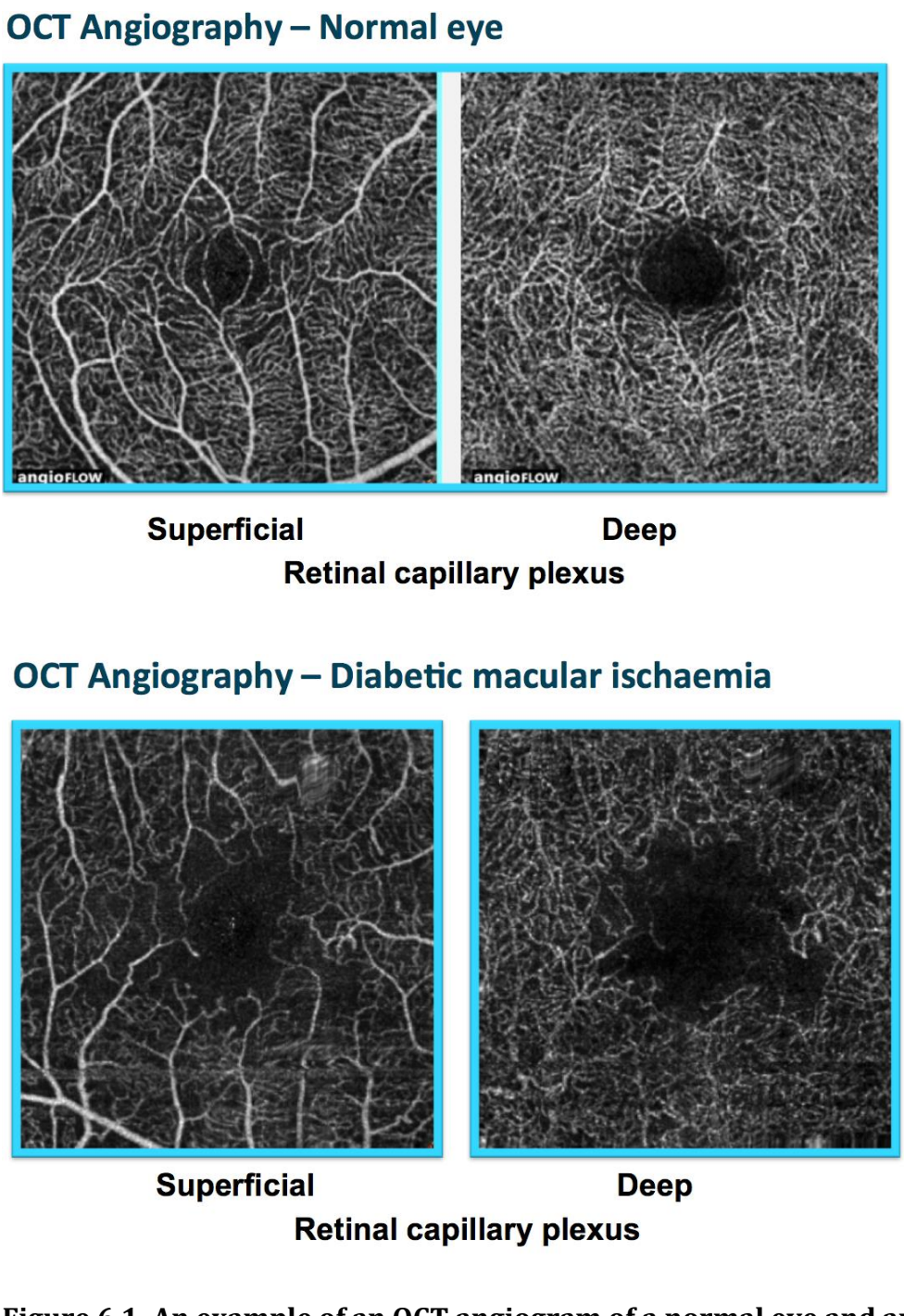

Figure 6.1. An example of an OCT angiogram of a normal eye and an eye with diabetic macular ischaemia.

Superficial (left) and deep (right) capillary plexus in the macula of a normal subject (Top row) and in diabetic macular ischaemia (Bottom row)

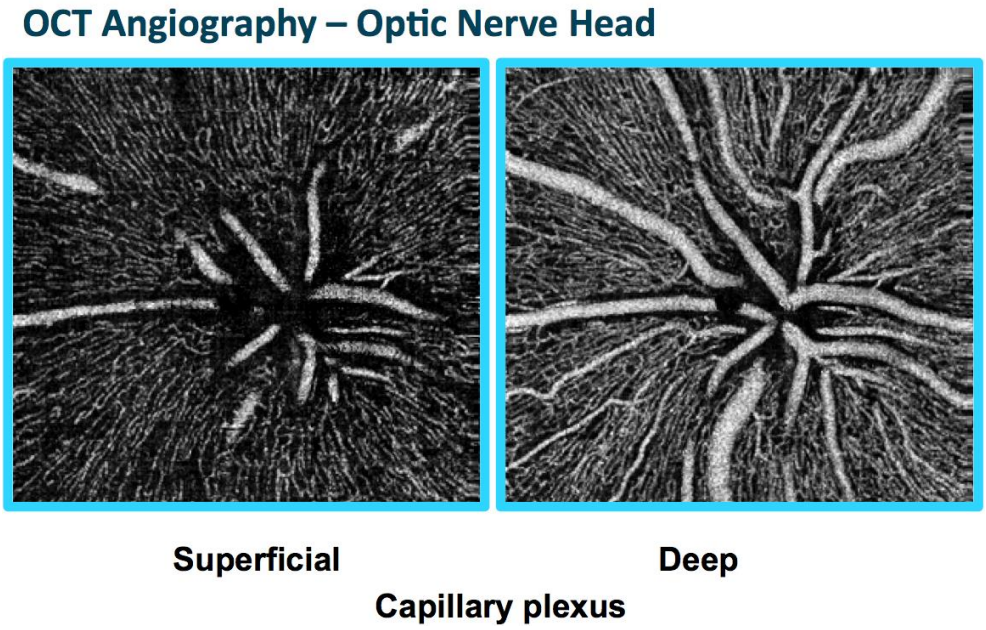

Figure 6.2. An example of an OCT angiogram of an optic nerve head.

Superficial (left) retinal nerve fibre layer capillary plexus and deep (right) ganglion cell layer capillary plexus from a patient with type 2 diabetes.

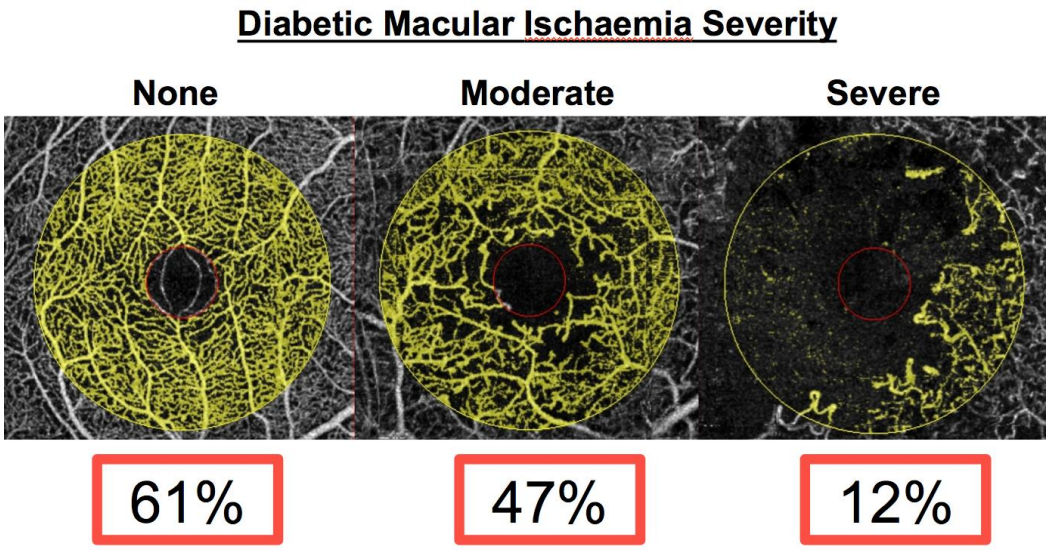

Figure 6.3. Quantification of capillary density on OCT angiograms.

Different severities of diabetic macular ischaemia; none (left) moderate (middle) and severe (right).

re-infused into the circulation. In this work, we developed more direct measures for inflammation in the eye using state-of-the-art retinal imaging technology-OCT, and further developed a simple method using ICG to label cells in vivo. In the field of regenerative medicine, this latter technique may further allow direct visualisation of cell-mediated inflammation regardless of the type of cell or tissue transplanted.

In chapter 5, we assessed EPC and monocyte profiles in the context of diabetic eye disease. Although we observed elevated levels of EPCs as defined by CD34+ CD309+, we failed to find any differences between subsets of diabetic eye disease as previously reported (93), or identify any associations with the progression of disease. This may reflect the limitations of and difficulties encountered when analysing a rare cell population; comparing proportions as low as 0.001% of the total PBMC population. The use of different technique for examining EPCs will, in future, improve our ability to accuracy detect differences between groups. Transcriptome analysis is one example that has been successfully used to characterise different culture-derived EPC subsets.(449, 450) Gene-expression profiling has highlighted the changes in which EPCs undergo during culture, and it was further able to detect changes in gene transcription in the context of disease. Results were consistent in both groups, demonstrating high similarities between a population of cultured EPCs and CD14+ monocytes. However, these studies did not examine the circulating EPC (without a culture step), possibly due to the rarity of this cell population in peripheral blood and potential difficulties obtaining sufficient numbers for analysis. A limitation of this method is that biological effects do not take place at a transcriptional level; and future efforts will likely require the integration of proteomic and metabolomics approaches in order to perform comprehensive profiling of the EPC.

In this chapter, differences in monocytes subsets were observed in the context of progression. Interestingly, there were no initial associations between monocyte subsets and eye disease severity at the outset. The expansion of CD16+ monocytes in the context of inflammation has been previously reported several publications (502-505), and is consistent with our observations, which further supports the notion of diabetes being a disease of inflammation. A recent large

population-based cohort study has further underlined the importance of inflammatory and immune response in the development of type 2 diabetes; revealing elevation of biomarkers such as C-reactive protein (CRP), total leukocyte count, IL-1, and IL-18 years before the onset of diabetes. A limitation of our monocyte analysis was the potential presence of confounding cells which express CD16+ i.e. neutrophils and natural killer cells. Although, published gating strategies were used for the quantification of flow cytometry data, we did not perform multiparameter imaging cytometry or use high-dimensional automated clustering algorithms to confirm the robustness of our gating strategy. Further, there is debate regarding Ficoll-based purification techniques of blood monocytes resulting in expansion of the CD16+ fraction.(462, 506) Ideally, whole-blood FACS analysis should have been performed to confirm our findings.

6.2. Outlook:

Fictitious clinical scenario:

"Mrs Smith has had type 2 diabetes for over 25 years, she arrives in the eye clinic for her 6th appointment this year for an anti-VEGF intravitreal injection for diabetic macular oedema. This has improved anatomically but her vision has not recovered. OCT angiography reveals concurrent diabetic macular ischaemia with moderate severity and quantitative analysis shows an increase in FAZ area of 20% from baseline. Whole blood analysis for monocyte subsets has confirmed alterations in her monocyte fractions. She is offered targeted intravitreal immunomodulatory therapy, which she can receive at the same time as her anti-VEGF injection. If this fails, an alternative is discussed, which will involve an intraocular injection of autologous monocytes repaired ex-vivo. Regeneration of foveal capillaries will be monitored using OCT angiography, and location of transplanted cells visualised with ICG labelling"

Important barriers toward bringing this fictitious clinical scenario into the realms of reality include; the lack of understanding of the role of monocytes in the

retina, its microcirculation, and the difficulties encountered in visualising these cells in in vivo. Nonetheless, there is evidence to suggest that monocytes play a key role in microvascular diseases, and their relative larger numbers in the peripheral circulation (compared to EPCs) make cells more suitable for autologous transplantation. However, its plasticity in culture, i.e. displaying endothelial-like genes when co-cultured with endothelium, or changes in antigenic phenotype when co-cultured with lymphocytes, and propensity to stick to plastic within minutes, are all factors that could arguably be considered equally as strengths or weaknesses in its campaign for candidacy in the field of regenerative therapy. In cell therapy, the challenges faced by monocytes lies not only in determining what subset to transplant, but also where to place it. Fortunately, monocytes have the pragmatic ability to home to sites of "injury" and there is evidence from hindlimb ischaemia models that intramuscular injections of these cells are equally effective as the intravenous route.(118) Another option for new treatment is intravitreal immunomodulatory therapy. The mainstay of which continues to be corticosteroids, which works via broad spectrum of action, potentially inhibiting both "good" and "bad" cells. More recently, newer-steroid sparing such as sirolimus, adalimumab, and gevokizumab, targetting specific inflammatory cytokines have been developed for intravitreal use in non-infectious uveitis and may be explored in the context of diabetic eye disease. In fact, systemic gevokizumab has entered phase 2 studies for the treatment of diabetic nephropathy. It is likely that a form of immune regulation will play a role in the treatment of diabetic eye disease in the future. Whether it will be a game changer the way anti-VEGF therapy has been over the past 5 years remains to be seen. Lastly, the importance of establishing meaningful clinical end-points and surrogate markers for efficacy must not be overlooked and defined at the outset of trials. These end-points should reflect clinical significance beyond statistical significance.

7. Appendix

7.1. Publications arising from this thesis

1. Karampelas M, Sim DA, Keane PA, Zarranz-Ventura J, Patel PJ, Tufail A, et al. Choroidal assessment in idiopathic panuveitis using optical coherence tomography. Graefes Arch Clin Exp Ophthalmol. 2013 Aug;251(8):2029-36. PubMed PMID: 23532454.
2. Sim DA, Keane PA, Mehta H, Fung S, Zarranz-Ventura J, Fruttiger M, et al. Repeatability and reproducibility of choroidal vessel layer measurements in diabetic retinopathy using enhanced depth optical coherence tomography. Invest Ophthalmol Vis Sci. 2013 Apr;54(4):2893-901. PubMed PMID: 23538058.
3. Sim DA, Keane PA, Zarranz-Ventura J, Bunce CV, Fruttiger M, Patel PJ, et al. Predictive factors for the progression of diabetic macular ischemia. Am J Ophthalmol. 2013 Oct;156(4):684-92. PubMed PMID: 23891332.
4. Sim DA, Keane PA, Zarranz-Ventura J, Fung S, Powner MB, Platteau E, et al. The effects of macular ischemia on visual acuity in diabetic retinopathy. Invest Ophthalmol Vis Sci. 2013 Mar;54(3):2353-60. PubMed PMID: 23449720.
5. Keane PA, Karampelas M, Sim DA, Sadda SR, Tufail A, Sen HN, et al. Objective measurement of vitreous inflammation using optical coherence tomography. Ophthalmology. 2014 Sep;121(9):1706-14. PubMed PMID: 24835759. Pubmed Central PMCID: 4507470.
6. Sim DA, Keane PA, Fung S, Karampelas M, Sadda SR, Fruttiger M, et al. Quantitative analysis of diabetic macular ischemia using optical coherence tomography. Invest Ophthalmol Vis Sci. 2014 Jan;55(1):417-23. PubMed PMID: 24398090.
7. Sim DA, Keane PA, Rajendram R, Karampelas M, Selvam S, Powner MB, et al. Patterns of peripheral retinal and central macula ischemia in diabetic retinopathy as evaluated by ultra-widefield fluorescein angiography. Am J Ophthalmol. 2014 Jul;158(1):144-53 e1. PubMed PMID: 24709807.
8. Zarranz-Ventura J, Sim DA, Keane PA, Patel PJ, Westcott MC, Lee RW, et al. Characterization of punctate inner choroidopathy using enhanced depth imaging optical coherence tomography. Ophthalmology. 2014 Sep;121(9):1790-7. PubMed PMID: 24856311.
9. Karampelas M, Sim DA, Chu C, Carreno E, Keane PA, Zarranz-Ventura J, et al. Quantitative analysis of peripheral vasculitis, ischemia, and vascular leakage in uveitis using ultra-widefield fluorescein angiography. Am J Ophthalmol. 2015 Jun;159(6):1161-8 e1. PubMed PMID: 25709064.
10. Keane PA, Balaskas K, Sim DA, Aman K, Denniston AK, Aslam T, et al. Automated Analysis of Vitreous Inflammation Using Spectral-Domain Optical Coherence Tomography. Translational vision science & technology. 2015 Sep;4(5):4. PubMed PMID: 26396930. Pubmed Central PMCID: 4572940.
11. Lee CS, Lee AY, Sim DA, Keane PA, Mehta H, Zarranz-Ventura J, et al. Reevaluating the definition of intraretinal microvascular abnormalities and neovascularization elsewhere in diabetic retinopathy using optical coherence

tomography and fluorescein angiography. Am J Ophthalmol. 2015 Jan;159(1):101-10 e1. PubMed PMID: 25284762.
12. Liew G, Sim DA, Keane PA, Tan AG, Mitchell P, Wang JJ, et al. Diabetic macular ischaemia is associated with narrower retinal arterioles in patients with type 2 diabetes. Acta Ophthalmol. 2015 Feb;93(1):e45-51. PubMed PMID: 25613127.
13. Liew G, Tufail A, Cosatto VF, Tan AG, Zarranz-Ventura J, Sim DA, et al. Retinal vessel caliber changes in vasculitis. Retina. 2015 Apr;35(4):803-8. PubMed PMID: 25526098.
14. Mehta H, Sim DA, Keane PA, Zarranz-Ventura J, Gallagher K, Egan CA, et al. Structural changes of the choroid in sarcoid- and tuberculosis-related granulomatous uveitis. Eye (Lond). 2015 Aug;29(8):1060-8. PubMed PMID: 26021867. Pubmed Central PMCID: 4541349.
15. Sim DA, Chu CJ, Selvam S, Powner MB, Liyanage S, Copland DA, et al. A simple method for in vivo labelling of infiltrating leukocytes in the retina using Indocyanine green dye. Disease models & mechanisms. 2015 Aug 20. PubMed PMID: 26398933.

7.2. Publications pertaining to but not included in this thesis

1. Alasil T, Keane PA, Sim DA, Tufail A, Rauser ME. Optical coherence tomography in pediatric ophthalmology: current roles and future directions. Ophthalmic surgery, lasers & imaging retina. 2013 Nov-Dec;44(6 Suppl):S19-29. PubMed PMID: 24220880.
2. Nobre Cardoso J, Keane PA, Sim DA, Bradley P, Agrawal R, Addison PK, et al. Systematic Evaluation of Optical Coherence Tomography Angiography in Retinal Vein Occlusion. American journal of ophthalmology. 2016 Mar;163:93-107 e6. PubMed PMID: 26621685.
3. Zarranz-Ventura J, Keane PA, Sim DA, Llorens V, Tufail A, Sadda SR, et al. Evaluation of Objective Vitritis Grading Method Using Optical Coherence Tomography: Influence of Phakic Status and Previous Vitrectomy. American journal of ophthalmology. 2016 Jan;161:172-80 e1-4. PubMed PMID: 26476212.
4. Keane PA, Balaskas K, Sim DA, Aman K, Denniston AK, Aslam T, et al. Automated Analysis of Vitreous Inflammation Using Spectral-Domain Optical Coherence Tomography. Translational vision science & technology. 2015 Sep;4(5):4. PubMed PMID: 26396930. Pubmed Central PMCID: 4572940.
5. Ang M, Cai Y, Shahipasand S, Sim DA, Keane PA, Sng CC, et al. En face optical coherence tomography angiography for corneal neovascularisation. The British journal of ophthalmology. 2016 May;100(5):616-21. PubMed PMID: 26311064.
6. Ang M, Sim DA, Keane PA, Sng CC, Egan CA, Tufail A, et al. Optical Coherence Tomography Angiography for Anterior Segment Vasculature Imaging. Ophthalmology. 2015 Sep;122(9):1740-7. PubMed PMID: 26088621.
7. Keane PA, de Salvo G, Sim DA, Goverdhan S, Agrawal R, Tufail A. Strategies for improving early detection and diagnosis of neovascular age-related macular degeneration. Clinical ophthalmology. 2015;9:353-66. PubMed PMID: 25733802. Pubmed Central PMCID: 4337735.
8. Carreno E, Fernandez-Sanz G, Sim DA, Keane PA, Westcott MC, Tufail A, et al. Multimodal imaging of macular serpiginous choroidopathy from acute presentation to quiescence. Ophthalmic surgery, lasers & imaging retina. 2015 Feb;46(2):266-70. PubMed PMID: 25707056.

9. Sim DA, Keane PA, Tufail A, Egan CA, Aiello LP, Silva PS. Automated retinal image analysis for diabetic retinopathy in telemedicine. Current diabetes reports. 2015 Mar;15(3):14. PubMed PMID: 25697773.
10. Sreekantam S, Macdonald T, Keane PA, Sim DA, Murray PI, Denniston AK. Quantitative analysis of vitreous inflammation using optical coherence tomography in patients receiving sub-Tenon's triamcinolone acetonide for uveitic cystoid macular oedema. The British journal of ophthalmology. 2016 May 5. PubMed PMID: 27150826.
11. Bradley PD, Sim DA, Keane PA, Cardoso J, Agrawal R, Tufail A, et al. The Evaluation of Diabetic Macular Ischemia Using Optical Coherence Tomography Angiography. Investigative ophthalmology & visual science. 2016 Feb;57(2):626-31. PubMed PMID: 26903223.
12. Sim DA, Mitry D, Alexander P, Mapani A, Goverdhan S, Aslam T, et al. The Evolution of Teleophthalmology Programs in the United Kingdom: Beyond Diabetic Retinopathy Screening. Journal of diabetes science and technology. 2016;10(2):308-17. PubMed PMID: 26830492. Pubmed Central PMCID: 4773982.
13. Ang M, Cai Y, MacPhee B, Sim DA, Keane PA, Sng CC, et al. Optical coherence tomography angiography and indocyanine green angiography for corneal vascularisation. The British journal of ophthalmology. 2016 Jan 28. PubMed PMID: 26823396.
14. Agrawal R, Salman M, Tan KA, Karampelas M, Sim DA, Keane PA, et al. Choroidal Vascularity Index (CVI)--A Novel Optical Coherence Tomography Parameter for Monitoring Patients with Panuveitis? PloS one. 2016;11(1):e0146344. PubMed PMID: 26751702. Pubmed Central PMCID: 4713828.
15. Vaz-Pereira S, Zarranz-Ventura J, Sim DA, Keane PA, Smith R, Egan CA, et al. Optical Coherence Tomography Features Of Active And Inactive Retinal Neovascularization In Proliferative Diabetic Retinopathy. Retina. 2016 Jun;36(6):1132-42. PubMed PMID: 26630315.

8. References

1. Banting FG, Best CH, Collip JB, Campbell WR, Fletcher AA. Pancreatic Extracts in the Treatment of Diabetes Mellitus. Canadian Medical Association journal. 1922 Mar;12(3):141-6. PubMed PMID: 20314060. Pubmed Central PMCID: 1524425.
2. Kempen JH, O'Colmain BJ, Leske MC, Haffner SM, Klein R, Moss SE, et al. The prevalence of diabetic retinopathy among adults in the United States. Arch Ophthalmol. 2004 Apr;122(4):552-63. PubMed PMID: 15078674.
3. Roy MS, Klein R, O'Colmain BJ, Klein BE, Moss SE, Kempen JH. The prevalence of diabetic retinopathy among adult type 1 diabetic persons in the United States. Arch Ophthalmol. 2004 Apr;122(4):546-51. PubMed PMID: 15078673.
4. Klein R, Klein BE, Moss SE, Davis MD, DeMets DL. The Wisconsin epidemiologic study of diabetic retinopathy. II. Prevalence and risk of diabetic retinopathy when age at diagnosis is less than 30 years. Archives of ophthalmology. 1984 Apr;102(4):520-6. PubMed PMID: 6367724. Epub 1984/04/01. eng.
5. Klein R, Klein BE, Moss SE, Davis MD, DeMets DL. The Wisconsin epidemiologic study of diabetic retinopathy. III. Prevalence and risk of diabetic retinopathy when age at diagnosis is 30 or more years. Arch Ophthalmol. 1984 Apr;102(4):527-32. PubMed PMID: 6367725.
6. Jaeger E. Beitr zur Pathol des Auges. Wien. 1856;p. 33 Fig 12.
7. Nettleship G. On oedema or cystic disease of the retina. Roy Ophth Lond Hosp Rep. 1872;VII(3):343-51.
8. Klein R, Moss SE, Klein BE, Davis MD, DeMets DL. The Wisconsin epidemiologic study of diabetic retinopathy. XI. The incidence of macular edema. Ophthalmology. 1989 Oct;96(10):1501-10. PubMed PMID: 2587045.
9. Klein R, Klein BE, Moss SE, Linton KL. The Beaver Dam Eye Study. Retinopathy in adults with newly discovered and previously diagnosed diabetes mellitus. Ophthalmology. 1992 Jan;99(1):58-62. PubMed PMID: 1741141. Epub 1992/01/01. eng.
10. Cikamatana L, Mitchell P, Rochtchina E, Foran S, Wang JJ. Five-year incidence and progression of diabetic retinopathy in a defined older population: the Blue Mountains Eye Study. Eye (Lond). 2007 Apr;21(4):465-71. PubMed PMID: 17318200.
11. Mitchell P, Smith W, Wang JJ, Attebo K. Prevalence of diabetic retinopathy in an older community. The Blue Mountains Eye Study. Ophthalmology. 1998 Mar;105(3):406-11. PubMed PMID: 9499768.
12. The effect of intensive treatment of diabetes on the development and progression of long-term complications in insulin-dependent diabetes mellitus. The Diabetes Control and Complications Trial Research Group. N Engl J Med. 1993 Sep 30;329(14):977-86. PubMed PMID: 8366922.
13. Intensive blood-glucose control with sulphonylureas or insulin compared with conventional treatment and risk of complications in patients with type 2 diabetes (UKPDS 33). UK Prospective Diabetes Study (UKPDS) Group. Lancet. 1998 Sep 12;352(9131):837-53. PubMed PMID: 9742976.
14. Matthews DR, Stratton IM, Aldington SJ, Holman RR, Kohner EM, Group UKPDS. Risks of progression of retinopathy and vision loss related to tight blood pressure control in type 2 diabetes mellitus: UKPDS 69. Arch Ophthalmol. 2004 Nov;122(11):1631-40. PubMed PMID: 15534123.
15. Tight blood pressure control and risk of macrovascular and microvascular complications in type 2 diabetes: UKPDS 38. UK Prospective Diabetes Study Group. BMJ. 1998 Sep 12;317(7160):703-13. PubMed PMID: 9732337. Pubmed Central PMCID: 28659.

16. van Hecke MV, Dekker JM, Nijpels G, Moll AC, Heine RJ, Bouter LM, et al. Inflammation and endothelial dysfunction are associated with retinopathy: the Hoorn Study. Diabetologia. 2005 Jul;48(7):1300-6. PubMed PMID: 15918015.
17. Goldberg MF, Jampol LM. Knowledge of diabetic retinopathy before and 18 years after the Airlie House Symposium on Treatment of Diabetic Retinopathy. Ophthalmology. 1987 Jul;94(7):741-6. PubMed PMID: 2889177.
18. Diabetic retinopathy study. Report Number 6. Design, methods, and baseline results. Report Number 7. A modification of the Airlie House classification of diabetic retinopathy. Prepared by the Diabetic Retinopathy. Invest Ophthalmol Vis Sci. 1981 Jul;21(1 Pt 2):1-226. PubMed PMID: 7195893.
19. Grading diabetic retinopathy from stereoscopic color fundus photographs--an extension of the modified Airlie House classification. ETDRS report number 10. Early Treatment Diabetic Retinopathy Study Research Group. Ophthalmology. 1991 May;98(5 Suppl):786-806. PubMed PMID: 2062513.
20. Wilkinson CP, Ferris FL, 3rd, Klein RE, Lee PP, Agardh CD, Davis M, et al. Proposed international clinical diabetic retinopathy and diabetic macular edema disease severity scales. Ophthalmology. 2003 Sep;110(9):1677-82. PubMed PMID: 13129861.
21. Classification of diabetic retinopathy from fluorescein angiograms. ETDRS report number 11. Early Treatment Diabetic Retinopathy Study Research Group. Ophthalmology. 1991 May;98(5 Suppl):807-22. PubMed PMID: 2062514. Epub 1991/05/01. eng.
22. Writing Committee for the Diabetic Retinopathy Clinical Research N, Fong DS, Strauber SF, Aiello LP, Beck RW, Callanan DG, et al. Comparison of the modified Early Treatment Diabetic Retinopathy Study and mild macular grid laser photocoagulation strategies for diabetic macular edema. Arch Ophthalmol. 2007 Apr;125(4):469-80. PubMed PMID: 17420366. Pubmed Central PMCID: 2536574.
23. Treatment techniques and clinical guidelines for photocoagulation of diabetic macular edema. Early Treatment Diabetic Retinopathy Study Report Number 2. Early Treatment Diabetic Retinopathy Study Research Group. Ophthalmology. 1987 Jul;94(7):761-74. PubMed PMID: 3658348.
24. Focal photocoagulation treatment of diabetic macular edema. Relationship of treatment effect to fluorescein angiographic and other retinal characteristics at baseline: ETDRS report no. 19. Early Treatment Diabetic Retinopathy Study Research Group. Arch Ophthalmol. 1995 Sep;113(9):1144-55. PubMed PMID: 7661748. Epub 1995/09/01. eng.
25. A randomized trial comparing intravitreal triamcinolone acetonide and focal/grid photocoagulation for diabetic macular edema. Ophthalmology. 2008 Sep;115(9):1447-9, 9 e1-10. PubMed PMID: 18662829. Pubmed Central PMCID: 2748264. Epub 2008/07/30. eng.
26. Huang D, Swanson EA, Lin CP, Schuman JS, Stinson WG, Chang W, et al. Optical coherence tomography. Science. 1991 Nov 22;254(5035):1178-81. PubMed PMID: 1957169. Epub 1991/11/22. eng.
27. Keane PA, Patel PJ, Liakopoulos S, Heussen FM, Sadda SR, Tufail A. Evaluation of age-related macular degeneration with optical coherence tomography. Surv Ophthalmol. 2012 Sep;57(5):389-414. PubMed PMID: 22898648.
28. Lee DH, Kim JT, Jung DW, Joe SG, Yoon YH. The relationship between foveal ischemia and spectral-domain optical coherence tomography findings in ischemic diabetic macular edema. Invest Ophthalmol Vis Sci. 2013 Feb;54(2):1080-5. PubMed PMID: 23329668. Epub 2013/01/19. eng.
29. Comyn O, Heng LZ, Ikeji F, Bibi K, Hykin PG, Bainbridge JW, et al. Repeatability of Spectralis OCT measurements of macular thickness and volume in diabetic macular edema. Invest Ophthalmol Vis Sci. 2012 Nov;53(12):7754-9. PubMed PMID: 23111610. Epub 2012/11/01. eng.

30. Hatef E, Khwaja A, Rentiya Z, Ibrahim M, Shulman M, Turkcuoglu P, et al. Comparison of time domain and spectral domain optical coherence tomography in measurement of macular thickness in macular edema secondary to diabetic retinopathy and retinal vein occlusion. J Ophthalmol. 2012;2012:354783. PubMed PMID: 22888403. Pubmed Central PMCID: 3410350. Epub 2012/08/14. eng.
31. Otani T, Kishi S. Tomographic assessment of vitreous surgery for diabetic macular edema. Am J Ophthalmol. 2000 Apr;129(4):487-94. PubMed PMID: 10764858. Epub 2000/04/15. eng.
32. Cho H, Alwassia AA, Regiatieri CV, Zhang JY, Baumal C, Waheed N, et al. Retinal neovascularization secondary to proliferative diabetic retinopathy characterized by spectral domain optical coherence tomography. Retina. 2013 Mar;33(3):542-7. PubMed PMID: 23400083. Epub 2013/02/13. eng.
33. Chung EJ, Roh MI, Kwon OW, Koh HJ. Effects of macular ischemia on the outcome of intravitreal bevacizumab therapy for diabetic macular edema. Retina. 2008 Jul-Aug;28(7):957-63. PubMed PMID: 18698297. Epub 2008/08/14. eng.
34. Flynn HW, Jr., Chew EY, Simons BD, Barton FB, Remaley NA, Ferris FL, 3rd. Pars plana vitrectomy in the Early Treatment Diabetic Retinopathy Study. ETDRS report number 17. The Early Treatment Diabetic Retinopathy Study Research Group. Ophthalmology. 1992 Sep;99(9):1351-7. PubMed PMID: 1407968. Epub 1992/09/11. eng.
35. Fluorescein angiographic risk factors for progression of diabetic retinopathy. ETDRS report number 13. Early Treatment Diabetic Retinopathy Study Research Group. Ophthalmology. 1991 May;98(5 Suppl):834-40. PubMed PMID: 2062516. Epub 1991/05/01. eng.
36. Mason JO, 3rd, Colagross CT, Haleman T, Fuller JJ, White MF, Feist RM, et al. Visual outcome and risk factors for light perception and no light perception vision after vitrectomy for diabetic retinopathy. Am J Ophthalmol. 2005 Aug;140(2):231-5. PubMed PMID: 15992755. Epub 2005/07/05. eng.
37. Mitchell P, Bandello F, Schmidt-Erfurth U, Lang GE, Massin P, Schlingemann RO, et al. The RESTORE study: ranibizumab monotherapy or combined with laser versus laser monotherapy for diabetic macular edema. Ophthalmology. 2011 Apr;118(4):615-25. PubMed PMID: 21459215. Epub 2011/04/05. eng.
38. Goebel W, Kretzchmar-Gross T. Retinal thickness in diabetic retinopathy: a study using optical coherence tomography (OCT). Retina. 2002 Dec;22(6):759-67. PubMed PMID: 12476103. Epub 2002/12/12. eng.
39. Michaelides M, Fraser-Bell S, Hamilton R, Kaines A, Egan C, Bunce C, et al. Macular perfusion determined by fundus fluorescein angiography at the 4-month time point in a prospective randomized trial of intravitreal bevacizumab or laser therapy in the management of diabetic macular edema (Bolt Study): Report 1. Retina. 2010 May;30(5):781-6. PubMed PMID: 20464787. Epub 2010/05/14. eng.
40. Conrath J, Giorgi R, Raccah D, Ridings B. Foveal avascular zone in diabetic retinopathy: quantitative vs qualitative assessment. Eye (Lond). 2005 Mar;19(3):322-6. PubMed PMID: 15258601. Epub 2004/07/20. eng.
41. Arend O, Wolf S, Harris A, Reim M. The relationship of macular microcirculation to visual acuity in diabetic patients. Arch Ophthalmol. 1995 May;113(5):610-4. PubMed PMID: 7748131. Epub 1995/05/01. eng.
42. Arend O, Wolf S, Jung F, Bertram B, Postgens H, Toonen H, et al. Retinal microcirculation in patients with diabetes mellitus: dynamic and morphological analysis of perifoveal capillary network. Br J Ophthalmol. 1991 Sep;75(9):514-8. PubMed PMID: 1911651. Pubmed Central PMCID: 1042463. Epub 1991/09/01. eng.

43. Bresnick GH, Condit R, Syrjala S, Palta M, Groo A, Korth K. Abnormalities of the foveal avascular zone in diabetic retinopathy. Arch Ophthalmol. 1984 Sep;102(9):1286-93. PubMed PMID: 6477244. Epub 1984/09/01. eng.
44. Alm A, Bill A. The oxygen supply to the retina. II. Effects of high intraocular pressure and of increased arterial carbon dioxide tension on uveal and retinal blood flow in cats. A study with radioactively labelled microspheres including flow determinations in brain and some other tissues. Acta Physiol Scand. 1972 Mar;84(3):306-19. PubMed PMID: 4553229. Epub 1972/03/01. eng.
45. Yanoff M. Ocular pathology of diabetes mellitus. Am J Ophthalmol. 1969 Jan;67(1):21-38. PubMed PMID: 4178151. Epub 1969/01/01. eng.
46. Spaide RF, Koizumi H, Pozzoni MC. Enhanced depth imaging spectral-domain optical coherence tomography. Am J Ophthalmol. 2008 Oct;146(4):496-500. PubMed PMID: 18639219. Epub 2008/07/22. eng.
47. Esmaeelpour M, Povazay B, Hermann B, Hofer B, Kajic V, Hale SL, et al. Mapping choroidal and retinal thickness variation in type 2 diabetes using three-dimensional 1060-nm optical coherence tomography. Invest Ophthalmol Vis Sci. 2011 Jul;52(8):5311-6. PubMed PMID: 21508108. Epub 2011/04/22. eng.
48. Querques G, Lattanzio R, Querques L, Del Turco C, Forte R, Pierro L, et al. Enhanced depth imaging optical coherence tomography in type 2 diabetes. Invest Ophthalmol Vis Sci. 2012 Aug 9. PubMed PMID: 22879414. Epub 2012/08/11. Eng.
49. Regatieri CV, Branchini L, Carmody J, Fujimoto JG, Duker JS. Choroidal thickness in patients with diabetic retinopathy analyzed by spectral-domain optical coherence tomography. Retina. 2012 Mar;32(3):563-8. PubMed PMID: 22374157. Pubmed Central PMCID: 3393081. Epub 2012/03/01. eng.
50. Vujosevic S, Martini F, Cavarzeran F, Pilotto E, Midena E. Macular and Peripapillary Choroidal Thickness in Diabetic Patients. Retina. 2012 Aug 3. PubMed PMID: 22869022. Epub 2012/08/08. Eng.
51. Hidayat AA, Fine BS. Diabetic choroidopathy. Light and electron microscopic observations of seven cases. Ophthalmology. 1985 Apr;92(4):512-22. PubMed PMID: 2582331. Epub 1985/04/01. eng.
52. Cao J, McLeod S, Merges CA, Lutty GA. Choriocapillaris degeneration and related pathologic changes in human diabetic eyes. Arch Ophthalmol. 1998 May;116(5):589-97. PubMed PMID: 9596494. Epub 1998/05/22. eng.
53. Fukushima I, McLeod DS, Lutty GA. Intrachoroidal microvascular abnormality: a previously unrecognized form of choroidal neovascularization. Am J Ophthalmol. 1997 Oct;124(4):473-87. PubMed PMID: 9323938. Epub 1997/11/05. eng.
54. Weinberger D, Kramer M, Priel E, Gaton DD, Axer-Siegel R, Yassur Y. Indocyanine green angiographic findings in nonproliferative diabetic retinopathy. Am J Ophthalmol. 1998 Aug;126(2):238-47. PubMed PMID: 9727518. Epub 1998/09/04. eng.
55. Shiragami C, Shiraga F, Matsuo T, Tsuchida Y, Ohtsuki H. Risk factors for diabetic choroidopathy in patients with diabetic retinopathy. Graefes Arch Clin Exp Ophthalmol. 2002 Jun;240(6):436-42. PubMed PMID: 12107509. Epub 2002/07/11. eng.
56. Motaghiannezam R, Schwartz DM, Fraser SE. In vivo human choroidal vascular pattern visualization using high-speed swept-source optical coherence tomography at 1060 nm. Invest Ophthalmol Vis Sci. 2012;53(4):2337-48. PubMed PMID: 22410568. Epub 2012/03/14. eng.
57. Povazay B, Hermann B, Hofer B, Kajic V, Simpson E, Bridgford T, et al. Wide-field optical coherence tomography of the choroid in vivo. Invest Ophthalmol Vis Sci. 2009 Apr;50(4):1856-63. PubMed PMID: 19060289. Epub 2008/12/09. eng.
58. Carmeliet P. Mechanisms of angiogenesis and arteriogenesis. Nature medicine. 2000 Apr;6(4):389-95. PubMed PMID: 10742145. eng.

59. Asahara T, Murohara T, Sullivan A, Silver M, van der Zee R, Li T, et al. Isolation of putative progenitor endothelial cells for angiogenesis. Science (New York, NY. 1997 Feb 14;275(5302):964-7. PubMed PMID: 9020076. eng.
60. Rafii S, Lyden D. Therapeutic stem and progenitor cell transplantation for organ vascularization and regeneration. Nature medicine. 2003 Jun;9(6):702-12. PubMed PMID: 12778169. eng.
61. Stitt AW, O'Neill CL, O'Doherty MT, Archer DB, Gardiner TA, Medina RJ. Vascular stem cells and ischaemic retinopathies. Prog Retin Eye Res. 2011 May;30(3):149-66. PubMed PMID: 21352947.
62. Fadini GP, Miorin M, Facco M, Bonamico S, Baesso I, Grego F, et al. Circulating endothelial progenitor cells are reduced in peripheral vascular complications of type 2 diabetes mellitus. J Am Coll Cardiol. 2005 May 3;45(9):1449-57. PubMed PMID: 15862417.
63. Tepper OM, Galiano RD, Capla JM, Kalka C, Gagne PJ, Jacobowitz GR, et al. Human endothelial progenitor cells from type II diabetics exhibit impaired proliferation, adhesion, and incorporation into vascular structures. Circulation. 2002 Nov 26;106(22):2781-6. PubMed PMID: 12451003. Epub 2002/11/27. eng.
64. Loomans CJ, de Koning EJ, Staal FJ, Rookmaaker MB, Verseyden C, de Boer HC, et al. Endothelial progenitor cell dysfunction: a novel concept in the pathogenesis of vascular complications of type 1 diabetes. Diabetes. 2004 Jan;53(1):195-9. PubMed PMID: 14693715. Epub 2003/12/25. eng.
65. Segal MS, Shah R, Afzal A, Perrault CM, Chang K, Schuler A, et al. Nitric oxide cytoskeletal-induced alterations reverse the endothelial progenitor cell migratory defect associated with diabetes. Diabetes. 2006 Jan;55(1):102-9. PubMed PMID: 16380482.
66. O'Neill CL, O'Doherty MT, Wilson SE, Rana AA, Hirst CE, Stitt AW, et al. Therapeutic revascularisation of ischaemic tissue: the opportunities and challenges for therapy using vascular stem/progenitor cells. Stem cell research & therapy. 2012;3(4):31. PubMed PMID: 22897941. Pubmed Central PMCID: 3580469.
67. Thum T, Fraccarollo D, Schultheiss M, Froese S, Galuppo P, Widder JD, et al. Endothelial nitric oxide synthase uncoupling impairs endothelial progenitor cell mobilization and function in diabetes. Diabetes. 2007 Mar;56(3):666-74. PubMed PMID: 17327434.
68. Hibbert B, Olsen S, O'Brien E. Involvement of progenitor cells in vascular repair. Trends in cardiovascular medicine. 2003 Nov;13(8):322-6. PubMed PMID: 14596947.
69. Peichev M, Naiyer AJ, Pereira D, Zhu Z, Lane WJ, Williams M, et al. Expression of VEGFR-2 and AC133 by circulating human CD34(+) cells identifies a population of functional endothelial precursors. Blood. 2000 Feb 1;95(3):952-8. PubMed PMID: 10648408.
70. Hur J, Yoon CH, Kim HS, Choi JH, Kang HJ, Hwang KK, et al. Characterization of two types of endothelial progenitor cells and their different contributions to neovasculogenesis. Arteriosclerosis, thrombosis, and vascular biology. 2004 Feb;24(2):288-93. PubMed PMID: 14699017.
71. Schmeisser A, Garlichs CD, Zhang H, Eskafi S, Graffy C, Ludwig J, et al. Monocytes coexpress endothelial and macrophagocytic lineage markers and form cord-like structures in Matrigel under angiogenic conditions. Cardiovasc Res. 2001 Feb 16;49(3):671-80. PubMed PMID: 11166280.
72. Rehman J, Li J, Orschell CM, March KL. Peripheral blood "endothelial progenitor cells" are derived from monocyte/macrophages and secrete angiogenic growth factors. Circulation. 2003 Mar 4;107(8):1164-9. PubMed PMID: 12615796.
73. Polverini PJ, Cotran PS, Gimbrone MA, Jr., Unanue ER. Activated macrophages induce vascular proliferation. Nature. 1977 Oct 27;269(5631):804-6. PubMed PMID: 927505.
74. Urbich C, Heeschen C, Aicher A, Dernbach E, Zeiher AM, Dimmeler S. Relevance of monocytic features for neovascularization capacity of circulating endothelial progenitor cells. Circulation. 2003 Nov 18;108(20):2511-6. PubMed PMID: 14581410.

75. Urbich C, Dimmeler S. Endothelial progenitor cells: characterization and role in vascular biology. Circ Res. 2004 Aug 20;95(4):343-53. PubMed PMID: 15321944.
76. Lin Y, Weisdorf DJ, Solovey A, Hebbel RP. Origins of circulating endothelial cells and endothelial outgrowth from blood. The Journal of clinical investigation. 2000 Jan;105(1):71-7. PubMed PMID: 10619863. Pubmed Central PMCID: 382587.
77. Aird WC. Phenotypic heterogeneity of the endothelium: I. Structure, function, and mechanisms. Circ Res. 2007 Feb 2;100(2):158-73. PubMed PMID: 17272818.
78. Aird WC. Phenotypic heterogeneity of the endothelium: II. Representative vascular beds. Circ Res. 2007 Feb 2;100(2):174-90. PubMed PMID: 17272819.
79. Liu XF, Yu JQ, Dalan R, Liu AQ, Luo KQ. Biological factors in plasma from diabetes mellitus patients enhance hyperglycaemia and pulsatile shear stress-induced endothelial cell apoptosis. Integrative biology : quantitative biosciences from nano to macro. 2014 May;6(5):511-22. PubMed PMID: 24643402.
80. Piconi L, Quagliaro L, Assaloni R, Da Ros R, Maier A, Zuodar G, et al. Constant and intermittent high glucose enhances endothelial cell apoptosis through mitochondrial superoxide overproduction. Diabetes Metab Res Rev. 2006 May-Jun;22(3):198-203. PubMed PMID: 16453381.
81. Nomura S. Dynamic role of microparticles in type 2 diabetes mellitus. Current diabetes reviews. 2009 Nov;5(4):245-51. PubMed PMID: 19531024.
82. Fadini GP, Sartore S, Albiero M, Baesso I, Murphy E, Menegolo M, et al. Number and function of endothelial progenitor cells as a marker of severity for diabetic vasculopathy. Arteriosclerosis, thrombosis, and vascular biology. 2006 Sep;26(9):2140-6. PubMed PMID: 16857948.
83. Humpert PM, Neuwirth R, Battista MJ, Voronko O, von Eynatten M, Konrade I, et al. SDF-1 genotype influences insulin-dependent mobilization of adult progenitor cells in type 2 diabetes. Diabetes Care. 2005 Apr;28(4):934-6. PubMed PMID: 15793201.
84. Krankel N, Adams V, Linke A, Gielen S, Erbs S, Lenk K, et al. Hyperglycemia reduces survival and impairs function of circulating blood-derived progenitor cells. Arteriosclerosis, thrombosis, and vascular biology. 2005 Apr;25(4):698-703. PubMed PMID: 15662022.
85. Fadini GP, Boscaro E, de Kreutzenberg S, Agostini C, Seeger F, Dimmeler S, et al. Time course and mechanisms of circulating progenitor cell reduction in the natural history of type 2 diabetes. Diabetes Care. 2010 May;33(5):1097-102. PubMed PMID: 20150295. Pubmed Central PMCID: 2858183.
86. Schatteman GC, Hanlon HD, Jiao C, Dodds SG, Christy BA. Blood-derived angioblasts accelerate blood-flow restoration in diabetic mice. The Journal of clinical investigation. 2000 Aug;106(4):571-8. PubMed PMID: 10953032. Pubmed Central PMCID: 380249.
87. Herbrig K, Gebler K, Oelschlaegel U, Pistrosch F, Foerster S, Wagner A, et al. Kidney transplantation substantially improves endothelial progenitor cell dysfunction in patients with end-stage renal disease. Am J Transplant. 2006 Dec;6(12):2922-8. PubMed PMID: 17061996.
88. Naruse K, Hamada Y, Nakashima E, Kato K, Mizubayashi R, Kamiya H, et al. Therapeutic neovascularization using cord blood-derived endothelial progenitor cells for diabetic neuropathy. Diabetes. 2005 Jun;54(6):1823-8. PubMed PMID: 15919805.
89. Jeong JO, Kim MO, Kim H, Lee MY, Kim SW, Ii M, et al. Dual angiogenic and neurotrophic effects of bone marrow-derived endothelial progenitor cells on diabetic neuropathy. Circulation. 2009 Feb 10;119(5):699-708. PubMed PMID: 19171856. Pubmed Central PMCID: 2746559.
90. Busik JV, Tikhonenko M, Bhatwadekar A, Opreanu M, Yakubova N, Caballero S, et al. Diabetic retinopathy is associated with bone marrow neuropathy and a depressed peripheral clock. The Journal of experimental medicine. 2009 Dec 21;206(13):2897-906. PubMed PMID: 19934019. Pubmed Central PMCID: 2806461.

91. Fadini GP, Sartore S, Baesso I, Lenzi M, Agostini C, Tiengo A, et al. Endothelial progenitor cells and the diabetic paradox. Diabetes Care. 2006 Mar;29(3):714-6. PubMed PMID: 16505536.
92. Asnaghi V, Lattanzio R, Mazzolari G, Pastore MR, Ramoni A, Maestroni A, et al. Increased clonogenic potential of circulating endothelial progenitor cells in patients with type 1 diabetes and proliferative retinopathy. Diabetologia. 2006 May;49(5):1109-11. PubMed PMID: 16520918.
93. Brunner S, Schernthaner GH, Satler M, Elhenicky M, Hoellerl F, Schmid-Kubista KE, et al. Correlation of different circulating endothelial progenitor cells to stages of diabetic retinopathy: first in vivo data. Invest Ophthalmol Vis Sci. 2009 Jan;50(1):392-8. PubMed PMID: 18719083.
94. Eardley KS, Kubal C, Zehnder D, Quinkler M, Lepenies J, Savage CO, et al. The role of capillary density, macrophage infiltration and interstitial scarring in the pathogenesis of human chronic kidney disease. Kidney Int. 2008 Aug;74(4):495-504. PubMed PMID: 18528327.
95. Kaito M, Araya S, Gondo Y, Fujita M, Minato N, Nakanishi M, et al. Relevance of distinct monocyte subsets to clinical course of ischemic stroke patients. PLoS One. 2013;8(8):e69409. PubMed PMID: 23936327. Pubmed Central PMCID: 3732285.
96. Frantz S, Nahrendorf M. Cardiac macrophages and their role in ischaemic heart disease. Cardiovasc Res. 2014 May 1;102(2):240-8. PubMed PMID: 24501331. Pubmed Central PMCID: 3989449.
97. Patel AS, Smith A, Nucera S, Biziato D, Saha P, Attia RQ, et al. TIE2-expressing monocytes/macrophages regulate revascularization of the ischemic limb. EMBO molecular medicine. 2013 Jun;5(6):858-69. PubMed PMID: 23653322. Pubmed Central PMCID: 3779448.
98. Joussen AM, Murata T, Tsujikawa A, Kirchhof B, Bursell SE, Adamis AP. Leukocyte-mediated endothelial cell injury and death in the diabetic retina. Am J Pathol. 2001 Jan;158(1):147-52. PubMed PMID: 11141487. Pubmed Central PMCID: 1850259.
99. Ishida S, Usui T, Yamashiro K, Kaji Y, Amano S, Ogura Y, et al. VEGF164-mediated inflammation is required for pathological, but not physiological, ischemia-induced retinal neovascularization. The Journal of experimental medicine. 2003 Aug 4;198(3):483-9. PubMed PMID: 12900522. Pubmed Central PMCID: 2194095.
100. Gordon S, Taylor PR. Monocyte and macrophage heterogeneity. Nat Rev Immunol. 2005 Dec;5(12):953-64. PubMed PMID: 16322748.
101. Schinkel C, Sendtner R, Zimmer S, Faist E. Functional analysis of monocyte subsets in surgical sepsis. The Journal of trauma. 1998 May;44(5):743-8; discussion 8-9. PubMed PMID: 9603073.
102. Skinner NA, MacIsaac CM, Hamilton JA, Visvanathan K. Regulation of Toll-like receptor (TLR)2 and TLR4 on CD14dimCD16+ monocytes in response to sepsis-related antigens. Clin Exp Immunol. 2005 Aug;141(2):270-8. PubMed PMID: 15996191. Pubmed Central PMCID: 1809439.
103. Hijdra D, Vorselaars AD, Grutters JC, Claessen AM, Rijkers GT. Phenotypic characterization of human intermediate monocytes. Frontiers in immunology. 2013;4:339. PubMed PMID: 24155746. Pubmed Central PMCID: 3805031.
104. Rossol M, Kraus S, Pierer M, Baerwald C, Wagner U. The CD14(bright) CD16+ monocyte subset is expanded in rheumatoid arthritis and promotes expansion of the Th17 cell population. Arthritis Rheum. 2012 Mar;64(3):671-7. PubMed PMID: 22006178.
105. Moniuszko M, Bodzenta-Lukaszyk A, Kowal K, Lenczewska D, Dabrowska M. Enhanced frequencies of CD14++CD16+, but not CD14+CD16+, peripheral blood monocytes in severe asthmatic patients. Clin Immunol. 2009 Mar;130(3):338-46. PubMed PMID: 18952503.

106. Hijdra D, Vorselaars AD, Grutters JC, Claessen AM, Rijkers GT. Differential expression of TNFR1 (CD120a) and TNFR2 (CD120b) on subpopulations of human monocytes. Journal of inflammation. 2012;9(1):38. PubMed PMID: 23039818. Pubmed Central PMCID: 3542013.
107. Steppich B, Dayyani F, Gruber R, Lorenz R, Mack M, Ziegler-Heitbrock HW. Selective mobilization of CD14(+)CD16(+) monocytes by exercise. Am J Physiol Cell Physiol. 2000 Sep;279(3):C578-86. PubMed PMID: 10942707.
108. Timmerman KL, Flynn MG, Coen PM, Markofski MM, Pence BD. Exercise training-induced lowering of inflammatory (CD14+CD16+) monocytes: a role in the anti-inflammatory influence of exercise? J Leukoc Biol. 2008 Nov;84(5):1271-8. PubMed PMID: 18664531.
109. Menart-Houtermans B, Rutter R, Nowotny B, Rosenbauer J, Koliaki C, Kahl S, et al. Leukocyte profiles differ between type 1 and type 2 diabetes and are associated with metabolic phenotypes: results from the German Diabetes Study (GDS). Diabetes Care. 2014 Aug;37(8):2326-33. PubMed PMID: 25061140.
110. Ryba-Stanislawowska M, Mysliwska J, Juhas U, Mysliwiec M. Elevated levels of peripheral blood CD14(bright) CD16(+) and CD14(dim) CD16(+) monocytes may contribute to the development of retinopathy in patients with juvenile onset type 1 diabetes. APMIS : acta pathologica, microbiologica, et immunologica Scandinavica. 2015 Sep;123(9):793-9. PubMed PMID: 26200806.
111. Fadini GP, de Kreutzenberg SV, Boscaro E, Albiero M, Cappellari R, Krankel N, et al. An unbalanced monocyte polarisation in peripheral blood and bone marrow of patients with type 2 diabetes has an impact on microangiopathy. Diabetologia. 2013 Aug;56(8):1856-66. PubMed PMID: 23616239.
112. Bunce C, Xing W, Wormald R. Causes of blind and partial sight certifications in England and Wales: April 2007-March 2008. Eye (Lond). Nov;24(11):1692-9. PubMed PMID: 20847749. eng.
113. Aiello LM. Perspectives on diabetic retinopathy. Am J Ophthalmol. 2003 Jul 1;136(1):122-35. PubMed PMID: 12834680. eng.
114. Sharma NK, Gardiner TA, Archer DB. A morphologic and autoradiographic study of cell death and regeneration in the retinal microvasculature of normal and diabetic rats. American journal of ophthalmology. 1985 Jul 15;100(1):51-60. PubMed PMID: 4014380. eng.
115. Stitt AW, McGoldrick C, Rice-McCaldin A, McCance DR, Glenn JV, Hsu DK, et al. Impaired retinal angiogenesis in diabetes: role of advanced glycation end products and galectin-3. Diabetes. 2005 Mar;54(3):785-94. PubMed PMID: 15734857. eng.
116. Risau W. Mechanisms of angiogenesis. Nature. 1997 Apr 17;386(6626):671-4. PubMed PMID: 9109485.
117. Womble TA, Green S, Shahaduzzaman M, Grieco J, Sanberg PR, Pennypacker KR, et al. Monocytes are essential for the neuroprotective effect of human cord blood cells following middle cerebral artery occlusion in rat. Molecular and cellular neurosciences. 2014 Mar;59:76-84. PubMed PMID: 24472845. Pubmed Central PMCID: 4008706.
118. Awad O, Dedkov EI, Jiao C, Bloomer S, Tomanek RJ, Schatteman GC. Differential healing activities of CD34+ and CD14+ endothelial cell progenitors. Arteriosclerosis, thrombosis, and vascular biology. 2006 Apr;26(4):758-64. PubMed PMID: 16410458.
119. Bersenev A. Role of monocytes in regenerative cell therapies. Cell Trials; Current Trends in Cell Therapy. 2014.
120. Lyons TJ, Jenkins AJ, Zheng D, Lackland DT, McGee D, Garvey WT, et al. Diabetic retinopathy and serum lipoprotein subclasses in the DCCT/EDIC cohort. Investigative ophthalmology & visual science. 2004 Mar;45(3):910-8. PubMed PMID: 14985310.
121. van Leiden HA, Dekker JM, Moll AC, Nijpels G, Heine RJ, Bouter LM, et al. Blood pressure, lipids, and obesity are associated with retinopathy: the hoorn study. Diabetes care. 2002 Aug;25(8):1320-5. PubMed PMID: 12145228.

122. Colhoun HM, Betteridge DJ, Durrington PN, Hitman GA, Neil HA, Livingstone SJ, et al. Primary prevention of cardiovascular disease with atorvastatin in type 2 diabetes in the Collaborative Atorvastatin Diabetes Study (CARDS): multicentre randomised placebo-controlled trial. Lancet. 2004 Aug 21-27;364(9435):685-96. PubMed PMID: 15325833.
123. Keech A, Simes RJ, Barter P, Best J, Scott R, Taskinen MR, et al. Effects of long-term fenofibrate therapy on cardiovascular events in 9795 people with type 2 diabetes mellitus (the FIELD study): randomised controlled trial. Lancet. 2005 Nov 26;366(9500):1849-61. PubMed PMID: 16310551.
124. Keech AC, Mitchell P, Summanen PA, O'Day J, Davis TM, Moffitt MS, et al. Effect of fenofibrate on the need for laser treatment for diabetic retinopathy (FIELD study): a randomised controlled trial. Lancet. 2007 Nov 17;370(9600):1687-97. PubMed PMID: 17988728.
125. Group AS, Ginsberg HN, Elam MB, Lovato LC, Crouse JR, 3rd, Leiter LA, et al. Effects of combination lipid therapy in type 2 diabetes mellitus. The New England journal of medicine. 2010 Apr 29;362(17):1563-74. PubMed PMID: 20228404. Pubmed Central PMCID: 2879499.
126. Zanetti M, Stocca A, Dapas B, Farra R, Uxa L, Bosutti A, et al. Inhibitory effects of fenofibrate on apoptosis and cell proliferation in human endothelial cells in high glucose. Journal of molecular medicine. 2008 Feb;86(2):185-95. PubMed PMID: 17876565.
127. Varet J, Vincent L, Mirshahi P, Pille JV, Legrand E, Opolon P, et al. Fenofibrate inhibits angiogenesis in vitro and in vivo. Cellular and molecular life sciences : CMLS. 2003 Apr;60(4):810-9. PubMed PMID: 12785728.
128. Villarroel M, Garcia-Ramirez M, Corraliza L, Hernandez C, Simo R. Fenofibric acid prevents retinal pigment epithelium disruption induced by interleukin-1beta by suppressing AMP-activated protein kinase (AMPK) activation. Diabetologia. 2011 Jun;54(6):1543-53. PubMed PMID: 21369818.
129. Garcia-Ramirez M, Hernandez C, Palomer X, Vazquez-Carrera M, Simo R. Fenofibrate prevents the disruption of the outer blood retinal barrier through downregulation of NF-kappaB activity. Acta diabetologica. 2016 Feb;53(1):109-18. PubMed PMID: 25936740.
130. Cheung N, Wong TY. Fenofibrate and diabetic retinopathy. Lancet. 2008 Mar 1;371(9614):721-2; author reply 2. PubMed PMID: 18313493.
131. Arakawa R, Tamehiro N, Nishimaki-Mogami T, Ueda K, Yokoyama S. Fenofibric acid, an active form of fenofibrate, increases apolipoprotein A-I-mediated high-density lipoprotein biogenesis by enhancing transcription of ATP-binding cassette transporter A1 gene in a liver X receptor-dependent manner. Arteriosclerosis, thrombosis, and vascular biology. 2005 Jun;25(6):1193-7. PubMed PMID: 15790930.
132. Takeuchi M, Sato T, Tanaka A, Muraoka T, Taguchi M, Sakurai Y, et al. Elevated Levels of Cytokines Associated with Th2 and Th17 Cells in Vitreous Fluid of Proliferative Diabetic Retinopathy Patients. PLoS One. 2015;10(9):e0137358. PubMed PMID: 26352837. Pubmed Central PMCID: 4564282.
133. Yoshida S, Kubo Y, Kobayashi Y, Zhou Y, Nakama T, Yamaguchi M, et al. Increased vitreous concentrations of MCP-1 and IL-6 after vitrectomy in patients with proliferative diabetic retinopathy: possible association with postoperative macular oedema. Br J Ophthalmol. 2015 Jul;99(7):960-6. PubMed PMID: 25631486.
134. McAuley AK, Sanfilippo PG, Hewitt AW, Liang H, Lamoureux E, Wang JJ, et al. Vitreous biomarkers in diabetic retinopathy: a systematic review and meta-analysis. J Diabetes Complications. 2014 May-Jun;28(3):419-25. PubMed PMID: 24630762.
135. Yoshida S, Kobayashi Y, Nakama T, Zhou Y, Ishikawa K, Arita R, et al. Increased expression of M-CSF and IL-13 in vitreous of patients with proliferative diabetic retinopathy: implications for M2 macrophage-involving fibrovascular membrane formation. Br J Ophthalmol. 2015 May;99(5):629-34. PubMed PMID: 25355804.

136. Scott IU, Jackson GR, Quillen DA, Larsen M, Klein R, Liao J, et al. Effect of doxycycline vs placebo on retinal function and diabetic retinopathy progression in patients with severe nonproliferative or non-high-risk proliferative diabetic retinopathy: a randomized clinical trial. JAMA ophthalmology. 2014 May;132(5):535-43. PubMed PMID: 24604308.
137. Mansour AM, Schachat A, Bodiford G, Haymond R. Foveal avascular zone in diabetes mellitus. Retina. 1993;13(2):125-8. PubMed PMID: 8337493. Epub 1993/01/01. eng.
138. Varma R, Torres M, Pena F, Klein R, Azen SP. Prevalence of diabetic retinopathy in adult Latinos: the Los Angeles Latino eye study. Ophthalmology. 2004 Jul;111(7):1298-306. PubMed PMID: 15234129. Epub 2004/07/06. eng.
139. Wong TY, Klein R, Islam FM, Cotch MF, Folsom AR, Klein BE, et al. Diabetic retinopathy in a multi-ethnic cohort in the United States. Am J Ophthalmol. 2006 Mar;141(3):446-55. PubMed PMID: 16490489. Pubmed Central PMCID: 2246042. Epub 2006/02/24. eng.
140. Nguyen QD, Brown DM, Marcus DM, Boyer DS, Patel S, Feiner L, et al. Ranibizumab for diabetic macular edema: results from 2 phase III randomized trials: RISE and RIDE. Ophthalmology. 2012 Apr;119(4):789-801. PubMed PMID: 22330964. Epub 2012/02/15. eng.
141. Elman MJ, Qin H, Aiello LP, Beck RW, Bressler NM, Ferris FL, 3rd, et al. Intravitreal Ranibizumab for Diabetic Macular Edema with Prompt versus Deferred Laser Treatment: Three-Year Randomized Trial Results. Ophthalmology. 2012 Sep 19. PubMed PMID: 22999634. Epub 2012/09/25. Eng.
142. Eppens MC, Craig ME, Cusumano J, Hing S, Chan AK, Howard NJ, et al. Prevalence of diabetes complications in adolescents with type 2 compared with type 1 diabetes. Diabetes Care. 2006 Jun;29(6):1300-6. PubMed PMID: 16732012. Epub 2006/05/30. eng.
143. Klein R, Knudtson MD, Lee KE, Gangnon R, Klein BE. The Wisconsin Epidemiologic Study of Diabetic Retinopathy: XXII the twenty-five-year progression of retinopathy in persons with type 1 diabetes. Ophthalmology. 2008 Nov;115(11):1859-68. PubMed PMID: 19068374. Pubmed Central PMCID: 2761813. Epub 2008/12/11. eng.
144. Ding J, Wong TY. Current epidemiology of diabetic retinopathy and diabetic macular edema. Current diabetes reports. 2012 Aug;12(4):346-54. PubMed PMID: 22585044.
145. Yau JW, Rogers SL, Kawasaki R, Lamoureux EL, Kowalski JW, Bek T, et al. Global prevalence and major risk factors of diabetic retinopathy. Diabetes Care. 2012 Mar;35(3):556-64. PubMed PMID: 22301125. Pubmed Central PMCID: 3322721.
146. Kook D, Wolf A, Kreutzer T, Neubauer A, Strauss R, Ulbig M, et al. Long-term effect of intravitreal bevacizumab (avastin) in patients with chronic diffuse diabetic macular edema. Retina. 2008 Oct;28(8):1053-60. PubMed PMID: 18779710. Epub 2008/09/10. eng.
147. Jonas JB, Martus P, Degenring RF, Kreissig I, Akkoyun I. Predictive factors for visual acuity after intravitreal triamcinolone treatment for diabetic macular edema. Arch Ophthalmol. 2005 Oct;123(10):1338-43. PubMed PMID: 16219724. Epub 2005/10/13. eng.
148. Lee CS, Koh HJ. Multiple retinal haemorrhages in diabetic retinopathy after adjunctive intravitreal bevacizumab (Avastin) with pars plana vitrectomy. Acta Ophthalmol. 2008 Nov;86(7):812-3. PubMed PMID: 18093262. Epub 2007/12/21. eng.
149. Wong LJ, Desai RU, Jain A, Feliciano D, Moshfeghi DM, Sanislo SR, et al. Surveillance for potential adverse events associated with the use of intravitreal bevacizumab for retinal and choroidal vascular disease. Retina. 2008 Oct;28(8):1151-8. PubMed PMID: 18685542. Epub 2008/08/08. eng.
150. Rouvas AA, Papakostas TD, Ladas ID, Vergados I. Enlargement of the hypofluorescent post photodynamic therapy treatment spot after a combination of photodynamic therapy with an intravitreal injection of bevacizumab for retinal angiomatous proliferation. Graefes Arch Clin Exp Ophthalmol. 2008 Feb;246(2):315-8. PubMed PMID: 17957379. Epub 2007/10/25. eng.

151. Campochiaro PA, Bhisitkul RB, Shapiro H, Rubio RG. Vascular Endothelial Growth Factor Promotes Progressive Retinal Nonperfusion in Patients with Retinal Vein Occlusion. Ophthalmology. 2012 Dec 20. PubMed PMID: 23260261. Epub 2012/12/25. Eng.
152. Hahl J, Simell T, Kupila A, Keskinen P, Knip M, Ilonen J, et al. A simulation model for estimating direct costs of type 1 diabetes prevention. PharmacoEconomics. 2003;21(5):295-303. PubMed PMID: 12627983.
153. Kimpimaki T, Kulmala P, Savola K, Kupila A, Korhonen S, Simell T, et al. Natural history of beta-cell autoimmunity in young children with increased genetic susceptibility to type 1 diabetes recruited from the general population. J Clin Endocrinol Metab. 2002 Oct;87(10):4572-9. PubMed PMID: 12364437.
154. MacFarlane AJ, Burghardt KM, Kelly J, Simell T, Simell O, Altosaar I, et al. A type 1 diabetes-related protein from wheat (Triticum aestivum). cDNA clone of a wheat storage globulin, Glb1, linked to islet damage. J Biol Chem. 2003 Jan 3;278(1):54-63. PubMed PMID: 12409286.
155. Li ZG, Zhang W, Grunberger G, Sima AA. Hippocampal neuronal apoptosis in type 1 diabetes. Brain research. 2002 Aug 16;946(2):221-31. PubMed PMID: 12137925.
156. Knip M, Kukko M, Kulmala P, Veijola R, Simell O, Akerblom HK, et al. Humoral beta-cell autoimmunity in relation to HLA-defined disease susceptibility in preclinical and clinical type 1 diabetes. American journal of medical genetics. 2002 May 30;115(1):48-54. PubMed PMID: 12116176.
157. Ilonen J, Sjoroos M, Knip M, Veijola R, Simell O, Akerblom HK, et al. Estimation of genetic risk for type 1 diabetes. American journal of medical genetics. 2002 May 30;115(1):30-6. PubMed PMID: 12116174.
158. Kupila A, Keskinen P, Simell T, Erkkila S, Arvilommi P, Korhonen S, et al. Genetic risk determines the emergence of diabetes-associated autoantibodies in young children. Diabetes. 2002 Mar;51(3):646-51. PubMed PMID: 11872662.
159. Blomqvist M, Juhela S, Erkkila S, Korhonen S, Simell T, Kupila A, et al. Rotavirus infections and development of diabetes-associated autoantibodies during the first 2 years of life. Clin Exp Immunol. 2002 Jun;128(3):511-5. PubMed PMID: 12067306. Pubmed Central PMCID: 1906266.
160. Kimpimaki T, Kupila A, Hamalainen AM, Kukko M, Kulmala P, Savola K, et al. The first signs of beta-cell autoimmunity appear in infancy in genetically susceptible children from the general population: the Finnish Type 1 Diabetes Prediction and Prevention Study. J Clin Endocrinol Metab. 2001 Oct;86(10):4782-8. PubMed PMID: 11600541.
161. Juhela S, Hyoty H, Roivainen M, Harkonen T, Putto-Laurila A, Simell O, et al. T-cell responses to enterovirus antigens in children with type 1 diabetes. Diabetes. 2000 Aug;49(8):1308-13. PubMed PMID: 10923630.
162. Li ZG, Britton M, Sima AA, Dunbar JC. Diabetes enhances apoptosis induced by cerebral ischemia. Life Sci. 2004 Dec 3;76(3):249-62. PubMed PMID: 15531378.
163. Hanninen H, Takala P, Makijarvi M, Montonen J, Korhonen P, Oikarinen L, et al. Recording locations in multichannel magnetocardiography and body surface potential mapping sensitive for regional exercise-induced myocardial ischemia. Basic research in cardiology. 2001 Jul;96(4):405-14. PubMed PMID: 11518197.
164. Bogaty P, Kingma JG, Jr., Robitaille NM, Plante S, Simard S, Charbonneau L, et al. Attenuation of myocardial ischemia with repeated exercise in subjects with chronic stable angina: relation to myocardial contractility, intensity of exercise and the adenosine triphosphate-sensitive potassium channel. J Am Coll Cardiol. 1998 Nov 15;32(6):1665-71. PubMed PMID: 9822094.
165. Kohner EM, Henkind P. Correlation of fluorescein angiogram and retinal digest in diabetic retinopathy. Am J Ophthalmol. 1970 Mar;69(3):403-14. PubMed PMID: 4907465. Epub 1970/03/01. eng.

166. Bresnick GH, Engerman R, Davis MD, de Venecia G, Myers FL. Patterns of ischemia in diabetic retinopathy. Trans Sect Ophthalmol Am Acad Ophthalmol Otolaryngol. 1976 Jul-Aug;81(4 Pt 1):OP694-709. PubMed PMID: 822560. Epub 1976/07/01. eng.
167. Bresnick GH, De Venecia G, Myers FL, Harris JA, Davis MD. Retinal ischemia in diabetic retinopathy. Arch Ophthalmol. 1975 Dec;93(12):1300-10. PubMed PMID: 1200895. Epub 1975/12/01. eng.
168. Byeon SH, Chu YK, Lee H, Lee SY, Kwon OW. Foveal ganglion cell layer damage in ischemic diabetic maculopathy: correlation of optical coherence tomographic and anatomic changes. Ophthalmology. 2009 Oct;116(10):1949-59 e8. PubMed PMID: 19699533. Epub 2009/08/25. eng.
169. Reznicek L, Kernt M, Haritoglou C, Kampik A, Ulbig M, Neubauer AS. In vivo characterization of ischemic retina in diabetic retinopathy. Clin Ophthalmol. 2010;5:31-5. PubMed PMID: 21311655. Pubmed Central PMCID: 3033002. Epub 2011/02/12. eng.
170. Alasil T, Keane PA, Updike JF, Dustin L, Ouyang Y, Walsh AC, et al. Relationship between optical coherence tomography retinal parameters and visual acuity in diabetic macular edema. Ophthalmology. 2010 Dec;117(12):2379-86. PubMed PMID: 20561684. Epub 2010/06/22. eng.
171. Keane PA, Heussen FM, Ouyang Y, Mokwa N, Walsh AC, Tufail A, et al. Assessment of differential pharmacodynamic effects using optical coherence tomography in neovascular age-related macular degeneration. Invest Ophthalmol Vis Sci. 2012 Mar;53(3):1152-61. PubMed PMID: 22281826. Pubmed Central PMCID: 3339900. Epub 2012/01/28. eng.
172. Sadda SR, Wu Z, Walsh AC, Richine L, Dougall J, Cortez R, et al. Errors in retinal thickness measurements obtained by optical coherence tomography. Ophthalmology. 2006 Feb;113(2):285-93. PubMed PMID: 16406542. Epub 2006/01/13. eng.
173. Sadda SR, Joeres S, Wu Z, Updike P, Romano P, Collins AT, et al. Error correction and quantitative subanalysis of optical coherence tomography data using computer-assisted grading. Invest Ophthalmol Vis Sci. 2007 Feb;48(2):839-48. PubMed PMID: 17251486. Epub 2007/01/26. eng.
174. Hermann R, Turpeinen H, Laine AP, Veijola R, Knip M, Simell O, et al. HLA DR-DQ-encoded genetic determinants of childhood-onset type 1 diabetes in Finland: an analysis of 622 nuclear families. Tissue antigens. 2003 Aug;62(2):162-9. PubMed PMID: 12889996.
175. Hermann R, Veijola R, Sipila I, Knip M, Akerblom HK, Simell O, et al. -to: Pani MA, Van Autreve J, Van Der Auwera BJ, Gorus FK, Badenhoop K (2002) Non-transmitted maternal HLA DQ2 or DQ8 alleles and risk of Type I diabetes in offspring: the importance of foetal or post partum exposure to diabetogenic molecules. Diabetologia 45:1340-1343. Diabetologia. 2003 Apr;46(4):588-9; author reply 91-2. PubMed PMID: 12684751.
176. Kukko M, Kimpimaki T, Kupila A, Korhonen S, Kulmala P, Savola K, et al. Signs of beta-cell autoimmunity and HLA-defined diabetes susceptibility in the Finnish population: the sib cohort from the Type 1 Diabetes Prediction and Prevention Study. Diabetologia. 2003 Jan;46(1):65-70. PubMed PMID: 12637984.
177. Dorman JS, Charron-Prochownik D, Siminerio L, Ryan C, Poole C, Becker D, et al. Need for genetic education for type 1 diabetes. Archives of pediatrics & adolescent medicine. 2003 Sep;157(9):935-6; author reply 6. PubMed PMID: 12963603.
178. Serban V, Enache A, Vlad A, Sima A, Rosu M, Rosca A, et al. GADA and islet cell antibodies in Romanian children and adolescents with diabetes mellitus. Romanian journal of internal medicine = Revue roumaine de medecine interne. 2004;42(2):325-32. PubMed PMID: 15529623.
179. Parr JC, Spears GF. General caliber of the retinal arteries expressed as the equivalent width of the central retinal artery. Am J Ophthalmol. 1974 Apr;77(4):472-7. PubMed PMID: 4819451.

180. Hubbard LD, Brothers RJ, King WN, Clegg LX, Klein R, Cooper LS, et al. Methods for evaluation of retinal microvascular abnormalities associated with hypertension/sclerosis in the Atherosclerosis Risk in Communities Study. Ophthalmology. 1999 Dec;106(12):2269-80. PubMed PMID: 10599656.
181. Sherry LM, Wang JJ, Rochtchina E, Wong T, Klein R, Hubbard L, et al. Reliability of computer-assisted retinal vessel measurementin a population. Clin Experiment Ophthalmol. 2002 Jun;30(3):179-82. PubMed PMID: 12010210.
182. Keane PA, Liakopoulos S, Ongchin SC, Heussen FM, Msutta S, Chang KT, et al. Quantitative subanalysis of optical coherence tomography after treatment with ranibizumab for neovascular age-related macular degeneration. Invest Ophthalmol Vis Sci. 2008 Jul;49(7):3115-20. PubMed PMID: 18408176. Pubmed Central PMCID: 2673192. Epub 2008/04/15. eng.
183. Pons ME, Garcia-Valenzuela E. Redefining the limit of the outer retina in optical coherence tomography scans. Ophthalmology. 2005 Jun;112(6):1079-85. PubMed PMID: 15882904. Epub 2005/05/11. eng.
184. Costa RA, Calucci D, Skaf M, Cardillo JA, Castro JC, Melo LA, Jr., et al. Optical coherence tomography 3: Automatic delineation of the outer neural retinal boundary and its influence on retinal thickness measurements. Invest Ophthalmol Vis Sci. 2004 Jul;45(7):2399-406. PubMed PMID: 15223823. Epub 2004/06/30. eng.
185. Bland JM, Altman DG. Measurement error. BMJ. 1996 Sep 21;313(7059):744. PubMed PMID: 8819450. Pubmed Central PMCID: 2352101. Epub 1996/09/21. eng.
186. Bland JM, Altman DG. Statistical methods for assessing agreement between two methods of clinical measurement. Lancet. 1986 Feb 8;1(8476):307-10. PubMed PMID: 2868172. Epub 1986/02/08. eng.
187. Sim DA, Keane PA, Zarranz-Ventura J, Fung S, Powner MB, Platteau E, et al. The effects of macular ischemia on visual acuity in diabetic retinopathy. Investigative ophthalmology & visual science. 2013 Mar;54(3):2353-60. PubMed PMID: 23449720.
188. Sakata K, Funatsu H, Harino S, Noma H, Hori S. Relationship of macular microcirculation and retinal thickness with visual acuity in diabetic macular edema. Ophthalmology. 2007 Nov;114(11):2061-9. PubMed PMID: 17445900. Epub 2007/04/21. eng.
189. Sander B, Larsen M, Engler C, Lund-Andersen H, Parving HH. Early changes in diabetic retinopathy: capillary loss and blood-retina barrier permeability in relation to metabolic control. Acta Ophthalmol (Copenh). 1994 Oct;72(5):553-9. PubMed PMID: 7887152. Epub 1994/10/01. eng.
190. Hilmantel G, Applegate RA, van Heuven WA, Stowers SP, Bradley A, Lee BL. Entoptic foveal avascular zone measurement and diabetic retinopathy. Optom Vis Sci. 1999 Dec;76(12):826-31. PubMed PMID: 10612403. Epub 1999/12/28. eng.
191. Sleightholm MA, Arnold J, Kohner EM. Diabetic retinopathy: I. The measurement of intercapillary area in normal retinal angiograms. J Diabet Complications. 1988 Jul-Sep;2(3):113-6. PubMed PMID: 2975658. Epub 1988/07/01. eng.
192. Dubis AM, Hansen BR, Cooper RF, Beringer J, Dubra A, Carroll J. The Relationship Between the Foveal Avascular Zone and Foveal Pit Morphology. Invest Ophthalmol Vis Sci. 2012 Feb 8. PubMed PMID: 22323466. Epub 2012/02/11. Eng.
193. Tam J, Dhamdhere KP, Tiruveedhula P, Manzanera S, Barez S, Bearse MA, Jr., et al. Disruption of the retinal parafoveal capillary network in type 2 diabetes before the onset of diabetic retinopathy. Invest Ophthalmol Vis Sci. 2011 Nov;52(12):9257-66. PubMed PMID: 22039250. Epub 2011/11/01. eng.
194. Hamanaka T, Akabane N, Yajima T, Takahashi T, Tanabe A. Retinal ischemia and angle neovascularization in proliferative diabetic retinopathy. Am J Ophthalmol. 2001 Nov;132(5):648-58. PubMed PMID: 11704026. Epub 2001/11/13. eng.

195. Mehre KS. Incidence of Cilio-Retinal Artery in Indians. Br J Ophthalmol. 1965 Jan;49:52-3. PubMed PMID: 14255602. Pubmed Central PMCID: 506062. Epub 1965/01/01. eng.
196. Wang RS. [Cilioretinal arteries under fundus fluorescein angiography]. Zhonghua Yan Ke Za Zhi. 1991 Jul;27(4):219-20. PubMed PMID: 1935448. Epub 1991/07/01. chi.
197. Knudsen LL, Lervang HH. Can a cilio-retinal artery influence diabetic maculopathy? Br J Ophthalmol. 2002 Nov;86(11):1252-5. PubMed PMID: 12386082. Pubmed Central PMCID: 1771374. Epub 2002/10/19. eng.
198. Landa G, Amde W, Haileselassie Y, Rosen RB. Cilioretinal arteries in diabetic eyes are associated with increased retinal blood flow velocity and occurrence of diabetic macular edema. Retina. 2011 Feb;31(2):304-11. PubMed PMID: 21102372. Epub 2010/11/26. eng.
199. Carpineto P, Ciancaglini M, Di Antonio L, Gavalas C, Mastropasqua L. Fundus microperimetry patterns of fixation in type 2 diabetic patients with diffuse macular edema. Retina. 2007 Jan;27(1):21-9. PubMed PMID: 17218911. Epub 2007/01/16. eng.
200. Al Shafaee M, Shenoy R, Bialasiewicz AA, Ganguly SS, Bhargava K. Macular function in prediabetic and diabetic Omani adults: a microperimetric evaluation. Eur J Ophthalmol. 2011 Nov-Dec;21(6):771-6. PubMed PMID: 21319136. Epub 2011/02/15. eng.
201. Nakamura Y, Mitamura Y, Ogata K, Arai M, Takatsuna Y, Yamamoto S. Functional and morphological changes of macula after subthreshold micropulse diode laser photocoagulation for diabetic macular oedema. Eye (Lond). 2010 May;24(5):784-8. PubMed PMID: 19680274. Epub 2009/08/15. eng.
202. Hatef E, Colantuoni E, Wang J, Ibrahim M, Shulman M, Adhi F, et al. The relationship between macular sensitivity and retinal thickness in eyes with diabetic macular edema. Am J Ophthalmol. 2011 Sep;152(3):400-5 e2. PubMed PMID: 21696702. Epub 2011/06/24. eng.
203. Soliman W, Hasler P, Sander B, Larsen M. Local retinal sensitivity in relation to specific retinopathy lesions in diabetic macular oedema. Acta Ophthalmol. 2010 Aug 31. PubMed PMID: 20809906. Epub 2010/09/03. Eng.
204. Tyrberg M, Ponjavic V, Lovestam-Adrian M. Multifocal electroretinogram (mfERG) in patients with diabetes mellitus and an enlarged foveal avascular zone (FAZ). Doc Ophthalmol. 2008 Nov;117(3):185-9. PubMed PMID: 18324430. Epub 2008/03/08. eng.
205. Hee MR, Puliafito CA, Duker JS, Reichel E, Coker JG, Wilkins JR, et al. Topography of diabetic macular edema with optical coherence tomography. Ophthalmology. 1998 Feb;105(2):360-70. PubMed PMID: 9479300. Pubmed Central PMCID: 2923575. Epub 1998/02/28. eng.
206. Forooghian F, Stetson PF, Meyer SA, Chew EY, Wong WT, Cukras C, et al. Relationship between photoreceptor outer segment length and visual acuity in diabetic macular edema. Retina. 2010 Jan;30(1):63-70. PubMed PMID: 19952996. Pubmed Central PMCID: 3021331. Epub 2009/12/03. eng.
207. Browning DJ, Glassman AR, Aiello LP, Beck RW, Brown DM, Fong DS, et al. Relationship between optical coherence tomography-measured central retinal thickness and visual acuity in diabetic macular edema. Ophthalmology. 2007 Mar;114(3):525-36. PubMed PMID: 17123615. Pubmed Central PMCID: 2585542. Epub 2006/11/25. eng.
208. Bandello F, Polito A, Del Borrello M, Zemella N, Isola M. "Light" versus "classic" laser treatment for clinically significant diabetic macular oedema. Br J Ophthalmol. 2005 Jul;89(7):864-70. PubMed PMID: 15965168. Pubmed Central PMCID: 1772712. Epub 2005/06/21. eng.
209. Laursen ML, Moeller F, Sander B, Sjoelie AK. Subthreshold micropulse diode laser treatment in diabetic macular oedema. Br J Ophthalmol. 2004 Sep;88(9):1173-9. PubMed PMID: 15317711. Pubmed Central PMCID: 1772323. Epub 2004/08/20. eng.

210. Rossi EA, Roorda A. The relationship between visual resolution and cone spacing in the human fovea. Nat Neurosci. 2010 Feb;13(2):156-7. PubMed PMID: 20023654. Pubmed Central PMCID: 2822659. Epub 2009/12/22. eng.
211. Frangieh GT, Green WR, Barraquer-Somers E, Finkelstein D. Histopathologic study of nine branch retinal vein occlusions. Arch Ophthalmol. 1982 Jul;100(7):1132-40. PubMed PMID: 6178389. Epub 1982/07/01. eng.
212. Green WR, Chan CC, Hutchins GM, Terry JM. Central retinal vein occlusion: a prospective histopathologic study of 29 eyes in 28 cases. Retina. 1981;1(1):27-55. PubMed PMID: 15633406. Epub 1981/01/01. eng.
213. van Dijk HW, Kok PH, Garvin M, Sonka M, Devries JH, Michels RP, et al. Selective loss of inner retinal layer thickness in type 1 diabetic patients with minimal diabetic retinopathy. Invest Ophthalmol Vis Sci. 2009 Jul;50(7):3404-9. PubMed PMID: 19151397. Pubmed Central PMCID: 2937215. Epub 2009/01/20. eng.
214. Yeung L, Lima VC, Garcia P, Landa G, Rosen RB. Correlation between spectral domain optical coherence tomography findings and fluorescein angiography patterns in diabetic macular edema. Ophthalmology. 2009 Jun;116(6):1158-67. PubMed PMID: 19395034. Epub 2009/04/28. eng.
215. Kaiser PK. Prospective evaluation of visual acuity assessment: a comparison of snellen versus ETDRS charts in clinical practice (An AOS Thesis). Transactions of the American Ophthalmological Society. 2009 Dec;107:311-24. PubMed PMID: 20126505. Pubmed Central PMCID: 2814576.
216. Do DV, Schmidt-Erfurth U, Gonzalez VH, Gordon CM, Tolentino M, Berliner AJ, et al. The DA VINCI Study: phase 2 primary results of VEGF Trap-Eye in patients with diabetic macular edema. Ophthalmology. 2011 Sep;118(9):1819-26. PubMed PMID: 21546089. Epub 2011/05/07. eng.
217. Elman MJ, Aiello LP, Beck RW, Bressler NM, Bressler SB, Edwards AR, et al. Randomized trial evaluating ranibizumab plus prompt or deferred laser or triamcinolone plus prompt laser for diabetic macular edema. Ophthalmology. 2010 Jun;117(6):1064-77 e35. PubMed PMID: 20427088. Pubmed Central PMCID: 2937272. Epub 2010/04/30. eng.
218. Massin P, Bandello F, Garweg JG, Hansen LL, Harding SP, Larsen M, et al. Safety and efficacy of ranibizumab in diabetic macular edema (RESOLVE Study): a 12-month, randomized, controlled, double-masked, multicenter phase II study. Diabetes Care. 2010 Nov;33(11):2399-405. PubMed PMID: 20980427. Pubmed Central PMCID: 2963502. Epub 2010/10/29. eng.
219. Michaelides M, Kaines A, Hamilton RD, Fraser-Bell S, Rajendram R, Quhill F, et al. A prospective randomized trial of intravitreal bevacizumab or laser therapy in the management of diabetic macular edema (BOLT study) 12-month data: report 2. Ophthalmology. 2010 Jun;117(6):1078-86 e2. PubMed PMID: 20416952. Epub 2010/04/27. eng.
220. Ticho U, Patz A. The role of capillary perfusion in the management of diabetic macular edema. Am J Ophthalmol. 1973 Dec;76(6):880-6. PubMed PMID: 4796764. Epub 1973/12/01. eng.
221. Hussain B, Saleh GM, Sivaprasad S, Hammond CJ. Changing from Snellen to LogMAR: debate or delay? Clin Experiment Ophthalmol. 2006 Jan-Feb;34(1):6-8. PubMed PMID: 16451251. Epub 2006/02/03. eng.
222. Kniestedt C, Stamper RL. Visual acuity and its measurement. Ophthalmol Clin North Am. 2003 Jun;16(2):155-70, v. PubMed PMID: 12809155. Epub 2003/06/18. eng.
223. Mackenzie S, Schmermer C, Charnley A, Sim D, Vikas T, Dumskyj M, et al. SDOCT imaging to identify macular pathology in patients diagnosed with diabetic maculopathy by a digital photographic retinal screening programme. PloS one. 2011;6(5):e14811. PubMed PMID: 21573106. Pubmed Central PMCID: 3089611.

224. Wessel MM, Nair N, Aaker GD, Ehrlich JR, D'Amico DJ, Kiss S. Peripheral retinal ischaemia, as evaluated by ultra-widefield fluorescein angiography, is associated with diabetic macular oedema. Br J Ophthalmol. 2012 May;96(5):694-8. PubMed PMID: 22423055. Pubmed Central PMCID: 3329634.
225. Klein R, Klein BE, Moss SE, Cruickshanks KJ. The Wisconsin Epidemiologic Study of diabetic retinopathy. XIV. Ten-year incidence and progression of diabetic retinopathy. Arch Ophthalmol. 1994 Sep;112(9):1217-28. PubMed PMID: 7619101.
226. Wong TY, Cheung N, Tay WT, Wang JJ, Aung T, Saw SM, et al. Prevalence and risk factors for diabetic retinopathy: the Singapore Malay Eye Study. Ophthalmology. 2008 Nov;115(11):1869-75. PubMed PMID: 18584872.
227. Farkas E, de Vos RA, Donka G, Jansen Steur EN, Mihaly A, Luiten PG. Age-related microvascular degeneration in the human cerebral periventricular white matter. Acta neuropathologica. 2006 Feb;111(2):150-7. PubMed PMID: 16453142.
228. Kador PF, Takahashi Y, Akagi Y, Blessing K, Randazzo J, Wyman M. Age-dependent retinal capillary pericyte degeneration in galactose-fed dogs. J Ocul Pharmacol Ther. 2007 Feb;23(1):63-9. PubMed PMID: 17341153.
229. Mullins RF, Johnson MN, Faidley EA, Skeie JM, Huang J. Choriocapillaris vascular dropout related to density of drusen in human eyes with early age-related macular degeneration. Invest Ophthalmol Vis Sci. 2011 Mar;52(3):1606-12. PubMed PMID: 21398287. Pubmed Central PMCID: 3101687.
230. Roy MS, Klein R, Janal MN. Relationship of retinal vessel caliber to cardiovascular disease and mortality in African Americans with type 1 diabetes mellitus. Arch Ophthalmol. 2012 May;130(5):561-7. PubMed PMID: 22652842.
231. Ding J, Cheung CY, Ikram MK, Zheng YF, Cheng CY, Lamoureux EL, et al. Early retinal arteriolar changes and peripheral neuropathy in diabetes. Diabetes Care. 2012 May;35(5):1098-104. PubMed PMID: 22374638. Pubmed Central PMCID: 3329839.
232. Lindley RI, Wang JJ, Wong MC, Mitchell P, Liew G, Hand P, et al. Retinal microvasculature in acute lacunar stroke: a cross-sectional study. The Lancet Neurology. 2009 Jul;8(7):628-34. PubMed PMID: 19481977.
233. Wang L, Wong TY, Sharrett AR, Klein R, Folsom AR, Jerosch-Herold M. Relationship between retinal arteriolar narrowing and myocardial perfusion: multi-ethnic study of atherosclerosis. Hypertension. 2008 Jan;51(1):119-26. PubMed PMID: 17998474.
234. Hemminki V, Laakso J, Kahonen M, Turjanmaa V, Uusitalo H, Lehtimaki T, et al. Plasma asymmetric dimethylarginine and retinal vessel diameters in middle-aged men. Metabolism. 2007 Oct;56(10):1305-10. PubMed PMID: 17884437.
235. Klein R, Klein BE, Moss SE, Wong TY, Sharrett AR. Retinal vascular caliber in persons with type 2 diabetes: the Wisconsin Epidemiological Study of Diabetic Retinopathy: XX. Ophthalmology. 2006 Sep;113(9):1488-98. PubMed PMID: 16828517.
236. Kifley A, Wang JJ, Cugati S, Wong TY, Mitchell P. Retinal vascular caliber, diabetes, and retinopathy. Am J Ophthalmol. 2007 Jun;143(6):1024-6. PubMed PMID: 17524767.
237. Klein R, Klein BE, Moss SE, Wong TY, Hubbard L, Cruickshanks KJ, et al. The relation of retinal vessel caliber to the incidence and progression of diabetic retinopathy: XIX: the Wisconsin Epidemiologic Study of Diabetic Retinopathy. Arch Ophthalmol. 2004 Jan;122(1):76-83. PubMed PMID: 14718299.
238. Tolentino MJ, McLeod DS, Taomoto M, Otsuji T, Adamis AP, Lutty GA. Pathologic features of vascular endothelial growth factor-induced retinopathy in the nonhuman primate. Am J Ophthalmol. 2002 Mar;133(3):373-85. PubMed PMID: 11860975.
239. Tolentino MJ, Miller JW, Gragoudas ES, Jakobiec FA, Flynn E, Chatzistefanou K, et al. Intravitreous injections of vascular endothelial growth factor produce retinal ischemia and microangiopathy in an adult primate. Ophthalmology. 1996 Nov;103(11):1820-8. PubMed PMID: 8942877.

240. Malik RA, Li C, Aziz W, Olson JA, Vohra A, McHardy KC, et al. Elevated plasma CD105 and vitreous VEGF levels in diabetic retinopathy. J Cell Mol Med. 2005 Jul-Sep;9(3):692-7. PubMed PMID: 16202216.
241. Pakter HM, Fuchs SC, Maestri MK, Moreira LB, Dei Ricardi LM, Pamplona VF, et al. Computer-assisted methods to evaluate retinal vascular caliber: what are they measuring? Investigative ophthalmology & visual science. 2011 Feb;52(2):810-5. PubMed PMID: 21051725.
242. Nejentsev S, Laine AP, Simell O, Ilonen J. Intercellular adhesion molecule-1 (ICAM-1) K469E polymorphism: no association with type 1 diabetes among Finns. Tissue antigens. 2000 Jun;55(6):568-70. PubMed PMID: 10902613.
243. Vukovic R, Simic M, Tasic M. [Analysis of ischemic lesions of the liver after various periods of warm and cold ischemia]. Medicinski pregled. 1996;49(7-8):263-7. PubMed PMID: 8926941. Analiza ishemijskih lezija jetre u razlicitim intervalima tople i hladne ishemije.
244. Koltz MT, Tosun C, Kurland DB, Coksaygan T, Castellani RJ, Ivanova S, et al. Tandem insults of prenatal ischemia plus postnatal raised intrathoracic pressure in a novel rat model of encephalopathy of prematurity. Journal of neurosurgery Pediatrics. 2011 Dec;8(6):628-39. PubMed PMID: 22132923. Pubmed Central PMCID: 3465975.
245. Simerabet M, Robin E, Aristi I, Adamczyk S, Tavernier B, Vallet B, et al. Preconditioning by an in situ administration of hydrogen peroxide: involvement of reactive oxygen species and mitochondrial ATP-dependent potassium channel in a cerebral ischemia-reperfusion model. Brain research. 2008 Nov 13;1240:177-84. PubMed PMID: 18793617.
246. Durrani OM, Meads CA, Murray PI. Uveitis: a potentially blinding disease. Ophthalmologica. 2004 Jul-Aug;218(4):223-36. PubMed PMID: 15258410. Epub 2004/07/20. eng.
247. Darrell RW, Wagener HP, Kurland LT. Epidemiology of uveitis. Incidence and prevalence in a small urban community. Arch Ophthalmol. 1962 Oct;68:502-14. PubMed PMID: 13883604. Epub 1962/10/01. eng.
248. Wakefield D, Chang JH. Epidemiology of uveitis. Int Ophthalmol Clin. 2005 Spring;45(2):1-13. PubMed PMID: 15791154. Epub 2005/03/26. eng.
249. Nussenblatt RB. The natural history of uveitis. Int Ophthalmol. 1990 Oct;14(5-6):303-8. PubMed PMID: 2249907. Epub 1990/10/01. eng.
250. Rothova A, Suttorp-van Schulten MS, Frits Treffers W, Kijlstra A. Causes and frequency of blindness in patients with intraocular inflammatory disease. Br J Ophthalmol. 1996 Apr;80(4):332-6. PubMed PMID: 8703885. Pubmed Central PMCID: 505460. Epub 1996/04/01. eng.
251. Denniston AK, Dick AD. Systemic therapies for inflammatory eye disease: past, present and future. BMC Ophthalmol. 2013;13:18. PubMed PMID: 23617902. Pubmed Central PMCID: 3639939. Epub 2013/04/27. eng.
252. Rothova A, Buitenhuis HJ, Meenken C, Brinkman CJ, Linssen A, Alberts C, et al. Uveitis and systemic disease. Br J Ophthalmol. 1992 Mar;76(3):137-41. PubMed PMID: 1540555. Pubmed Central PMCID: 504190.
253. Weiner A, BenEzra D. Clinical patterns and associated conditions in chronic uveitis. Am J Ophthalmol. 1991 Aug 15;112(2):151-8. PubMed PMID: 1867298.
254. Henderly DE, Genstler AJ, Smith RE, Rao NA. Changing patterns of uveitis. Am J Ophthalmol. 1987 Feb 15;103(2):131-6. PubMed PMID: 3812615.
255. Marcus EI, Do DV, Shah SM, Nguyen QD, Biswas J, Levinson R. Diagnostic and therapeutic challenges. Granulomatous panuveitis. Retina. 2008 Nov-Dec;28(10):1544-9. PubMed PMID: 19009682.
256. Jones NP. Sarcoidosis and uveitis. Ophthalmol Clin North Am. 2002 Sep;15(3):319-26, vi. PubMed PMID: 12434480. Epub 2002/11/19. eng.

257. Iannuzzi MC, Rybicki BA, Teirstein AS. Sarcoidosis. N Engl J Med. 2007 Nov 22;357(21):2153-65. PubMed PMID: 18032765. Epub 2007/11/23. eng.
258. Massaro D, Katz S, Sachs M. Choroidal Tubercles. A Clue to Hematogenous Tuberculosis. Annals of internal medicine. 1964 Feb;60:231-41. PubMed PMID: 14114443.
259. Gupta A, Bansal R, Gupta V, Sharma A, Bambery P. Ocular signs predictive of tubercular uveitis. Am J Ophthalmol. 2010 Apr;149(4):562-70. PubMed PMID: 20149341.
260. Gupta V, Gupta A, Rao NA. Intraocular tuberculosis--an update. Surv Ophthalmol. 2007 Nov-Dec;52(6):561-87. PubMed PMID: 18029267. Epub 2007/11/22. eng.
261. Yeh S, Sen HN, Colyer M, Zapor M, Wroblewski K. Update on ocular tuberculosis. Curr Opin Ophthalmol. Nov;23(6):551-6. PubMed PMID: 23047173. Epub 2012/10/11. eng.
262. Babu K, Kini R, Mehta R, Philips M, Subbakrishna DK, Murthy KR. Predictors for tubercular uveitis: a comparison between biopsy-proven cases of tubercular and sarcoid uveitis. Retina. May;32(5):1017-20. PubMed PMID: 22146129. Epub 2011/12/08. eng.
263. Miserocchi E, Modorati G, Di Matteo F, Galli L, Rama P, Bandello F. Visual outcome in ocular sarcoidosis: retrospective evaluation of risk factors. Eur J Ophthalmol. Nov-Dec;21(6):802-10. PubMed PMID: 21374555. Epub 2011/03/05. eng.
264. Manousaridis K, Ong E, Stenton C, Gupta R, Browning AC, Pandit R. Clinical presentation, treatment, and outcomes in presumed intraocular tuberculosis: experience from Newcastle upon Tyne, UK. Eye (Lond). 2013 Apr;27(4):480-6. PubMed PMID: 23429412. Pubmed Central PMCID: 3626011.
265. Imrie FR, Dick AD. Biologics in the treatment of uveitis. Curr Opin Ophthalmol. 2007 Nov;18(6):481-6. PubMed PMID: 18163000.
266. Kempen JH, Daniel E, Dunn JP, Foster CS, Gangaputra S, Hanish A, et al. Overall and cancer related mortality among patients with ocular inflammation treated with immunosuppressive drugs: retrospective cohort study. Bmj. 2009;339:b2480. PubMed PMID: 19578087. Pubmed Central PMCID: 2714688.
267. Herbort CP, Tugal-Tutkun I. Editorial: Laser flare (cell) photometry: 20 years already. International ophthalmology. 2010 Oct;30(5):445-7. PubMed PMID: 20593221.
268. Herbort CP. Fluorescein and indocyanine green angiography for uveitis. Middle East African journal of ophthalmology. 2009 Oct;16(4):168-87. PubMed PMID: 20404985. Pubmed Central PMCID: 2855659.
269. Ouyang Y, Heussen FM, Mokwa N, Walsh AC, Durbin MK, Keane PA, et al. Spatial distribution of posterior pole choroidal thickness by spectral domain optical coherence tomography. Invest Ophthalmol Vis Sci. Aug;52(9):7019-26. PubMed PMID: 21810980. Pubmed Central PMCID: 3176017. Epub 2011/08/04. eng.
270. Margolis R, Spaide RF. A pilot study of enhanced depth imaging optical coherence tomography of the choroid in normal eyes. Am J Ophthalmol. 2009 May;147(5):811-5. PubMed PMID: 19232559. Epub 2009/02/24. eng.
271. Keane PA, Allie M, Turner SJ, Southworth HS, Sadda SR, Murray PI, et al. Characterization of birdshot chorioretinopathy using extramacular enhanced depth optical coherence tomography. JAMA Ophthalmol. 2013 Mar;131(3):341-50. PubMed PMID: 23307137.
272. Karampelas M, Sim DA, Keane PA, Zarranz-Ventura J, Patel PJ, Tufail A, et al. Choroidal assessment in idiopathic panuveitis using optical coherence tomography. Graefes Arch Clin Exp Ophthalmol. 2013 Aug;251(8):2029-36. PubMed PMID: 23532454.
273. Zhang X, Zuo C, Li M, Chen H, Huang S, Wen F. Spectral-Domain Optical Coherence Tomographic Findings at Each Stage of Punctate Inner Choroidopathy. Ophthalmology. 2013 Jun 11. PubMed PMID: 23769333.
274. Zarranz-Ventura J, Sim DA, Keane PA, Patel PJ, Westcott MC, Lee RW, et al. Characterization of Punctate Inner Choroidopathy Using Enhanced Depth Imaging Optical Coherence Tomography. Ophthalmology. 2014 May 20. PubMed PMID: 24856311.

275. Keane PA, Karampelas M, Sim DA, Sadda SR, Tufail A, Sen HN, et al. Objective Measurement of Vitreous Inflammation Using Optical Coherence Tomography. Ophthalmology. 2014 May 15. PubMed PMID: 24835759.
276. Nakayama M, Keino H, Okada AA, Watanabe T, Taki W, Inoue M, et al. Enhanced depth imaging optical coherence tomography of the choroid in Vogt-Koyanagi-Harada disease. Retina. 2012 Nov-Dec;32(10):2061-9. PubMed PMID: 23095726.
277. Amer R, Lois N. Punctate inner choroidopathy. Survey of ophthalmology. 2011 Jan-Feb;56(1):36-53. PubMed PMID: 21056447. Epub 2010/11/09. eng.
278. Essex RW, Wong J, Fraser-Bell S, Sandbach J, Tufail A, Bird AC, et al. Punctate inner choroidopathy: clinical features and outcomes. Archives of ophthalmology. 2010 Aug;128(8):982-7. PubMed PMID: 20696997. Epub 2010/08/11. eng.
279. Watzke RC, Packer AJ, Folk JC, Benson WE, Burgess D, Ober RR. Punctate inner choroidopathy. Am J Ophthalmol. 1984 Nov;98(5):572-84. PubMed PMID: 6208783. Epub 1984/11/01. eng.
280. Brown J, Jr., Folk JC, Reddy CV, Kimura AE. Visual prognosis of multifocal choroiditis, punctate inner choroidopathy, and the diffuse subretinal fibrosis syndrome. Ophthalmology. 1996 Jul;103(7):1100-5. PubMed PMID: 8684800. Epub 1996/07/01. eng.
281. Zhang H, Liu ZL, Sun P, Gu F. Intravitreal bevacizumab as primary treatment of choroidal neovascularization secondary to punctate inner choroidopathy: results of a 1-year prospective trial. Retina. 2012 Jun;32(6):1106-13. PubMed PMID: 22481479. Epub 2012/04/07. eng.
282. Cornish KS, Williams GJ, Gavin MP, Imrie FR. Visual and optical coherence tomography outcomes of intravitreal bevacizumab and ranibizumab in inflammatory choroidal neovascularization secondary to punctate inner choroidopathy. Eur J Ophthalmol. 2011 Jul-Aug;21(4):440-5. PubMed PMID: 21188681. Epub 2010/12/29. eng.
283. Rouvas A, Petrou P, Douvali M, Ntouraki A, Vergados I, Georgalas I, et al. Intravitreal ranibizumab for the treatment of inflammatory choroidal neovascularization. Retina. 2011 May;31(5):871-9. PubMed PMID: 21358461. Epub 2011/03/02. eng.
284. Menezo V, Cuthbertson F, Downes SM. Positive response to intravitreal ranibizumab in the treatment of choroidal neovascularization secondary to punctate inner choroidopathy. Retina. 2010 Oct;30(9):1400-4. PubMed PMID: 20224465. Epub 2010/03/13. eng.
285. Chan WM, Lai TY, Liu DT, Lam DS. Intravitreal bevacizumab (avastin) for choroidal neovascularization secondary to central serous chorioretinopathy, secondary to punctate inner choroidopathy, or of idiopathic origin. Am J Ophthalmol. 2007 Jun;143(6):977-83. PubMed PMID: 17459318. Epub 2007/04/27. eng.
286. Gerstenblith AT, Thorne JE, Sobrin L, Do DV, Shah SM, Foster CS, et al. Punctate inner choroidopathy: a survey analysis of 77 persons. Ophthalmology. 2007 Jun;114(6):1201-4. PubMed PMID: 17434588. Epub 2007/04/17. eng.
287. Tiffin PA, Maini R, Roxburgh ST, Ellingford A. Indocyanine green angiography in a case of punctate inner choroidopathy. Br J Ophthalmol. 1996 Jan;80(1):90-1. PubMed PMID: 8664243. Pubmed Central PMCID: 505392. Epub 1996/01/01. eng.
288. Sivaprasad S, Ikeji F, Xing W, Lightman S. Tomographic assessment of therapeutic response to uveitic macular oedema. Clinical & experimental ophthalmology. 2007 Nov;35(8):719-23. PubMed PMID: 17997774. Epub 2007/11/14. eng.
289. Iannetti L, Accorinti M, Liverani M, Caggiano C, Abdulaziz R, Pivetti-Pezzi P. Optical coherence tomography for classification and clinical evaluation of macular edema in patients with uveitis. Ocul Immunol Inflamm. 2008 Jul-Aug;16(4):155-60. PubMed PMID: 18716950. Epub 2008/08/22. eng.
290. Gallagher MJ, Yilmaz T, Cervantes-Castaneda RA, Foster CS. The characteristic features of optical coherence tomography in posterior uveitis. Br J Ophthalmol. 2007

Dec;91(12):1680-5. PubMed PMID: 17591668. Pubmed Central PMCID: 2095553. Epub 2007/06/27. eng.
291. Chen FK, Tufail A. Multifocal outer retinopathy in a patient with multifocal inner choroidopathy. Clinical & experimental ophthalmology. 2011 Sep-Oct;39(7):700-3. PubMed PMID: 22452687. Epub 2012/03/29. eng.
292. Sim DA, Sheth HG, Kaines A, Tufail A. Punctate inner choroidopathy-associated choroidal neovascular membranes during pregnancy. Eye (Lond). 2008 May;22(5):725-7. PubMed PMID: 18369374. Epub 2008/03/29. eng.
293. Yukari J, Gomi F, Ikuno Y. Spectral-Domain Optical Coherence Tomographic findings in punctate inner choroidopathy. Retinal Cases and Brief Reports. 2012;6:189-92.
294. Channa R, Ibrahim M, Sepah Y, Turkcuoglu P, Lee JH, Khwaja A, et al. Characterization of macular lesions in punctate inner choroidopathy with spectral domain optical coherence tomography. Journal of ophthalmic inflammation and infection. 2012 Sep;2(3):113-20. PubMed PMID: 22210152. Pubmed Central PMCID: 3438299. Epub 2012/01/03. eng.
295. Stepien KE, Carroll J. Using spectral-domain optical coherence tomography to follow outer retinal structure changes in a patient with recurrent punctate inner choroidopathy. J Ophthalmol. 2011;2011:753741. PubMed PMID: 21772986. Pubmed Central PMCID: 3136150. Epub 2011/07/21. eng.
296. Fong AH, Li KK, Wong D. Choroidal evaluation using enhanced depth imaging spectral-domain optical coherence tomography in Vogt-Koyanagi-Harada disease. Retina. 2011 Mar;31(3):502-9. PubMed PMID: 21336069.
297. Fujiwara T, Imamura Y, Margolis R, Slakter JS, Spaide RF. Enhanced depth imaging optical coherence tomography of the choroid in highly myopic eyes. Am J Ophthalmol. 2009 Sep;148(3):445-50. PubMed PMID: 19541286. Epub 2009/06/23. eng.
298. Nussenblatt RB, Palestine AG, Chan CC, Roberge F. Standardization of vitreal inflammatory activity in intermediate and posterior uveitis. Ophthalmology. 1985 Apr;92(4):467-71. PubMed PMID: 4000641. Epub 1985/04/01. eng.
299. Jabs DA, Nussenblatt RB, Rosenbaum JT. Standardization of uveitis nomenclature for reporting clinical data. Results of the First International Workshop. Am J Ophthalmol. 2005 Sep;140(3):509-16. PubMed PMID: 16196117. Epub 2005/10/01. eng.
300. Madow B, Galor A, Feuer WJ, Altaweel MM, Davis JL. Validation of a photographic vitreous haze grading technique for clinical trials in uveitis. Am J Ophthalmol. 2011 Aug;152(2):170-6 e1. PubMed PMID: 21652026. Epub 2011/06/10. eng.
301. Davis JL, Madow B, Cornett J, Stratton R, Hess D, Porciatti V, et al. Scale for photographic grading of vitreous haze in uveitis. Am J Ophthalmol. 2010 Nov;150(5):637-41 e1. PubMed PMID: 20719302. Pubmed Central PMCID: 3220938. Epub 2010/08/20. eng.
302. Hee MR, Puliafito CA, Wong C, Duker JS, Reichel E, Rutledge B, et al. Quantitative assessment of macular edema with optical coherence tomography. Arch Ophthalmol. 1995 Aug;113(8):1019-29. PubMed PMID: 7639652. Epub 1995/08/01. eng.
303. Keane PA, Liakopoulos S, Ongchin SC, Heussen FM, Msutta S, Chang KT, et al. Quantitative subanalysis of optical coherence tomography after treatment with ranibizumab for neovascular age-related macular degeneration. Invest Ophthalmol Vis Sci. 2008 Jul;49(7):3115-20. PubMed PMID: 18408176. Pubmed Central PMCID: 2673192. Epub 2008/04/15. eng.
304. Saito M, Barbazetto IA, Spaide RF. Intravitreal cellular infiltrate imaged as punctate spots by spectral-domain optical coherence tomography in eyes with posterior segment inflammatory disease. Retina. 2013 Mar;33(3):559-65. PubMed PMID: 23042101. Epub 2012/10/09. eng.
305. Sonoda S, Sakamoto T, Shirasawa M, Yamashita T, Otsuka H, Terasaki H. Correlation between reflectivity of subretinal fluid in OCT images and concentration of intravitreal VEGF

in eyes with diabetic macular edema. Invest Ophthalmol Vis Sci. 2013;Jul 16 ePub ahead of print.
306. Barthelmes D, Gillies MC, Sutter FK. Quantitative OCT analysis of idiopathic perifoveal telangiectasia. Invest Ophthalmol Vis Sci. 2008 May;49(5):2156-62. PubMed PMID: 18436849. Epub 2008/04/26. eng.
307. Barthelmes D, Sutter FK, Gillies MC. Differential optical densities of intraretinal spaces. Invest Ophthalmol Vis Sci. 2008 Aug;49(8):3529-34. PubMed PMID: 18441298. Epub 2008/04/29. eng.
308. Ahlers C, Golbaz I, Einwallner E, Dunavolgyi R, Malamos P, Stock G, et al. Identification of optical density ratios in subretinal fluid as a clinically relevant biomarker in exudative macular disease. Invest Ophthalmol Vis Sci. 2009 Jul;50(7):3417-24. PubMed PMID: 19168899. Epub 2009/01/27. eng.
309. Neudorfer M, Weinberg A, Loewenstein A, Barak A. Differential optical density of subretinal spaces. Invest Ophthalmol Vis Sci. 2012 May;53(6):3104-10. PubMed PMID: 22499985. Epub 2012/04/14. eng.
310. Horii T, Murakami T, Nishijima K, Akagi T, Uji A, Arakawa N, et al. Relationship between fluorescein pooling and optical coherence tomographic reflectivity of cystoid spaces in diabetic macular edema. Ophthalmology. 2012 May;119(5):1047-55. PubMed PMID: 22330965. Epub 2012/02/15. eng.
311. Murakami T, Nishijima K, Akagi T, Uji A, Horii T, Ueda-Arakawa N, et al. Optical coherence tomographic reflectivity of photoreceptors beneath cystoid spaces in diabetic macular edema. Invest Ophthalmol Vis Sci. 2012 Mar;53(3):1506-11. PubMed PMID: 22323463. Epub 2012/02/11. eng.
312. Herbort CP, Rao NA, Mochizuki M. International criteria for the diagnosis of ocular sarcoidosis: results of the first International Workshop On Ocular Sarcoidosis (IWOS). Ocul Immunol Inflamm. 2009 May-Jun;17(3):160-9. PubMed PMID: 19585358. Epub 2009/07/09. eng.
313. Takase H, Shimizu K, Yamada Y, Hanada A, Takahashi H, Mochizuki M. Validation of international criteria for the diagnosis of ocular sarcoidosis proposed by the first international workshop on ocular sarcoidosis. Jpn J Ophthalmol. Nov;54(6):529-36. PubMed PMID: 21191712. Epub 2010/12/31. eng.
314. Cunningham ET, Rathinam SR. TB or not TB? The perennial question. Br J Ophthalmol. 2001 Feb;85(2):127-8. PubMed PMID: 11159470. Pubmed Central PMCID: 1723846.
315. Ang M, Cheung G, Vania M, Chen J, Yang H, Li J, et al. Aqueous cytokine and chemokine analysis in uveitis associated with tuberculosis. Molecular vision. 2012;18:565-73. PubMed PMID: 22509092. Pubmed Central PMCID: 3325289.
316. Ang M, Wong WL, Li X, Chee SP. Interferon gamma release assay for the diagnosis of uveitis associated with tuberculosis: a Bayesian evaluation in the absence of a gold standard. Br J Ophthalmol. 2013 Aug;97(8):1062-7. PubMed PMID: 23723411.
317. Itty S, Bakri SJ, Pulido JS, Herman DC, Faia LJ, Tufty GT, et al. Initial results of QuantiFERON-TB Gold testing in patients with uveitis. Eye (Lond). 2009 Apr;23(4):904-9. PubMed PMID: 18451874.
318. Mackensen F, Becker MD, Wiehler U, Max R, Dalpke A, Zimmermann S. QuantiFERON TB-Gold--a new test strengthening long-suspected tuberculous involvement in serpiginous-like choroiditis. Am J Ophthalmol. 2008 Nov;146(5):761-6. PubMed PMID: 18718569.
319. La Distia Nora R, van Velthoven ME, Ten Dam-van Loon NH, Misotten T, Bakker M, van Hagen MP, et al. Clinical manifestations of patients with intraocular inflammation and positive QuantiFERON-TB gold in-tube test in a country nonendemic for tuberculosis. Am J Ophthalmol. 2014 Apr;157(4):754-61. PubMed PMID: 24262781.
320. Pepple KL, Van Gelder R, Forooghian F. Caveats about QuantiFERON-TB gold in-tube testing for uveitis. Am J Ophthalmol. 2014 Apr;157(4):752-3. PubMed PMID: 24630206.

321. Ang M, Htoon HM, Chee SP. Diagnosis of tuberculous uveitis: clinical application of an interferon-gamma release assay. Ophthalmology. 2009 Jul;116(7):1391-6. PubMed PMID: 19576501.
322. Spaide RF, Koizumi H, Pozzoni MC. Enhanced depth imaging spectral-domain optical coherence tomography. Am J Ophthalmol. 2008 Oct;146(4):496-500. PubMed PMID: 18639219. Epub 2008/07/22. eng.
323. Sadda SR, Keane PA, Ouyang Y, Updike JF, Walsh AC. Impact of scanning density on measurements from spectral domain optical coherence tomography. Invest Ophthalmol Vis Sci. Feb;51(2):1071-8. PubMed PMID: 19797199. Pubmed Central PMCID: 2868472. Epub 2009/10/03. eng.
324. Joeres S, Tsong JW, Updike PG, Collins AT, Dustin L, Walsh AC, et al. Reproducibility of quantitative optical coherence tomography subanalysis in neovascular age-related macular degeneration. Invest Ophthalmol Vis Sci. 2007 Sep;48(9):4300-7. PubMed PMID: 17724220. Epub 2007/08/29. eng.
325. Adhi M, Lau M, Liang MC, Waheed NK, Duker JS. Analysis of the Thickness and Vascular Layers of the Choroid in Eyes with Geographic Atrophy Using Spectral-Domain Optical Coherence Tomography. Retina. 2013 Jul 18. PubMed PMID: 23873163.
326. Sim DA, Keane PA, Mehta H, Fung S, Zarranz-Ventura J, Fruttiger M, et al. Repeatability and reproducibility of choroidal vessel layer measurements in diabetic retinopathy using enhanced depth optical coherence tomography. Investigative ophthalmology & visual science. 2013 Apr;54(4):2893-901. PubMed PMID: 23538058.
327. Branchini LA, Adhi M, Regatieri CV, Nandakumar N, Liu JJ, Laver N, et al. Analysis of Choroidal Morphologic Features and Vasculature in Healthy Eyes Using Spectral-Domain Optical Coherence Tomography. Ophthalmology. 2013 May 9. PubMed PMID: 23664466. Epub 2013/05/15. Eng.
328. Sadda SR, Keane PA, Ouyang Y, Updike JF, Walsh AC. Impact of scanning density on measurements from spectral domain optical coherence tomography. Invest Ophthalmol Vis Sci. 2010 Feb;51(2):1071-8. PubMed PMID: 19797199. Pubmed Central PMCID: 2868472. Epub 2009/10/03. eng.
329. Sadda SR, Joeres S, Wu Z, Updike P, Romano P, Collins AT, et al. Error correction and quantitative subanalysis of optical coherence tomography data using computer-assisted grading. Invest Ophthalmol Vis Sci. 2007 Feb;48(2):839-48. PubMed PMID: 17251486. Epub 2007/01/26. eng.
330. Pappuru RR, Ouyang Y, Nittala MG, Hemmati HD, Keane PA, Walsh AC, et al. Relationship between outer retinal thickness substructures and visual acuity in eyes with dry age-related macular degeneration. Invest Ophthalmol Vis Sci. 2011 Aug;52(9):6743-8. PubMed PMID: 21685337. Epub 2011/06/21. eng.
331. Joeres S, Tsong JW, Updike PG, Collins AT, Dustin L, Walsh AC, et al. Reproducibility of quantitative optical coherence tomography subanalysis in neovascular age-related macular degeneration. Invest Ophthalmol Vis Sci. 2007 Sep;48(9):4300-7. PubMed PMID: 17724220. Epub 2007/08/29. eng.
332. Guyer DRS, A.P.; Green, W.R. . The choroid: structural considerations. In: Ryan SJ, editor. Retina. Philadelphia: Elsevier. 2006:33-42.
333. Ikuno Y, Maruko I, Yasuno Y, Miura M, Sekiryu T, Nishida K, et al. Reproducibility of retinal and choroidal thickness measurements in enhanced depth imaging and high-penetration optical coherence tomography. Invest Ophthalmol Vis Sci. 2011 Jul;52(8):5536-40. PubMed PMID: 21508114.
334. Rahman W, Chen FK, Yeoh J, Patel P, Tufail A, Da Cruz L. Repeatability of manual subfoveal choroidal thickness measurements in healthy subjects using the technique of enhanced depth imaging optical coherence tomography. Invest Ophthalmol Vis Sci. 2011 Apr;52(5):2267-71. PubMed PMID: 21087970.

335. Maruko I, Iida T, Sugano Y, Oyamada H, Sekiryu T, Fujiwara T, et al. Subfoveal choroidal thickness after treatment of Vogt-Koyanagi-Harada disease. Retina. 2011 Mar;31(3):510-7. PubMed PMID: 20948460.
336. Aoyagi R, Hayashi T, Masai A, Mitooka K, Gekka T, Kozaki K, et al. Subfoveal choroidal thickness in multiple evanescent white dot syndrome. Clinical & experimental optometry. 2012 Mar;95(2):212-7. PubMed PMID: 22023216.
337. Yuzawa M, Kawamura A, Matsui M. Indocyanine green video-angiographic findings in Harada's disease. Jpn J Ophthalmol. 1993;37(4):456-66. PubMed PMID: 8145391.
338. Oshima Y, Harino S, Hara Y, Tano Y. Indocyanine green angiographic findings in Vogt-Koyanagi-Harada disease. Am J Ophthalmol. 1996 Jul;122(1):58-66. PubMed PMID: 8659599.
339. Obana A, Kusumi M, Miki T. Indocyanine green angiographic aspects of multiple evanescent white dot syndrome. Retina. 1996;16(2):97-104. PubMed PMID: 8724951.
340. Howe LJ, Woon H, Graham EM, Fitzke F, Bhandari A, Marshall J. Choroidal hypoperfusion in acute posterior multifocal placoid pigment epitheliopathy. An indocyanine green angiography study. Ophthalmology. 1995 May;102(5):790-8. PubMed PMID: 7777278.
341. Machida S, Tanaka M, Murai K, Takahashi T, Tazawa Y. Choroidal circulatory disturbance in ocular sarcoidosis without the appearance of retinal lesions or loss of visual function. Jpn J Ophthalmol. 2004 Jul-Aug;48(4):392-6. PubMed PMID: 15295669.
342. Atmaca LS, Sonmez PA. Fluorescein and indocyanine green angiography findings in Behcet's disease. Br J Ophthalmol. 2003 Dec;87(12):1466-8. PubMed PMID: 14660454. Pubmed Central PMCID: 1920565.
343. Howe LJ, Stanford MR, Graham EM, Marshall J. Choroidal abnormalities in birdshot chorioretinopathy: an indocyanine green angiography study. Eye (Lond). 1997;11 (Pt 4):554-9. PubMed PMID: 9425423.
344. Vadala M, Lodato G, Cillino S. Multifocal choroiditis: indocyanine green angiographic features. Ophthalmologica. 2001 Jan-Feb;215(1):16-21. PubMed PMID: 11125264.
345. Yasuno Y, Okamoto F, Kawana K, Yatagai T, Oshika T. Investigation of multifocal choroiditis with panuveitis by three-dimensional high-penetration optical coherence tomography. J Biophotonics. 2009 Jul;2(6-7):435-41. PubMed PMID: 19575418.
346. Iaccarino G, Cennamo G, Forte R, Cennamo G. Evaluation of posterior pole with echography and optical coherence tomography in patients with Behcet's disease. Ophthalmologica. 2009;223(4):250-5. PubMed PMID: 19299906.
347. Gass JD, Olson CL. Sarcoidosis with optic nerve and retinal involvement. Arch Ophthalmol. 1976 Jun;94(6):945-50. PubMed PMID: 938285.
348. Campo RV, Aaberg TM. Choroidal granuloma in sarcoidosis. Am J Ophthalmol. 1984 Apr;97(4):419-27. PubMed PMID: 6720813. Epub 1984/04/01. eng.
349. Spalton DJ, Sanders MD. Fundus changes in histologically confirmed sarcoidosis. Br J Ophthalmol. 1981 May;65(5):348-58. PubMed PMID: 6166318. Pubmed Central PMCID: 1039517.
350. Demirci H, Shields CL, Shields JA, Eagle RC, Jr. Ocular tuberculosis masquerading as ocular tumors. Surv Ophthalmol. 2004 Jan-Feb;49(1):78-89. PubMed PMID: 14711441.
351. Gungor SG, Akkoyun I, Reyhan NH, Yesilirmak N, Yilmaz G. Choroidal Thickness in Ocular Sarcoidosis during Quiescent Phase Using Enhanced Depth Imaging Optical Coherence Tomography. Ocul Immunol Inflamm. 2014 Jun 9:1-7. PubMed PMID: 24912003.
352. Kim M, Kim H, Kwon HJ, Kim SS, Koh HJ, Lee SC. Choroidal Thickness in Behcet's Uveitis: An Enhanced Depth Imaging-Optical Coherence Tomography and its Association with Angiographic Changes. Invest Ophthalmol Vis Sci. 2013 Jul 30. PubMed PMID: 23900605.
353. Williams TJ. Oedema and vasodilatation in inflammation: the relevance of prostaglandins. Postgrad Med J. 1977 Nov;53(625):660-2. PubMed PMID: 593990. Pubmed Central PMCID: 2496818.

354. Rassam SM, Patel V, Chen HC, Kohner EM. Regional retinal blood flow and vascular autoregulation. Eye (Lond). 1996;10 (Pt 3):331-7. PubMed PMID: 8796158.
355. Bill A, Sperber GO. Control of retinal and choroidal blood flow. Eye (Lond). 1990;4 (Pt 2):319-25. PubMed PMID: 2199239.
356. Weiter JJ, Ernest JT. Anatomy of the choroidal vasculature. Am J Ophthalmol. 1974 Oct;78(4):583-90. PubMed PMID: 4412020.
357. Rahman W, Chen FK, Yeoh J, Patel P, Tufail A, Da Cruz L. Repeatability of manual subfoveal choroidal thickness measurements in healthy subjects using the technique of enhanced depth imaging optical coherence tomography. Invest Ophthalmol Vis Sci. Apr;52(5):2267-71. PubMed PMID: 21087970. Epub 2010/11/23. eng.
358. Li XQ, Larsen M, Munch IC. Subfoveal choroidal thickness in relation to sex and axial length in 93 Danish university students. Invest Ophthalmol Vis Sci. Oct;52(11):8438-41. PubMed PMID: 21917938. Epub 2011/09/16. eng.
359. Tan CS, Ouyang Y, Ruiz H, Sadda SR. Diurnal variation of choroidal thickness in normal, healthy subjects measured by spectral domain optical coherence tomography. Invest Ophthalmol Vis Sci. Jan;53(1):261-6. PubMed PMID: 22167095. Epub 2011/12/15. eng.
360. Flores-Moreno I, Lugo F, Duker JS, Ruiz-Moreno JM. The relationship between axial length and choroidal thickness in eyes with high myopia. Am J Ophthalmol. 2013 Feb;155(2):314-9 e1. PubMed PMID: 23036569.
361. Mrejen S, Spaide RF. Optical coherence tomography: Imaging of the choroid and beyond. Surv Ophthalmol. 2013 Aug 2. PubMed PMID: 23916620.
362. Adhi M, Duker JS. Optical coherence tomography--current and future applications. Curr Opin Ophthalmol. 2013 May;24(3):213-21. PubMed PMID: 23429598.
363. Atan D, Fraser-Bell S, Plskova J, Kuffova L, Hogan A, Tufail A, et al. Punctate inner choroidopathy and multifocal choroiditis with panuveitis share haplotypic associations with IL10 and TNF loci. Invest Ophthalmol Vis Sci. 2011 May;52(6):3573-81. PubMed PMID: 21357402. Epub 2011/03/02. eng.
364. Jampol LM, Becker KG. White spot syndromes of the retina: a hypothesis based on the common genetic hypothesis of autoimmune/inflammatory disease. Am J Ophthalmol. 2003 Mar;135(3):376-9. PubMed PMID: 12614757. Epub 2003/03/05. eng.
365. Akman A, Kadayifcilar S, Aydin P. Indocyanine green angiographic findings in a case of punctate inner choroidopathy. Eur J Ophthalmol. 1998 Jul-Sep;8(3):191-4. PubMed PMID: 9793776. Epub 1998/10/30. eng.
366. Folk J, Walker J, editors. Multifocal Choroiditis with Panuveitis, Diffuse Subretinal Fibrosis, and Punctate Inner Choroidopathy. Philadelphia: Elsevier; 2006.
367. Ishihara K, Hangai M, Kita M, Yoshimura N. Acute Vogt-Koyanagi-Harada disease in enhanced spectral-domain optical coherence tomography. Ophthalmology. 2009 Sep;116(9):1799-807. PubMed PMID: 19643489. Epub 2009/08/01. eng.
368. Kimura SJ, Thygeson P, Hogan MJ. Signs and symptoms of uveitis. II. Classification of the posterior manifestations of uveitis. Am J Ophthalmol. 1959 May;47(5, Part 2):171-6. PubMed PMID: 13649856. Epub 1959/05/01. eng.
369. Kuchle M. Laser tyndallometry in anterior segment diseases. Curr Opin Ophthalmol. 1994 Aug;5(4):110-6. PubMed PMID: 10147336. Epub 1994/07/07. eng.
370. Tugal-Tutkun I, Herbort CP. Laser flare photometry: a noninvasive, objective, and quantitative method to measure intraocular inflammation. Int Ophthalmol. 2010 Oct;30(5):453-64. PubMed PMID: 19430730. Epub 2009/05/12. eng.
371. Csaky KG, Richman EA, Ferris FL, 3rd. Report from the NEI/FDA Ophthalmic Clinical Trial Design and Endpoints Symposium. Invest Ophthalmol Vis Sci. 2008 Feb;49(2):479-89. PubMed PMID: 18234989. Epub 2008/02/01. eng.

372. Lloyd R, Harris J, Wadhwa S, Chambers W. Food and Drug Administration approval process for ophthalmic drugs in the US. Curr Opin Ophthalmol. 2008 May;19(3):190-4. PubMed PMID: 18408492. Epub 2008/04/15. eng.
373. Kempen JH, Ganesh SK, Sangwan VS, Rathinam SR. Interobserver agreement in grading activity and site of inflammation in eyes of patients with uveitis. Am J Ophthalmol. 2008 Dec;146(6):813-8 e1. PubMed PMID: 18687418. Epub 2008/08/09. eng.
374. Malamos P, Ahlers C, Mylonas G, Schutze C, Deak G, Ritter M, et al. Evaluation of segmentation procedures using spectral domain optical coherence tomography in exudative age-related macular degeneration. Retina. 2011 Mar;31(3):453-63. PubMed PMID: 21221050. Epub 2011/01/12. eng.
375. Penha FM, Rosenfeld PJ, Gregori G, Falcao M, Yehoshua Z, Wang F, et al. Quantitative imaging of retinal pigment epithelial detachments using spectral-domain optical coherence tomography. Am J Ophthalmol. 2012 Mar;153(3):515-23. PubMed PMID: 22030354. Epub 2011/10/28. eng.
376. Keane PA, Mand PS, Liakopoulos S, Walsh AC, Sadda SR. Accuracy of retinal thickness measurements obtained with Cirrus optical coherence tomography. Br J Ophthalmol. 2009 Nov;93(11):1461-7. PubMed PMID: 19574239. Epub 2009/07/04. eng.
377. Itakura H, Kishi S. Aging changes of vitreomacular interface. Retina. 2011 Jul-Aug;31(7):1400-4. PubMed PMID: 21233785. Epub 2011/01/15. eng.
378. Helb HM, Charbel Issa P, Fleckenstein M, Schmitz-Valckenberg S, Scholl HP, Meyer CH, et al. Clinical evaluation of simultaneous confocal scanning laser ophthalmoscopy imaging combined with high-resolution, spectral-domain optical coherence tomography. Acta Ophthalmol. 2010 Dec;88(8):842-9. PubMed PMID: 19706019. Epub 2009/08/27. eng.
379. Drexler W, Fujimoto JG. State-of-the-art retinal optical coherence tomography. Prog Retin Eye Res. 2008 Jan;27(1):45-88. PubMed PMID: 18036865. Epub 2007/11/27. eng.
380. Grulkowski I, Liu JJ, Potsaid B, Jayaraman V, Lu CD, Jiang J, et al. Retinal, anterior segment and full eye imaging using ultrahigh speed swept source OCT with vertical-cavity surface emitting lasers. Biomed Opt Express. 2012 Nov 1;3(11):2733-51. PubMed PMID: 23162712. Pubmed Central PMCID: 3493240. Epub 2012/11/20. eng.
381. Grulkowski I, Liu JJ, Zhang JY, Potsaid B, Jayaraman V, Cable AE, et al. Reproducibility of a Long-Range Swept-Source Optical Coherence Tomography Ocular Biometry System and Comparison with Clinical Biometers. Ophthalmology. 2013 Jun 4. PubMed PMID: 23755873. Epub 2013/06/13. Eng.
382. Lee RW, Nicholson LB, Sen HN, Chan CC, Wei L, Nussenblatt RB, et al. Autoimmune and autoinflammatory mechanisms in uveitis. Seminars in immunopathology. 2014 May 24. PubMed PMID: 24858699.
383. Whitcup SM, Sodhi A, Atkinson JP, Holers VM, Sinha D, Rohrer B, et al. The role of the immune response in age-related macular degeneration. International journal of inflammation. 2013;2013:348092. PubMed PMID: 23762772. Pubmed Central PMCID: 3676958.
384. Xu H, Chen M, Forrester JV. Para-inflammation in the aging retina. Prog Retin Eye Res. 2009 Sep;28(5):348-68. PubMed PMID: 19560552.
385. Simcox JA, McClain DA. Iron and diabetes risk. Cell metabolism. 2013 Mar 5;17(3):329-41. PubMed PMID: 23473030.
386. Simha V, Shah P. The surgical cure for diabetes? The National medical journal of India. 2012 Sep-Oct;25(5):281-3. PubMed PMID: 23448628.
387. Sima C, Glogauer M. Diabetes Mellitus and Periodontal Diseases. Current diabetes reports. 2013 Feb 21. PubMed PMID: 23430581.
388. Erlich HA, Valdes AM, McDevitt S, Simen BB, Blake LA, McGowan KR, et al. Next Generation Sequencing Reveals the Association of DRB3*02:02 with Type I Diabetes. Diabetes. 2013 Mar 5. PubMed PMID: 23462545.

389. Derbent AU, Simavli SA, Kaygusuz I, Gumus, II, Yilmaz S, Yildirim M, et al. Serum hepcidin is associated with parameters of glucose metabolism in women with gestational diabetes mellitus. The journal of maternal-fetal & neonatal medicine : the official journal of the European Association of Perinatal Medicine, the Federation of Asia and Oceania Perinatal Societies, the International Society of Perinatal Obstet. 2013 Feb 27. PubMed PMID: 23356500.
390. American Diabetes A, Anderson JE, Greene MA, Griffin JW, Jr., Kohrman DB, Lorber D, et al. Diabetes and employment. Diabetes Care. 2013 Jan;36 Suppl 1:S93-7. PubMed PMID: 23264429. Pubmed Central PMCID: 3537279.
391. Jensen RA, Sim X, Li X, Cotch MF, Ikram MK, Holliday EG, et al. Genome-wide association study of retinopathy in individuals without diabetes. PLoS One. 2013;8(2):e54232. PubMed PMID: 23393555. Pubmed Central PMCID: 3564946.
392. American Diabetes A, Clarke W, Deeb LC, Jameson P, Kaufman F, Klingensmith G, et al. Diabetes care in the school and day care setting. Diabetes Care. 2013 Jan;36 Suppl 1:S75-9. PubMed PMID: 23264426. Pubmed Central PMCID: 3537280.
393. Saxena R, Saleheen D, Been LF, Garavito ML, Braun T, Bjonnes A, et al. Genome-wide association study identifies a novel locus contributing to type 2 diabetes susceptibility in sikhs of punjabi origin from India. Diabetes. 2013 May;62(5):1746-55. PubMed PMID: 23300278. Pubmed Central PMCID: 3636649.
394. Helgeson VS, Reynolds KA, Snyder PR, Palladino DK, Becker DJ, Siminerio L, et al. Characterizing the transition from paediatric to adult care among emerging adults with Type 1 diabetes. Diabet Med. 2013 May;30(5):610-5. PubMed PMID: 23157171. Pubmed Central PMCID: 3628931.
395. Helgeson VS, Becker D, Escobar O, Siminerio L. Families with children with diabetes: implications of parent stress for parent and child health. Journal of pediatric psychology. 2012 May;37(4):467-78. PubMed PMID: 22267104. Pubmed Central PMCID: 3334535.
396. Virtanen SM, Nevalainen J, Kronberg-Kippila C, Ahonen S, Tapanainen H, Uusitalo L, et al. Food consumption and advanced beta cell autoimmunity in young children with HLA-conferred susceptibility to type 1 diabetes: a nested case-control design. Am J Clin Nutr. 2012 Feb;95(2):471-8. PubMed PMID: 22237062.
397. Dick AD, McMenamin PG, Korner H, Scallon BJ, Ghrayeb J, Forrester JV, et al. Inhibition of tumor necrosis factor activity minimizes target organ damage in experimental autoimmune uveoretinitis despite quantitatively normal activated T cell traffic to the retina. European journal of immunology. 1996 May;26(5):1018-25. PubMed PMID: 8647162.
398. Dick AD, Ford AL, Forrester JV, Sedgwick JD. Flow cytometric identification of a minority population of MHC class II positive cells in the normal rat retina distinct from CD45lowCD11b/c+CD4low parenchymal microglia. Br J Ophthalmol. 1995 Sep;79(9):834-40. PubMed PMID: 7488603. Pubmed Central PMCID: 505270.
399. Quellec G, Lamard M, Josselin PM, Cazuguel G, Cochener B, Roux C. Optimal wavelet transform for the detection of microaneurysms in retina photographs. IEEE transactions on medical imaging. 2008 Sep;27(9):1230-41. PubMed PMID: 18779064. Pubmed Central PMCID: 2567825.
400. Horie S, Robbie SJ, Liu J, Wu WK, Ali RR, Bainbridge JW, et al. CD200R signaling inhibits pro-angiogenic gene expression by macrophages and suppresses choroidal neovascularization. Scientific reports. 2013;3:3072. PubMed PMID: 24170042. Pubmed Central PMCID: 3812658.
401. Liu J, Copland DA, Horie S, Wu WK, Chen M, Xu Y, et al. Myeloid cells expressing VEGF and arginase-1 following uptake of damaged retinal pigment epithelium suggests potential mechanism that drives the onset of choroidal angiogenesis in mice. PLoS One. 2013;8(8):e72935. PubMed PMID: 23977372. Pubmed Central PMCID: 3745388.

402. Miyahara S, Kiryu J, Miyamoto K, Katsuta H, Hirose F, Tamura H, et al. In vivo three-dimensional evaluation of leukocyte behavior in retinal microcirculation of mice. Invest Ophthalmol Vis Sci. 2004 Nov;45(11):4197-201. PubMed PMID: 15505075.
403. Shen J, Xie B, Dong A, Swaim M, Hackett SF, Campochiaro PA. In vivo immunostaining demonstrates macrophages associate with growing and regressing vessels. Invest Ophthalmol Vis Sci. 2007 Sep;48(9):4335-41. PubMed PMID: 17724225.
404. Hulten MA, Gould CP, Goldman AS, Waters JJ. Chromosome in situ suppression hybridisation in clinical cytogenetics. J Med Genet. 1991 Sep;28(9):577-82. PubMed PMID: 1956055. Pubmed Central PMCID: 1015785.
405. Bernardes R, Nunes S, Pereira I, Torrent T, Rosa A, Coelho D, et al. Computer-assisted microaneurysm turnover in the early stages of diabetic retinopathy. Ophthalmologica. 2009;223(5):284-91. PubMed PMID: 19372722.
406. Donald DE, Yipintsoi T. Comparison of measured and indocyanine green blood flows in various organs and systems. Mayo Clinic proceedings. 1973 Jul;48(7):492-500. PubMed PMID: 4577311.
407. DiNardo MM, Gibson JM, Siminerio L, Morell AR, Lee ES. Complementary and alternative medicine in diabetes care. Current diabetes reports. 2012 Dec;12(6):749-61. PubMed PMID: 22986889.
408. Lee MG, Jeong MH, Lee KH, Park KH, Sim DS, Yoon HJ, et al. Prognostic impact of diabetes mellitus and hypertension for mid-term outcome of patients with acute myocardial infarction who underwent percutaneous coronary intervention. Journal of cardiology. 2012 Oct;60(4):257-63. PubMed PMID: 22819036.
409. Ingram DA, Mead LE, Tanaka H, Meade V, Fenoglio A, Mortell K, et al. Identification of a novel hierarchy of endothelial progenitor cells using human peripheral and umbilical cord blood. Blood. 2004 Nov 1;104(9):2752-60. PubMed PMID: 15226175.
410. Yoder MC, Mead LE, Prater D, Krier TR, Mroueh KN, Li F, et al. Redefining endothelial progenitor cells via clonal analysis and hematopoietic stem/progenitor cell principals. Blood. 2007 Mar 1;109(5):1801-9. PubMed PMID: 17053059. Pubmed Central PMCID: 1801067.
411. Sen T, Aksu T. Endothelial progenitor cell and adhesion molecules determine the quality of the coronary collateral circulation/Endothelial progenitor cells (CD34+KDR+) and monocytes may provide the development of good coronary collaterals despite the vascular risk factors and extensive atherosclerosis. Anadolu kardiyoloji dergisi : AKD = the Anatolian journal of cardiology. 2012 Aug;12(5):447; author reply -8. PubMed PMID: 22626655.
412. Georgescu A, Alexandru N, Andrei E, Titorencu I, Dragan E, Tarziu C, et al. Circulating microparticles and endothelial progenitor cells in atherosclerosis: pharmacological effects of irbesartan. Journal of thrombosis and haemostasis : JTH. 2012 Apr;10(4):680-91. PubMed PMID: 22303879.
413. Werner N, Wassmann S, Ahlers P, Schiegl T, Kosiol S, Link A, et al. Endothelial progenitor cells correlate with endothelial function in patients with coronary artery disease. Basic research in cardiology. 2007 Nov;102(6):565-71. PubMed PMID: 17932708.
414. Du F, Zhou J, Gong R, Huang X, Pansuria M, Virtue A, et al. Endothelial progenitor cells in atherosclerosis. Frontiers in bioscience. 2012;17:2327-49. PubMed PMID: 22652782. Pubmed Central PMCID: 3368338.
415. Glowinska-Olszewska B, Moniuszko M, Hryniewicz A, Jeznach M, Rusak M, Dabrowska M, et al. Relationship between circulating endothelial progenitor cells and endothelial dysfunction in children with type 1 diabetes: a novel paradigm of early atherosclerosis in high-risk young patients. European journal of endocrinology / European Federation of Endocrine Societies. 2013 Feb;168(2):153-61. PubMed PMID: 23111589.
416. Guven H, Shepherd RM, Bach RG, Capoccia BJ, Link DC. The number of endothelial progenitor cell colonies in the blood is increased in patients with angiographically significant

coronary artery disease. J Am Coll Cardiol. 2006 Oct 17;48(8):1579-87. PubMed PMID: 17045891.
417. Cuadrado-Godia E, Regueiro A, Nunez J, Diaz-Ricard M, Novella S, Oliveras A, et al. Endothelial Progenitor Cells Predict Cardiovascular Events after Atherothrombotic Stroke and Acute Myocardial Infarction. A PROCELL Substudy. PLoS One. 2015;10(9):e0132415. PubMed PMID: 26332322. Pubmed Central PMCID: 4557832.
418. Pelliccia F, Pasceri V, Rosano G, Pristipino C, Roncella A, Speciale G, et al. Endothelial progenitor cells predict long-term prognosis in patients with stable angina treated with percutaneous coronary intervention: five-year follow-up of the PROCREATION study. Circulation journal : official journal of the Japanese Circulation Society. 2013;77(7):1728-35. PubMed PMID: 23575363.
419. Seo SG, Yeo JH, Kim JH, Kim JB, Cho TJ, Lee DY. Negative-pressure wound therapy induces endothelial progenitor cell mobilization in diabetic patients with foot infection or skin defects. Exp Mol Med. 2013;45:e62. PubMed PMID: 24232261. Pubmed Central PMCID: 3849576.
420. Kulwas A, Drela E, Jundzill W, Goralczyk B, Ruszkowska-Ciastek B, Rosc D. Circulating endothelial progenitor cells and angiogenic factors in diabetes complicated diabetic foot and without foot complications. J Diabetes Complications. 2015 Jul;29(5):686-90. PubMed PMID: 25872462.
421. Yao Y, Sheng Z, Li Y, Fu C, Ma G, Liu N, et al. Tissue kallikrein-modified human endothelial progenitor cell implantation improves cardiac function via enhanced activation of akt and increased angiogenesis. Laboratory investigation; a journal of technical methods and pathology. 2013 May;93(5):577-91. PubMed PMID: 23508045. Pubmed Central PMCID: 4051305.
422. Oikonomou E, Siasos G, Zaromitidou M, Hatzis G, Mourouzis K, Chrysohoou C, et al. Atorvastatin treatment improves endothelial function through endothelial progenitor cells mobilization in ischemic heart failure patients. Atherosclerosis. 2015 Feb;238(2):159-64. PubMed PMID: 25525743.
423. Zhou J, Cheng M, Liao YH, Hu Y, Wu M, Wang Q, et al. Rosuvastatin enhances angiogenesis via eNOS-dependent mobilization of endothelial progenitor cells. PLoS One. 2013;8(5):e63126. PubMed PMID: 23704894. Pubmed Central PMCID: 3660394.
424. Suzuki R, Fukuda N, Katakawa M, Tsunemi A, Tahira Y, Matsumoto T, et al. Effects of an angiotensin II receptor blocker on the impaired function of endothelial progenitor cells in patients with essential hypertension. American journal of hypertension. 2014 May;27(5):695-701. PubMed PMID: 24200748.
425. Ye L, Zhang P, Duval S, Su L, Xiong Q, Zhang J. Thymosin beta4 increases the potency of transplanted mesenchymal stem cells for myocardial repair. Circulation. 2013 Sep 10;128(11 Suppl 1):S32-41. PubMed PMID: 24030419. Pubmed Central PMCID: 3886821.
426. Asai J, Takenaka H, Kusano KF, Ii M, Luedemann C, Curry C, et al. Topical sonic hedgehog gene therapy accelerates wound healing in diabetes by enhancing endothelial progenitor cell-mediated microvascular remodeling. Circulation. 2006 May 23;113(20):2413-24. PubMed PMID: 16702471.
427. Jujo K, Hamada H, Iwakura A, Thorne T, Sekiguchi H, Clarke T, et al. CXCR4 blockade augments bone marrow progenitor cell recruitment to the neovasculature and reduces mortality after myocardial infarction. Proc Natl Acad Sci U S A. 2010 Jun 15;107(24):11008-13. PubMed PMID: 20534467. Pubmed Central PMCID: 2890743.
428. Roncalli J, Renault MA, Tongers J, Misener S, Thorne T, Kamide C, et al. Sonic hedgehog-induced functional recovery after myocardial infarction is enhanced by AMD3100-mediated progenitor-cell mobilization. J Am Coll Cardiol. 2011 Jun 14;57(24):2444-52. PubMed PMID: 21658566. Pubmed Central PMCID: 3117426.

429. Horie T, Onodera R, Akamastu M, Ichikawa Y, Hoshino J, Kaneko E, et al. Long-term clinical outcomes for patients with lower limb ischemia implanted with G-CSF-mobilized autologous peripheral blood mononuclear cells. Atherosclerosis. 2010 Feb;208(2):461-6. PubMed PMID: 19720375.
430. Fisher SA, Brunskill SJ, Doree C, Mathur A, Taggart DP, Martin-Rendon E. Stem cell therapy for chronic ischaemic heart disease and congestive heart failure. The Cochrane database of systematic reviews. 2014;4:CD007888. PubMed PMID: 24777540.
431. Losordo DW, Henry TD, Davidson C, Sup Lee J, Costa MA, Bass T, et al. Intramyocardial, autologous CD34+ cell therapy for refractory angina. Circ Res. 2011 Aug 5;109(4):428-36. PubMed PMID: 21737787. Pubmed Central PMCID: 3190575.
432. Chen YL, Tsai TH, Wallace CG, Chen YL, Huang TH, Sung PH, et al. Intra-carotid arterial administration of autologous peripheral blood-derived endothelial progenitor cells improves acute ischemic stroke neurological outcomes in rats. International journal of cardiology. 2015 Dec 15;201:668-83. PubMed PMID: 26363631.
433. Tanaka R, Masuda H, Kato S, Imagawa K, Kanabuchi K, Nakashioya C, et al. Autologous G-CSF-mobilized peripheral blood CD34+ cell therapy for diabetic patients with chronic nonhealing ulcer. Cell transplantation. 2014 Feb;23(2):167-79. PubMed PMID: 23107450.
434. Risau W, Flamme I. Vasculogenesis. Annual review of cell and developmental biology. 1995;11:73-91. PubMed PMID: 8689573.
435. Chen H, Campbell RA, Chang Y, Li M, Wang CS, Li J, et al. Pleiotrophin produced by multiple myeloma induces transdifferentiation of monocytes into vascular endothelial cells: a novel mechanism of tumor-induced vasculogenesis. Blood. 2009 Feb 26;113(9):1992-2002. PubMed PMID: 19060246. Pubmed Central PMCID: 2651013.
436. Hill JM, Zalos G, Halcox JP, Schenke WH, Waclawiw MA, Quyyumi AA, et al. Circulating endothelial progenitor cells, vascular function, and cardiovascular risk. The New England journal of medicine. 2003 Feb 13;348(7):593-600. PubMed PMID: 12584367.
437. Prater DN, Case J, Ingram DA, Yoder MC. Working hypothesis to redefine endothelial progenitor cells. Leukemia. 2007 Jun;21(6):1141-9. PubMed PMID: 17392816.
438. Rohde E, Bartmann C, Schallmoser K, Reinisch A, Lanzer G, Linkesch W, et al. Immune cells mimic the morphology of endothelial progenitor colonies in vitro. Stem Cells. 2007 Jul;25(7):1746-52. PubMed PMID: 17395771.
439. van Beem RT, Noort WA, Voermans C, Kleijer M, ten Brinke A, van Ham SM, et al. The presence of activated CD4(+) T cells is essential for the formation of colony-forming unit-endothelial cells by CD14(+) cells. J Immunol. 2008 Apr 1;180(7):5141-8. PubMed PMID: 18354240.
440. Vasa M, Fichtlscherer S, Aicher A, Adler K, Urbich C, Martin H, et al. Number and migratory activity of circulating endothelial progenitor cells inversely correlate with risk factors for coronary artery disease. Circ Res. 2001 Jul 6;89(1):E1-7. PubMed PMID: 11440984.
441. Vasa M, Fichtlscherer S, Adler K, Aicher A, Martin H, Zeiher AM, et al. Increase in circulating endothelial progenitor cells by statin therapy in patients with stable coronary artery disease. Circulation. 2001 Jun 19;103(24):2885-90. PubMed PMID: 11413075.
442. Mukai N, Akahori T, Komaki M, Li Q, Kanayasu-Toyoda T, Ishii-Watabe A, et al. A comparison of the tube forming potentials of early and late endothelial progenitor cells. Experimental cell research. 2008 Feb 1;314(3):430-40. PubMed PMID: 18083163.
443. Zhang SJ, Zhang H, Wei YJ, Su WJ, Liao ZK, Hou M, et al. Adult endothelial progenitor cells from human peripheral blood maintain monocyte/macrophage function throughout in vitro culture. Cell research. 2006 Jun;16(6):577-84. PubMed PMID: 16775629.
444. Sieveking DP, Buckle A, Celermajer DS, Ng MK. Strikingly different angiogenic properties of endothelial progenitor cell subpopulations: insights from a novel human angiogenesis assay. J Am Coll Cardiol. 2008 Feb 12;51(6):660-8. PubMed PMID: 18261686.

445. Li B, Cohen A, Hudson TE, Motlagh D, Amrani DL, Duffield JS. Mobilized human hematopoietic stem/progenitor cells promote kidney repair after ischemia/reperfusion injury. Circulation. 2010 May 25;121(20):2211-20. PubMed PMID: 20458011. Pubmed Central PMCID: 2919223.
446. Rookmaaker MB, Vergeer M, van Zonneveld AJ, Rabelink TJ, Verhaar MC. Endothelial progenitor cells: mainly derived from the monocyte/macrophage-containing CD34- mononuclear cell population and only in part from the hematopoietic stem cell-containing CD34+ mononuclear cell population. Circulation. 2003 Nov 25;108(21):e150; author reply e. PubMed PMID: 14638532.
447. Timmermans F, Plum J, Yoder MC, Ingram DA, Vandekerckhove B, Case J. Endothelial progenitor cells: identity defined? J Cell Mol Med. 2009 Jan;13(1):87-102. PubMed PMID: 19067770. Pubmed Central PMCID: 3823038.
448. Pula G, Mayr U, Evans C, Prokopi M, Vara DS, Yin X, et al. Proteomics identifies thymidine phosphorylase as a key regulator of the angiogenic potential of colony-forming units and endothelial progenitor cell cultures. Circ Res. 2009 Jan 2;104(1):32-40. PubMed PMID: 19023133.
449. Medina RJ, O'Neill CL, Sweeney M, Guduric-Fuchs J, Gardiner TA, Simpson DA, et al. Molecular analysis of endothelial progenitor cell (EPC) subtypes reveals two distinct cell populations with different identities. BMC medical genomics. 2010;3:18. PubMed PMID: 20465783. Pubmed Central PMCID: 2881111.
450. Gremmels H, Fledderus JO, van Balkom BW, Verhaar MC. Transcriptome analysis in endothelial progenitor cell biology. Antioxidants & redox signaling. 2011 Aug 15;15(4):1029-42. PubMed PMID: 20812873.
451. Yoon CH, Hur J, Park KW, Kim JH, Lee CS, Oh IY, et al. Synergistic neovascularization by mixed transplantation of early endothelial progenitor cells and late outgrowth endothelial cells: the role of angiogenic cytokines and matrix metalloproteinases. Circulation. 2005 Sep 13;112(11):1618-27. PubMed PMID: 16145003.
452. Elsheikh E, Uzunel M, He Z, Holgersson J, Nowak G, Sumitran-Holgersson S. Only a specific subset of human peripheral-blood monocytes has endothelial-like functional capacity. Blood. 2005 Oct 1;106(7):2347-55. PubMed PMID: 15985545.
453. Dernbach E, Urbich C, Brandes RP, Hofmann WK, Zeiher AM, Dimmeler S. Antioxidative stress-associated genes in circulating progenitor cells: evidence for enhanced resistance against oxidative stress. Blood. 2004 Dec 1;104(12):3591-7. PubMed PMID: 15161665.
454. Schirmer SH, Fledderus JO, Bot PT, Moerland PD, Hoefer IE, Baan J, Jr., et al. Interferon-beta signaling is enhanced in patients with insufficient coronary collateral artery development and inhibits arteriogenesis in mice. Circ Res. 2008 May 23;102(10):1286-94. PubMed PMID: 18420941.
455. Shantsila E, Tapp LD, Wrigley BJ, Montoro-Garcia S, Lip GY. CXCR4 positive and angiogenic monocytes in myocardial infarction. Thromb Haemost. 2013 Feb;109(2):255-62. PubMed PMID: 23223950.
456. Shantsila E, Wrigley BJ, Shantsila A, Tapp LD, Gill PS, Lip GY. Monocyte-derived and CD34+/KDR+ endothelial progenitor cells in heart failure. Journal of thrombosis and haemostasis : JTH. 2012 Jul;10(7):1252-61. PubMed PMID: 22519984.
457. Pulford K, Micklem K, McCarthy S, Cordell J, Jones M, Mason DY. A monocyte/macrophage antigen recognized by the four antibodies GHI/61, Ber-MAC3, Ki-M8 and SM4. Immunology. 1992 Apr;75(4):588-95. PubMed PMID: 1592433. Pubmed Central PMCID: 1384835.
458. Backe E, Schwarting R, Gerdes J, Ernst M, Stein H. Ber-MAC3: new monoclonal antibody that defines human monocyte/macrophage differentiation antigen. Journal of

clinical pathology. 1991 Nov;44(11):936-45. PubMed PMID: 1721628. Pubmed Central PMCID: 496636.
459. Topoll HH, Zwadlo G, Lange DE, Sorg C. Phenotypic dynamics of macrophage subpopulations during human experimental gingivitis. Journal of periodontal research. 1989 Mar;24(2):106-12. PubMed PMID: 2524575.
460. Zwadlo G, Voegeli R, Schulze Osthoff K, Sorg C. A monoclonal antibody to a novel differentiation antigen on human macrophages associated with the down-regulatory phase of the inflammatory process. Experimental cell biology. 1987;55(6):295-304. PubMed PMID: 3450546.
461. Noble PB, Cutts JH. Isolation of individual leukocyte types from peripheral blood. J Lab Clin Med. 1968 Sep;72(3):533-8. PubMed PMID: 5674084.
462. Corkum CP, Ings DP, Burgess C, Karwowska S, Kroll W, Michalak TI. Immune cell subsets and their gene expression profiles from human PBMC isolated by Vacutainer Cell Preparation Tube (CPT()) and standard density gradient. BMC immunology. 2015;16(1):48. PubMed PMID: 26307036. Pubmed Central PMCID: 4549105.
463. Riedhammer C, Halbritter D, Weissert R. Peripheral Blood Mononuclear Cells: Isolation, Freezing, Thawing, and Culture. Methods in molecular biology. 2016;1304:53-61. PubMed PMID: 25092056.
464. Shantsila E, Wrigley B, Tapp L, Apostolakis S, Montoro-Garcia S, Drayson MT, et al. Immunophenotypic characterization of human monocyte subsets: possible implications for cardiovascular disease pathophysiology. Journal of thrombosis and haemostasis : JTH. 2011 May;9(5):1056-66. PubMed PMID: 21342432.
465. Cros J, Cagnard N, Woollard K, Patey N, Zhang SY, Senechal B, et al. Human CD14dim monocytes patrol and sense nucleic acids and viruses via TLR7 and TLR8 receptors. Immunity. 2010 Sep 24;33(3):375-86. PubMed PMID: 20832340. Pubmed Central PMCID: 3063338.
466. Fernandez Pujol B, Lucibello FC, Gehling UM, Lindemann K, Weidner N, Zuzarte ML, et al. Endothelial-like cells derived from human CD14 positive monocytes. Differentiation; research in biological diversity. 2000 May;65(5):287-300. PubMed PMID: 10929208.
467. Romagnani P, Annunziato F, Liotta F, Lazzeri E, Mazzinghi B, Frosali F, et al. CD14+CD34low cells with stem cell phenotypic and functional features are the major source of circulating endothelial progenitors. Circ Res. 2005 Aug 19;97(4):314-22. PubMed PMID: 16020753.
468. Fadini GP, Simoni F, Cappellari R, Vitturi N, Galasso S, Vigili de Kreutzenberg S, et al. Pro-inflammatory monocyte-macrophage polarization imbalance in human hypercholesterolemia and atherosclerosis. Atherosclerosis. 2014 Dec;237(2):805-8. PubMed PMID: 25463124.
469. Tippett E, Cheng WJ, Westhorpe C, Cameron PU, Brew BJ, Lewin SR, et al. Differential expression of CD163 on monocyte subsets in healthy and HIV-1 infected individuals. PLoS One. 2011;6(5):e19968. PubMed PMID: 21625498. Pubmed Central PMCID: 3098854.
470. Buechler C, Ritter M, Orso E, Langmann T, Klucken J, Schmitz G. Regulation of scavenger receptor CD163 expression in human monocytes and macrophages by pro- and antiinflammatory stimuli. J Leukoc Biol. 2000 Jan;67(1):97-103. PubMed PMID: 10648003.
471. Schmidt-Lucke C, Fichtlscherer S, Aicher A, Tschope C, Schultheiss HP, Zeiher AM, et al. Quantification of circulating endothelial progenitor cells using the modified ISHAGE protocol. PLoS One. 2010;5(11):e13790. PubMed PMID: 21072182. Pubmed Central PMCID: 2972200.
472. Zawada AM, Fell LH, Untersteller K, Seiler S, Rogacev KS, Fliser D, et al. Comparison of two different strategies for human monocyte subsets gating within the large-scale prospective CARE FOR HOMe Study. Cytometry A. 2015 Aug;87(8):750-8. PubMed PMID: 26062127.

473. Fadini GP, Losordo D, Dimmeler S. Critical reevaluation of endothelial progenitor cell phenotypes for therapeutic and diagnostic use. Circ Res. 2012 Feb 17;110(4):624-37. PubMed PMID: 22343557. Pubmed Central PMCID: 3382070.
474. Kondo T, Hayashi M, Takeshita K, Numaguchi Y, Kobayashi K, Iino S, et al. Smoking cessation rapidly increases circulating progenitor cells in peripheral blood in chronic smokers. Arteriosclerosis, thrombosis, and vascular biology. 2004 Aug;24(8):1442-7. PubMed PMID: 15191940.
475. Lanuti P, Rotta G, Almici C, Avvisati G, Budillon A, Doretto P, et al. Endothelial progenitor cells, defined by the simultaneous surface expression of VEGFR2 and CD133, are not detectable in healthy peripheral and cord blood. Cytometry A. 2015 Aug 25. PubMed PMID: 26305912.
476. Case J, Mead LE, Bessler WK, Prater D, White HA, Saadatzadeh MR, et al. Human CD34+AC133+VEGFR-2+ cells are not endothelial progenitor cells but distinct, primitive hematopoietic progenitors. Exp Hematol. 2007 Jul;35(7):1109-18. PubMed PMID: 17588480.
477. Shih YT, Wang MC, Peng HH, Chen TF, Chen L, Chang JY, et al. Modulation of chemotactic and pro-inflammatory activities of endothelial progenitor cells by hepatocellular carcinoma. Cellular signalling. 2012 Mar;24(3):779-93. PubMed PMID: 22120522.
478. Brunner M, Thurnher D, Heiduschka G, Grasl M, Brostjan C, Erovic BM. Elevated levels of circulating endothelial progenitor cells in head and neck cancer patients. Journal of surgical oncology. 2008 Dec 1;98(7):545-50. PubMed PMID: 18792958.
479. Kleinman ME, Tepper OM, Capla JM, Bhatt KA, Ceradini DJ, Galiano RD, et al. Increased circulating AC133+ CD34+ endothelial progenitor cells in children with hemangioma. Lymphatic research and biology. 2003;1(4):301-7. PubMed PMID: 15624558.
480. Hilbe W, Dirnhofer S, Oberwasserlechner F, Schmid T, Gunsilius E, Hilbe G, et al. CD133 positive endothelial progenitor cells contribute to the tumour vasculature in non-small cell lung cancer. Journal of clinical pathology. 2004 Sep;57(9):965-9. PubMed PMID: 15333659. Pubmed Central PMCID: 1770433.
481. Park A, Barrera-Ramirez J, Ranasinghe I, Pilon S, Sy R, Fergusson D, et al. Use of Statins to Augment Progenitor Cell Function in Preclinical and Clinical Studies of Regenerative Therapy: a Systematic Review. Stem cell reviews. 2016 Jun;12(3):327-39. PubMed PMID: 26873165.
482. Kawanaka N, Yamamura M, Aita T, Morita Y, Okamoto A, Kawashima M, et al. CD14+,CD16+ blood monocytes and joint inflammation in rheumatoid arthritis. Arthritis Rheum. 2002 Oct;46(10):2578-86. PubMed PMID: 12384915.
483. Ramirez R, Carracedo J, Merino A, Soriano S, Ojeda R, Alvarez-Lara MA, et al. CD14+CD16+ monocytes from chronic kidney disease patients exhibit increased adhesion ability to endothelial cells. Contrib Nephrol. 2011;171:57-61. PubMed PMID: 21625090.
484. Shibuya M. VEGF-VEGFR System as a Target for Suppressing Inflammation and other Diseases. Endocrine, metabolic & immune disorders drug targets. 2015;15(2):135-44. PubMed PMID: 25772179.
485. Favre J, Terborg N, Horrevoets AJ. The diverse identity of angiogenic monocytes. Eur J Clin Invest. 2013 Jan;43(1):100-7. PubMed PMID: 23083351.
486. Nowak G, Karrar A, Holmen C, Nava S, Uzunel M, Hultenby K, et al. Expression of vascular endothelial growth factor receptor-2 or Tie-2 on peripheral blood cells defines functionally competent cell populations capable of reendothelialization. Circulation. 2004 Dec 14;110(24):3699-707. PubMed PMID: 15381639.
487. Wara AK, Croce K, Foo S, Sun X, Icli B, Tesmenitsky Y, et al. Bone marrow-derived CMPs and GMPs represent highly functional proangiogenic cells: implications for ischemic cardiovascular disease. Blood. 2011 Dec 8;118(24):6461-4. PubMed PMID: 21828132. Pubmed Central PMCID: 3236127.

488. Willenborg S, Lucas T, van Loo G, Knipper JA, Krieg T, Haase I, et al. CCR2 recruits an inflammatory macrophage subpopulation critical for angiogenesis in tissue repair. Blood. 2012 Jul 19;120(3):613-25. PubMed PMID: 22577176.
489. Grunewald M, Avraham I, Dor Y, Bachar-Lustig E, Itin A, Jung S, et al. VEGF-induced adult neovascularization: recruitment, retention, and role of accessory cells. Cell. 2006 Jan 13;124(1):175-89. PubMed PMID: 16413490.
490. Kim SJ, Kim JS, Papadopoulos J, Wook Kim S, Maya M, Zhang F, et al. Circulating monocytes expressing CD31: implications for acute and chronic angiogenesis. Am J Pathol. 2009 May;174(5):1972-80. PubMed PMID: 19349357. Pubmed Central PMCID: 2671284.
491. Hamann W, Floter A, Schmutzler W, Zwadlo-Klarwasser G. Characterization of a novel anti-inflammatory factor produced by RM3/1 macrophages derived from glucocorticoid treated human monocytes. Inflammation research : official journal of the European Histamine Research Society [et al]. 1995 Dec;44(12):535-40. PubMed PMID: 8788234.
492. Kodelja V, Muller C, Tenorio S, Schebesch C, Orfanos CE, Goerdt S. Differences in angiogenic potential of classically vs alternatively activated macrophages. Immunobiology. 1997 Nov;197(5):478-93. PubMed PMID: 9413747.
493. Lad EM, Cousins SW, Van Arnam JS, Proia AD. Abundance of infiltrating CD163+ cells in the retina of postmortem eyes with dry and neovascular age-related macular degeneration. Graefes Arch Clin Exp Ophthalmol. 2015 Jul 7. PubMed PMID: 26148801.
494. Chmielewski PP, Boryslawski K, Chmielowiec K, Chmielowiec J, Strzelec B. The association between total leukocyte count and longevity: Evidence from longitudinal and cross-sectional data. Annals of anatomy = Anatomischer Anzeiger : official organ of the Anatomische Gesellschaft. 2015 Sep 30. PubMed PMID: 26434754.
495. Price SA, Gorelik A, Fourlanos S, Colman PG, Wentworth JM. Obesity is associated with retinopathy and macrovascular disease in type 1 diabetes. Obesity research & clinical practice. 2014 Mar-Apr;8(2):e178-82. PubMed PMID: 24743014.
496. Gray N, Picone G, Sloan F, Yashkin A. Relation between BMI and diabetes mellitus and its complications among US older adults. Southern medical journal. 2015 Jan;108(1):29-36. PubMed PMID: 25580754. Pubmed Central PMCID: 4457375.
497. Kyari F, Tafida A, Sivasubramaniam S, Murthy GV, Peto T, Gilbert CE, et al. Prevalence and risk factors for diabetes and diabetic retinopathy: results from the Nigeria national blindness and visual impairment survey. BMC public health. 2014;14:1299. PubMed PMID: 25523434. Pubmed Central PMCID: 4301086.
498. Schlitt A, Heine GH, Blankenberg S, Espinola-Klein C, Dopheide JF, Bickel C, et al. CD14+CD16+ monocytes in coronary artery disease and their relationship to serum TNF-alpha levels. Thromb Haemost. 2004 Aug;92(2):419-24. PubMed PMID: 15269840.
499. Devevre EF, Renovato-Martins M, Clement K, Sautes-Fridman C, Cremer I, Poitou C. Profiling of the three circulating monocyte subpopulations in human obesity. J Immunol. 2015 Apr 15;194(8):3917-23. PubMed PMID: 25786686.
500. Panasiuk A, Zak J, Kasprzycka E, Janicka K, Prokopowicz D. Blood platelet and monocyte activations and relation to stages of liver cirrhosis. World J Gastroenterol. 2005 May 14;11(18):2754-8. PubMed PMID: 15884116. Pubmed Central PMCID: 4305910.
501. Spaide RF, Klancnik JM, Jr., Cooney MJ. Retinal vascular layers imaged by fluorescein angiography and optical coherence tomography angiography. JAMA ophthalmology. 2015 Jan;133(1):45-50. PubMed PMID: 25317632.
502. Fingerle-Rowson G, Auers J, Kreuzer E, Fraunberger P, Blumenstein M, Ziegler-Heitbrock LH. Expansion of CD14+CD16+ monocytes in critically ill cardiac surgery patients. Inflammation. 1998 Aug;22(4):367-79. PubMed PMID: 9675608.
503. Fingerle G, Pforte A, Passlick B, Blumenstein M, Strobel M, Ziegler-Heitbrock HW. The novel subset of CD14+/CD16+ blood monocytes is expanded in sepsis patients. Blood. 1993 Nov 15;82(10):3170-6. PubMed PMID: 7693040.

504. Skrzeczynska J, Kobylarz K, Hartwich Z, Zembala M, Pryjma J. CD14+CD16+ monocytes in the course of sepsis in neonates and small children: monitoring and functional studies. Scandinavian journal of immunology. 2002 Jun;55(6):629-38. PubMed PMID: 12028567.
505. Hepburn AL, Mason JC, Davies KA. Expression of Fcgamma and complement receptors on peripheral blood monocytes in systemic lupus erythematosus and rheumatoid arthritis. Rheumatology (Oxford). 2004 May;43(5):547-54. PubMed PMID: 14747618.
506. Mukherjee R, Kanti Barman P, Kumar Thatoi P, Tripathy R, Kumar Das B, Ravindran B. Non-Classical monocytes display inflammatory features: Validation in Sepsis and Systemic Lupus Erythematous. Scientific reports. 2015;5:13886. PubMed PMID: 26358827. Pubmed Central PMCID: 4566081.